SUPPORTING BRIDGE MANAGEMENT WITH ADVANCED ANALYSIS AND MACHINE LEARNING

FINAL REPORT

Principal Investigator: Joshua S. Steelman, Ph.D., P.E.
Graduate Research Assistant: Francisco Garcia

Department of Civil and Environmental Engineering
University of Nebraska-Lincoln
900 N. 16th Street
Nebraska Hall W181
PO Box 880531
Lincoln, NE 68588-0531

Sponsored By
Nebraska Department of Transportation and U.S. Department of Transportation Federal Highway Administration

September 1, 2020

NEBRASKA
Good Life. Great Journey.
DEPARTMENT OF TRANSPORTATION

UNIVERSITY OF Nebraska Lincoln

TECHNICAL REPORT DOCUMENTATION PAGE

1. Report No. SPR-1(19) M088	**2. Government Accession No.**	**3. Recipient's Catalog No.**
4. Title and Subtitle Supporting Bridge Management with Advanced Analysis and Machine Learning		**5. Report Date** September 1, 2020 **6. Performing Organization Code**
7. Author(s) Joshua Steelman, Francisco Garcia		**8. Performing Organization Report No.**
9. Performing Organization Name and Address Department of Civil and Environmental Engineering University of Nebraska-Lincoln 900 N. 16th Street Nebraska Hall W181 PO Box 880531 Lincoln, NE 68588-0531		**10. Work Unit No.** **11. Contract** SPR-1(19) M088
12. Sponsoring Agency Name and Address Nebraska Department of Transportation Research Section 1400 Hwy 2 Lincoln, NE 68502		**13. Type of Report and Period Covered** Final Report July 2018-August 2020 **14. Sponsoring Agency Code**
15. Supplementary Notes		

16. Abstract

A supplemental Artificial Neural Network (ANN)-based tool was developed to support the Nebraska Department of Transportation (NDOT) in optimizing bridge management investments when choosing between refined modeling, field testing, retrofitting, or bridge replacement. Load ratings typically increase by approximately 15% to 20% when using detailed finite element analysis (FEA) instead of AASHTO approximate analysis methods. The ANN tool is implemented in an Excel spreadsheet to accept ten input parameters readily available to NDOT engineers performing typical load ratings, and predicts FEA-equivalent critical girder distribution factors (GDFs), removing unnecessary conservativism from approximate AASHTO GDFs, potentially justifying load posting removal for existing bridges, and enabling more optimized design for new construction. The Excel tool outputs direct ANN-predicted GDFs and adjusted GDFs penalized to account for ANN error by reliability calibration philosophically consistent with AASHTO Load and Resistance Factor Rating. The study included detailed FEA for 174 simple span, steel girder bridges with concrete decks. Subsets of 163 and 161 bridges within these available cases comprised the ANN design and training datasets for critical moment and shear live load effects, respectively. The reliability calibration found that the ANN live load effect prediction error with mean absolute independent testing error of 3.65% could be conservatively accommodated by increasing the live load factor by less than 0.05. The study also demonstrates application of the neural network model validated with a diagnostic field test, including discussion of potential adjustments to account for noncomposite bridge capacity and Load Factor Rating instead of Load and Resistance Factor Rating.

17. Key Words Bridge Load Ratings, Finite Element Modeling, Artificial Neural Networks, Reliability Calibration, Load Testing	**18. Distribution Statement** No restrictions.

19. Security Classification (of this report) Unclassified	**20. Security Classification (of this page)** Unclassified	**21. No. of Pages** 304	**22. Price** N/A

Form DOT F 1700.7 (8-72) Reproduction of completed page authorized

DISCLAIMER

The contents of this report reflect the views of the authors, who are responsible for the facts and the accuracy of the information presented herein. The contents do not necessarily reflect the official views or policies neither of the Nebraska Department of Transportations nor the University of Nebraska-Lincoln. This report does not constitute a standard, specification, or regulation. Trade or manufacturers' names, which may appear in this report, are cited only because they are considered essential to the objectives of the report.

The United States (U.S.) government and the State of Nebraska do not endorse products or manufacturers. This material is based upon work supported by the Federal Highway Administration under SPR-1(19) (M088). Any opinions, findings and conclusions or recommendations expressed in this publication are those of the author(s) and do not necessarily reflect the views of the Federal Highway Administration."

ACKNOWLEDGEMENTS

The authors of this project would like to thank the members of the Technical Advisory Committee and the Bridge Management Section at the Nebraska Department of Transportation for all of their help with attaining bridge information, performing load tests, and providing feedback through progress meetings. The authors would also like to thank Mr. Khalilullah Sultani, Ms. Xinyu Lin, and Mr. Juan Pablo Perez Garfias for their contributions to this project.

TABLE OF CONTENTS

LIST OF FIGURES

LIST OF TABLES

1 Introduction

1.1 Motivation

State governments are required by law to load rate all state-owned structures and to ensure the rating of local government structures (Hearn 2014). Load ratings establish safe loading limits for heavy truck traffic, and load posting is required to restrict bridge use when a bridge is deemed insufficiently safe to support legal loads. Nebraska's bridge inventory is subject to concerns particular to rural Mid-America, where a significant portion of transportation infrastructure was built off-system from state and national highway networks, and in many cases the bridges are aged and approaching or exceeding design lives. These same bridges are now desired to carry heavy husbandry vehicles or crop harvests.

The National Bridge Inventory (NBI 2019) reports that 10% of all bridges in the United States, and 19% of bridges in Nebraska (98% of which are locally owned), are posted to limit the allowable load on the bridge. The NBI also reports the design loading for 89% of posted bridges in Nebraska as "unknown", reflecting the bridges' age and off-system locations. Load postings can require truck rerouting, which generates negative economic and environmental impacts. It is therefore desirable to reduce the number of load posted bridges in the existing inventory.

Load posting is generally removed by either retrofitting to enhance the capacity of a particular asset, or performing a more rigorous load rating evaluation with physical load testing and/or refined analysis. Bridges can often carry appreciably higher loads than those used for design, because design procedures typically use conservative analytical modeling simplifications. More rigorous analysis can reveal the margin of reserve capacity beyond design loads accommodated by realistic load distribution among structural elements, but requires time and expertise on the part of the load rating engineer. The costs of designing, installing,

inspecting, and maintaining a retrofit must be compared to the costs of conducting a load test or refined analysis to determine the most efficient bridge management approach for each asset. This study aims to provide a supplementary tool that will enable a load rating engineer to quickly and easily estimate the likely benefit available from more rigorous evaluations.

1.2 Load Ratings

Load ratings are used to assess the load-carrying capacity of bridges, and are expressed as rating factors (RFs). The rating is the ratio of the available capacity of the bridge (i.e., total capacity reduced to account for permanent loads) to the required load effect produced by a rating vehicle. The rating factor is exactly 1 when the available capacity equals the required demand, more than 1 when the bridge has a higher capacity than the demand, and less than 1 when the demand is higher than the available capacity. Typical load rating is performed at two rating levels: Inventory and Operating. Inventory capacity describes the lower bound of the safe load capacity, which can be applied indefinitely, and corresponding to a reliability index that is consistent with current design codes. The operating capacity describes the maximum load capacity that a structure can nominally safely withstand, corresponding to a lower reliability index than the one used in typical design today. Bridges with Operating RFs less than 1 are further assessed using Legal loads, which are typically a suite of truck configurations and can vary by state. A bridge with a Legal RF less than 1 must be posted to warn and restrict heavy vehicles from traversing the bridge.

For girder bridges, engineers determine the RF for each girder of the bridge in question, and the girder with the lowest rating factor governs the load rating. Load rating engineers analyze each component and connection subjected to a “single force effect” (e.g. axial force, flexure, or shear) (AASHTO LRFD 2013). The general load rating equation, shown in Eqn. 1, is

written as a function of nominal capacity (C), dead load (D), live load effect (LL), and impact factor (IM).

$$RF = \frac{\Phi C - \gamma_d * D}{\gamma_L * LL(1 + IM)} \quad \text{Eqn. 1}$$

AASHTO rating factors tend to be conservative because the derivation of the live load utilizes girder distribution factors (GDFs or DFs). GDFs are intentionally conservative because they are primarily intended to facilitate new design and employ semi-empirical equations that must reasonably represent a wide variety of bridge geometries. Furthermore, AASHTO code neglects some bridge parameters and behavior such as additional stiffness provided by parapets and bridge rails, unintended composite behavior, and additional support restraint (i.e. rotational restraint at nominally simple supports). Since GDFs evaluate each girder as an element with approximated load demands, higher capacities can often be found when evaluating the bridge as a 3D system.

An alternative way to attain a more accurate load rating is to perform diagnostic load tests. The AASHTO Manual for Bridge Evaluation (2013) provides a procedure for adjusting analytic load ratings based on diagnostic tests, and will be discussed in Chapter 8. Load tests reveal live load effects induced in bridge elements by known load magnitudes and placements acting on a bridge. One of the primary benefits of a load test is to capture structural system response, thereby reducing biases introduced by AASHTO GDFs.

Most bridge tests are non-destructive tests. Destructive tests are performed in research labs or on decommissioned bridges in the field to understand how bridge structures behave as the load approaches the ultimate capacity. Diagnostic tests can be performed at a reliably safe load,

so that damage to the bridge is highly unlikely. Results of diagnostic tests can be used to calibrate a theoretical prediction of structural response to live loads. Diagnostic tests can be static or moving load tests, depending on the engineer's goals.

Alternatively, a proof test can be performed at a higher load level, by testing a bridge until a target load is reached or the bridge shows signs of distress. Since the load incrementally increases closer to the bridge capacity, damage into the structure is much more likely than a diagnostic load test. For this reason, the testing team must be highly qualified and carefully calculate the appropriate proof load before such a test can be performed.

Finite element analysis (FEA) is a powerful tool that can be used to assess more accurate load ratings. However, FEA takes a considerable amount of time and expertise, as well as investment in analysis software to develop accurate models. Artificial neural networks (ANNs) present an appealing supplementary option to complement AASHTO- and FEA-based computational load ratings. With the increasing accessibility of ANNs in commercial computing software, ANNs have recently been implemented to address an extensive range of complex problems in engineering. The primary benefit of using artificial neural networks is that, after initial development and calibration, ANNs can quickly provide reliable predictions for complex phenomena from readily available known parameter inputs. ANNs implemented in structural engineering do not formulate predictions explicitly from mechanics or advanced structural analysis. Instead, ANNs formulate predictions implicitly by using relationships detected during training, mimicking the human heuristic thought process.

Typical ANNs in engineering employ a multi-layered feedforward architecture. Multi-layer refers to layers of nodes in between the input and output. All of the nodes from one layer are connected to all of the nodes in the next layer by weighted connections. The weights and

biases of the nodes are established and refined during the training of the ANN. The ANN is trained by comparing the desired prediction and the actual ANN prediction. The difference between the ANN prediction and desired prediction is the error. As the ANN trains, the error backpropagates through the node connections and adjusts weights and biases to iteratively mitigate and minimize prediction errors.

In this project, ANNs were trained to predict FEA-based 3D structural system live load effects. The significance of this project is that bridges that are load posted can be load rated by using the ANN predictions to determine whether the investment of more rigorous structural analysis and/or field testing would be warranted to remove load posting.

2 Literature Review

2.1 Scope of Review

The literature review for this study focused on the following topics:

- AASHTO load rating specifications
- AASTHO design specifications
- Diagnostic field testing for bridges
- Artificial neural network applications in civil engineering
- Reliability analysis and calibration for structures

This chapter contains a selected set of key references. Additional references are discussed in Appendix 11.1.1.

2.2 Studies of Bridge Analysis and Load Ratings

Armendariz, R.R. and Bowman, M.D., 2018, Bridge Load Rating

The Indiana Department of Transportation (INDOT) was posed with the problem of determining bridge load ratings for bridges that had incomplete or no plans at all. The researchers formulated a general load rating plan that can be used for any bridge, regardless of how much information is known. The general procedure, shown in Figure 1, can be summarized by performing the following steps: 1) conduct a bridge characterization, 2) create a bridge database from the previous step, 3) conduct a field survey and inspection, and 4) perform the bridge load rating. INDOT provided the researchers with a list of bridges without plans. The list was made up of 53 bridges, 29 of which were bridges with soil covers. The proposed methodology for load rating the bridges was implemented for several bridges.

The first bridge is a soil covered bridge made up of three corrugated metal pipes. Based on the field inspections and conservative estimates for the three corrugated steel deck pipes,

AASHTO LRFR and LFR load ratings were calculated at inventory and operating rating levels, which were all above 1.

The second bridge, referred to as the Doan's Creek Bridge, was an earthen-filled concrete bridge. The bridge has two symmetrical arches with a pier in the middle that divides oncoming traffic. A SAP2000 model was created to capture axial and bending effects of the bridge. The model was created by dividing the arches in portions. The portions of the arches were approximated by straight frame element members. An interaction diagram was produced that described the failure bounds of the bridge. Finally, the bridge was also load tested with two trucks with strain gauge instrumentation on one of the concrete arches. The model and load test rating factors aligned closely, and showed that the bridge did not need a load posting.

A third bridge, referred to as the Roaring Creek Bridge, was investigated as well. This bridge did have plans, however the open-spandrel reinforced concrete bridge was load posted based on simple analyses performed by INDOT. This bridge was studied more closely with the goal of removing the load posting. This bridge was load tested with two trucks and instrumentation located at the face of the floor beams. A variety of static load tests were performed to use recorded strains to determine elastic neutral axis locations and moments. A 3D FE model was made that used strain measurements from the test in ABAQUS. It was found that the simplified load rating methods used by INDOT were conservative. The measurements from the load test were used to find an experimental load rating that was high enough to remove the load posting.

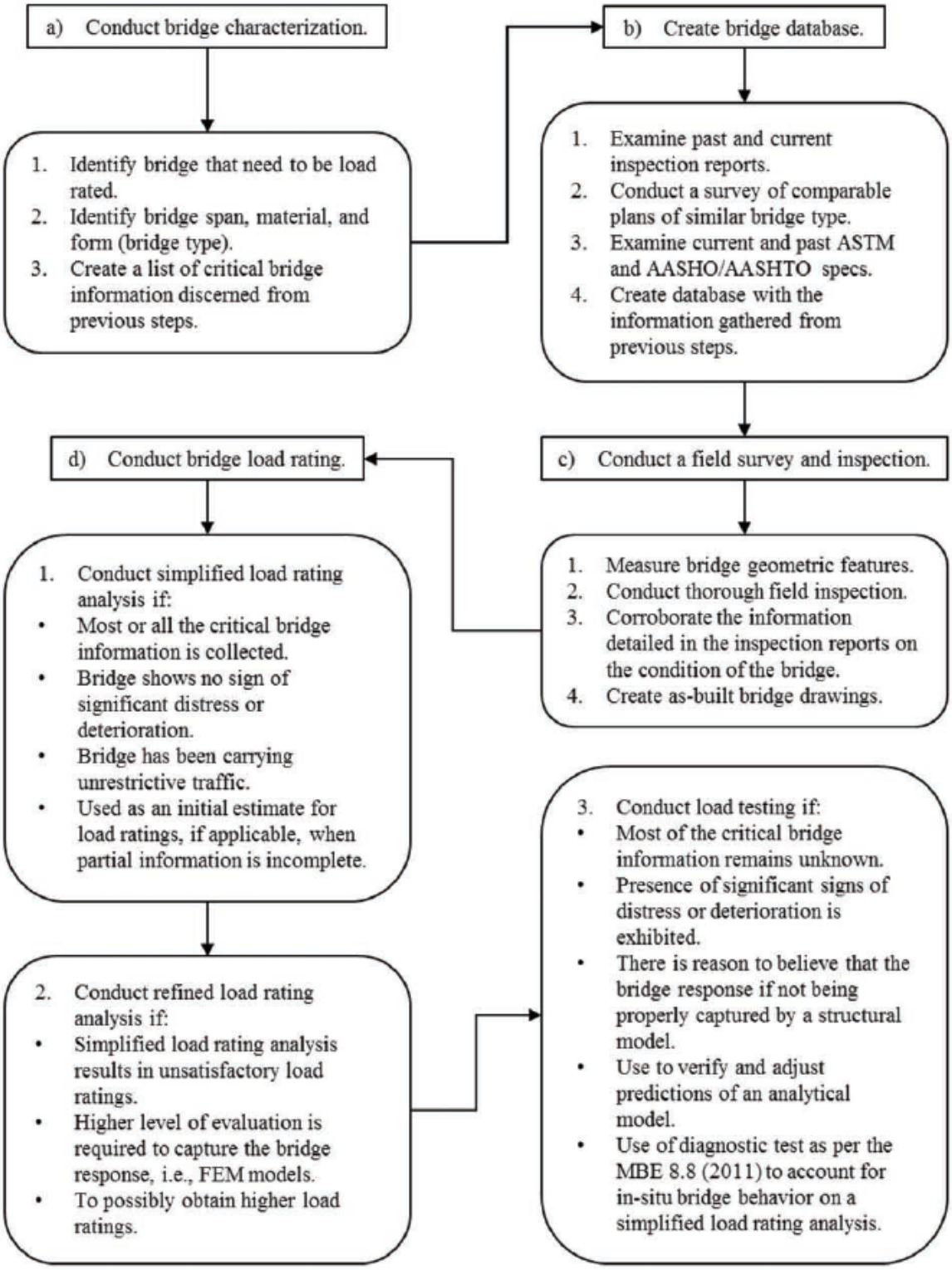

Figure 1. Flowchart of General Rating Procedure

Hearn, G., NCHRP Synthesis 453, 2014, State Bridge Load Posting Processes and Practices

This report gives a summary of the status of bridge load postings, load vehicle types, non-technical load rating processes, load posting signs, and fines associated with overweight vehicle violations. According to the report, ten percent of bridges and culverts in the U.S. are load posted, 77% of load posted bridges and culverts have unknown design live loads or were designed for live loads less than or equal to H15, and 95% of load posted structures are bridges, not culverts. The 10 most numerous structure types and the number of bridges posted is shown in Table 1. Many agencies have vehicles that are exempt from load postings, including vehicles that are related to agriculture, construction, firefighting, forest products, materials, and towing.

Table 1. Ten Most Numerous Structure Types and Load Posting

Item 43 Structure Type, Main		Structures	Posted	% of Group	% of Load Posted
Steel	Stringer/multi-beam or girder	101,454	22,481	22.2	36.8
Concrete	Culvert, includes frame culvert	89,624	2,038	2.3	3.3
Prestressed Concrete	Stringer/multi-beam or girder	54,317	383	0.71	0.63
Steel Continuous	Stringer/multi-beam or girder	47,005	2,710	5.8	4.4
Prestressed Concrete	Box beam or girders—Multiple	40,686	710	1.7	1.2
Concrete	Slab	33,123	3,907	11.8	6.4
Concrete Continuous	Slab	31,940	1,489	4.7	2.4
Concrete Continuous	Culvert, includes frame culvert	27,795	215	0.77	0.35
Concrete	Tee beam	20,295	1,997	9.8	3.3
Wood or Timber	Stringer/multi-beam or girder	18,180	9,373	51.6	15.4

Condition ratings, load rating revaluations, load rating vehicles, load rating signs and installation, and excess weight fines are briefly summarized in the report. The report discusses ASR, LFR, and LRFR load rating methods and how they differ. The report claims that all of the

states surveyed use beam line analysis for load rating, but that 24 of the 43 do refined analysis methods for some load rating computations. Of those 24 agencies, 18 of them perform refined analysis to avoid load postings, 14 of them do it for complex bridges, and six do it for both cases. Of the states surveyed, only 19 states used load tests for rating purposes. Of the states surveyed, 22 states set load postings based on operating rating capacities, 5 set load postings based on inventory rating capacities, and 12 set load postings based on another rating. 4 states used Eqn. 2 from AASHTO, to determine the safe posting load, where W is the gross weight of a rating vehicle and RF is the rating factor for the same vehicle.

$$Safe\ Posting\ Load = \frac{W}{0.7}(RF - 0.3) \qquad \text{Eqn. 2}$$

Legal loads are established by the U.S. Code Title 23; however, states can establish their own legal loads. Code 23 has legal load limits of 20,000 lb. for single axle, 34,000 lb. for tandem axle, and 80,000 lb. for gross vehicle weight. However, legal loads are higher than one or more of the legal loads recommended by Code 23 in 32 states. Nebraska uses the Code 23 single axle and tandem axle limits. However, Nebraska uses 95,000 lb. as the gross vehicle weight maximum legal load instead of 80,000 lb.

According to the report, states can issue overweight permits for vehicles that exceed the legal limit. Typically, overweight permits are issued for non-divisible weights and longer combination vehicles. Overweight permits can be issued for single trips or multiple trips.

The following gaps in knowledge and needs for further research were identified by the author: effectiveness of decisions in load posting, effectiveness of quality control of load rating in load posting, effectiveness of implementation of load postings, effectiveness of load rating in

load posting, hazard at un-rated structures, effectiveness of weight limit signs in restricting use of structures, effectiveness of communication of weight restrictions, effectiveness of maintenance of weight limit signs, effectiveness of enforcement, practices of local governments in load posting, and transience of load posting.

2.3 Studies of Neural Networks in Engineering

Sofi, F., 2017, Structural System-Based Evaluation of Steel Girder Highway Bridges and Artificial Neutral Network (ANN) Implementation for Bridge Asset Management

Due to the conservative nature of AASHTO line girder rating methods, Sofi developed a methodology that provides a load rating prediction based on finite element modeling via ANN training. The bridge data in this study is made up of 61 bridges in Nebraska and 193 hypothetically-generated bridges. The scope of the data is limited to single span, multi-girder composite bridges with a concrete deck. The hypothetically generated bridges were randomly made with the most economical rolled W-shapes being used that satisfies AASHTO design requirements.

FEM was performed on ANSYS to obtain girder response to determine a more realistic live load effect that would be used to calculate a refined load rating. An Excel Visual Basic Application (VBA) was used in conjunction with the ANSYS capabilities to perform the analyses. This process modeling technique creates solid elements for the concrete slab. The girders were modeled as shell elements and the cross frames at supports were modeled with Timoshenko beam elements. The bridges in this study were modeled to act compositely by using multipoint constraint (MPC) rigid beam elements. The modeling process used in this study matched with the results of a full-scale ultimate load test on a simply supported model bridge at

the University of Nebraska-Lincoln (Kathol et al.1995) and The Elk River Bridge ultimate load test performed in Tennessee (Burdette and Goodpasture 1971).

The bridge tested at the University of Nebraska-Lincoln, referred to as the Nebraska Bridge, was a steel girder composite bridge with a reinforced concrete deck that was designed in accordance with AASHTO LFD (AASHTO 1992). The test was performed to investigate the load-carrying capacity of the superstructure. Truck loads were applied with post-tensioning rods in 12 locations to simulate two HS-20 design trucks. The longitudinal spacing of the loads was 12 ft. and 15 ft., instead of 14 ft. axle spacing, to match the laboratory's strong floor hole locations. The bridge's geometry and loading configuration is shown in Figure 2.

Loads were applied in increments of HS-20 trucks (8 kip front axle and 32 kips on middle and back axle). The bridge experienced its first yield after an equivalent weight of 9 HS-20 trucks (648 kips). The exterior girders yielded after an equivalent weight of 12 HS-20 trucks (864 kips). The test came to an end due to local punching shear failure in the concrete after the equivalent weight of 16 HS-20 (1,152 kips) was applied. Girder deflection comparisons between the lab test documentation and the developed models are shown in Figure 3. The maximum interior girder deflection error was 8%, but the mean absolute percent difference was 4%. Sofi claims, "The discrepancy between the load-deflection curve results for the interior girder was attributed to residual stresses in the steel-plate girders and precomposite dead load-induced stresses unaccounted for in the analytical model, which would cause an earlier onset of inelasticity in the girders than predicted by the FE model."

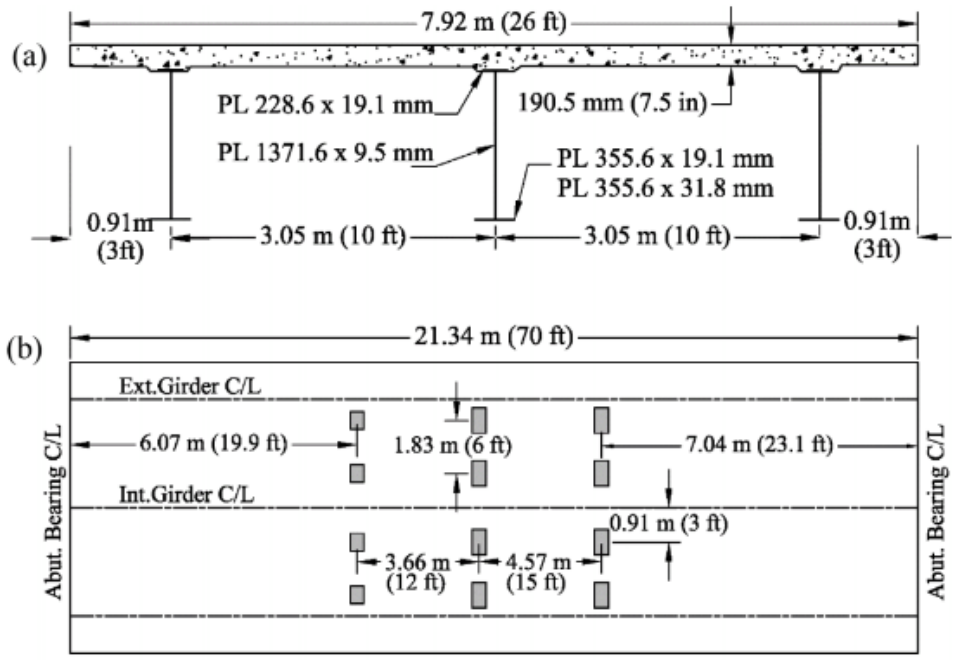

Figure 2. Nebraska Bridge Ultimate Load Test: (a) Cross section; (b) Loading Configuration

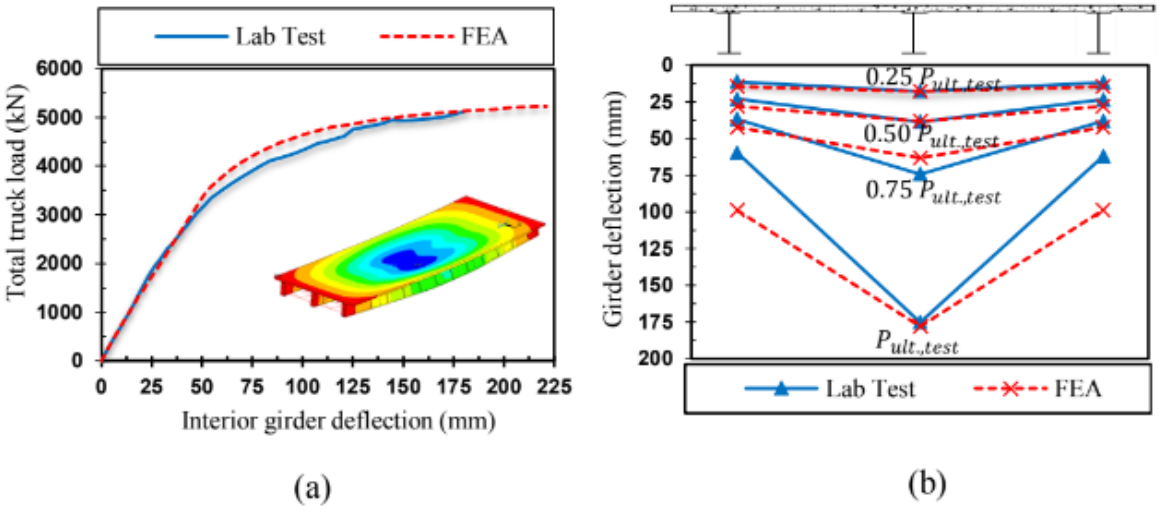

Figure 3. Nebraska Bridge FE Model Comparison with Load Test Results: (a) Interior Girder Deflection; (b) Girder-Deflection Profile at Midspan

Discrepancies between the exterior girder deflections were attributed to a higher stiffness in the experimental exterior girders due to the parapets not being modeled in ANSYS. The

difference in deflections became more pronounced at higher loads because more of the loads were distributed to the exterior girders as the interior girders reached their plastic limit.

Once the FEM methodology was validated, the live load distribution of the 243 bridges was used to update load rating predictions and train the ANNs. 10 governing bridge parameters were determined for ANN training. The governing parameters and their effective ranges are shown in Table 2. The ANNs in this study were trained to map the 10 governing inputs to the inventory rating factor of an HS-20 truck. Single ANNs were optimized by creating ANNs with single or two hidden layers, 2-10 nodes per hidden layer, and either Bayesian-Regularization or Levenberg Marquardt training algorithms. The ANNs were made with 250 retraining iterations to ensure a low mean square error. 15% of the design set was randomly selected for testing. In addition to the 15%, a reduced design set size was used to ensure additional bridges could test the efficacy of the ANN prediction. The ANNs with the best performance were found to have an average absolute error between 6 and 7%.

A shortcoming of a single network is that the error associated for one bridge may be high even though the average error is low. To mitigate this error, Sofi produced committee networks that are made up of subcommittee networks. Subcommittee networks are multiple ANNs of the same architecture. Combined with other subcommittees, the committee network should produce a more robust prediction than a single network. The committee networks produced slightly better predictions on average than the single-best-network. The committee networks and single-best-network had a coefficient-of-correlation with the FEM data of 0.967 and 0.955, respectively.

Table 2. Governing Parameters and their Effective Ranges

Parameter number	Bridge parameter	Effective range
1	Span length (L)	20-89 ft (6.10-27.13 m)
2	Girder spacing (s)	32-99 in (813-2,515 mm)
3	Longitudinal stiffness (Kg)	6,200-325,800 in^4 (2.58×10^9-135.61×10^9 mm^4)
4	Cross frames	Present or absent
5	Number of girders (n_b)	4-11
6	Skew angle (α)	0-45°
7	Barrier distance (d_e)	(-) 8-34 in (-203-864 mm)
8	Deck thickness (t_s)	5-9 in (127-228.6 mm)
9	Conc. compressive strength (f_c')	2.5-4 ksi (17.24-27.58 MPa)
10	Steel yield stress (f_y)	30–50 ksi (206.85–344.75 MPa)

The FEM load ratings produced rating factors that were on average 27% higher than AASHTO. Due to the close agreement between the ANN predictions and the FEM load ratings, Sofi proposes a user application procedure that could be implemented at state agencies.

The first step of the proposed procedure is to create a reliable ANN. Next, the weights and biases should be copied into a spreadsheet where the ANN prediction calculations and nonlinear transfer functions can be programmed. These calculations should be intended to be in hidden sheets so that the user does not have to interact with them. The spreadsheet should prompt the user for the ten governing parameters, normalize the inputs, perform calculations and transfer functions, reverse the normalization, and produce a load rating prediction. Finally, the user should check the applicability of the prediction by ensuring that the governing parameter are

within the design set scatterplot boundaries, otherwise, the ANN would be extrapolating beyond its initial training scope.

2.4 Studies of Structural Reliability

Nowak, A.J., 1999, NCHRP Report 368, Calibration of LRFD Bridge Design Code

The motivation for this research was to produce a bridge design code that is based on probabilistic design. LRFD was created to provide a consistent a "uniform safety level" for bridges – an attribute of LRFD that is not shared with the Allowable Stress Method or Load Factor Design. The probability of failure is described by the reliability index, β, which is shown in Eqn. 3. The reliability index is the inverse standard normal distribution function of the probability of failure. The formula for the reliability index is a function of the nominal resistance (R_n), the resistance bias factor (λ_R), the resistance coefficient of variation (V_R), the mean load (μ_Q), the standard deviation of load (σ_Q), and the parameter k which depends on the location of the design point. Typically, k is taken as 2.

$$\beta = \frac{R_n \lambda_R (1 - kV_R)[1 - \ln(1 - kV_R)] - \mu_Q}{\sqrt{[R_n V_R \lambda_R (1 - kV_R)]^2 + {\sigma_Q}^2}} \qquad \text{Eqn. 3}$$

A visual representation of the probability failure is shown in Figure 4. The probability of failure and its corresponding reliability index is shown in Table 3.

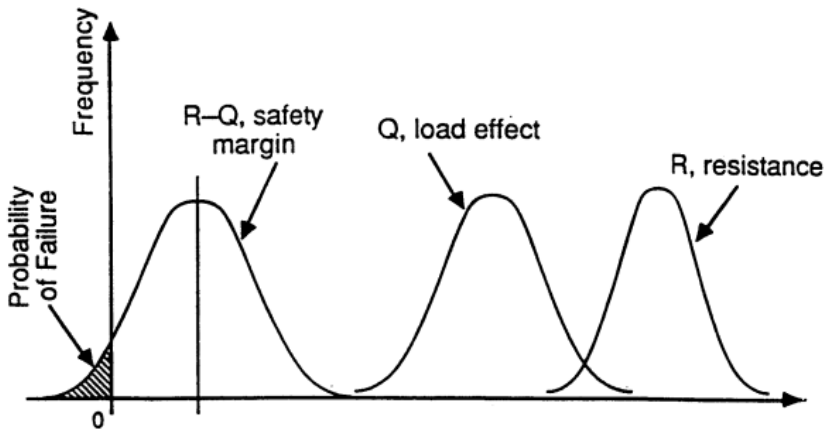

Figure 4. Probability Distribution Functions (PDF) of Load, Resistance, and Safety Reserve

Table 3. Probability of Failure and β.

reliability index β	reliability $S\ (=1-P_f)$	probability of failure P_f
0.0	0.500	$0.500\times10^{+0}$
0.5	0.691	$0.309\times10^{+0}$
1.0	0.841	$0.159\times10^{+0}$
1.5	0.933 2	0.668×10^{-1}
2.0	0.977 2	0.228×10^{-1}
2.5	0.993 79	0.621×10^{-2}
3.0	0.998 65	0.135×10^{-2}
3.5	0.999 767	0.233×10^{-3}
4.0	0.999 968 3	0.317×10^{-4}
4.5	0.999 996 60	0.340×10^{-5}
5.0	0.999 999 713	0.287×10^{-6}
5.5	0.999 999 981 0	0.190×10^{-7}
6.0	0.999 999 999 013	0.987×10^{-9}
6.5	0.999 999 999 959 8	0.402×10^{-10}
7.0	0.999 999 999 998 72	0.128×10^{-11}
7.5	0.999 999 999 999 968 1	0.319×10^{-13}
8.0	0.999 999 999 999 999 389	0.611×10^{-15}

The inconsistent reliability indices are illustrated in Figure 5, Figure 6, Figure 7, and Figure 8. It can be seen that by using the contemporary code, reliability is not consistent for varying span lengths nor girder spacings.

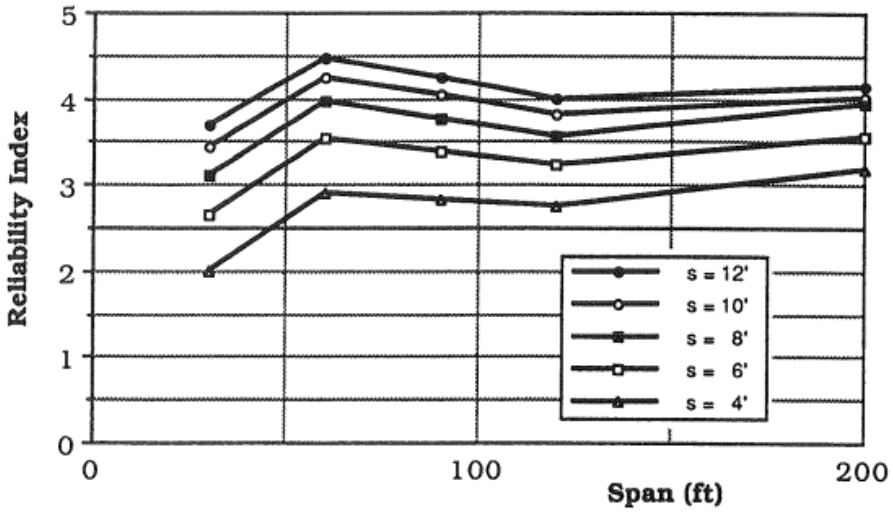

Figure 5. Reliability Indices for Contemporary AASHTO; Simple Span Moment in Noncomposite Steel Girders

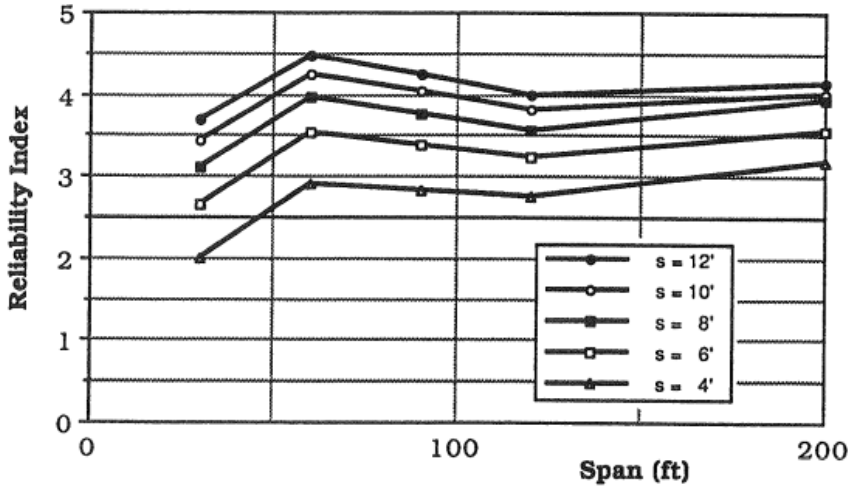

Figure 6. Reliability Indices for Contemporary AASHTO; Simple Span Moment in Composite Steel Girders

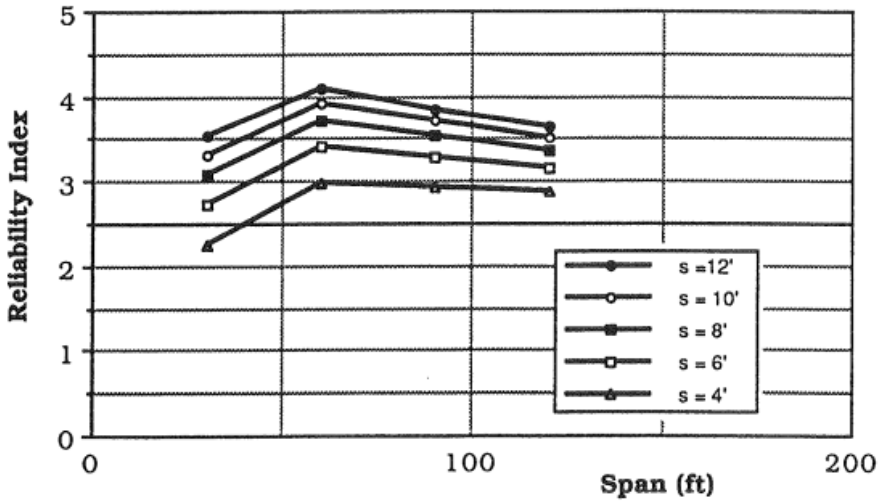

Figure 7. Reliability Indices for Contemporary AASHTO; Simple Span Moment in Reinforced Concrete T-Beams

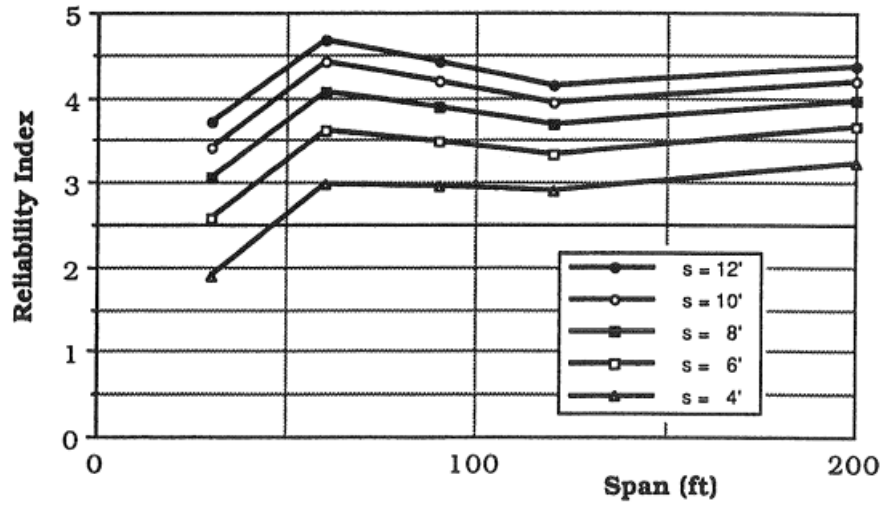

Figure 8. Reliability Indices for Contemporary AASHTO; Simple Span Moment in Prestressed Concrete Girders

The calibration procedure for LRFD is broken down into six steps described below.

1. **Bridge Selection**

   Roughly 200 bridges were selected from various places in the United States. An emphasis was placed on contemporary and future trends instead of focusing on old bridges. Load effects and capacities were evaluated.

2. **Establishing the Statistical Data Base for Load and Resistance Parameters**

   Load data was gathered from surveys, measurements, and weigh-in-motion (WIM) data. Since there is little field data for dynamic loads, a numerical procedure was created to simulate data. As for the resistance parameters, material and component tests were performed.

3. **Development of Load and Resistance Models**

   Cumulative Distribution Functions (CDF) were found for loads by using the available statistical data base. Live load models were created with single and multiple adjacent trucks on the bridge that account for multilane reduction factors for wide bridges.

4. **Development of the Reliability Analysis Procedure**

   Limit states were used to assess the probability of failure and realibility index, β_T, based off of the Rackwitz and Fiessler procedure.

5. **Selection of the Target Reliability Index**

   A target reliability index, which corresponds to a target probability of failure, is selected.

6. **Calculation of Load and Resistance Factors**

   Based off of the target reliability selected in the previous step, load factors, γ, and resistance factors, ϕ, are calculated. Based off of this procedure, a target reliability set

at 3.5, and k being equal to 2, load and reliability factors were found. The dead load factor was found to be 1.25 while the asphalt dead load factor was 1.5. The live load factor was found to be approximately 1.6, but a more conservative value of 1.7 was proposed for the LRFD code.

Suggested research topics include creating a large and reliable WIM data base, creating a data base for bridge dynamic loads, further development of serviceability criteria, performing calibration on timber structures, performing calibration on substructures, creating more bridge component test data, creating load models for wind, earthquake, temperature and other load combinations, and investigating how to incorporate bridge component deterioration into the code.

Moses, F., 2001, NCHRP Report 454, Calibration of Load Factors for LRFR Bridge Evaluation

The purpose of this report was to provide the rationale behind the live load factors incorporated to the then proposed AASHTO Manual for Condition Evaluation and Load and Resistance Factor Rating of Highway Bridges. More specifically, the report presents recommendations for legal load rating analysis and permit loadings and postings.

The goal of this project was to select load and resistance factors that correspond to a uniform reliability index. The calibration process was similar to the NCHRP Report 368 (Nowak 1999). First, limit states were checked. The standard limit state function, g, is a function of random variables. The random variables that the limit state function depends on are resistance, R, dead load effect, D, and live load effect, L. The limit state function is shown below in Eqn. 4.

$$g(R, D, L) = R - D - L = 0 \qquad \text{Eqn. 4}$$

Next, the random variables in the limit state function are defined. After that, load and resistance data is gathered for the calibration process. At a minimum, each variable should have a coefficient of variation (COV), which describes the "scatter of the variable", and a bias factor, which is the ratio of mean value to the nominal design value. Finally, a target reliability index is selected and the load and resistance factors can be determined.

The report notes that the NCHRP Report 368 (Nowak 1999) does not specify whether or not site-to-site uncertainties are considered for load intensities. That report used the average beta value from a database using designs that correspond to an extreme loading situation for a very heavy truck volume and weight distribution. However, bridges with lower traffic volumes are expected to have higher reliability indices. Another interpretation is that they did include site-to-site variability. If site-to-site variations are included in the calibration effort and the bias of the extreme loading intensity with respect to average site loading intensity were included, then the target beta of 3.5 would be the average beta of all the bridges. Some bridges would have higher and lower betas than this.

This report claims that they adopted site-to-site variabilities by modeling the live load COV. Furthermore, they used site-specific information such as traffic volume (ADTT) and weight intensities when the data was available.

The data from NCHRP Report 368 was used in this study to find equivalent weight parameters. However, due to the data being recorded for two weeks, heavy trucks avoiding static weight stations, and truck weights changing over time, the researchers decided to consider site-to-site variability and load growth as random variables in this project.

In this research, an operating target beta of 2.5 was used instead of 3.5 for inventory. The reason this is the case is because the 2.5 target beta reflects component failure, not system failure.

Based off of the statistical parameters shown in Table 4, partial safety factors were determined from ranging live-to-dead-load ratios from 0.5 to 2. They found that the required live load factor ranged between 1.65 and 1.77 for a reliability index that corresponds to inventory level rating. For operating level rating, the live load factor ranged between 1.28 and 1.35 for the same live-to-dead-load ratio range. A conservative operating live load factor of 1.35 was recommended by the researchers.

Table 4. Statistics for Safety Index Computations

Case	Bias	COV	Distribution
Dead Load	1.04	8%	Normal
Live Load	1.00	18%	Lognormal
Resistance	1.12	10%	Normal

2.5 Studies of Load Testing

Peiris, A., Harik, I., 2019, Bridge Load Testing Versus Bridge Load Rating

Sensormate's QE-1010 magnetic strain gauge and BDI ST350 strain gauges were evaluated and compared to traditional foil-type strain gauges. The two data acquisition systems were used to instrument members that were also instrumented by foil-type gauges in tensile and flexural laboratory tests. It was found that both systems performed adequately except for the magnetic strain gauge system because they slipped at strains higher than 400 microstrain. The magnetic strain gauge system was used to test a steel girder bridge referred to as the Lewis County Bridge and data was compared to that of foil gauges. The two systems had similar strain profiles, shown in Figure 9, that were interpreted as the bridge performing noncompositely. However, load rating benefits were found since the abutments behave more like fixed supports than simple supports.

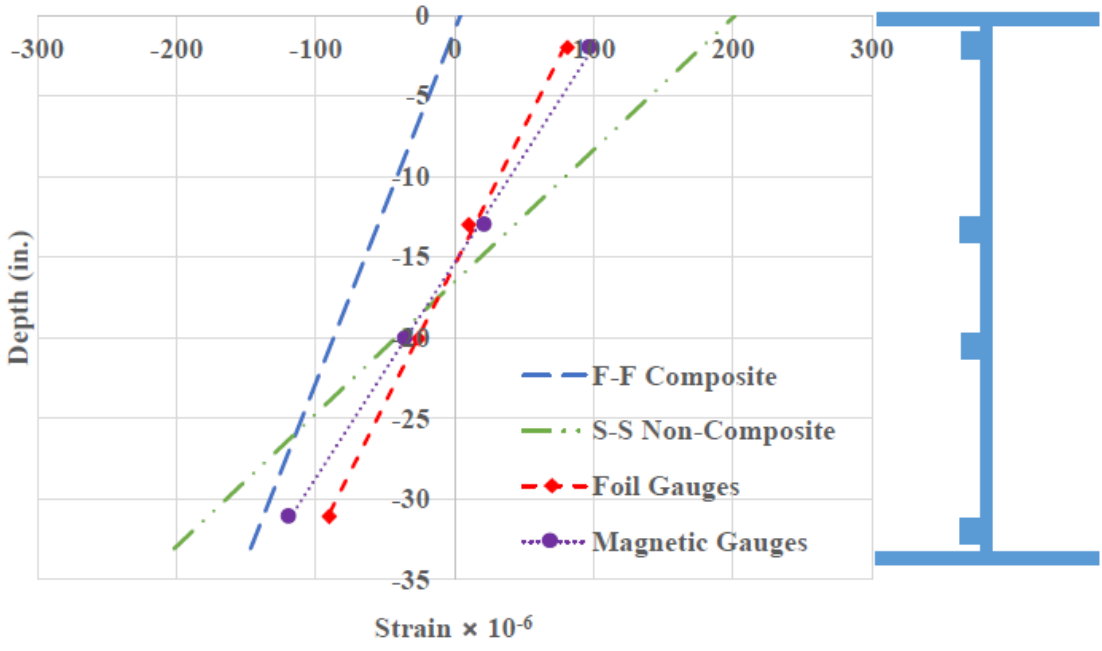

Figure 9. Lewis County Bridge Load Test Strain Data

The Hardin County Bridge was tested using both foil gauges and BDI strain transducers. This test revealed that this bridge benefits largely due to partial composite behavior, illustrated in Figure 10. Although the bridge was performing partially composite, the researchers assumed that the bridge's behavior could be scaled up by 33% since the steel had not yielded yet. It is a well known that the degree partial composite behavior can decrease as elastic yielding is approached.

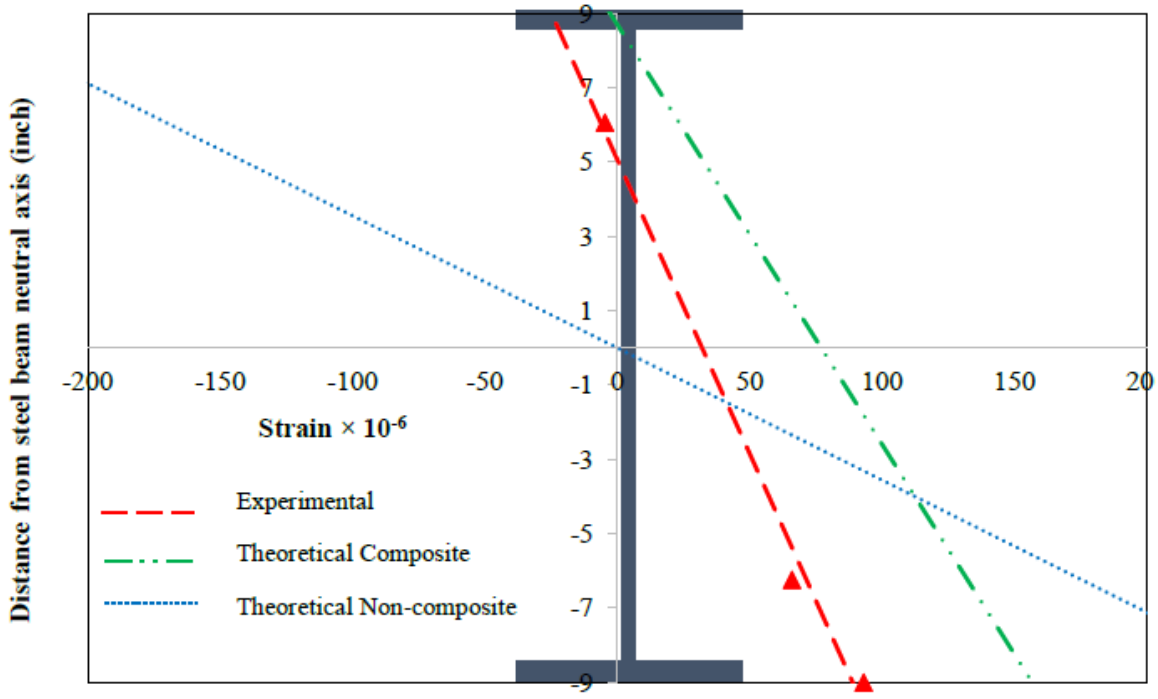

Figure 10. Hardin County Bridge Load Test Strain Data

Both bridges showed significant load carrying capacity benefits in the load test. However, only the Hardin bridge had a load test rating factor that is above 1. The load rating findings are summarized below in Table 5.

Table 5. Load Rating Results

Bridge	Governing Truck Type	AASHTO Analytical Rating Factor	Load Test Rating Factor
KY 1068 – Lewis County	KY Type 3	0.48	0.70
KY 220 – Hardin County	KY Type 3	0.62	1.25

Hosteng, T., and Phares, B., 2013, Demonstration of Load Rating Capabilities Through Physical Load Testing: Sioux County Bridge Case Study

Researchers performed load tests on a two-lane, three-span, continuous steel girder bridge built in 1939. Strain transducers were placed at the top and bottom flanges in locations specified in Figure 11. All of the load tests were performed at crawl speed. The truck locations are shown Figure 12. Two runs were performed to verify the data. Distribution factors were estimated by taking the ratio of girder strains to the girder strains experienced by all of the girders. The researchers found distribution factors significantly lower than what AASHTO prescribes.

By using the strain data, the researchers developed a two-dimensional FEM to perform LFR load rating analyses on AASHTO rating vehicles. The FEM software that the researchers used is BDI WinGEN and WinSAC was used to do structural analysis and data correlation. WinSAC was used to perform analysis at incremental locations of the truck load. The calibration procedure was done by modifying material properties and stiffnesses until an adequate level of agreement was reached. The calibrated model had a coefficient of correlation of 0.9762. An example of strain comparisons between the analytical model and the field strains is shown in Figure 13.

The operating load ratings for all of the analyses were found to be greater than one despite the bridge being load posted. A summary of the bridge critical rating factors is shown in Table 6.

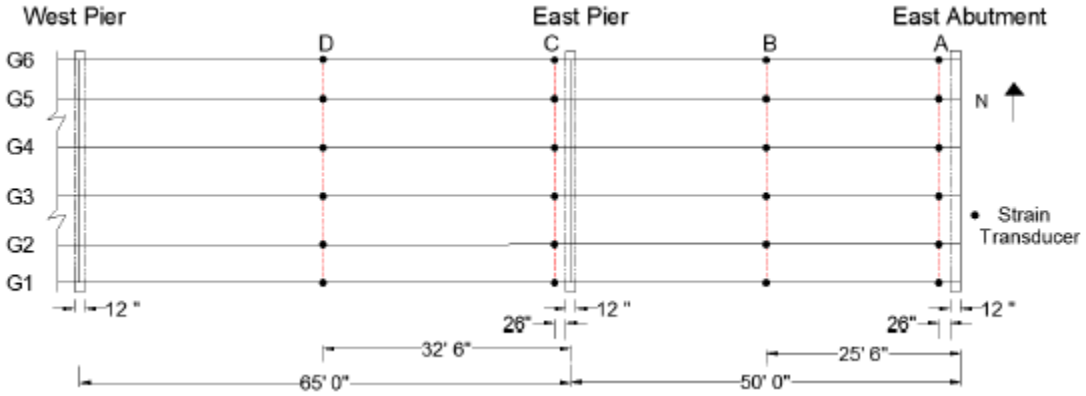

Figure 11. Sioux County Bridge Plan View of Strain Transducer Locations

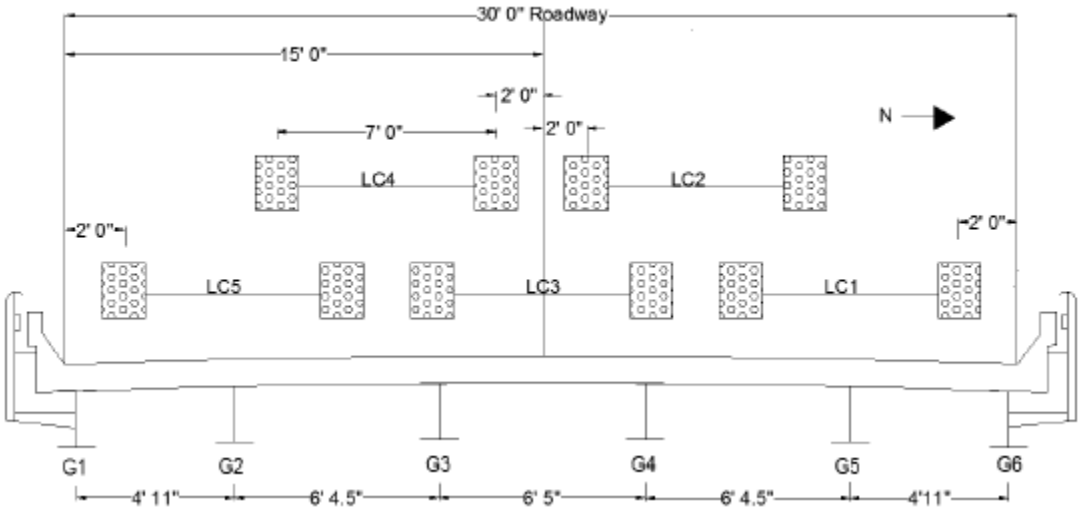

Figure 12. Sioux County Bridge Transverse Load Position

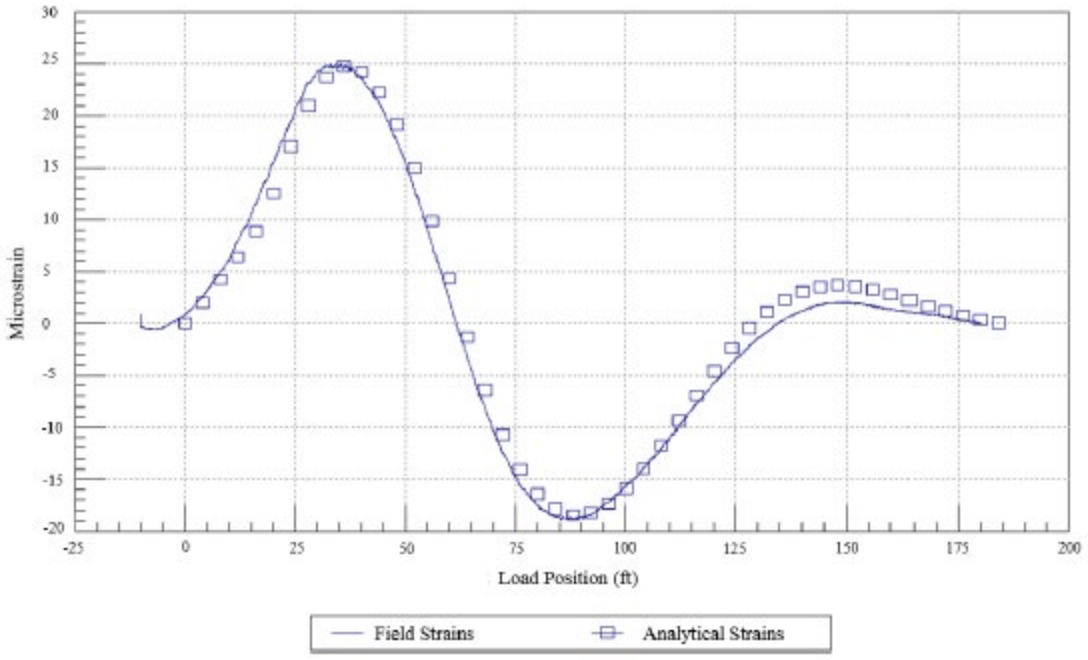

Figure 13. Sioux County Bridge Strain Comparison of G6 on LC3

Table 6. Sioux County Bridge Critical Rating Factors

Rating Vehicle	Location/Limiting Capacity	Inventory Rating Factor		Operating Rating Factor	
		Two Lane	One Lane	Two Lane	One Lane
HS-20(14)	Exterior, Center Span, (+) Flexure	0.61	0.80	1.02	1.33
HS-20(22)	Exterior, Center Span, (+) Flexure	0.72	0.95	1.21	1.59
HS-20(30)	Exterior, Center Span, (+) Flexure	0.86	1.12	1.43	1.88
Type 4	Exterior, Center Span, (+) Flexure	0.73	0.94	1.22	1.57
Type 3S3A	Exterior, Center Span, (+) Flexure	0.75	1.00	1.26	1.66
Type 3-3	Exterior, Center Span, (+) Flexure	0.72	0.96	1.20	1.60
Type 3S3B	Exterior, Center Span, (+) Flexure	0.93	1.16	1.55	1.93
Type 4S3	Exterior, Center Span, (+) Flexure	0.80	1.01	1.34	1.68
Type 3	Exterior, Center Span, (+) Flexure	0.81	1.04	1.35	1.74
Type 3S2B	Exterior, Center Span, (+) Flexure	0.86	1.09	1.43	1.82
Type 3S2A	Exterior, Center Span, (+) Flexure	0.79	1.05	1.32	1.75
Midspan and Endspan Lane Load	Exterior, Center Span, (+) Flexure	0.92	1.19	1.53	1.99
Both Endspans Lane Load	Exterior, Pier, (-) Flexure	1.95	2.61	3.25	4.36
Midspan Lane Load	Exterior, Center Span, (+) Flexure	1.33	1.77	2.23	2.95
Single Endspan Lane Load	Exterior, Pier, (-) Flexure	1.89	2.52	3.15	4.21

3 Objective and Scope

3.1 Research Objective

The objective of this research project was to augment and extend existing ANNs that predict the load rating of steel-girder bridges. The ANN modifications include:

- ✓ replacing hypothetical bridge ANN training data with additional existing Nebraska bridge training data,
- ✓ reconfiguring existing ANNs to predict AASHTO truck live load effects rather than load ratings, and
- ✓ accounting for ANN uncertainty in the load rating predictions.

This research was performed with the goal of providing a tool that could be used as a supplement to existing tools available to load rating engineers at the Nebraska Department of Transportation (NDOT).

3.2 Research Scope

This research aimed to address bridges in fair or better condition, for which no penalties would be required to represent deterioration. Since ANNs were trained using the results of FEMs, the scope of the project is limited by the ranges of attributes represented by the bridges selected for FEM analyses. The bridges selected for training were simple span, steel girder bridges in Nebraska. All bridges were assumed to be composite with concrete decks at the outset of the study, although discussions with state and county bridge engineers during the study revealed that this assumption is not entirely valid. Additional discussion related to composite effectiveness is included with Chapter 8 – Field Testing Case Study.

Ten bridge parameters were used to predict live load distribution factors using ANNs, similarly to Sofi (2017). Sofi selected these parameters because they were believed to be

influential to live load distribution behavior and load rating. In order for ANN predictions to be reliable, inputs should be similar to those used in training to avoid extrapolation. ANNs were trained using only data that excluded outliers (refer to the chapter discussing Finite Element Modeling), with some bridges identified as outliers for moment but not shear, or vice versa. Accordingly, ANNs used to estimate moment and shear rating factors have slightly different ranges of application reflecting the characteristics of bridges comprising the respective training bridge populations. Moment GDF ANN and shear GDF ANN ranges of applicability are shown below in Table 7. It should be noted that these are ranges for each individual attribute, but that users should always verify that their inputs are within the scatter of training data shown in Chapter 6.

Table 7. ANN Governing Parameters' Effective Ranges

Bridge Parameters	**Effective Range for Moment GDF ANNs**	**Effective Range for Shear GDF ANNs**
Span Length (L)	20-81.6 ft	
Girder Spacing (s)	32-99 in	32-92.5 in
Longitudinal Stiffness (K_g)	11,900-346,225 in^4	7,540.6-415,400.16 in^4
Cross Frames	Present or Absent	
Number of Girders (n_b)	4-11	
Skew Angle (α)	0-45°	
Barrier Distance (d_e)	(-) 4.5-31.25 in	(-) 4.5-32 in
Deck Thickness (t_s)	5-9 in	5-8 in
Concrete Compressive Strength (f_c')	2.5-4 ksi	
Steel Yield Stress (f_y)	30-50 ksi	

Lastly, reliability calibration was performed to augment the AASHTO LRFR paradigm to account for additional live load uncertainty introduced by ANNs. This study was limited to consider only the AASHTO LRFR Strength I limit state. The general methodology could be implemented with other similar reliability frameworks or limit states. Neither AASHTO LFR nor AASHTO LRFR Serviceability limit states were calibrated for a target reliability. The developed FEA-based GDFs represent linear elastic structural behavior and are theoretically representative of Serviceability conditions, but it is not possible to rationally state a recommendation for reliability-calibrated Serviceability GDFs, because Serviceability limit states fundamentally are not reliability-targeted. Extrapolation to LFR was considered, but only on an approximate basis.

4 Bridge Population

4.1 Background and Previous Work

Sofi's goal (2017) was to create ANNs that could accurately predict the inventory load rating of a bridge based on 10 governing parameters that are representative of bridge behavior. In order to create ANNs, the 10 governing parameters need target values. For Sofi, every bridge's 10 governing parameters use the inventory rating factor based on FEM load distribution as targets. Before ANN training, bridges needed to be identified and modeled to provide a refined rating factor. The previous work by Sofi, excluding outliers that were not used in ANN training, included 61 real bridges supplemented with 193 hypothetical bridges efficiently designed according to current AASHTO LRFD criteria. Sofi's pilot study created and used hypothetical bridges because retrieving bridge data from DOT records is time-consuming, and Sofi's work focused on FEA and ANN development. Reasonable designs could by generated from hypothetical combinations of governing parameters, allowing Sofi to devote the requisite time for foundational FEA and ANN development and calibration. NDOT bridge documentation often provides only measurement plans. This documentation can be illegible, unclearly organized, or can exclude critical information. Figures 14 through 17 show example measurements available from NDOT for Bridge C007805310P.

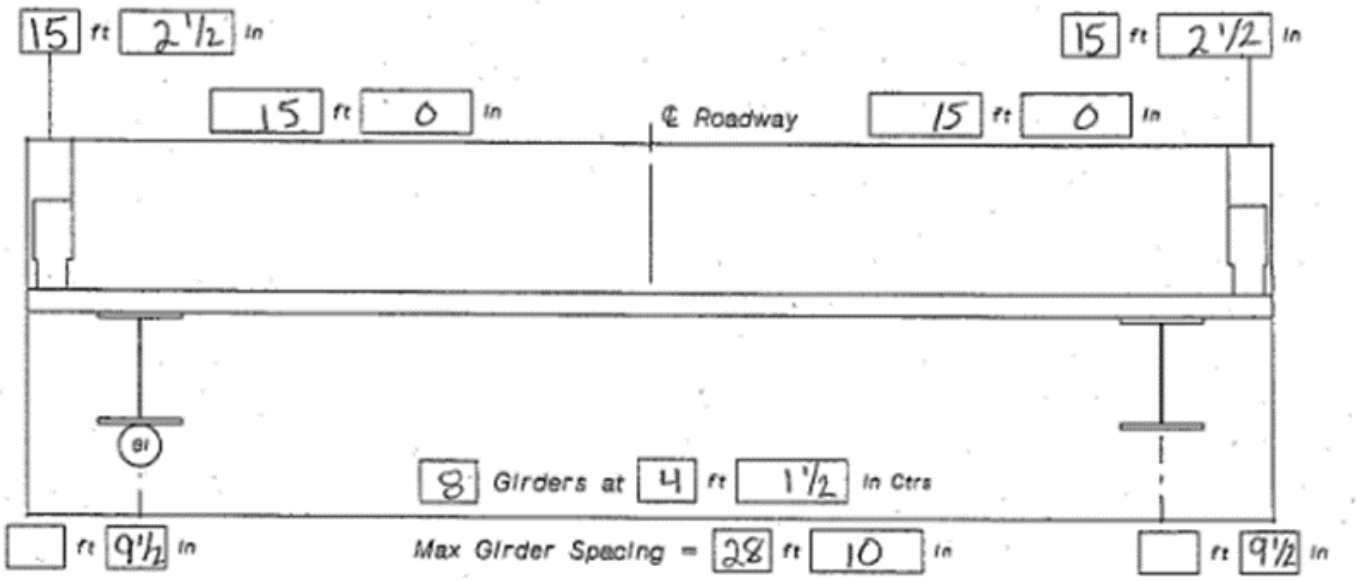

Figure 14. Bridge C007805310P Transverse Measurements

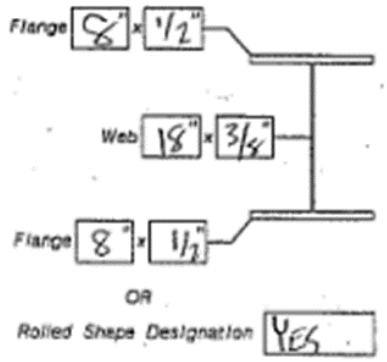

Figure 15. Bridge C007805310P Girder Measurements

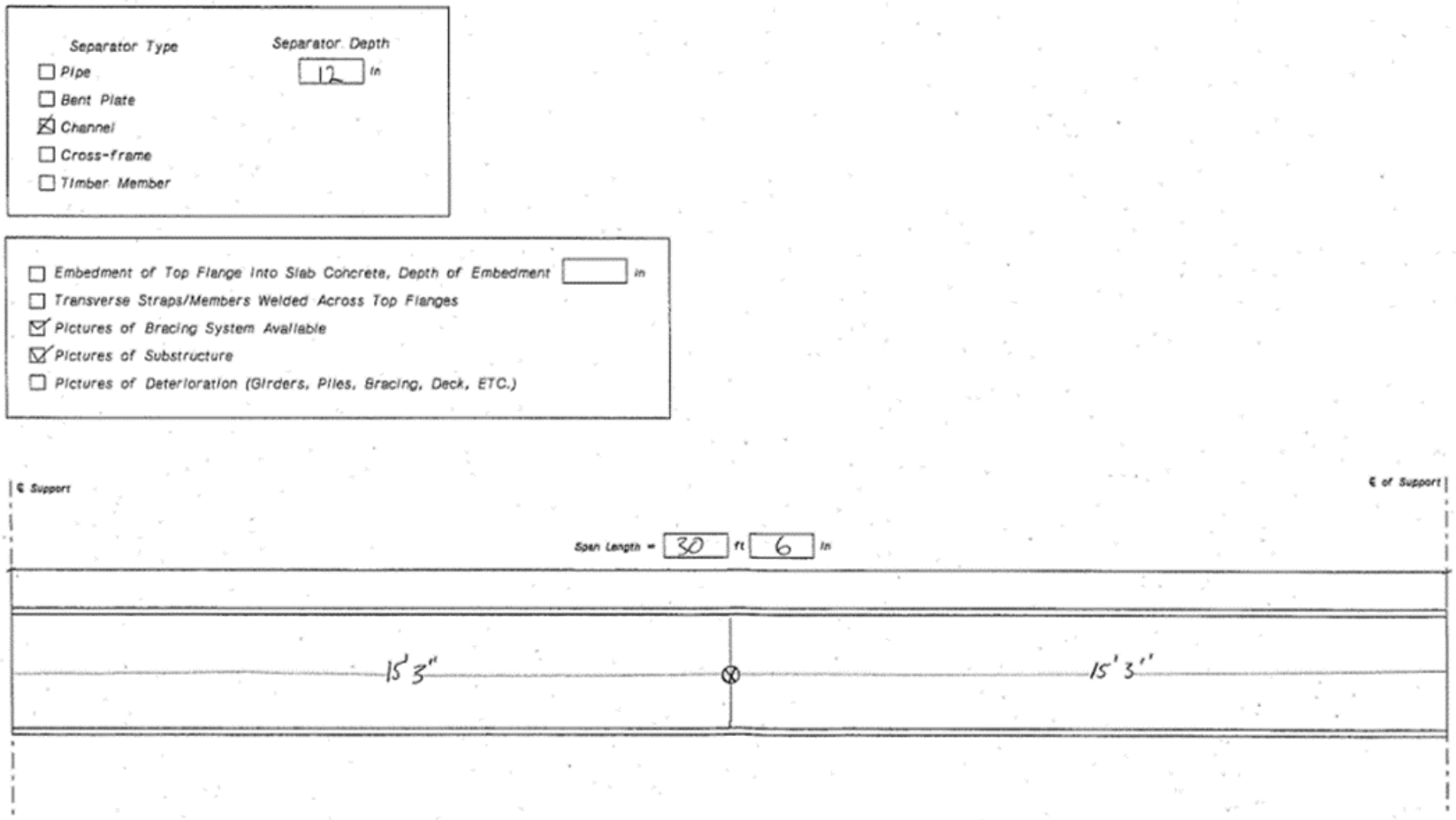

Figure 16. Bridge C007805310P Longitudinal Measurements

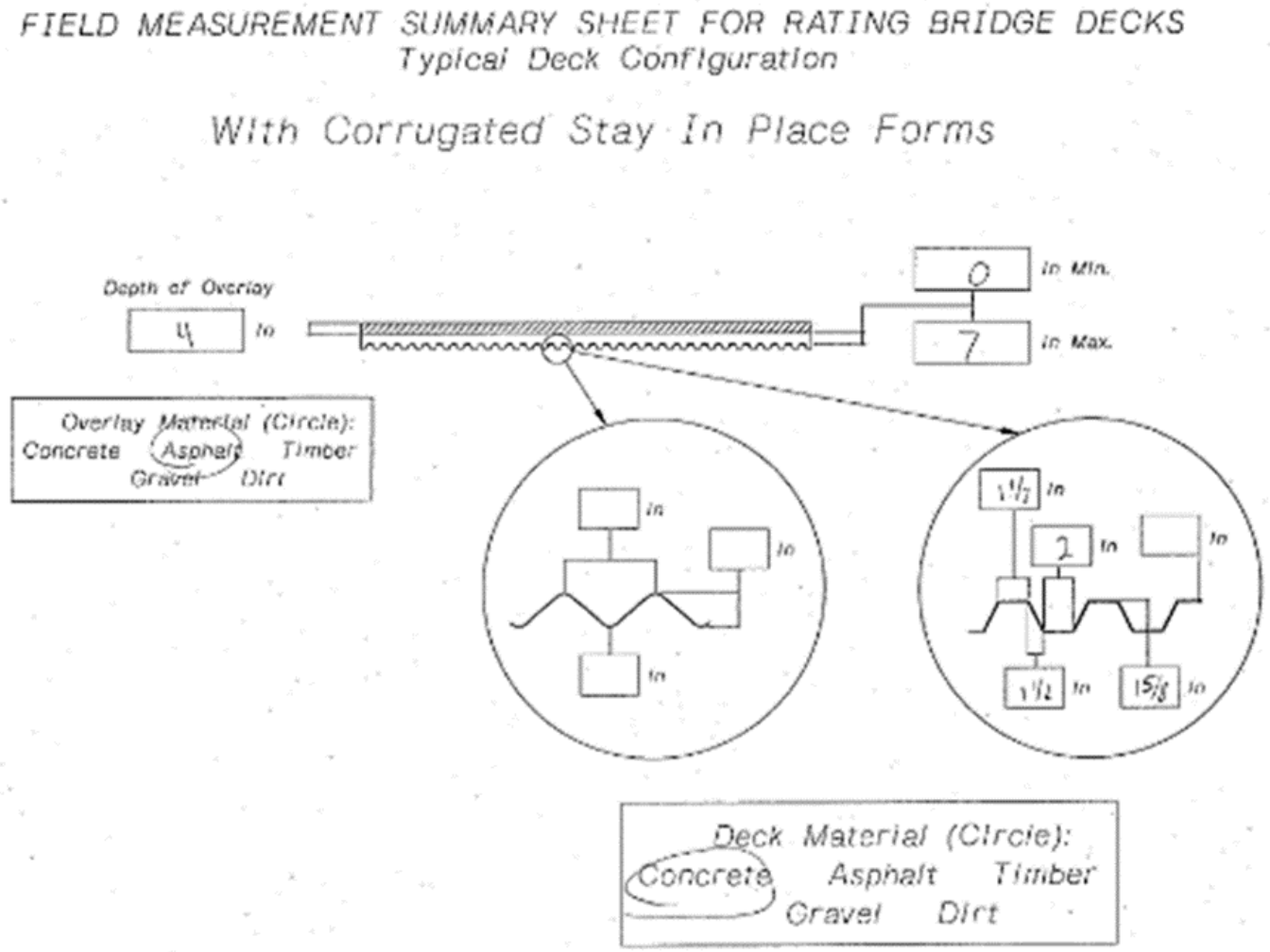

Figure 17. Bridge C007805310P Deck Measurements

4.2 Bridge Population Modifications

The present study included the collection of additional real bridges, allowing hypothetical bridges to be excluded this study to avoid potential bias. 74 Nebraska bridge parameters were made available from Sofi's preliminary pilot study (2017). NDOT aided in retrieving bridge measurement plans and design drawings for 100 additional bridges. The bridges provided from NDOT all have load restrictions, are not fracture critical, and have decks, superstructures, and substructures that have a condition rating of 5 (Fair) or better. Most governing parameter and FEA modeling data were obtained from drawings showing field measurements taken after the bridges' construction. Because of this, details such as presence of composite shear studs or material properties were often undocumented. In such cases, AASHTO 2nd Edition MBE (AASHTO 2013) Tables 6A.5.2.1-1 and 6A.6.2.1-1 were used to select assumed minimum compressive strengths and steel yield strengths, respectively, based on year of construction.

4.3 Bridge Parametric Data

The bridge acquisition task revealed characteristics about single-span bridges in Nebraska. 80% of the bridges were straight and 78% had an assumed concrete compressive strength of 3 ksi. 78% of the bridges had between five and seven girders, with 76% of girder spacings between 3 ft and 6 ft, and 90% of the bridges span less than 60 ft. Histograms that illustrate the study population's governing parameters are shown in Figures 18 to 27. Appendix 11.1.3.1 includes all of the individual bridge characteristics.

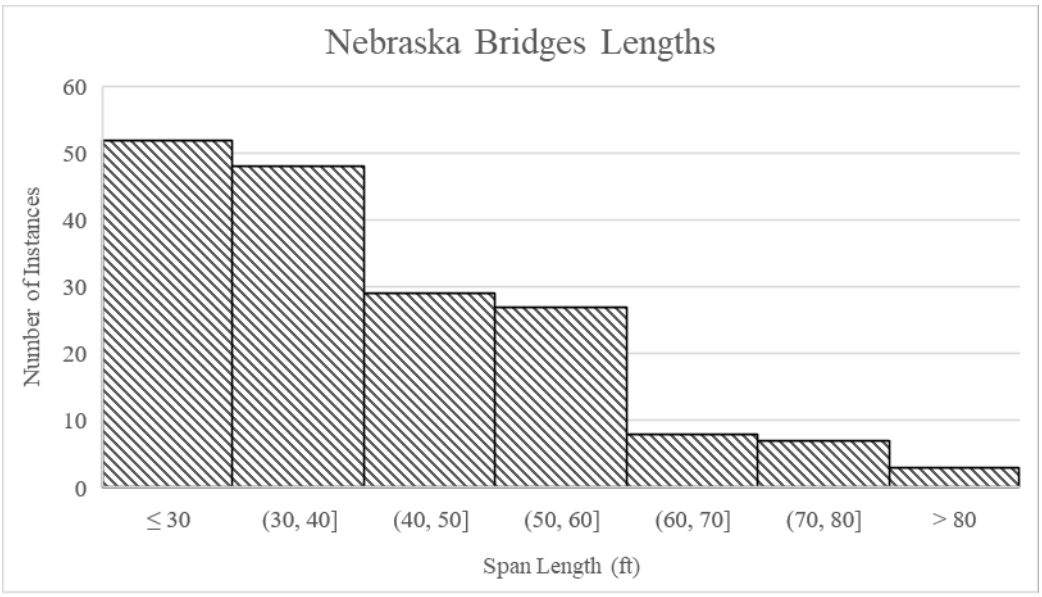

Figure 18. Histogram of Bridge Lengths

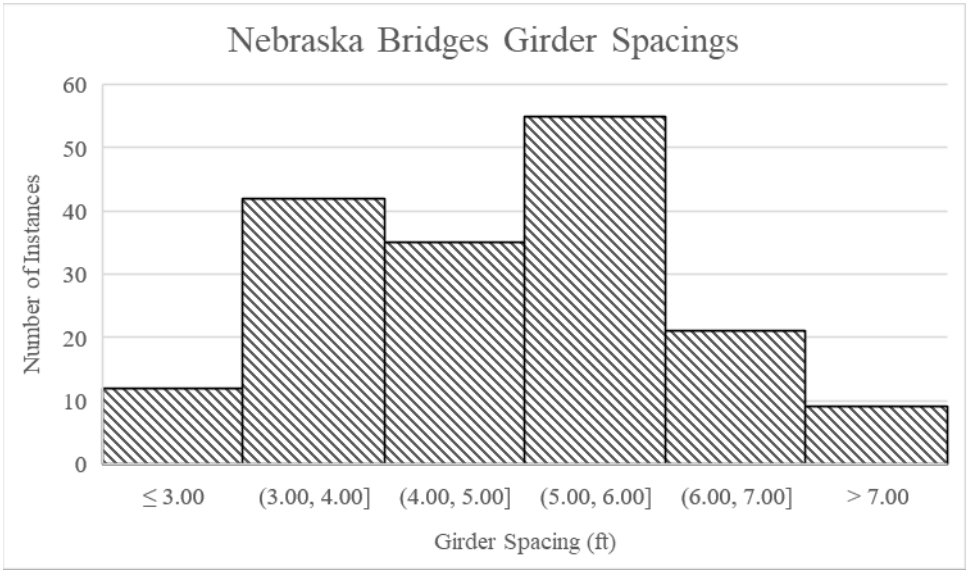

Figure 19. Histogram of Girder Spacings

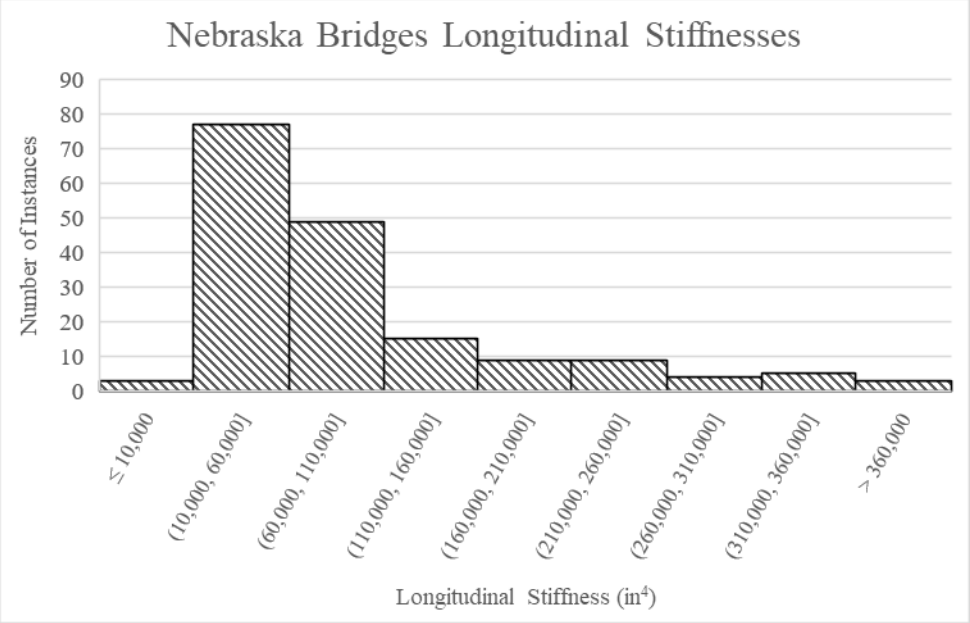

Figure 20. Histogram of Longitudinal Stiffnesses

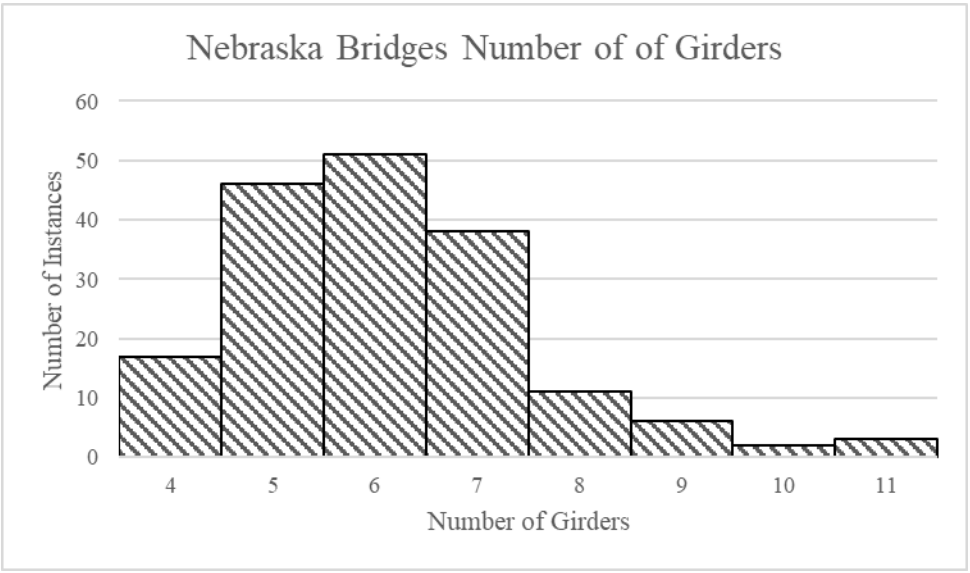

Figure 21. Histogram of Numbers of Girders

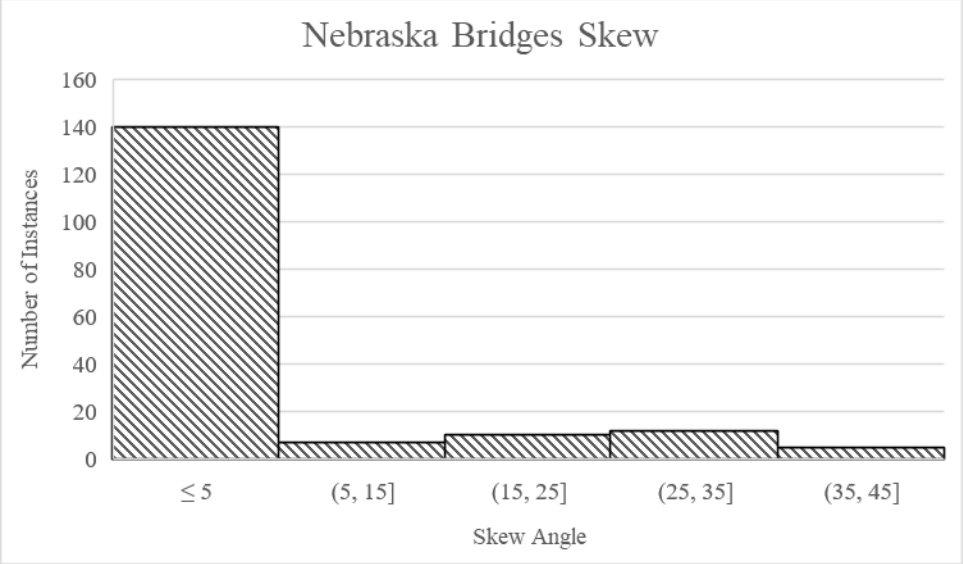

Figure 22. Histogram of Bridge Skews

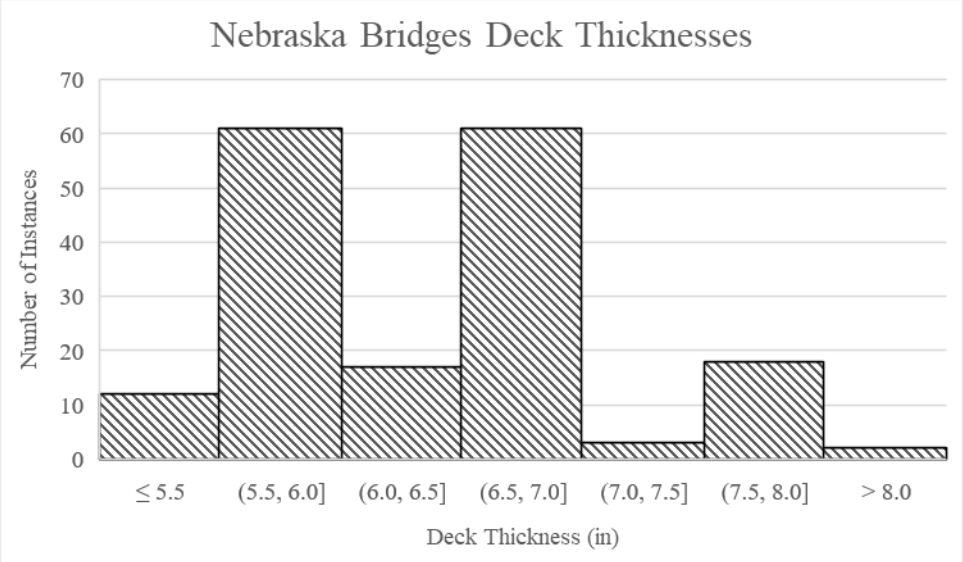

Figure 23. Histogram of Deck Thicknesses

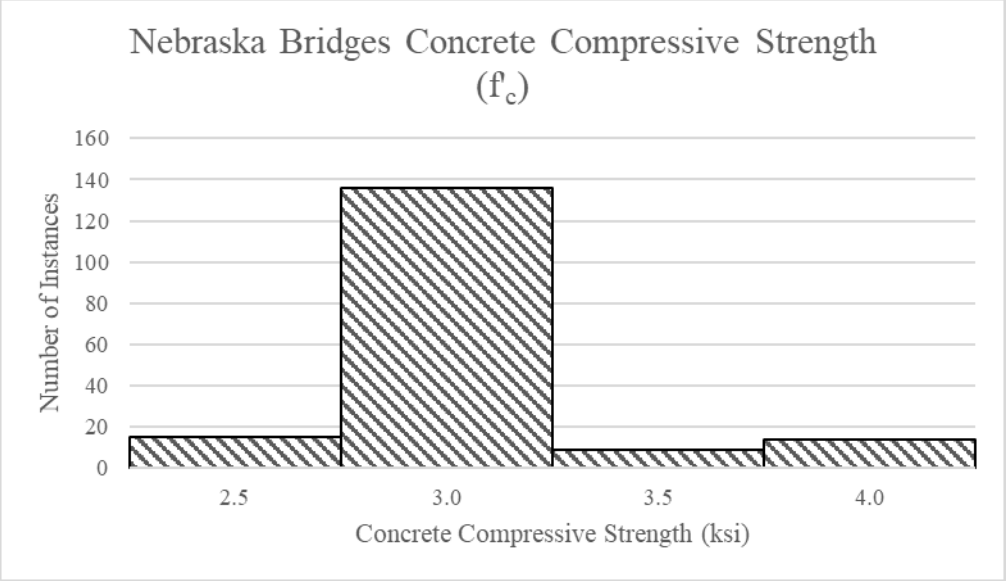

Figure 24. Histogram of Concrete Compressive Strengths

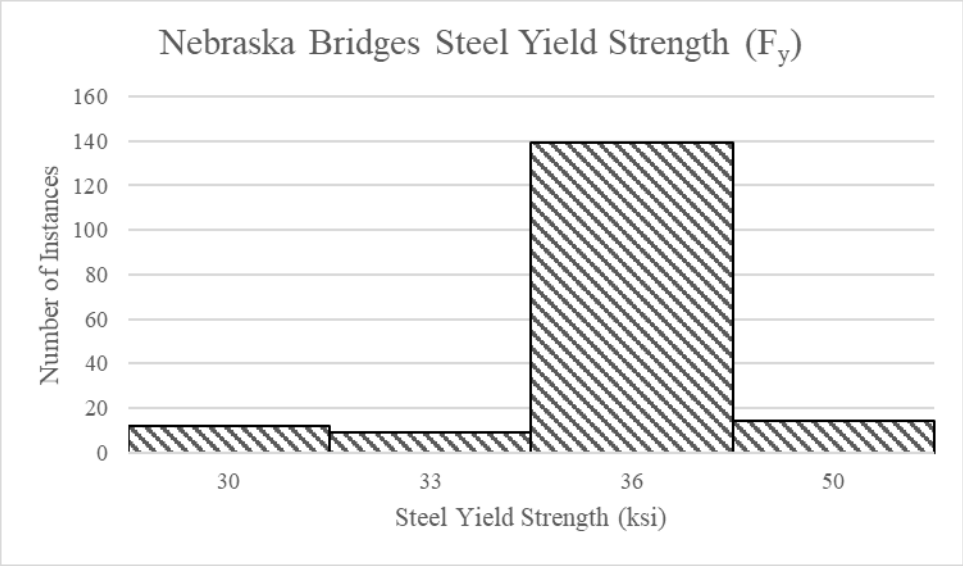

Figure 25. Histogram of Steel Yield Strengths

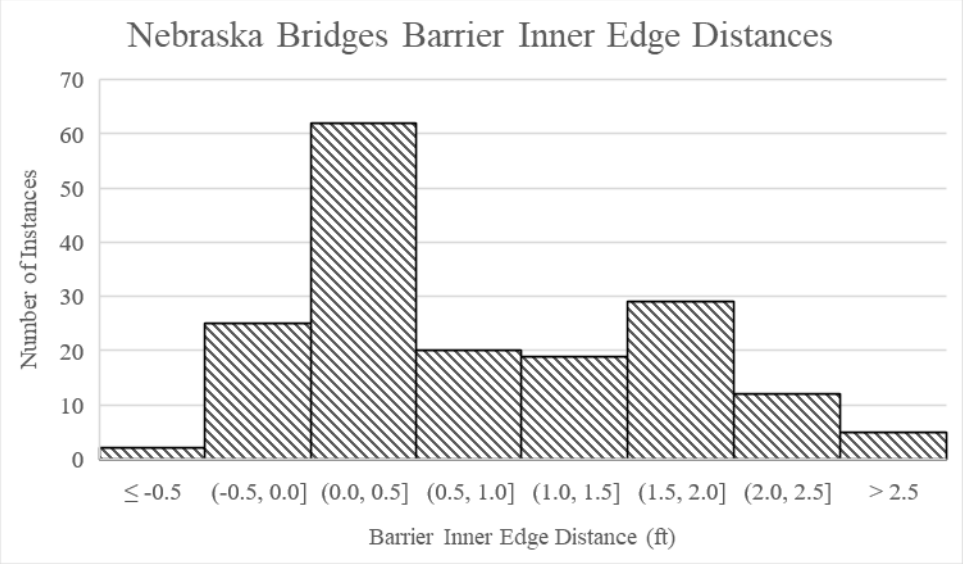

Figure 26. Histogram of Bridge Barrier Inner Edge Distances

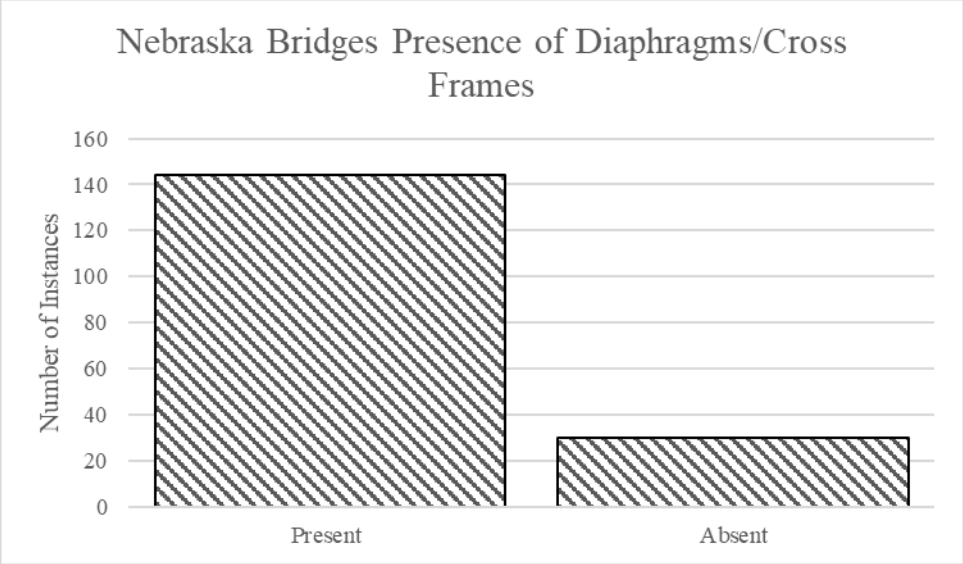

Figure 27. Histogram of Presence of Diaphragms or Cross Frames

5 Finite Element Modeling

5.1 ANSYS Modeling

5.1.1 Background and Previous Modeling Framework

As noted from literature, AASHTO usually estimates live load distribution conservatively, but detailed FEM can capture realistic internal load effects in a structural system closer to those expected from a field load test, which may justify removing load posting from a bridge. It was therefore desirable to generate and implement FEM results as ANN training targets. Sofi (2017) created an FEM procedure to efficiently generate 3D continuum models for single span, composite steel girder bridges. Governing parameters, bridge configuration, loading vehicle details, and FEM meshing details were input into excel sheets for each of the 174 individual bridges from the Nebraska inventory included in this study. Input files for ANSYS were automatically created with an ANSYS parametric design language (APDL) in conjunction with excel VBA macros. The steel girders were modeled as shell elements (Shell 181) and the diaphragms or cross-frames were modeled as beam elements (Beam 188). The bridge deck was modeled using brick elements (Solid65) connected to girders with rigid links (Link180). All bridge models' restraints were modeled as simply supported at the girder ends. Additional details of Sofi's bridge models and validation are available in Sofi and Steelman (2017, 2019). Deck nonlinearity and reinforcement was neglected for these bridge models.

Critical moment loading corresponds to a condition when the loading vehicles' middle axle is located at midspan. However, the maximum moment does not necessarily correspond to the midspan. Sofi specified an analysis location at midspan for bending moments. An example of a bridge FEM is shown in Figure 28 (Sofi and Steelman 2017).

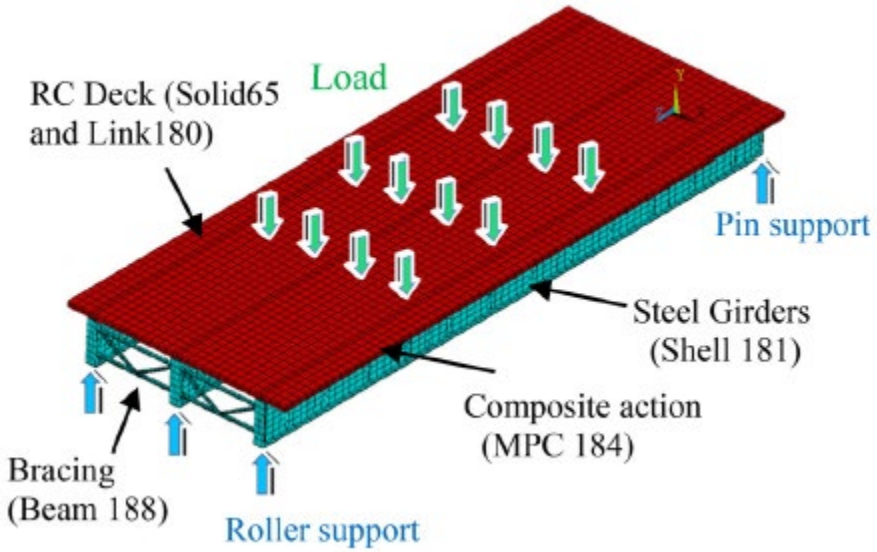

Figure 28. ANSYS Model

5.1.2 Previous ANSYS Modeling and Post-Processing

Sofi's previous work possessed the capability to investigate shear by placing simulated wheel load patches at appropriate alternate locations nearer supports, but primarily focused on flexure. All loads were defined using simulated HS-20 wheel patch loads as described in Sofi and Steelman (2017), and did not account for lane loads in either modeling or post-processing. Four analysis cases were considered: one lane loaded at the critical interior girder position, one lane loaded at the critical exterior girder position, two lanes loaded at the critical interior girder position, and two lanes loaded at the critical exterior girder position. Simulated truck load was placed longitudinally to simulate critical moment demands for all cases.

APDLs were used to post-process element force and stress data to provide the maximum resultant bending moment for each bridge girder following ANSYS analyses. Single lane-loaded analysis results were scaled by a multiple presence factor, *m*, of 1.2. Two-lane loaded analysis

results were not modified to account for multiple presence (i.e., $m = 1$). Maximum moment effects for critical interior and exterior girders were divided by the midspan moment effect of a single lane of HS-20 load. Finally, the analysis results were used to calculate interior and exterior girder moment rating factors, which were then used as output targets in ANN training.

5.1.3 Current Study Modeling and Post-Processing Modifications

As noted previously, Sofi's previous work focused on flexure. The current study expanded to also examine shear. Each bridge was analyzed for eight potential critical scenarios with combinations of: load placement for critical exterior or interior girder loading, load placement for critical shear or moment loading, one- to two-lane loading. A summary of all load cases performed for all bridges in this study is presented in

Table 8. Cases 1 to 4 were identical to Sofi's previous work. Transverse load placement correlated to Critical Girder and Lanes Loaded. Longitudinal load placement correlated to the critical Load Effect of interest for the analysis Case.

Moment GDFs were calculated by dividing maximum moment effects for critical interior and exterior girders by the midspan moment induced by a single lane of HS-20 load. Similarly, the shear GDFs were calculated by dividing maximum shear effects for critical interior and exterior girders by the total shear effect on the critical bridge section under a single lane of HS-20 load.

Table 8. FEM Load Placements

		Critical Girder		Lanes Loaded		Load Effect	
		Interior	**Exterior**	**One**	**Two**	**Moment**	**Shear**
Moment ANNs	**Case 1**	X		X		X	
	Case 2	X			X	X	
	Case 3		X	X		X	
	Case 4		X		X	X	
Shear ANNs	**Case 5**	X		X			X
	Case 6	X			X		X
	Case 7		X	X			X
	Case 8		X		X		X

All modeling in ANSYS assumed composite behavior. However, discussions with NDOT personnel indicated that a significant number of bridges in the anticipated study population were noncomposite. Composite effectiveness will implicitly influence transverse load distribution through the longitudinal stiffness term. Noncomposite bridge models were not included in the study, but the study will extend to load rating noncomposite bridges, provided that the noncomposite bridge of interest possesses characteristics (particularly longitudinal stiffness) represented in the ANN training data.

5.1.4 ANSYS ANN Training and Testing Data

This study aimed to obtain ANSYS-equivalent GDFs from ANNs. After completing ANSYS analyses for all bridges in the study population, the resulting GDFs were plotted with respect to each governing parameter to identify outliers. Figure 29-Figure 32 and Figure 33-

Figure 36 show plots of moment and shear GDFs, respectively. Bridges that were identified as outliers are shown as purple data points and were excluded from ANN training and testing. 11 outliers were identified in the moment GDF scatterplots, which left 163 bridges for moment ANN development. 13 outliers were identified for shear GDF scatterplots, which left 161 bridges for shear ANN development.

It should be noted that some data points may not be outliers in all plots. For example, a bridge may be an outlier because it has a moment GDF and longitudinal stiffness combination that is clearly aberrant compared to the population scatter cloud. However, the same bridge may also have a moment GDF and length that are similar to other bridges. Outliers were assigned a label number so that bridge outlier data points can be noted for multiple plots. Shear ANN outliers do not necessarily correspond to moment ANN outliers.

As anticipated, the GDFs from the modeling procedures were on average lower than AASHTO LRFD GDFs. The AASHTO GDFs were on average 35% and 24% higher than the moment and shear GDFs, respectively. If girder spacing, number of girders, span length, deck thickness, longitudinal stiffness, edge distance, or skew angle fall outside the ranges of applicability for AASHTO LRFR GDF equations, the lever rule was used to calculate GDFs instead. 150 out of 174 (86%) and 141 out of 174 (81%) of moment and shear GDF ratios were between 1 and 1.5, as shown in Figure 37 and Figure 38 . The moment and shear GDFs were post-processed and composite operating rating factors were determined. In this study, it was found that 30 bridges were governed by shear. All of these bridges span 35 ft or less. The moment to shear rating factor ratio is 1.87 and is shown in Figure 39.

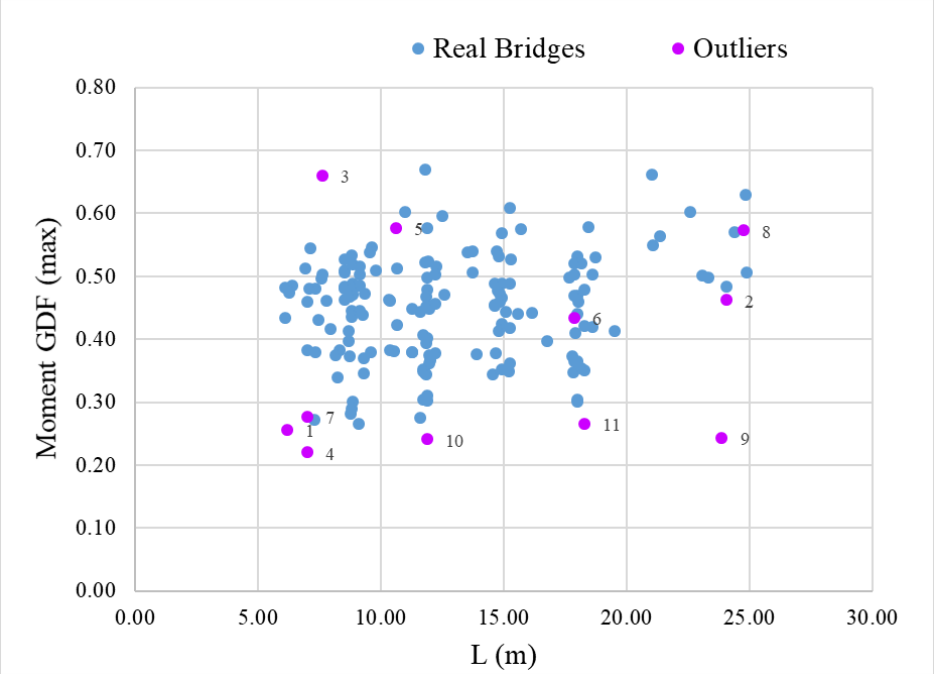

Figure 29. Length vs. FEM-Based Moment GDF

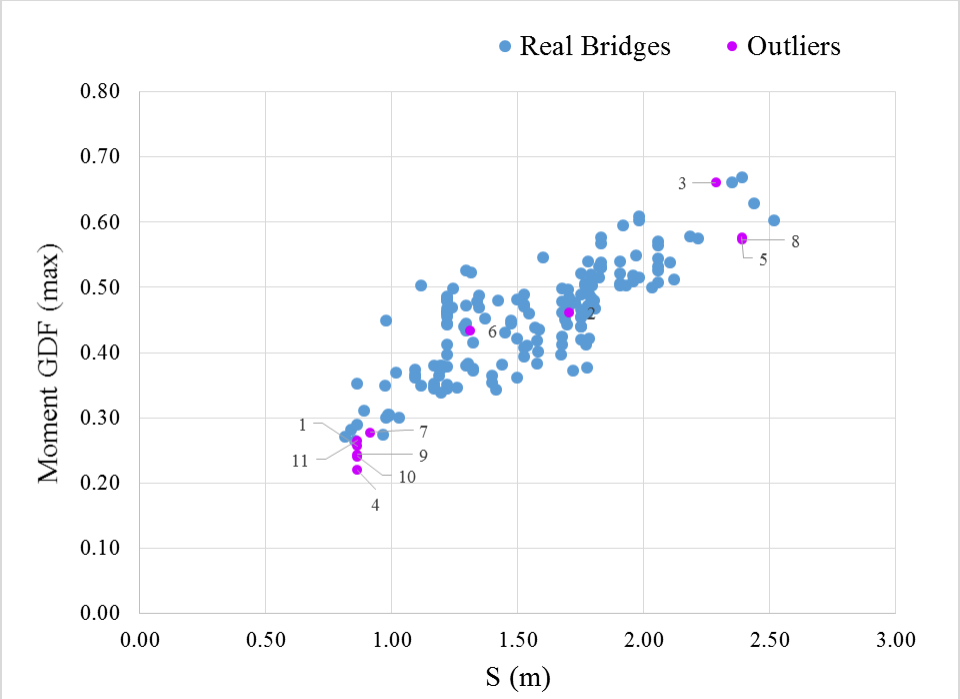

Figure 30. Girder Spacing vs. FEM-Based Moment GDF

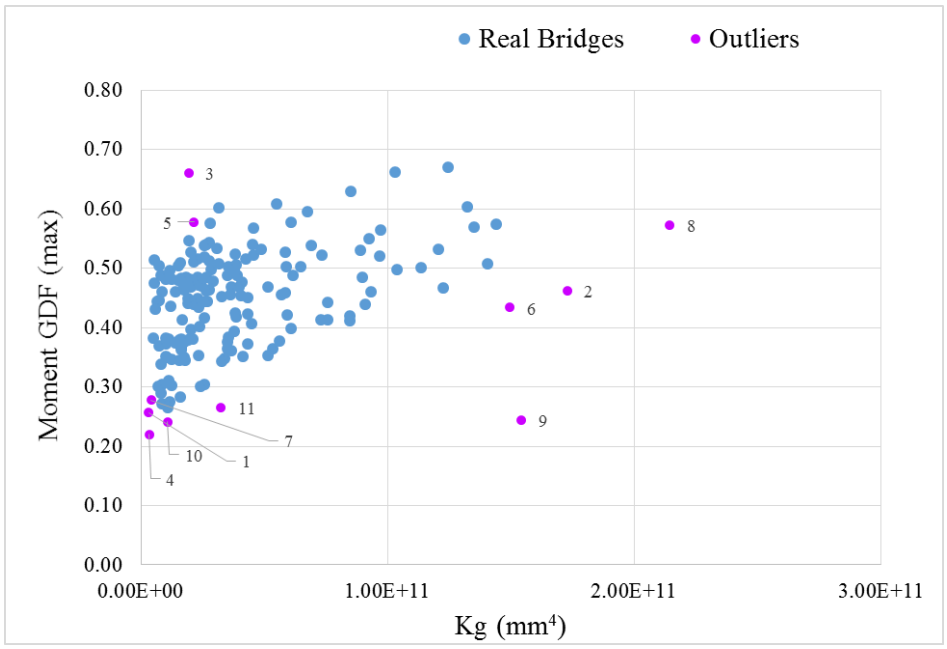

Figure 31. Longitudinal Stiffness vs. FEM-Based Moment GDF

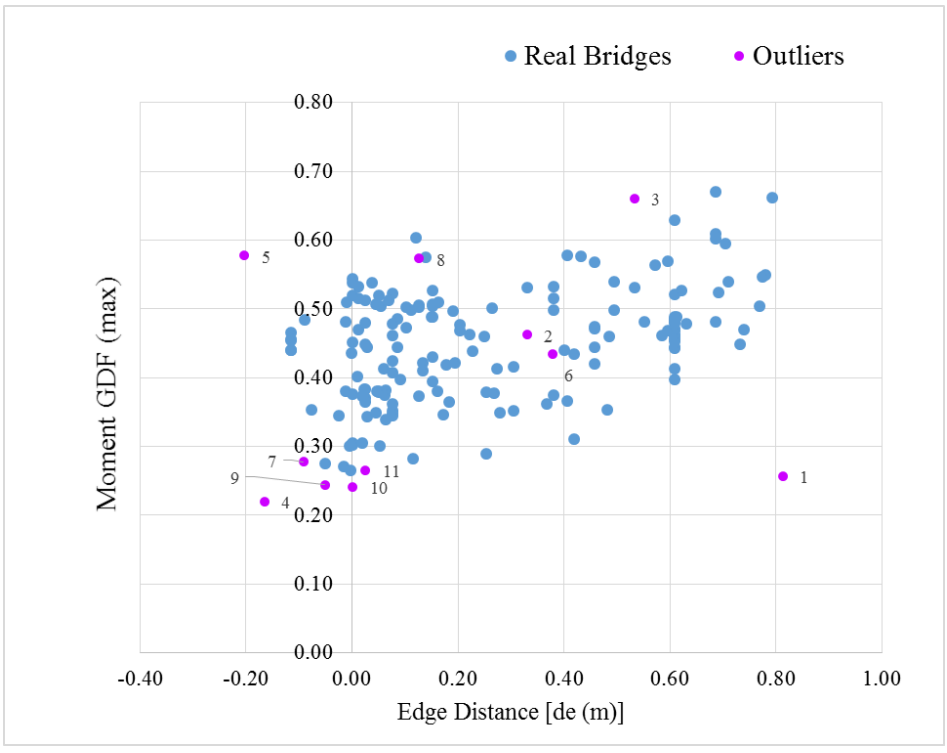

Figure 32. Edge Distance vs FEM-Based Moment GDF

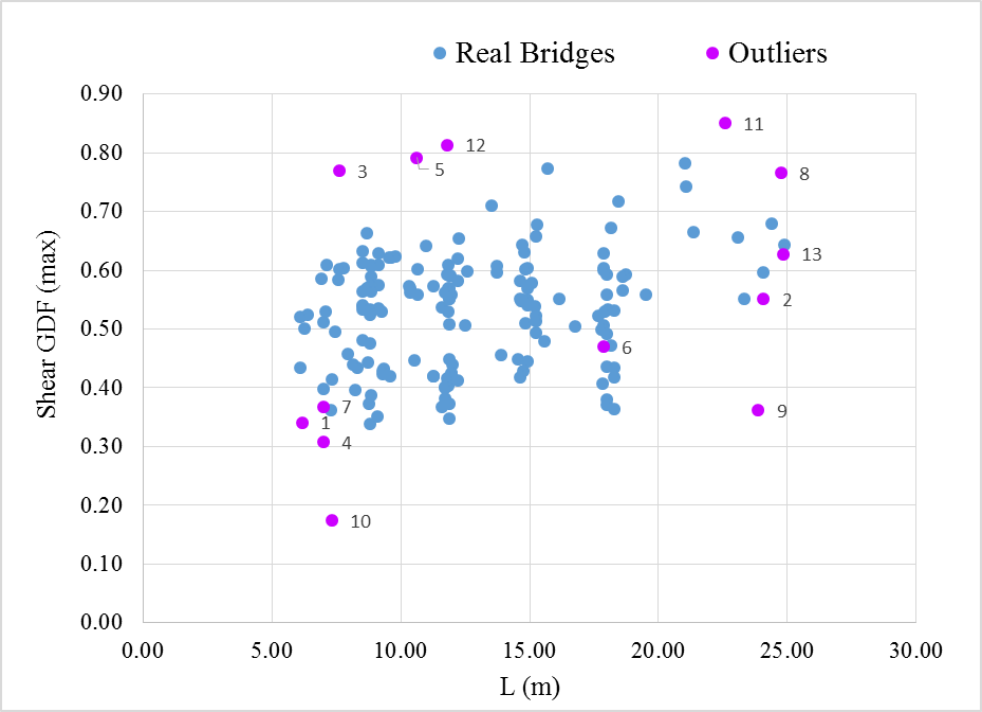

Figure 33. Length vs. FEM-Based Shear GDF

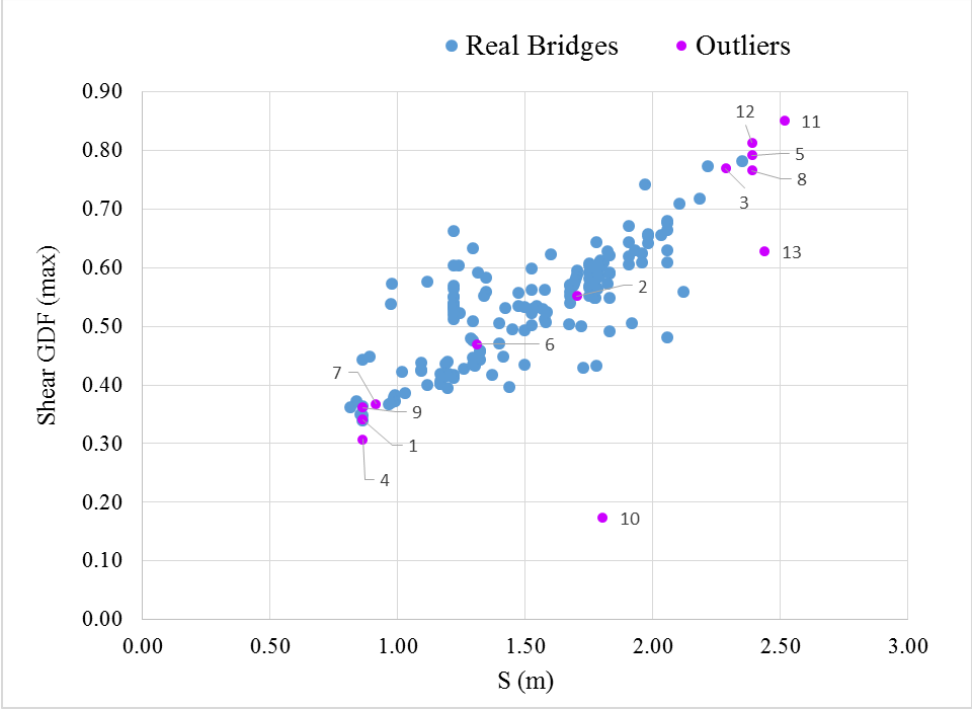

Figure 34. Girder Spacing vs. FEM-Based Shear GDF

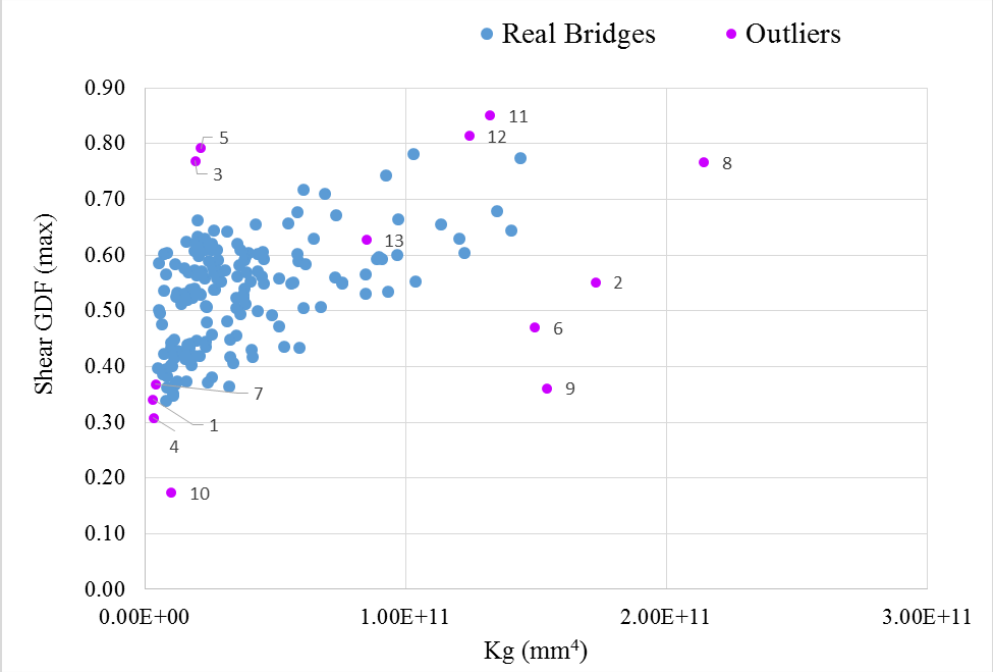

Figure 35. Longitudinal Stiffness vs. FEM-Based Shear GDF

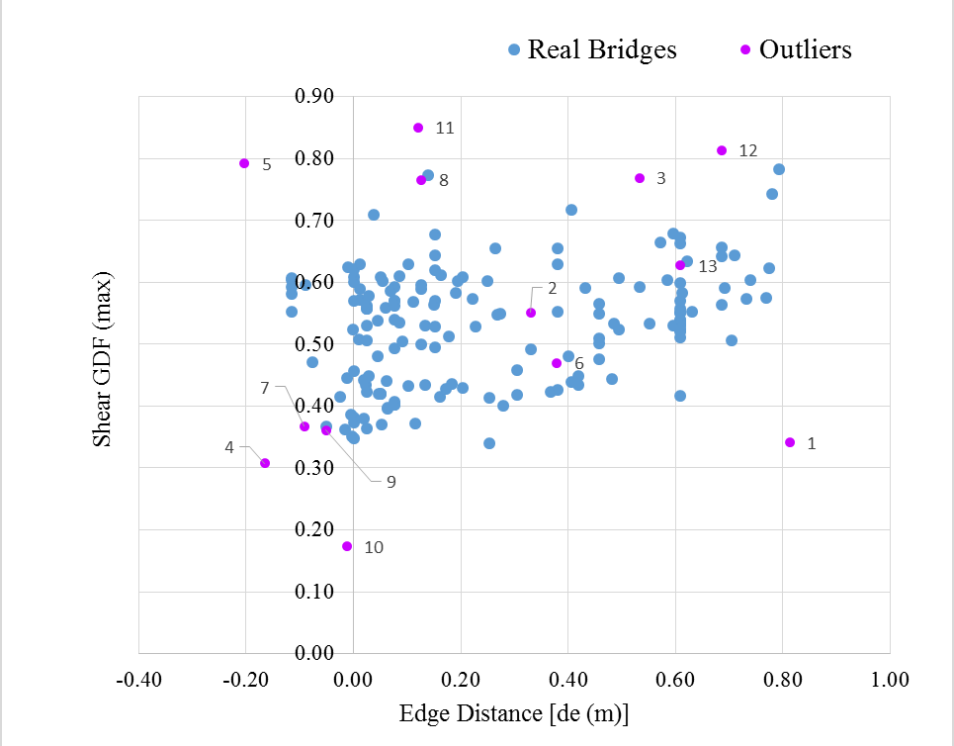

Figure 36. Edge Distance vs FEM-Based Shear GDF

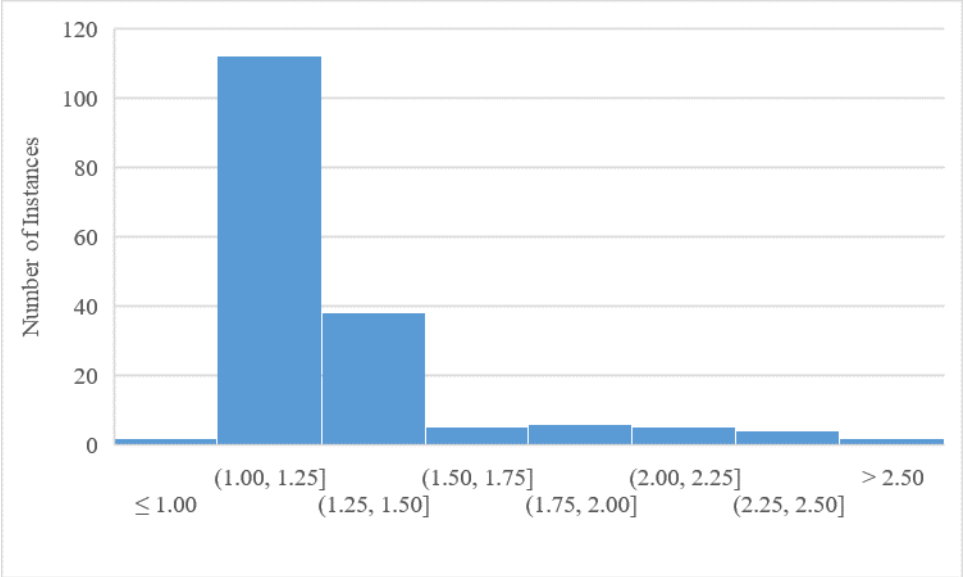

Figure 37. Histogram of Moment GDF Ratio (AASHTO/FEM)

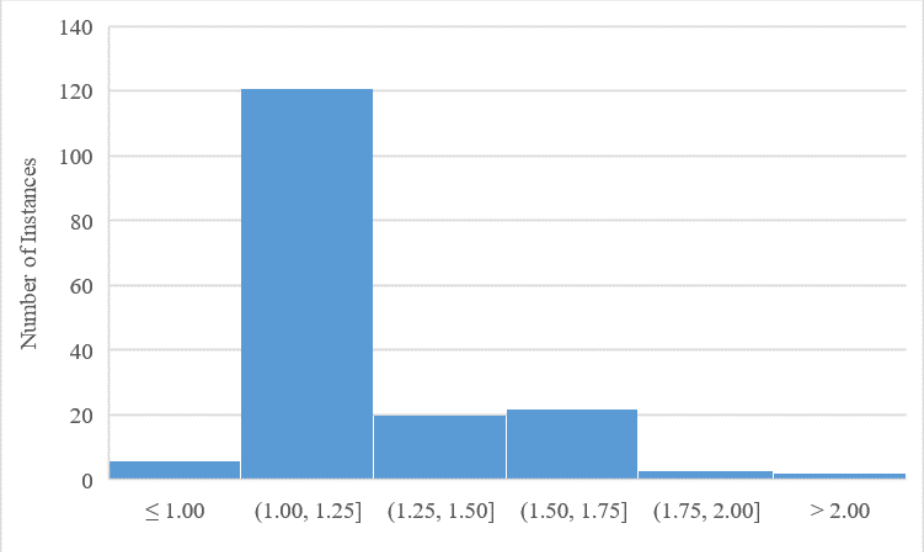

Figure 38. Histogram of Shear GDF Ratio (AASHTO/FEM)

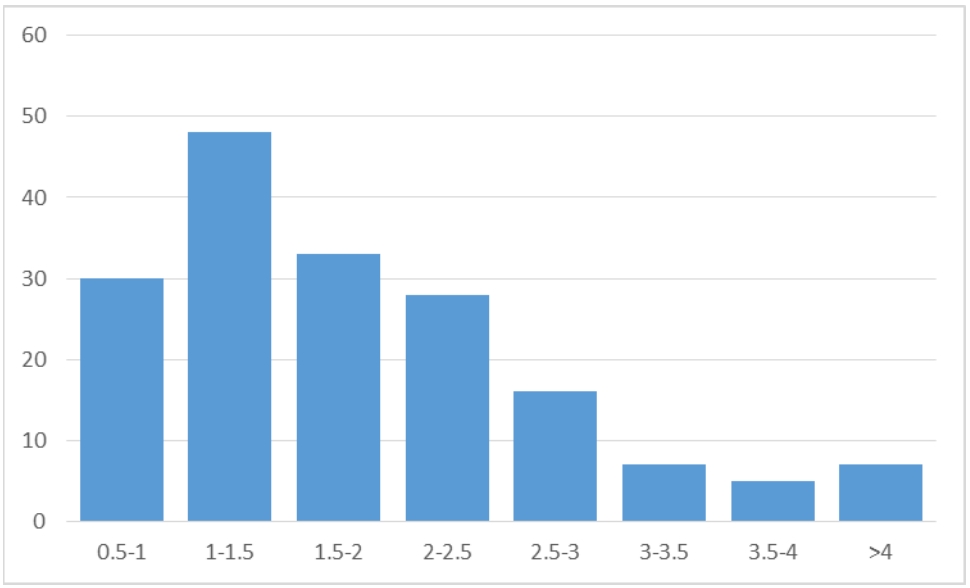

Figure 39. Moment to Shear Operating Rating Factor Ratio

5.2 CSiBridge Modeling

Complementary bridge modeling was performed in CSiBridge for bridges subjected to field load tests. CSiBridge provides a more simplified user experience than ANSYS, and can simulate moving vehicle loads to perform load rating analyses for composite and noncomposite bridges. Both ANSYS and CSiBridge modeled girders with shell elements, but CSiBridge also used shell elements to model the deck, rather than solid elements as in ANSYS.

Four vehicle loading lanes were modeled to represent critical interior and exterior girder load paths in order to be consistent with the loading in the ANSYS models. Material properties, such as yield strength of steel and compressive strength of concrete, were defined identically to those used in ANSYS. Similarly, girder, diaphragm, and deck section properties were identical to ANSYS, except that the deck was specified by its total thickness and axial and flexural shell geometric section properties were internally calculated by CSiBridge.

Once the elements were defined, the bridge was created as an area object model. An HL-93 load pre-defined and available in the software was selected, and an impact factor of 33% was specified consistent with AASHTO LRFR. It should be noted that this load vehicle includes the lane load specified by AASHTO Manual for Bridge Evaluation, which is 0.64 kip/ft for 10 ft wide lanes. Load factors were also specified in accordance with AASHTO LRFR to obtain both inventory and operating load ratings. Load ratings were obtained for both interior and exterior girders, as mentioned previously in the discussion of ANSYS modeling. CSiBridge also allows users specify whether the bridge is composite or noncomposite.

5.3 HS-20 and Tandem GDF Comparison

AASHTO LRFD/LRFR specifies that the maximum moment and shear effects for either HS-20 trucks or tandem loads should be used. For shorter bridge spans, tandem loads have a higher chance of governing moment and shear design. Since this study is predominantly focused on HS-20 loads, a study was performed to compare tandem-based moment and shear GDFs to HS-20 GDFs. The load distributions between HS-20 and tandem loads were compared for bridges C008101013P, C009202210, C003303710, and C006710205 which have span lengths of 20, 40, 60, and 80 ft, respectively. Tandem load GDFs were calculated with the methods mentioned earlier in this chapter. Finally, the percent differences between the GDFs for the two methods were calculated as shown in Eqn. 6. Moment and shear GDF comparisons are summarized below in Table 9 through Table 12.Additionally, the governing load effect is provided in Table 13 for the bridges in ascending span length.

$$Percent\ Difference = 100 * (\frac{GDF_{HS-20}}{GDF_{Tandem}} - 1)$$ Eqn. 5

Table 9. Tandem and HS-20 Moment and Shear GDF Difference for Bridge C008101013P (20')

	Moment GDF Difference	**Shear GDF Difference**
1 Truck Interior	0.7%	0.2%
2 Trucks Interior	1.2%	0.7%
1 Truck Exterior	0.6%	2.0%
2 Trucks Exterior	0.9%	-1.8%

Table 10. Tandem and HS-20 Moment and Shear GDF Difference for Bridge C009202210 (40')

	Moment GDF Difference	**Shear GDF Difference**
1 Truck Interior	0.7%	-8.5%
2 Trucks Interior	-0.9%	-2.5%
1 Truck Exterior	0.1%	-4.3%
2 Trucks Exterior	-0.5%	-2.6%

Table 11. Tandem and HS-20 Moment and Shear GDF Difference for Bridge C003303710 (60')

	Moment GDF Difference	**Shear GDF Difference**
1 Truck Interior	-4.4%	-11.5%
2 Trucks Interior	-3.6%	-3.7%
1 Truck Exterior	-0.9%	3.2%
2 Trucks Exterior	0.1%	-0.5%

Table 12. Tandem and HS-20 Moment and Shear GDF Difference for Bridge C006710205 (80')

	Moment GDF Difference	Shear GDF Difference
1 Truck Interior	21.5%	21.5%
2 Trucks Interior	19.9%	31.0%
1 Truck Exterior	20.7%	39.4%
2 Trucks Exterior	22.4%	29.3%

Table 13. Governing Load Effect

	Moment		Shear	
Bridge	**Tandem**	**HS-20**	**Tandem**	**HS-20**
C008101013P	X		X	
C009202210	X			X
C003303710		X		X
C006710205		X		X

In Table 9, the maximum absolute difference between tandem load and HS-20 moment and shear GDFs is 1.2% and 2%, respectively. Results are similar for the 40' bridge, except that the differences in shear GDFs are more pronounced, differing by up to 8.5%. Although this GDFs discrepancy is appreciably large for shear, the governing load effect is produced by the HS-20, as indicated in Table 13, which has a larger gross vehicle weight.

Ultimately, these results indicate that ANNs trained to produce HS-20 GDFs can also be used with tandem loads. A detailed discussion of reliability calibration is presented later, but it is noteworthy for this present discussion that NCHRP 20-07 / 186 (Kulicki et al., 2007) indicated that the coefficient of variation associated with GDFs was 12%. This aspect of uncertainty is already present and integral within a total 18% coefficient of variation for dynamic live load effects in AASHTO LRFD/R.

GDF predictions for HS-20 loading are generally conservative relative to tandem loading at small loads, to using HS-20 GDFs from ANNs with tandem loads will generally produce slightly conservative results. As span length increases to 40 ft, the HS-20 GDFs initially become unconservative for use with tandem loads, but the effect is only pronounced for shear effects, which are unlikely to govern over moment effects with increasing span lengths. Use of tandem loads with HS-20 GDFs for span lengths of 60 ft or larger is inadvisable. HS-20 loads tend to govern at these span lengths, and the tandem GDFs were also significantly lower for the 80 ft span. Use of tandem loads with HS-20 GDFs may therefore be excessively conservative with increasing span lengths and may negate the benefit of using GDFs from ANNs.

6 Artificial Neural Networks

6.1 Background and Previous Work

Sofi's preliminary study (2017) sought to produce ANNs capable of predicting moment-based load ratings from 10 governing parameters. Figure 40 shows an example of an ANN network architecture (Sofi 2017). Inputs and nodes are connected to each other by weights and each node also has a bias associated to it. Weights and biases are configured during ANN training. Sofi created ANNs using standard machine-learning methods such as using backpropogation algorithms, using testing data to evaluate the generalization of the ANNs, changing ANN architecture to minimize error, and retraining ANNs of the same configuration to account for random initial conditions for weights and biases. The proposed methodology used post-processed FEM live load effects (element-based moment and shear) as ANN training data, rather than extrapolating directly to load ratings within the ANNs.

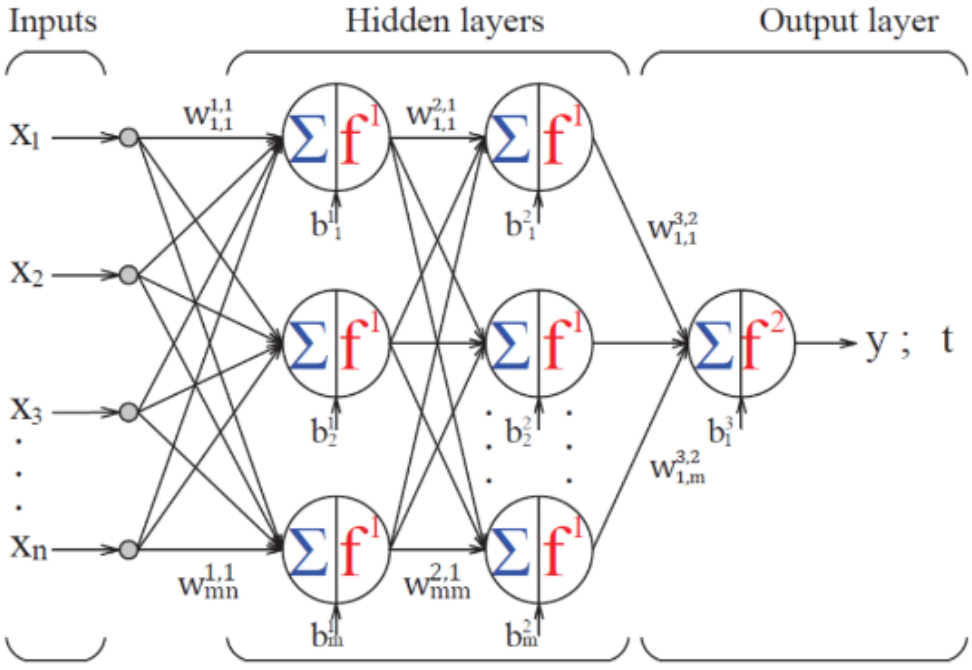

Figure 40. Artificial Neural Network Architecture with Two Hidden Layers and 1 Output

The resulting ANNs in this slightly revised approach can be used to produce rating factors more consistent with realistic bridge behavior when compared to routine AASHTO-based GDFs and load ratings, removing unnecessary conservativism (bias) from anticipated live load effects, similar to Sofi's work. However, the modified approach also facilitates reliability calibration as discussed in detail in Chapter 7 to reflect amplified live load effect uncertainty introduced by ANN prediction errors. The revised methodology also offers increased flexibility and can be easily modified to account for different load vehicles or noncomposite bridges. In addition to the ANN optimization procedure proposed by Sofi, the current study also expanded upon the comparison of ANN performance with varying training set sizes performed by Sofi.

6.2 Artificial Neural Network Training and Testing Data

Neural network modeling for this study was performed using the Neural Network Toolbox available in MATLAB 2017 and implemented a typical feedforward architecture with one input layer comprised of 10 neurons (one for each of the governing parameter inputs), one output layer containing a neuron for the predicted GDF, and either one or two hidden layers. As discussed in the following section, the number of neurons in the hidden layers was varied to optimize network performance.

A total of 163 and 161 bridges remained for moment and shear ANN development, respectively, after excluding outliers as discussed in the previous chapter. Neural network training is commonly performed by partitioning available *design* data into *training*, *validation*, and *testing* subsets. These design datasets are randomly partitioned during ANN training to ensure that the ANN is sufficiently generalized to avoid overfitting, which would result in very low errors for training data but significantly larger errors for samples outside the training data.

Similar to the Sofi's method, prior to any ANN training, a portion of the study population was partitioned and isolated as an *independent testing set*, which was distinct from the *design testing set* typically used in ANN training. Design and independent testing sets were assigned randomly, except that the assignment of bridges to the design set was strategically performed with extreme cases (relatively high and low GDF values with respect to governing parameters) to envelope the design data. The design set envelope was then supplemented with random additional samples to provide internal interpolation points within the population.

The design set ranged from 20 to 130 bridges in increments of 10 to investigate design set size influence on ANN prediction accuracy. Each design set population was randomly subdivided by MATLAB into 70% training, 15% validation, and 15% design testing subsets when the Levenberg-Marquardt algorithm was used. The design set population was randomly subdivided by MATLAB into 85% training and 15% design testing subsets when the Bayesian Regularization algorithm was used. While the design testing set size varied with the overall size of the design set under consideration, the independent testing set comprised 33 and 31 particular bridges for the moment and shear GDFs, respectively, which remained unchanged regardless of the design set size.

When less than the maximum 130 available bridges were used in the design set, the bridges not included in the design set were available for additional testing. Accordingly, these extra bridges excluded from the design set were classified as an "Additional testing set." Figure 41 shows moment GDF vs. governing parameter data points for 130 bridges in the design set and Figure 42 shows moment GDF vs. governing parameter data points for 90 bridges in the design set. The testing set, shown in orange, is the "independent" testing set, and remained the same for

the two design set sizes. The smaller design set left out 40 bridges, shown in magenta, that were used for additional testing (in addition to the independent testing set). The entire moment and shear data sets are in the Appendix 11.1.3.

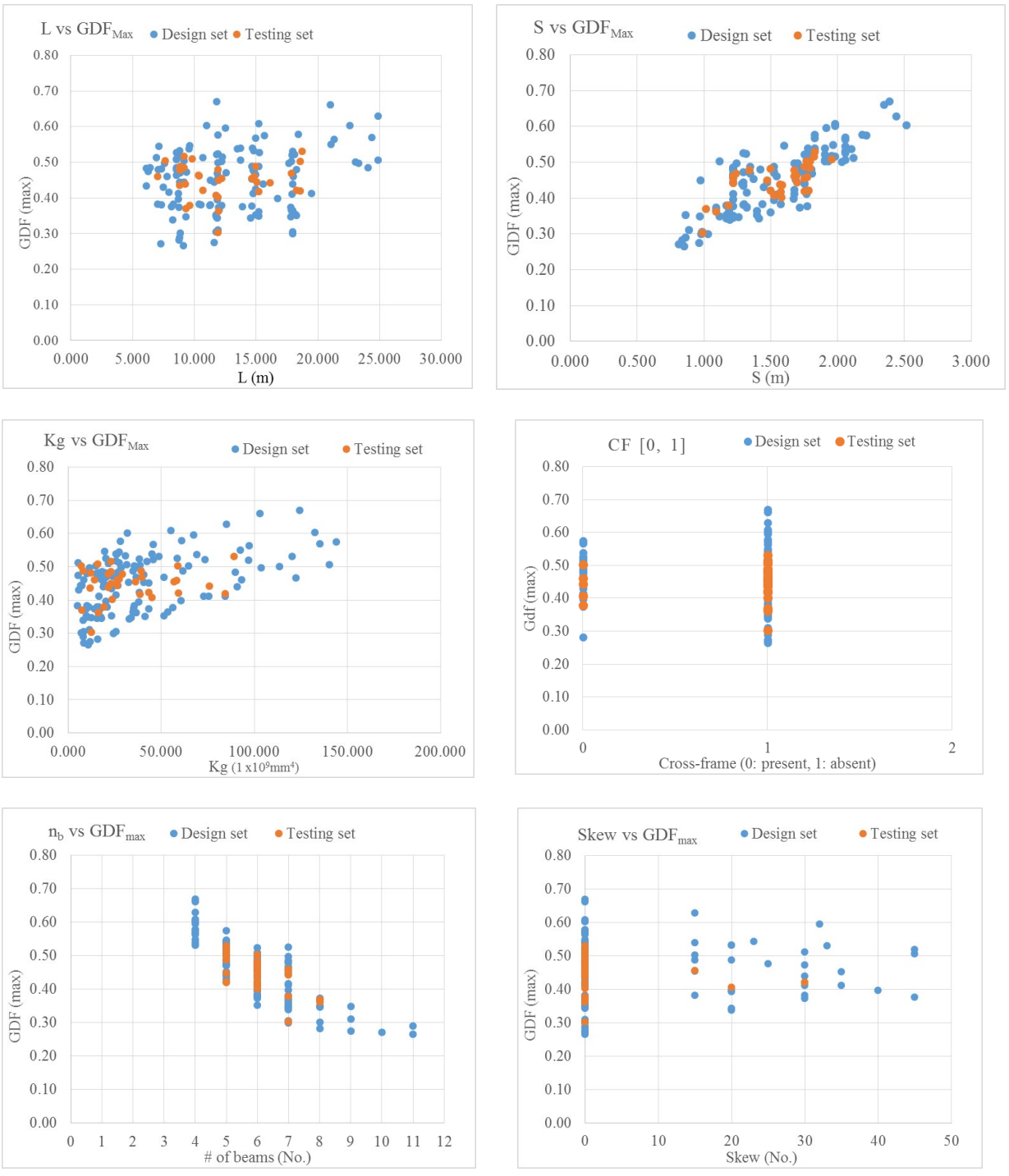

Figure 41. Moment GDFs vs. Governing Parameters for 130 Bridges in Design Set

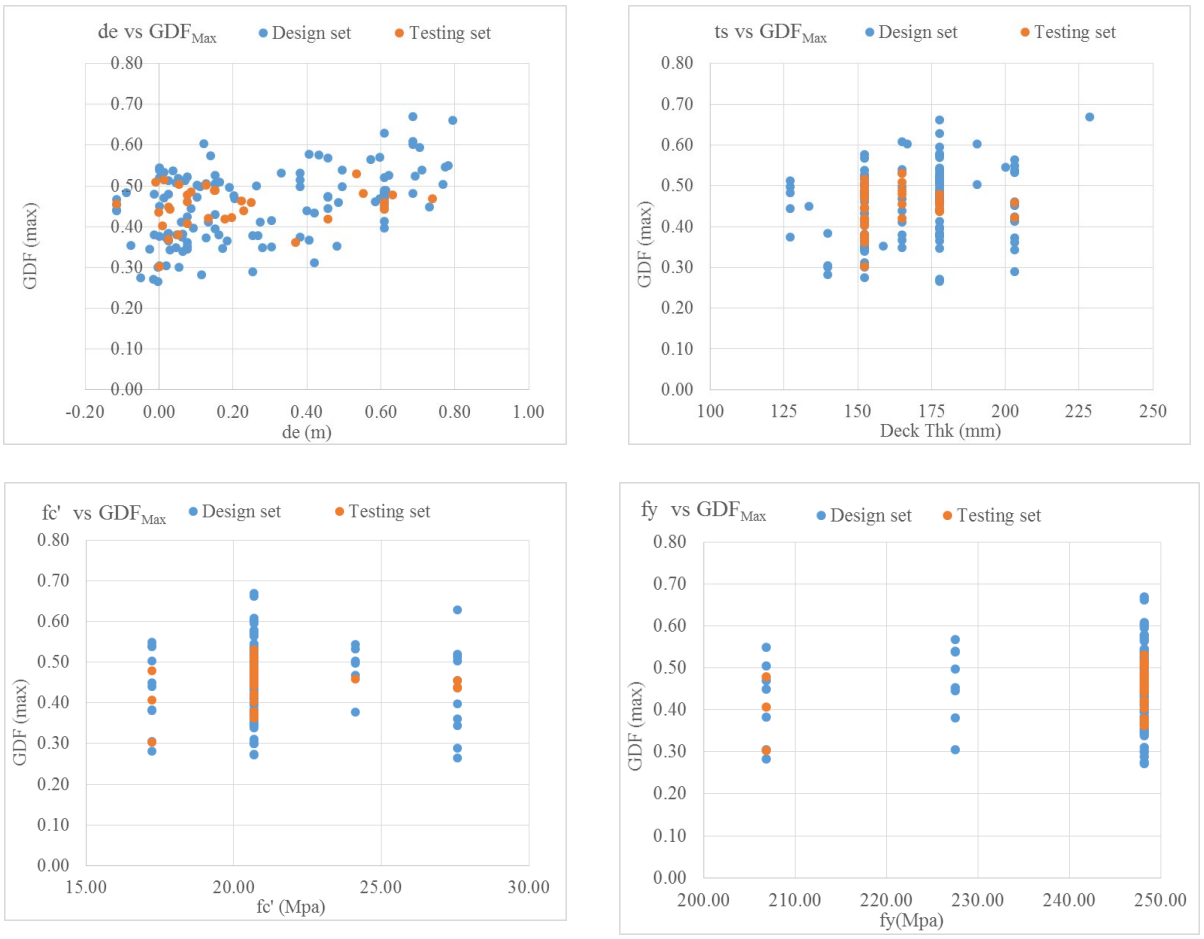

Figure 41. Moment GDFs vs. Governing Parameters for 130 Bridges in Design Set (continued)

Figure 42. Moment GDFs vs. Governing Parameters for 90 Bridges in Design Set

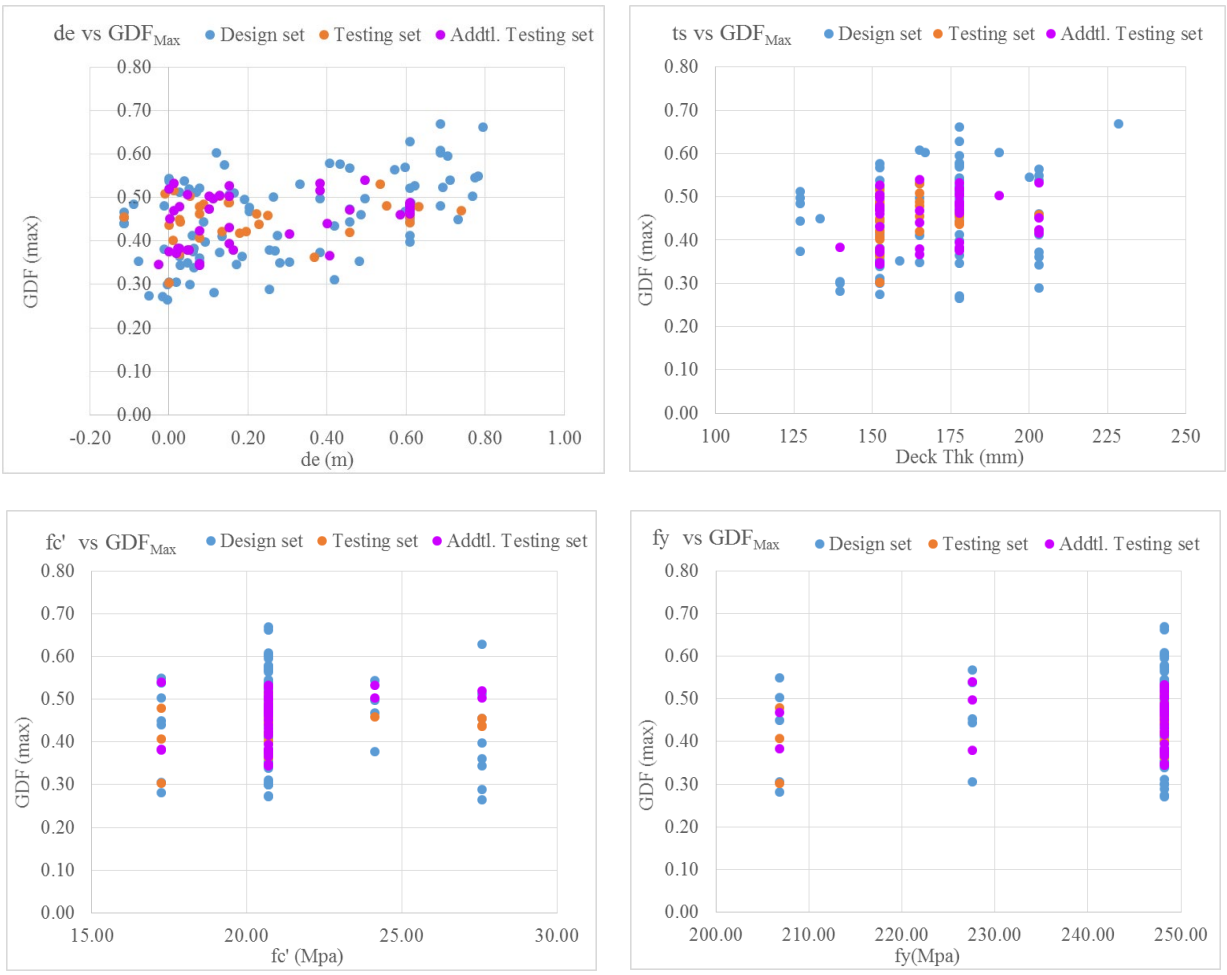

Figure 42. Moment GDFs vs. Governing Parameters for 90 Bridges in Design SetFigure 42. Moment GDFs vs. Governing Parameters for 90 Bridges in Design Set (continued)

6.3 Artificial Neural Network Optimization

The ANNs in this study were optimized with a similar scheme used by Sofi (2017). ANNs of the same design set size were configured and trained with combinations of the following parameters:

1) Training algorithm: ANNs were trained with either Bayesian-Regularization, BR, (MacKay 1992) or Levenberg-Marquardt, LM, (1963) backpropagation algorithms.

2) Number of hidden layers: 1 or 2 hidden layers

3) Number of nodes per hidden layer: 2-9 nodes per hidden layer

The same network architecture naming convention used by Sofi will be used herein. The four combinations are 10-m-1-BR, 10-m-m-1-BR, 10-m-1-LM, and 10-m-m-1-LM where the values read from left to right are the number of inputs (10 governing parameters), number of nodes in hidden layer (m), number of outputs (1 GDF prediction), and training algorithm (BR or LM). The number of nodes per hidden layer was varied between 2 and 10. ANNs with two hidden layers were configured to have the same quantity of nodes in both hidden layers.

ANNs were retrained 250 times with randomly initialized weights and biases. ANN performance was evaluated by mean square error (MSE). The formula for mean squared error is shown below in Eqn. 6, where *n* corresponds to a set of bridge inputs, *T* corresponds to the target value or the expected value of the ANN for a particular bridge (GDF from FEM post-processing), and *Y* is the ANN prediction for a bridge.

$$MSE = \frac{1}{n}\sum_{i}^{n}(T - Y)^2 \qquad \text{Eqn. 6}$$

The optimal ANN for each architecture minimized combined testing set MSE within the 250 ANN trials, where the combined testing set is comprised of the independent testing set and the 15% of the design set used for testing during ANN training. Figure 43 shows an example of how MSE can vary depending on the random initial weights and biases. Figure 44 and Figure 45 are examples of the ANN architecture optimization. The 130 bridge design set single best network that predicts moment GDFs is 10-5-5-1 BR with an average absolute error of 3.65% from independent testing. The single best network of the same for shear GDFs of the same

design set size is 10-3-3-1 BR and has an absolute error of 2.88%. The Appendix 11.1.3 has results for moment and shear neural network optimizations for all design set sizes tested.

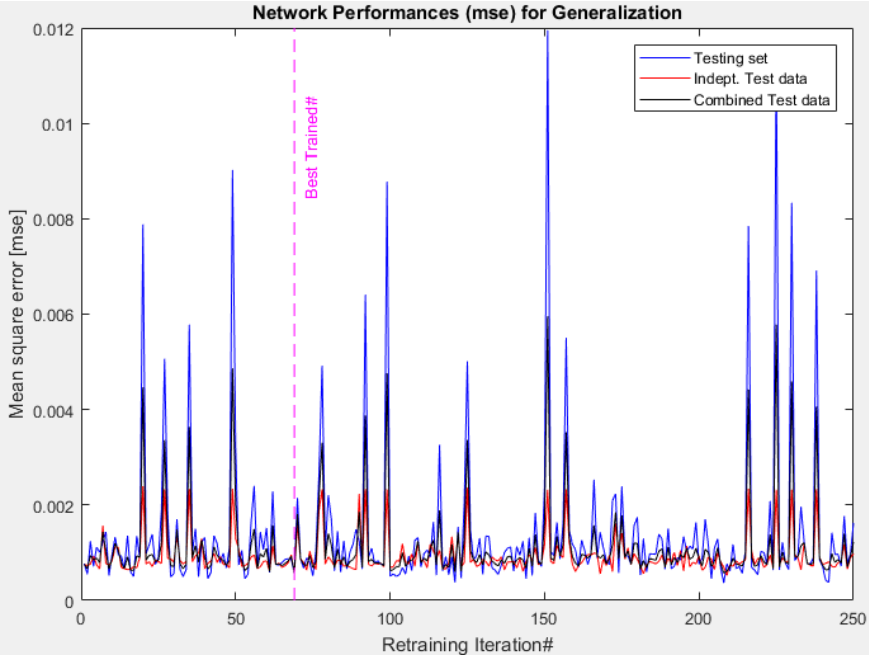

Figure 43. Moment 10-5-5-1 BR Best Network based on MSE of Combined Testing Set

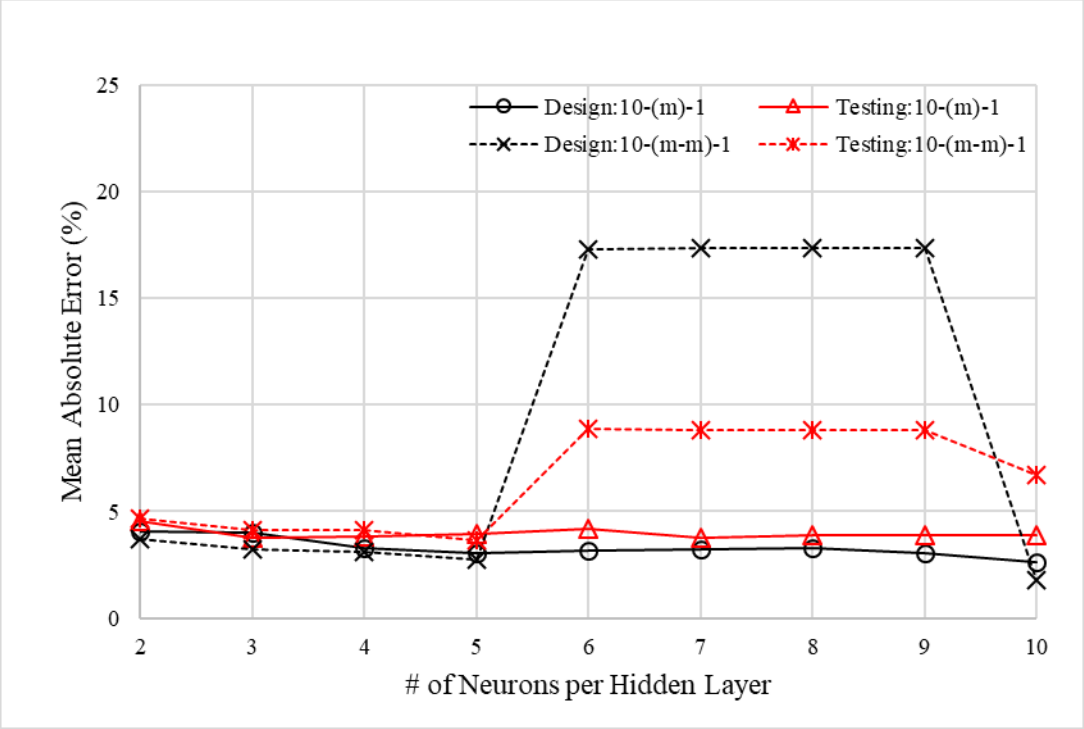

Figure 44. 130 Bridge Design Set Moment ANN Optimization for Bayesian-Regularization

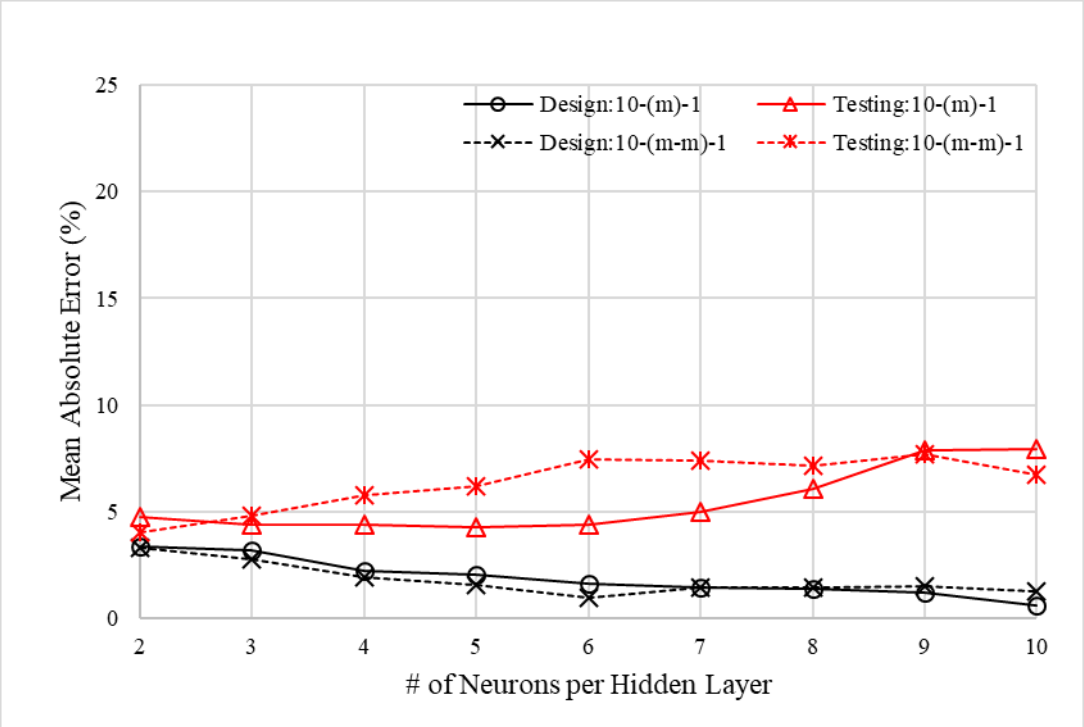

Figure 45. 130 Bridge Design Set Moment ANN Optimization for Levenberg-Marquardt

6.4 Effect of Sample Size

ANN architecture optimization was performed for ANN design sets of varying sizes to investigate ANN error with respect to varying design data sizes. The "best" ANNs for each design set size were defined to be those with the lowest independent testing error. Additional testing and independent testing errors were combined by using a weighted average formula shown in Eqn. 7. Subscripts "1" and "2" correspond to independent and additional testing set errors, respectively. The number of bridges in a testing set is designated by "*n*". Independent and combined testing errors are plotted for moment ANNs and shear ANNs in Figure 46 and Figure 47.

$$Combined\ Testing\ Error = \frac{Error_1 * n_1 + Error_2 * n_2}{n_1 + n_2} \quad \text{Eqn. 7}$$

As expected, the best-performing moment and shear ANNs were those with the largest number of training bridges. For the moment ANNs, the independent testing error is relatively insensitive to design set size. This is because the data points used for the testing set are within the envelope of the design set. However, the combined testing error increases as the number of training bridges decreases because as more bridges are removed from the training set, additional testing set bridges are increasingly likely to fall at an edge of the population where prediction accuracy begins to degrade. Interestingly, the independent and combined testing error are surprisingly low for an ANN trained using only 20 bridges.

Shear ANNs exhibit similar trends, though with generally higher error, and particularly high sensitivity at very low ANN design set size (sharp jump from 20 to 30 bridges in the design set). The combined testing error is also higher than the independent testing error by a larger gap for shear than for moment ANNs for most design set sizes.

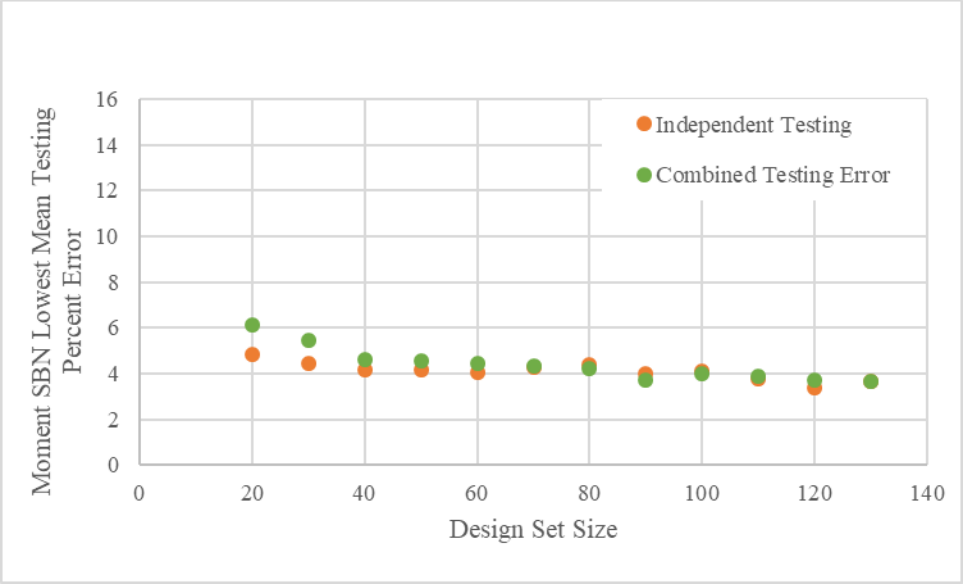

Figure 46. Lowest Mean Absolute Testing Error for Moment ANNs vs. Design Set Size

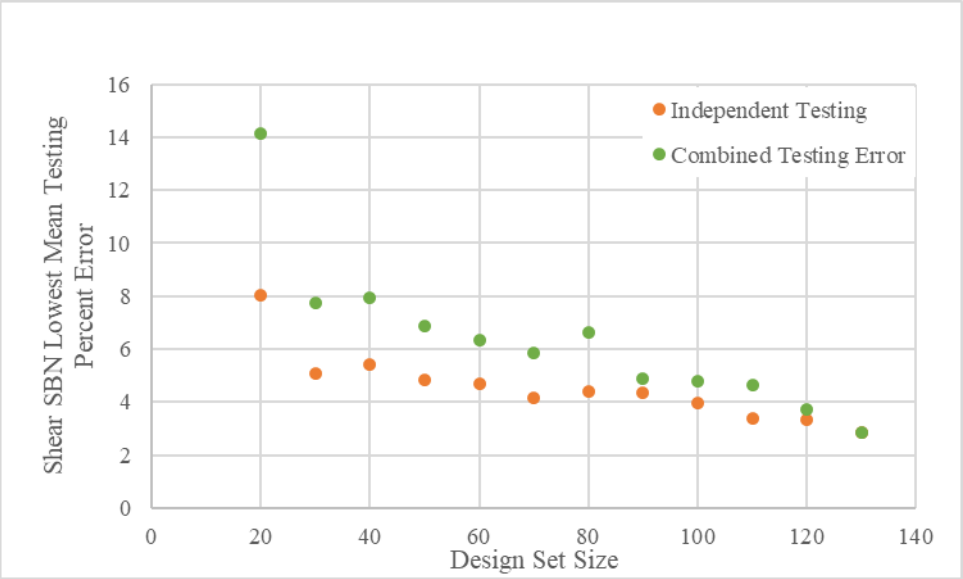

Figure 47. Lowest Mean Absolute Testing Error for Shear ANNs vs. Design Set Size

6.5 Contributions of Governing Parameters

10 governing parameters were used to train ANNs to predict girder distributions factors. Weights connect all of the inputs to all of the nodes in the first hidden layer and are taken as a value between -1 and 1. The weights between the inputs and the first hidden layer for the best moment ANN is shown below in Table 14. The matrix is a 5 by 10 matrix. The 5 corresponds to the best hidden network architecture (10-5-5-1) which has 5 nodes in the first hidden layer. The 10 corresponds to the governing parameters in the following order: length, girder spacing, longitudinal stiffness, cross-frame presence, number of girders, skew, barrier inner edge distance, deck thickness, concrete compressive strength, and steel yield strength.

Table 14. Weights between 10 Inputs and Nodes of 1st Hidden Layer

-0.792	0.309	0.227	-0.312	-0.284	-0.146	-0.106	0.079	-0.180	0.146
0.569	0.069	-0.131	-0.022	-0.353	0.247	-0.030	-0.371	0.246	-0.323
-0.098	-0.145	0.258	-0.029	0.516	0.048	1.014	-0.361	-0.137	0.063
-0.093	-0.368	0.224	-0.229	-0.042	-0.081	0.308	-0.389	-0.124	-0.248
-0.153	-0.351	0.055	-0.118	0.316	0.376	-0.086	-0.082	0.092	0.178

The columns of the weights shown in Table 14 correspond to the weights of the governing parameters. Weights that are close to 0 reflect an inconsequential parameter for the ANN. Each parameter's weight was averaged to examine the relative significance among the parameters with respect to the trained ANN. Table 15 presents the absolute values of arithmetic averages for each column in Table 14. Deck thickness and barrier inner edge distance are observed to have the highest absolute average influence, while concrete compressive stress, steel yield stress, and number of girders had the least absolute average influence. As expected, terms relating to stiffness (generally depth and span) tend to be more influential than material properties when the objective is to determine girder distribution factors, rather than load ratings (as in Sofi's original study).

Table 15. Absolute Value of the Average Weight for Best Moment ANN

Governing Parameter	**Absolute Value of the Average Weight**
Deck Thickness	0.22
Barrier Inner Edge Distance	0.22
Presence of Cross Frames/Diaphragms	0.14
Longitudinal Stiffness	0.13
Length	0.11
Girder Spacing	0.10
Skew	0.09
Steel Yield Stress	0.04
Number of Girders	0.03
Concrete Compressive Stress	0.02

7 Reliability Calibration

7.1 Introduction

ANN prediction error introduces additional uncertainty into live loads, which must be integrated into load rating evaluations. Although ANN error is on average small, approximately 50% of rating factors will be unconservative if AASHTO LRFR partial safety factors are used without calibration. To mitigate potentially unconservative load ratings, a reliability calibration was performed to account for additional live load uncertainty from ANN error. The goal of these analyses was to produce an updated live load partial safety factor that corresponds with the same reliability index targeted in AASHTO LRFR. Reliability calibration methods are described in NCHRP Project 20-07, Task 186 (Kulicki et al. 2007), NCHRP Report 368 (Nowak 1999), NCHRP Report 454 (Moses 2001), and Nowak and Collins (2013). Two reliability determination methods described in literature were used in this study: First Order Reliability Method using Rackwitz-Fiessler and Monte Carlo Simulation. Distribution types, coefficient of variations, and dynamic amplification characterization are consistent with NCHRP Project 20-07, Task 186 (Kulicki et al. 2001). All uncertain parameters, including ANN-predicted GDFs, are assumed to be statistically independent.

7.2 Reliability Determination and Calibration Methodology

One objective of this study was to calibrate reliability to reflect ANN prediction uncertainty. However, the suite of bridges in the study reflected a wide range of engineering designers, who could exercise varying levels of diligence and conservativism. Additionally, older bridges were often designed to unknown standards. Such structures may have been designed for

lower loads and using either more conservative or liberal practice methodologies. To avoid these potential sources of bias across the population, baseline reliability indices for each bridge in the study were calculated using FEM live load demands.

The proposed theoretical reliability calibration procedure progresses through two Stages, as summarized in Table 16. The Baseline Stage, which will be indicated in equations with a 0 subscript, represents current AASHTO LRFD/R calibration in the Bridge Design Specifications (2015) and Manual for Bridge Evaluation (2013). The only modification from routine load rating is the use of detailed modeling to determine static live load effects. The load rating factor is therefore generally higher than routine load rating.

When the live load demand is determined from ANN predictions, rather than detailed modeling, the nominal and mean static live loads are nearly identical to those from Baseline detailed modeling. However, the ANN-based live load is more uncertain because of prediction errors. The Updated Stage, which will be indicated in equations with a 1 subscript, produces a load rating factor reflecting an increased live load factor to accommodate additional uncertainty introduced by ANN prediction error.

Table 16. Nomenclature of Live Load, Live Load Partial Safety Factors, and Rating Factors

		L	γ	RF
Stage	Baseline	FEA static live load effect with typical AASHTO live load COV	Unadjusted AASHTO LRFR	Corresponds to FEA live load and unadjusted AASHTO LRFR γ
	Updated	ANN static live load effect with increased COV from ANN uncertainty	Increased for live load, unchanged for other terms	Reduced from Baseline to account for additional LL uncertainty.

7.2.1 AASHTO LRFR Strength I Calibration Format

The general form of the governing AASHTO strength-based limit state function, g, is written below in Eqn. 6:

$$g(R, DC, DW, L) = R - DC - DW - L = 0 \quad \text{Eqn. 8}$$

Where R represents resistance, DC represents dead load from components (e.g., girders, deck), DW represents dead load from a wearing surface, and L represents the effect of traffic live load. Each term represents an uncertain quantity characterized by probabilistic parameters, such as mean and standard deviation, or related terms such as nominal values, biases, and coefficients of variation. Nominal values will be indicated with a subscript *n*. Additionally, AASHTO considers dynamic amplification as an integral component of live load traffic demand on bridge structures. In the following methodology, static and dynamic live loads will be indicated with *st* and *dyn* subscripts, respectively.

A probabilistic limit state function can be characterized with deterministic values for each probabilistic parameter corresponding to the critical design condition (a unique point in hyperdimensional space) along the limit state surface, referred to as the design point:

$$g = {x_R}^* - {x_{DC}}^* - {x_{DW}}^* - {x_{L,dyn}}^* = 0 \quad \text{Eqn. 9}$$

In Eqn. 9, the terms are marked with "*" to indicate that the terms are deterministic values at the design point, rather that uncertain probabilistic terms as in Eqn. 6. A convenient form of the resulting equation at the design point represents parameters mean values, μ, scaled by partial safety factors, γ, as shown in Eqn. 10:

$$g = \gamma_{R,0}\mu_R - \gamma_{DC,0}\mu_{DC} - \gamma_{DW,0}\mu_{DW} - \gamma_{L,0}\mu_{L,dyn,0} = 0 \quad \text{Eqn. 10}$$

Design codes typically implement a format in terms of nominal values, rather than mean values. For example, specified compressive strength of concrete, f'_c, is a nominal value. The actual strength of concrete supplied to job sites will vary from batch to batch, even when supplied by the same manufacturer and using the same raw materials, because of tolerances in measurements and inherent variabilities such as aggregate particle sizes, mixing proportions, heterogeneous distributions of constituent materials, and curing conditions. Actual supplied concrete strength is likely to be higher than the nominal specified value, so the mean-to-nominal concrete strength is expected to be greater than one. The discrepancy between mean and nominal values for each term is incorporated into reliability calibrations through a bias factor, λ, as shown in Eqn. 11 for a general parameter probabilistic parameter X:

$$\mu_X = \lambda_X X_n \qquad \text{Eqn. 11}$$

Substituting bias and nominal values for mean values, the governing limit state characterized at the design point becomes:

$$g = \gamma_{R,0}\lambda_R R_n - \gamma_{DC,0}\lambda_{DC} DC_n - \gamma_{DW,0}\lambda_{DW} DW_n - \gamma_{L,0}\lambda_L L_{n,dyn,0} = 0 \qquad \text{Eqn. 12}$$

According to NCHRP 20-07 / 186 (Kulicki et al. 2007), AASHTO LRFD has been calibrated based on an assumption that the probabilistic mean live load dynamic amplification effect relative to static load is 10%. However, the deterministic AASHTO design and evaluation format has been calibrated such that 33% is typically applied to the truck load (lane load is not amplified). Partitioning nominal dynamic live load into nominal static live load and a dynamic amplification factor:

$$x_L{}^* = \gamma_{L,0}\mu_{L,dyn,0} = \gamma_{L,0}\mu_I\mu_{L,st,0} = \ where\ \mu_I = 1.1 \qquad \text{Eqn. 13}$$

The AASHTO LRFD calibration effectively introduces a supplemental bias for dynamic amplification complementary to the general live load bias, $\lambda_{L,dyn}$. The AASHTO code live load amplification is represented below as I_{AASHTO}:

$$x_L{}^* = \gamma_{L,0}\left[\lambda_{L,dyn} L_{n,st,0} \mu_I\right] \frac{(1 + I_{AASHTO})}{(1 + I_{AASHTO})} \quad \text{Eqn. 14}$$

Defining the supplemental AASHTO LRFD live load amplification calibration bias as:

$$\lambda_I = \frac{\mu_I}{(1 + I_{AASHTO})} \quad \text{Eqn. 15}$$

Eqn. 14 can be rearranged to a format similar to that found in AASHTO LRFD:

$$x_L{}^* = [\gamma_{L,0} \lambda_{L,st} \lambda_I][L_{n,st,0}(1 + I_{AASHTO})] \quad \text{Eqn. 16}$$

In Eqn. 16, the multiplicative product of terms in the first set of square brackets represent the live load factor adopted in AASHTO LRFD.

The nominal live load term represents an induced load effect in a structural element, and is therefore influenced not only by vehicle weight traveling across a bridge, but also by analysis method. Static traffic gravity load is proportioned to individual girders similar to the approximate analysis method available in AASHTO, using girder distribution factors (GDFs). In the present study, analysis is performed either using detailed FEMs (Baseline, 0), or by substituting ANN-predicted GDFs (Updated, 1). For the Baseline stage:

$$L_{n,st,0} = L_{HL-93} GDF_0 \quad \text{Eqn. 17}$$

For design with LRFD, live load is specified, and a required resistance is calculated that will provide acceptable minimum reliability. For bridge load rating evaluations with LRFR, capacity is known, and the objective is to determine the scaled value of live load that can safely

be carried. Multiplying the nominal live load by a scaling factor, RF, theoretically configures the rating evaluation to represent a target reliability.

$$x_L{}^* = [\gamma_{L,0}\lambda_{L,st}\lambda_I][L_{HL-93}GDF_0RF_0(1 + I_{AASHTO})] \quad \text{Eqn. 18}$$

$$\gamma_L^n = [\gamma_{L,0}\lambda_{L,st}\lambda_I] \quad \text{Eqn. 19}$$

$$Nominal\ Live\ Load\ Term = [L_{HL-93}GDF_0RF_0(1 + I_{AASHTO})] \quad \text{Eqn. 20}$$

7.2.2 Determining β with the Modified Rackwitz-Fiessler Method

The Rackwitz-Fiessler method was implemented as described in Nowak and Collins (2013). The first step to evaluate bridge reliability for strength is to quantify probabilistic characteristics for live load, dead load, and resistance. The stastistical parameters used in this study are shown in Table 16, which were taken from NCHRP Project 20-07 / 186 (Kulicki et al. 2007). These values correspond to a 75-year bridge design life. Live load uncertainties are associated with the load vehicle (weight, axle spacing, etc.), number of lanes loaded, and dynamic load amplification.

Table 17. Assumed Statistical Parameters

Case	Bias	COV	Distribution
Component Dead Load	1.05	0.1	Normal
Wearing Dead Load	1.00	0.25	Normal
Live Load	1.18	0.18	Normal
Resistance	1.12	0.1	Lognormal

The COV for live load correlates to dynamic live load (static plus dynamic amplification). Dynamic live load amplification was assumed equal to 10% of the static live load, consistent with Kulicki et al (2007). The method to account for probabilistic versus code-based dynamic impact was discussed in the preceding section. The limit state equation is shown below in Eqn. 21. Inclusion of the RF term should result in reasonably uniform reliabilities across the study population. RF values were determined for each bridge using the LRFR method. The anticipated reliability index for the limit state with the inclusion of RF is therefore approximately 2.5.

$$g(R, DC, DW, L) = \mathrm{R} - \mathrm{DC} - \mathrm{DW} - RF_0 * L_{dyn,0} = 0 \quad \text{Eqn. 21}$$

Next, initial design points (x_i^*) are determined. Mean values are used as a starting point for all parameters except live load (Eqn. 22 – Eqn. 25). The live load initial design point is constrained to coincide with the limit state failure surface (Eqn. 26).

$$g = x_R^* - x_{DC}^* - x_{DW}^* - x_L^* = 0 \quad \text{Eqn. 22}$$

$$x_R^* = \mu_R = \lambda_R * R_n \quad \text{Eqn. 23}$$

$$x_{DC}^* = \mu_{DC} = \lambda_{DC} * DC_n \quad \text{Eqn. 24}$$

$$x_{DW}^* = \mu_{DW} = \lambda_{DW} * DW_n \quad \text{Eqn. 25}$$

$$x_L^* = x_R^* - x_{DC}^* - x_{DW}^* \quad \text{Eqn. 26}$$

The mean live load, including the rating factor as noted previously, is:

$$\mu_L = \lambda_L RF_0 L_{dyn,0} = \lambda_L RF_0 L_{n,st,0} \mu_I \quad \text{Eqn. 27}$$

Eqn. 28 and Eqn. 29 convert non-normal random distributions (i.e., lognormal resistance) to equivalent normal distributions at the design point, where Φ and ϕ represent the standard normal cumulative distribution function (CDF) and probability density function (PDF).

$$\sigma_X{}^e = \frac{1}{f_X(x_i{}^*)}\phi[\phi^{-1}(F_X(x_i{}^*))] \quad \text{Eqn. 28}$$

$$\mu_X{}^e = x_i{}^* - \sigma_X{}^e[\phi^{-1}(F_X(x_i{}^*))] \quad \text{Eqn. 29}$$

The limit state function with normalized distributions is next written in terms of reduced variates, $z_i{}^*$, as shown in Eqn. 30 and Eqn. 31. A column vector, $\{G\}$, is then determined by calculating and compiling partial derivatives of the limit state function, as shown in Eqn. 32 and Eqn. 33.

$$z_i{}^* = \frac{x_i{}^* - \mu_i}{\sigma_i} \quad \text{Eqn. 30}$$

$$g = \mu_{R,O}{}^e + z_R{}^*\sigma_R{}^e - (\mu_{DC} + z_{DC}{}^*\sigma_{DC}) - (\mu_{DW} + z_{DW}{}^*\sigma_{DW}) - (\mu_L + z_L{}^*\sigma_L) = 0 \quad \text{Eqn. 31}$$

$$\{G\} = \begin{pmatrix} G_1 \\ G_2 \\ \vdots \\ G_n \end{pmatrix}, \text{ where } G_i = -\frac{\partial g}{\partial Z_i}|\{z_i{}^*\} \quad \text{Eqn. 32}$$

$$\{G\} = \begin{pmatrix} -\sigma_R{}^e \\ \sigma_{DC} \\ RF_0\sigma_{DW} \\ \sigma_L \end{pmatrix} \quad \text{Eqn. 33}$$

Next, α and β can be estimated based on the sensitivy factors, $\{G\}$.

$$\beta = \frac{\{G\}^T * \{z^*\}}{\sqrt{\{G\}^T * \{G\}}} \quad \text{Eqn. 34}$$

$$where\ \{z^*\} = \begin{pmatrix} z_1{}^* \\ z_2{}^* \\ \vdots \\ z_n{}^* \end{pmatrix} \quad \text{Eqn. 35}$$

$$\alpha = \frac{\{G\}}{\sqrt{\{G\}^T\{G\}}} \quad \text{Eqn. 36}$$

Lastly, the design point in reduced variates is updated using α and β and converted back to original coordinates, according to Eqn. 37 – Eqn. 39. The design point is updated and iterated until β converges to a minimum value.

$$z_i^* = \alpha_i \beta \quad \text{Eqn. 37}$$

$$x_i^* = \mu_{x_i}^e + z_i^* \sigma_{x_i}^e \quad \text{Eqn. 38}$$

$$x_L^* = x_R^* - x_{DC}^* - x_{DW}^* \quad \text{Eqn. 39}$$

7.2.3 Determining β with Monte Carlo Simulation

Monte Carlo Simulation (MCS) was performed to validate the results of the modified Rackwitz-Fiessler Method. MCS is performed by generating an arbitrarily large number of sample points for each random variables according to their respective probabilistic distributions. The limit state equation was evaluated by substituting the randomly generated parameter values, and the probability of failure was determined by counting the number of instances in which the limit state equation was violated (i.e., total dead and live load exceeded capacity) and dividing the number of failure outcomes by total trials. Finally, the reliability index, β, was determined by taking the negative inverse of the standard normal cumulative distribution function evaluated at the sampled failure probability. Eqn. 40 – Eqn. 43 illustrate the procedure. Sample sizes were increased until the probability of failure converged. Ultimately, a total of one million samples was used for reported MCS results to reliably capture a probability of failure approximately 0.62% (corresponding to an Operating level reliability index of 2.5).

$$g(R, DC, DW, L) = \mathrm{R} - \mathrm{DC} - \mathrm{DW} - \left(L = RF_0 * L_{0,dyn}\right) = 0 \quad \text{Eqn. 40}$$

$$if\ g_i < 0, Failure\ is\ Recorded \quad \text{Eqn. 41}$$

$$Prob.of\ Failure = \frac{Sum\ of\ Failures\ Recorded}{Number\ of\ Limit\ State\ Scenarios} \quad \text{Eqn. 42}$$

$$\beta = \Phi^{-1}(Prob.of\ Failure) \quad \text{Eqn. 43}$$

7.2.4 Study Population Baseline Reliability

Both the modified Rackwitz-Fiessler and Monte Carlo procedures were performed for all bridges in the inventory. When an Operating rating factor was used in the two procedures with an impact factor of 33%, the resulting reliabilities were found to be slightly below the target reliability nominally expected for Operating capacities (2.5). The modified Rackwitz-Fiessler and Monte Carlo methods resulted in average β values of 2.22 and 2.23, respectively, for moment analyses. Histograms of β values from the two methods are shown below in Figures 48 and 49 for moment and shear, respectively, confirming excellent agreement between the two methods. The maximum difference between reliability indexes for a given bridge is less than 2%. Reliability indices were similarly calculated corresponding to LRFR Inventory ratings. Inventory reliability indices are shown for moment and shear in Figure 50 and Figure 51.

The Inventory reliability indices are similar to data presented in Kulicki et al. (2007). The AASHTO MBE (2019) states in C6A.1.3 that the "LRFR procedures … adopt a reduced target reliability index of approximately 2.5 calibrated to past AASHTO operating level load rating." This statement echoes Moses (2001), which noted that Operating reliability indices corresponded to a target in the range of 2.3 to 2.5. Therefore, the Operating reliability results are reasonably consistent with the approximate basis implemented by AASHTO when establishing LRFR live load factors.

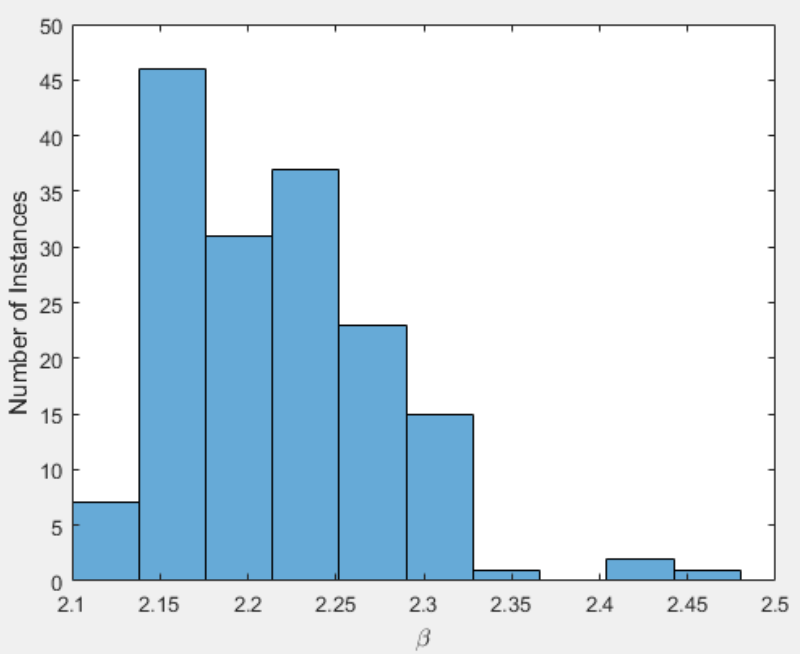

(a)

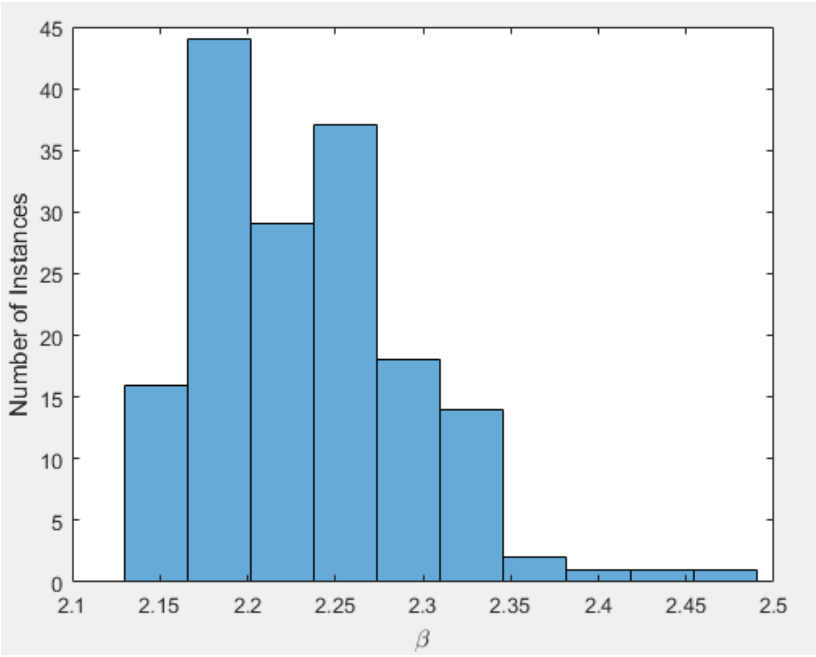

(b)

Figure 48. Operating Level FEM Moment β results from (a) the modified Rackwitz-Fiessler Method and (b) Monte Carlo Simulations.

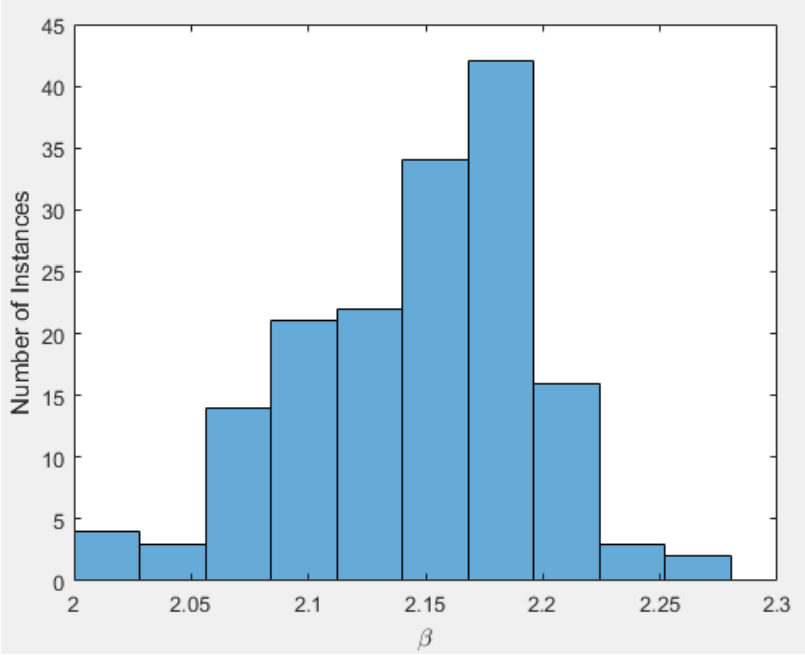

(a)

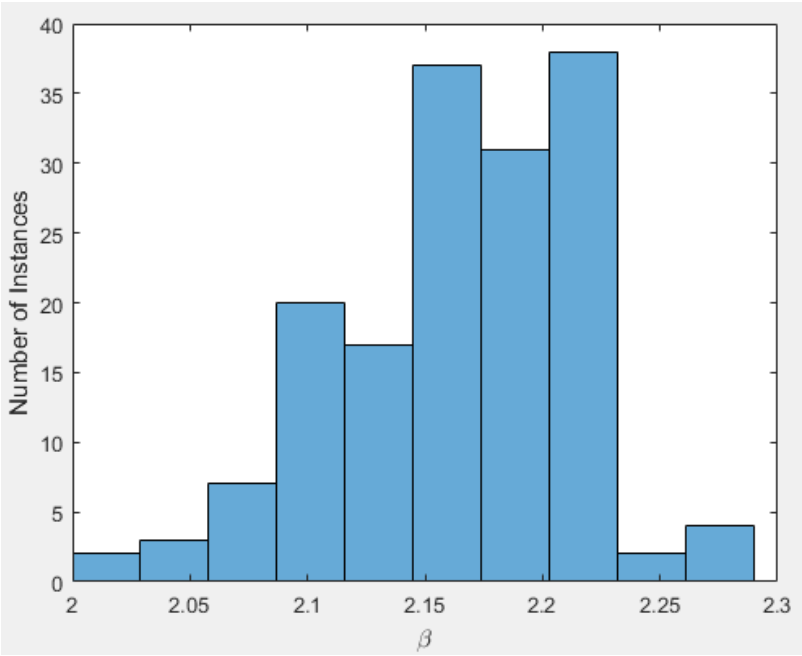

(b)

Figure 49. Operating Level FEM Shear β results from (a) the modified Rackwitz-Fiessler Method and (b) Monte Carlo Simulations.

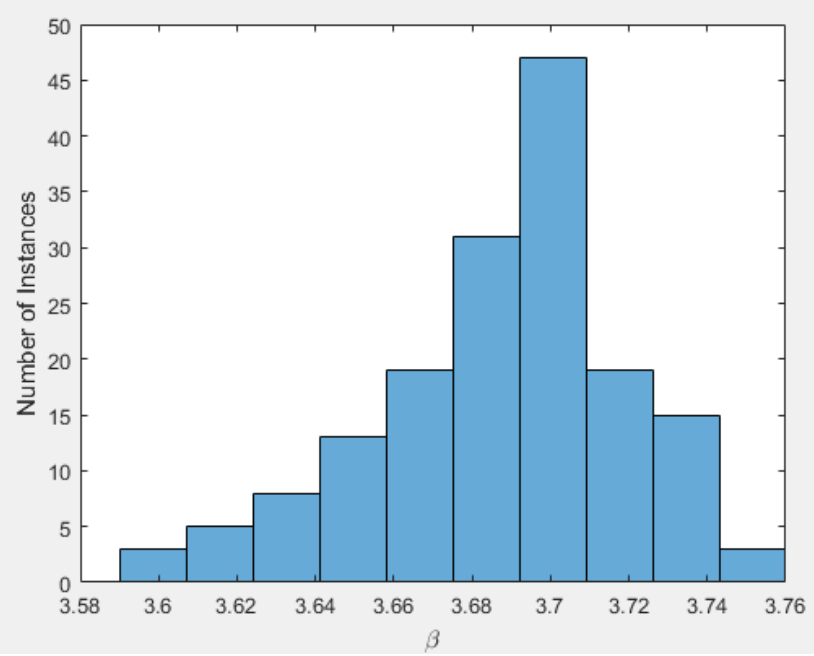

(a)

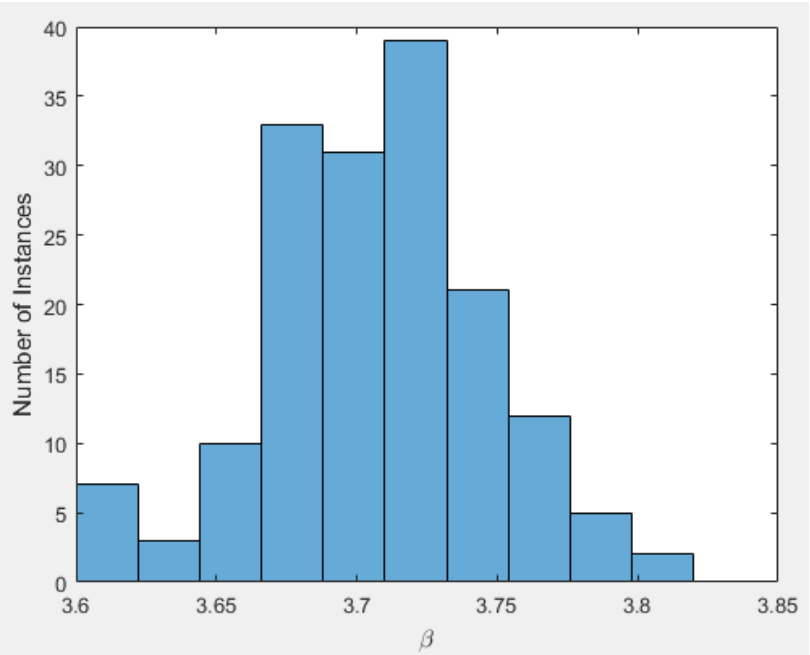

(b)

Figure 50. Inventory Level FEM Moment β results from (a) the modified Rackwitz-Fiessler Method and (b) Monte Carlo Simulations.

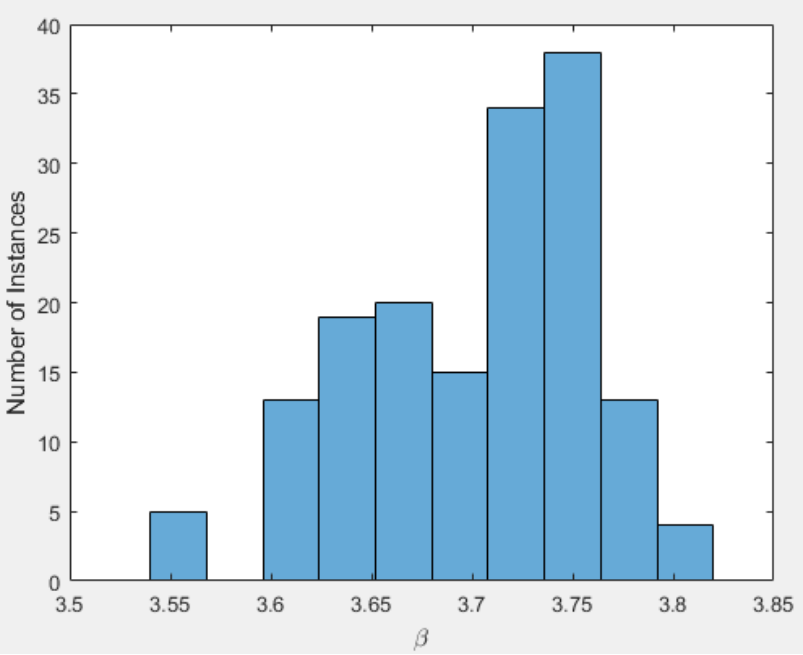

(a)

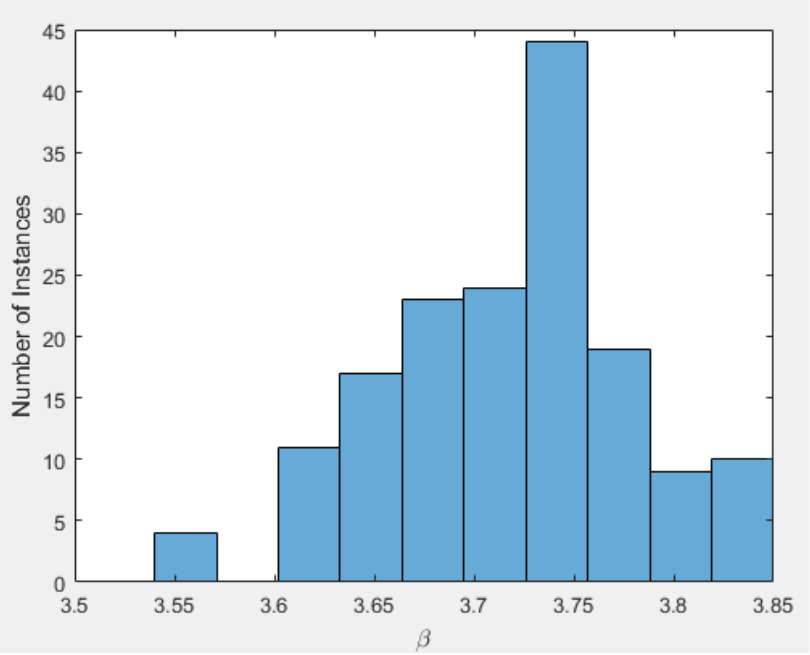

(b)

Figure 51. Inventory Level FEM Shear β results from (a) the modified Rackwitz-Fiessler Method and (b) Monte Carlo Simulations.

7.3 Live Load Statistical Parameters Including Additional ANN Uncertainty

If live load GDFs are determined from ANNs rather than mechanistic models, additional live load uncertainty must be incorporated to account for ANN prediction errors. A numerical method was used to explicitly reflect prediction bias. First, a random normal distribution that corresponds to the live load model was created. For simplicity, a mean of 1 was used. A COV of 18% was used to create an initial distribution, consistent with AASHTO LRFD/R dynamic live load variation. This distribution will be referred to as the original distribution, herein.

In the following step, the ANN uncertainties are used to generate a new random distribution that reflects ANN tendencies. ANN error appears to be roughly normal. The single best moment ANN produced a mean GDF ratio of 1.0 (as expected for a well-trained network) with a standard deviation of 5.70% based on independent testing. Since the live load random variable corresponds to the product of the ANN-produced GDF and the dynamic load effect, the expected mean is the product of the ANN prediction error and the mean of the original distribution. Likewise, the new distribution error will be the product of the ANN standard deviation and the mean of the original distribution. It should be noted that $\mu_{Combined}$ is only used to derive $\sigma_{Combined}$.

$$Error_{ANN,Cal} = \frac{GDF_{FEM}}{GDF_{ANN}} \quad \text{Eqn. 44}$$

$$\mu_{Combined} = \left(Average\ Error_{ANN,Cal}\right) * \mu_{Original} \quad \text{Eqn. 45}$$

$$\sigma_{Combined} = \mu_{Combined} * \sigma_{ANN} \quad \text{Eqn. 46}$$

Finally, the new distribution can be used to find the new COV to use in the rest of the reliability procedure. The new distribution was created by scaling the original distribution by the expected ANN-percent error shown in Eqn. 45. Next, a new point was randomly generated around the updated point with the standard deviation calculated in Eqn. 46. Finally, the new distribution's statistical parameters are calculated. It is anticipated that the COV would be higher, since the live load distribution would be more spread out due to a higher standard deviation caused by ANN error. The new live load COV that accounts for the ANN error is 18.88%, which is higher than the 18% live load COV used to calibrate AASHTO. Figure 52 shows how the updated live load distribution is attenuated and more spread out, however, only slightly. Compared to uncertainties associated to the live load, ANN uncertainty barely adds additional uncertainty.

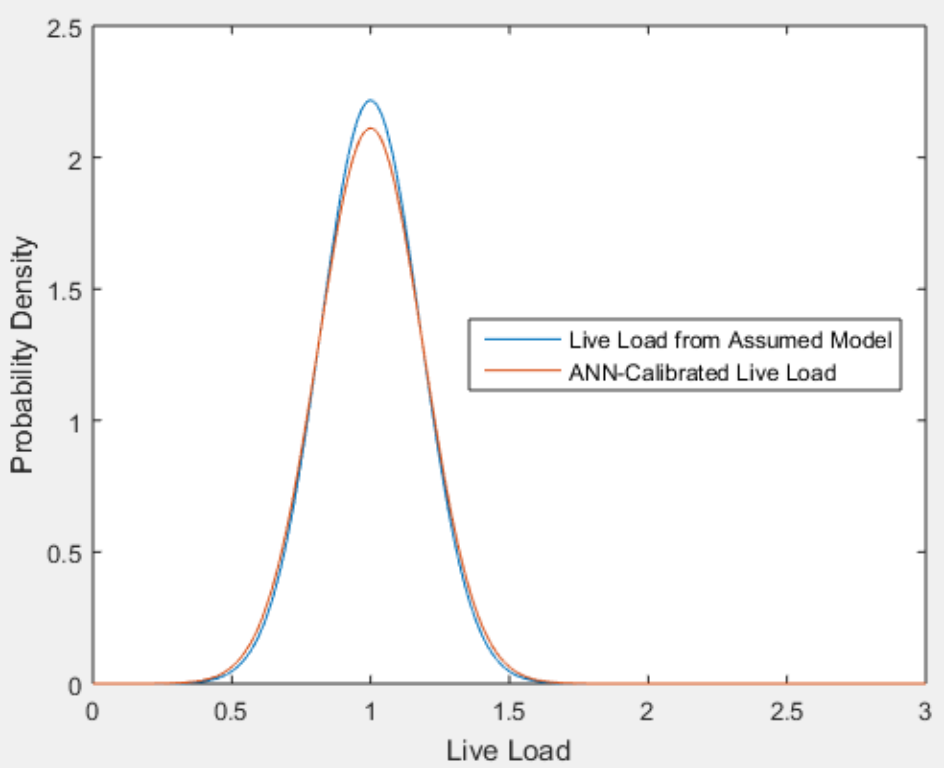

Figure 52. Comparison between Assumed and ANN-Updated Live Load Distributions

A commonly used equation used to combine uncorrelated random distributions is shown below in Eqn. 47 (Nowak and Collins 2013). If the mean values are equivalent, the equation can be rewritten in terms of COV, shown in Eqn. 48. Since the updated live load COV was calculated using an assumed distribution used by Kulicki, the additional COV provided by the ANN can be estimated by using Eqn. 50, which is Eqn. 49 rewritten.

The COV of the ANN, using Eqn. 50, was found to be 5.70%, which is nearly the standard deviation of the ANN of 5.71 when the mean live load is assumed to be 1. Discrepancies are believed to have been introduced by the fact that the true mean values of the ANN are changed slightly due to the average ANN error bias that is neglected in this calculation.

$$\sigma_{Combined} = \sqrt{{\sigma_1}^2 + {\sigma_2}^2} \quad \text{Eqn. 47}$$

$$COV = \frac{\mu}{\sigma} \quad \text{Eqn. 48}$$

$$COV_{Updated} = \sqrt{{COV_{Live\ Load}}^2 + {COV_{ANN}}^2} \quad \text{Eqn. 49}$$

$$COV_{ANN} = \sqrt{{COV_{Updated}}^2 - {COV_{Live\ Load}}^2} \quad \text{Eqn. 50}$$

Since the best shear ANN performed better than the moment ANN, the COV increase is smaller. The ANN-adjusted COV for the shear ANN was found to be 18.48%.

7.4 Partial Safety Factor Recalibrations

7.4.1 Calibration based on Modified Rackwitz-Fiessler Method

The next step is to update live load and, therefore, load rating factors by recalibrating to maintain reliability with additional ANN prediction uncertainty. A "1" subscript is now used to indicate that the reliability calibration reflects additional uncertainty associated with ANN-predicted GDFs.

$$g(R, DC, \mathrm{DW}, L) = 0 = \mathrm{R} - \mathrm{DC} - \mathrm{DW} - RF_1 L_{dyn,1} \quad \text{Eqn. 51}$$

$$g = x_R{}^* - x_{DC}{}^* - x_{DW}{}^* - x_L{}^* = 0 \quad \text{Eqn. 52}$$

The Rackwitz-Fiessler method was implemented similar to the Baseline Stage, except that the reliability index is a target and RF_1 is unknown. As in Stage 0, an initial trial design point was selected using mean values for all parameters except live load, and the live load design point value was calculated to intercept the limit state surface. Accordingly, the initial design point trial was:

$$x_R{}^* = \mu_R = \lambda_R * M_R \quad \text{Eqn. 53}$$

$$x_{DC}{}^* = \mu_{DC} = \lambda_{DC} * M_{DC} \quad \text{Eqn. 54}$$

$$x_{DW}{}^* = \mu_{DW} = \lambda_{DW} * M_{DW} \quad \text{Eqn. 55}$$

$$x_L{}^* = x_R{}^* - x_{DC}{}^* - x_{DW}{}^* \quad \text{Eqn. 56}$$

The mean live load becomes:

$$\mu_L = \lambda_L RF_1 L_{dyn,1} = \lambda_L RF_1 L_{n,st,1} \mu_I \quad \text{Eqn. 57}$$

$L_{n,st,1}$ differs from $L_{n,st,0}$ only in that the GDF is supplied by an ANN for the Updated (subscript 1) case versus FEMs for the Baseline (subscript 0) case. RF_1 was initially assumed equal to RF_0. Equivalent normal parameters were calculated for the lognormal resistance (recall Eqn. 28 and Eqn. 29). The remainder of the procedure is the same as described previously to

arrive at a converged reliability index and design point for a particular assumed RF_1 value (recall Eqn. 30 – Eqn. 39).

After the first iteration, the target reliability is not met since the live load COV has increased from Baseline to Updated Stages. The mean live load term is updated for the next iteration by using the following set of equations. Since the uncertainty has increased, the mean live load value must compensate by decreasing to maintain a consistent probability of failure and reliability index. A scalar, $\zeta_{reduction}$, was introduced to reduce the mean live load. $\zeta_{reduction}$ was incrementally reduced in successive iterations until the target reliability was reached.

$$\mu_L = \lambda_L[RF_1 = \zeta_{reduction} RF_0]L_{1,dyn} \quad \text{Eqn. 58}$$

$$if\ \beta < \beta_{target}, \zeta_{reduction,i+1} = \zeta_{reduction,i} - 0.001 \quad \text{Eqn. 59}$$

Finally, the reduction factor was related to the updated live load partial safety factor as shown in the following equations. The limit state must be satisfied for Baseline and Updated cases, but the resistance and dead load terms are unchanged. The ratio of GDF_0 to GDF_1 can be neglected (taken as 1) because the ANN-predicted GDF is expected to be very similar to that predicted by FEMs.

$$g = \gamma_{R,0}\lambda_R R_n - \gamma_{DC,0}\lambda_{DC} DC_n - \gamma_{DW,0}\lambda_{DW} DW_n - \gamma_{L,0}\lambda_L L_{n,dyn,0} = 0 \quad \text{Eqn. 60}$$

$$g = \gamma_{R,0}\lambda_R R_n - \gamma_{DC,0}\lambda_{DC} DC_n - \gamma_{DW,0}\lambda_{DW} DW_n - \gamma_{L,1}\lambda_L L_{n,dyn,1} = 0 \quad \text{Eqn. 61}$$

$$\gamma_{L,0}\lambda_L L_{n,dyn,0} = \gamma_{L,1}\lambda_L L_{n,dyn,1} \quad \text{Eqn. 62}$$

$$[\gamma_{L,0}\lambda_{L,st}\lambda_I][L_{HL-93} GDF_0 RF_0(1 + I_{AASHTO})] = [\gamma_{L,1}\lambda_{L,st}\lambda_I][L_{HL-93} GDF_1 RF_1(1 + I_{AASHTO})] \quad \text{Eqn. 63}$$

$$\gamma_{L,0} GDF_0 RF_0 = \gamma_{L,1} GDF_1 RF_1 \quad \text{Eqn. 64}$$

$$\gamma_{L,0} GDF_0 RF_0 = \gamma_{L,1} GDF_1 \zeta_{reduction} RF_0 \quad \text{Eqn. 65}$$

$$\gamma_{L,1} = \frac{\gamma_{L,0}}{\zeta_{reduction}} \left(\frac{GDF_0}{GDF_1} \approx 1 \right) \quad \text{Eqn. 66}$$

7.4.2 Calibration based on Monte Carlo Simulation

MCS was again used to validate the calibration results from the modified Rackwitz-Fiessler method. A similar approach was used to reduce the mean live load until the target reliability is met. The live load reduction factor is called $\xi_{reduction}$ in this section. The live load was successively reduced until the resulting probability of failure and reliability index satisfied the respective target values.

$$g(R, DC, DW, L) = \mathrm{R} - \mathrm{DC} - \mathrm{DW} - \xi_{reduction,n} * RF_0 * L_{,dyn} \quad \text{Eqn. 67}$$

$$if\ g_i < 0, Failure\ is\ Recorded \quad \text{Eqn. 68}$$

$$Prob.of\ Failure = \frac{Sum\ of\ Failures\ Recorded}{Number\ of\ Limit\ State\ Scenarios} \quad \text{Eqn. 69}$$

$$\beta = \Phi^{-1}(Prob.of\ Failure) \quad \text{Eqn. 70}$$

$$If\ \beta < \beta_{Target}, \quad \text{Eqn. 71}$$

$$repeat\ with\ \xi_{reduction,n+1} = \xi_{reduction,n} - 0.001$$

Finally, $\xi_{reduction,n}$ was used to update the live load partial safety factor, similar to the procedure shown previously for the modified Rackwitz-Fiessler method.

$$\gamma_{L,1} = \frac{\gamma_{L,0}}{\xi_{reduction,n}} \quad \text{Eqn. 72}$$

7.5 Reliability Calibration Results

Reliability calibration was performed for all bridges that had moment and shear GDF predictions. Distributions of live load safety factors corresponding to Operating rating capacities and targeting a uniform reliability index of 2.5 for the modified Rackwitz-Fiessler method and Monte Carlo Simulations are shown in Figures 53 and 54 for moment and shear, respectively. The resulting moment and shear partial safety range as high as 1.46 and 1.48, respectively. These results represent both accommodation of ANN prediction error uncertainty and a fundamental mean reliability deficiency in the bridge population resulting from the LRFR Operating live load factor (recall Figures 48 and 49).

To isolate the influence of ANN prediction uncertainty, an alternative method was implemented to characterize the influence of ANN error uncertainty on Operating live load factors. The previously described procedures were repeated with both modified Rackwitz-Fiessler and MCS, individually targeting original reliability indices for each bridge instead of a uniform reliability. The resulting calibrated live load factors are shown in Figures 55 and 56 for moment and shear, respectively.

Modified Rackwitz-Fiessler and MCS produced similar results in all reliability calibration analyses. The partial safety factors for both moment and shear decrease significantly when isolating the effect of ANN prediction uncertainty, with maximum live load partial safety factors for moment and shear increasing to 1.37 and 1.36, respectively, from the reference code-specified value of 1.35. The shear partial safety factor is slightly lower than the moment partial safety factor because ANN prediction error was smaller for shear than moment GDFs.

All presented reliability analyses and results assumed fully composite steel girder bridges. Moment reliability analyses were performed assuming noncomposite capacities and rating factors for all bridges having a noncomposite rating factor at least equal to 0.5. According to Kulicki et al. (2007), the resistance bias and coefficient of variation for compact noncomposite steel girders is identical to composite steel girders. The resulting operating level FEM reliabilities were very similar to those found using composite girder capacities. The reliability calibration data presented for composite steel girders is therefore also reasonably representative of noncomposite steel girders.

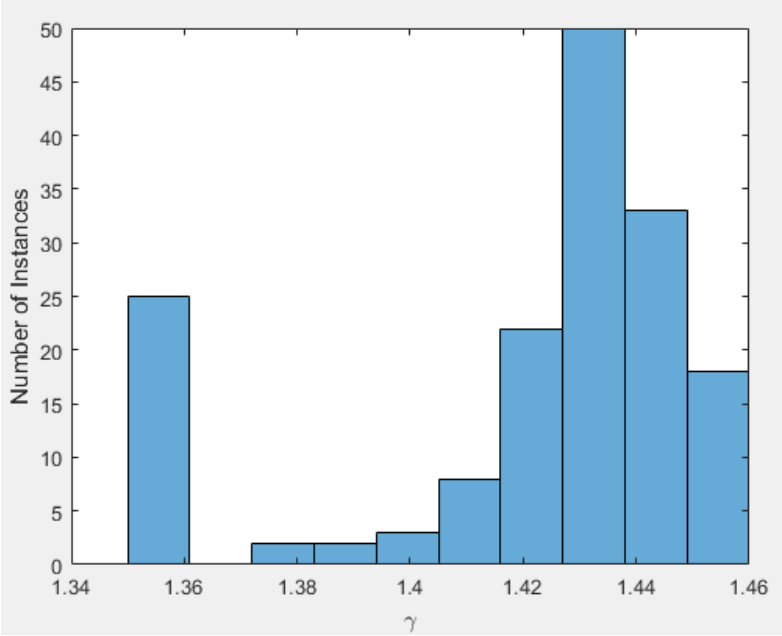

(a)

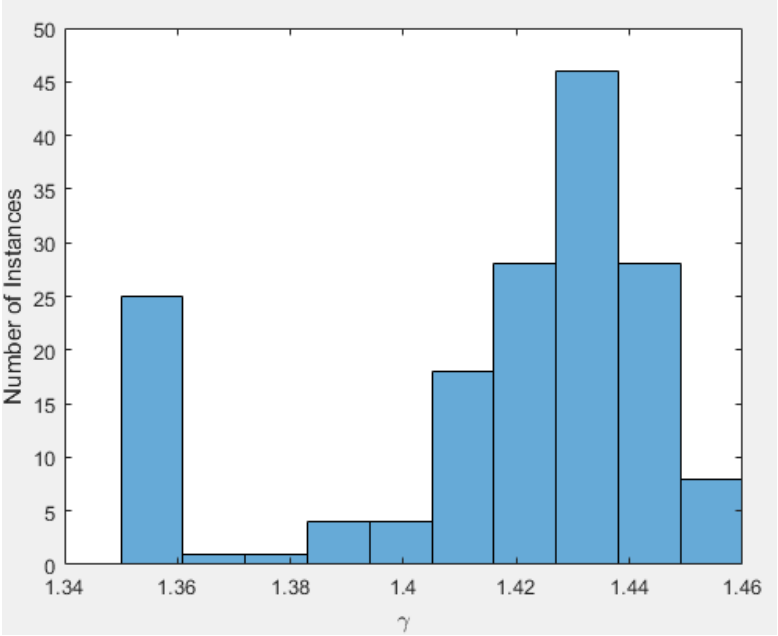

(b)

Figure 53. Calibrated Moment Partial Safety Factor based on a Uniform Target Reliability for (a) Modified Rackwitz-Fiessler Method and (b) Monte Carlo Sampling

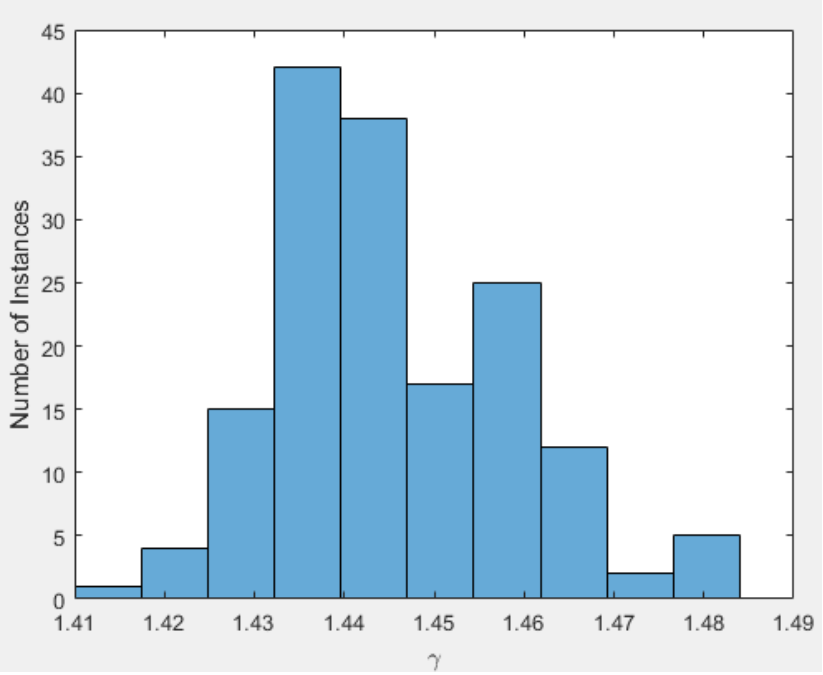

(a)

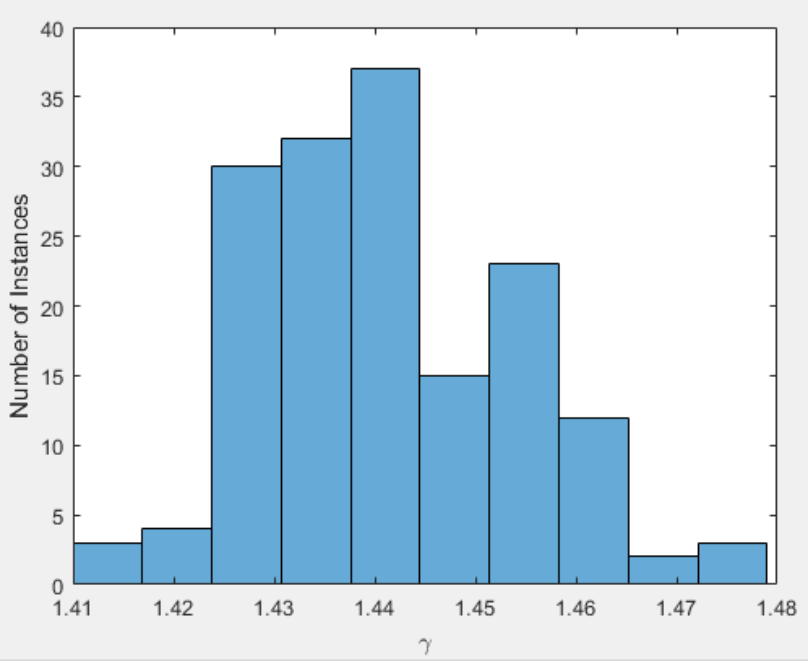

(b)

Figure 54. Calibrated Shear Partial Safety Factor based on a Uniform Target Reliability for (a) Modified Rackwitz-Fiessler Method and (b) Monte Carlo Sampling

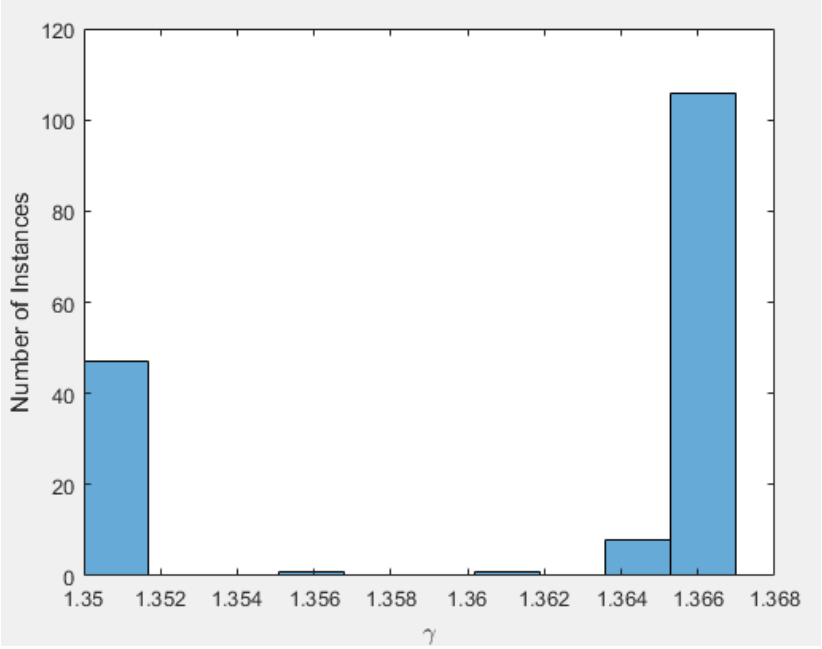

(a)

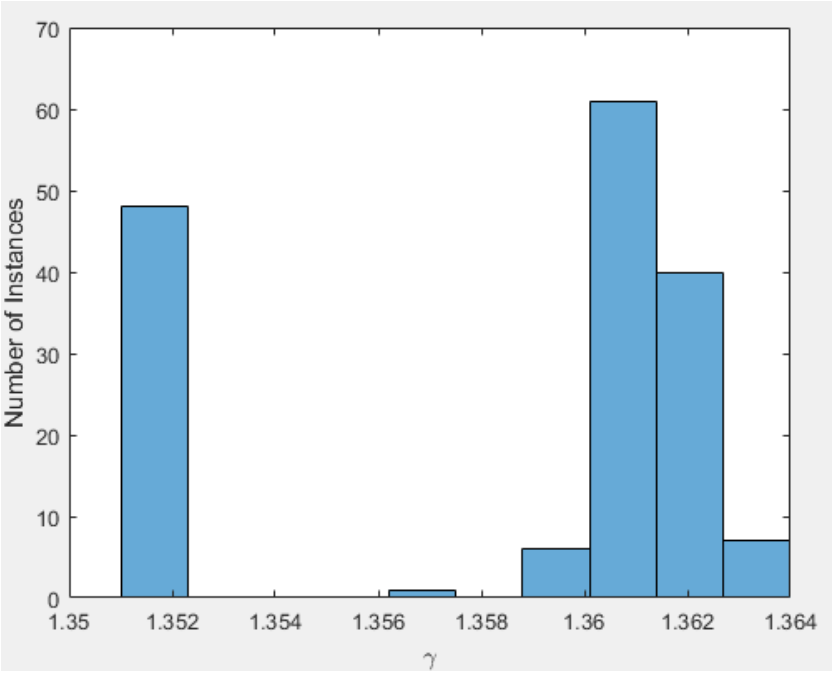

(b)

Figure 55. Calibrated Moment Partial Safety Factor based on FEM Reliability for (a) Modified Rackwitz-Fiessler Method and (b) Monte Carlo Sampling

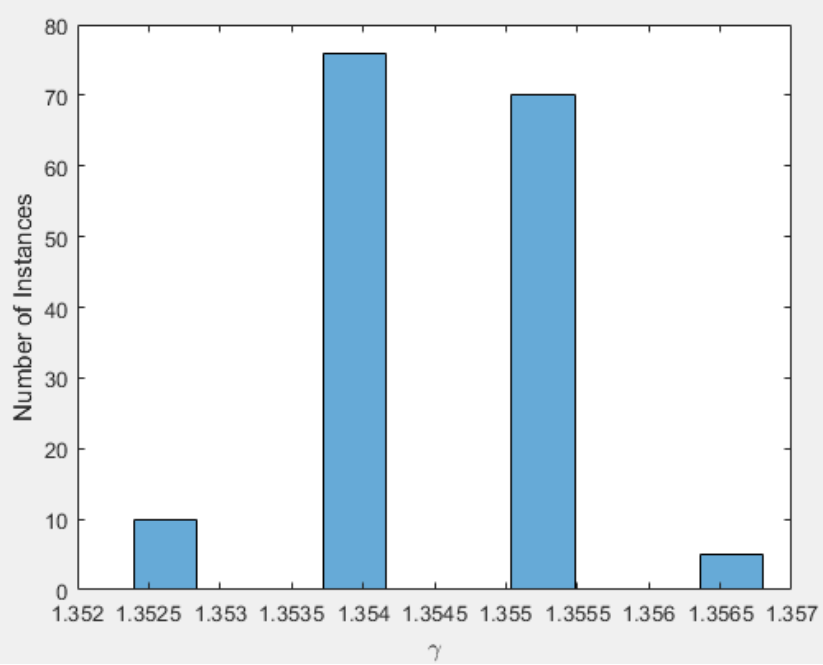

(a)

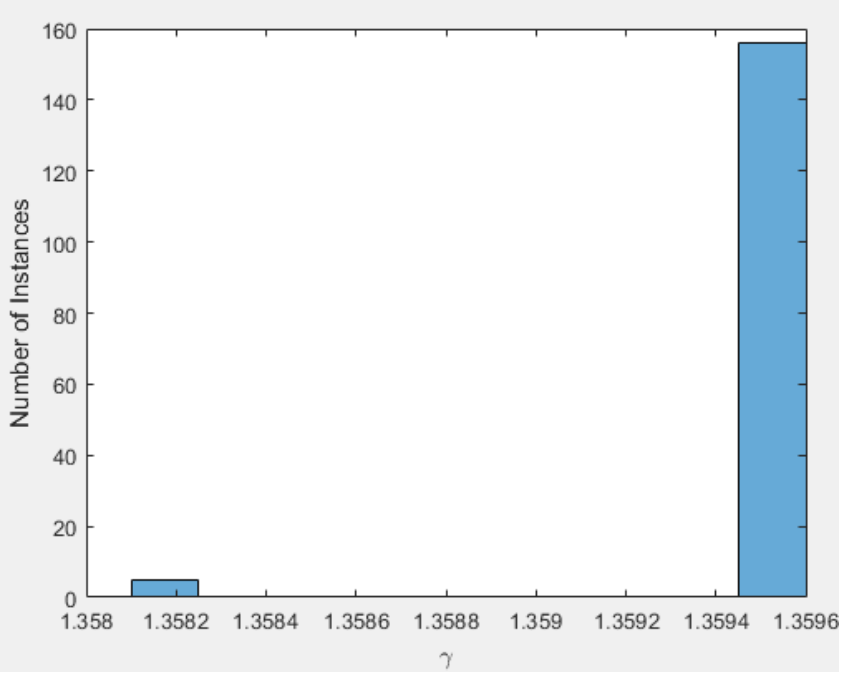

(b)

Figure 56. Calibrated Shear Partial Safety Factor based on FEM Reliability for (a) Modified Rackwitz-Fiessler Method and (b) Monte Carlo Sampling

8 Field Testing Case Study

8.1 Introduction

This project included diagnostic load testing to demonstrate the proposed methodology and potentially remove load restrictions from a currently posted bridge. Bridge C007805310P, shown in Figure 57 and referred to herein as the Yutan Bridge, was selected for a diagnostic load test in consultation with NDOT bridge rating and management personnel. The bridge is located in and owned by Saunders County. In addition to the potential removal of a load posting, the objective of this bridge test was to investigate and validate the suitability of the FEA methodology to accurately capture the live load distribution, which was used for ANN training, and to obtain an experimental load rating for comparison to and validation of a finite element model (FEM) load rating and an ANN load rating. After analyzing results from the load test, results and limitations from the first load test led the team to perform a retest on the bridge with additional instrumentation distributed across the bridge.

Figure 57. Yutan Bridge

The proposed methodology is presented as a flowchart in Figure 58, which is a slightly modified version of the global decision tree presented in Szerszen et al. (2019).

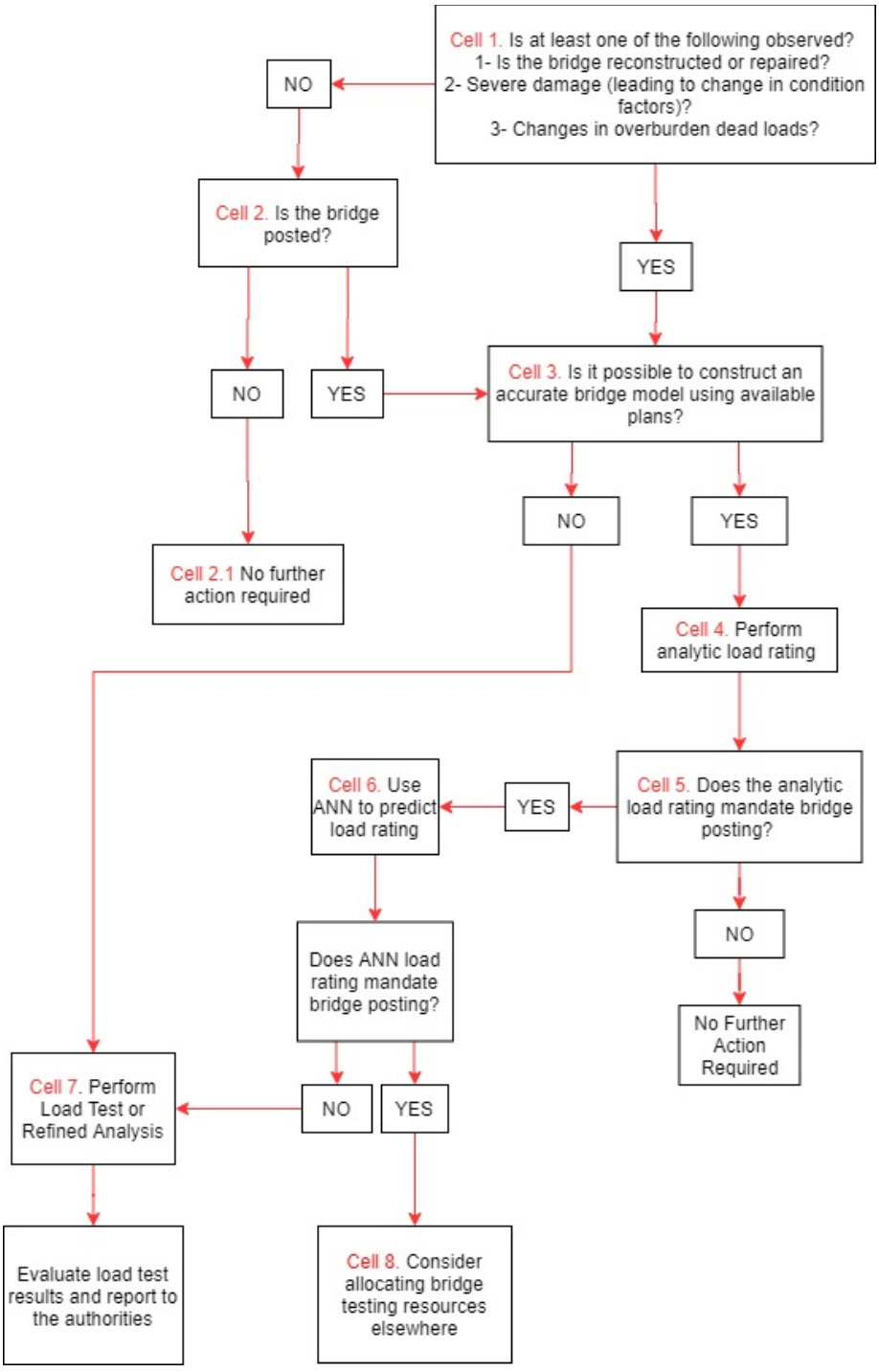

Figure 58. Proposed Methodology

Following the flowchart, none of the conditions in Cell 1 are met, so the procedure progresses to Cell 2. The bridge is posted according to NDOT records. Excerpts from October 2017 and July 2019 Load Rating Summary Sheets are shown in Figures 59 and 60. The 2017 sheet was in effect at the time the bridge was selected for testing in this project. The bridge was noted to have been rated according to Load Factor Rating (LFR) and governed by Strength for flexure. The documented Operating Ratings were 0.83 and 0.896 in 2017 and 2019, respectively. The discussion in this chapter will focus primarily on the Operating level and a Strength limit state. Additional discussion for various other considerations, such as serviceability, is provided at the end of this chapter.

Because the bridge was posted, the procedure continues to Cell 3. Whether or not an "accurate" bridge model could be constructed is subjective. The bridge was built and owned by a county, and documentation was sparse compared to that typically available for state or federally owned bridge assets. Images of the available documentation from NDOT for this bridge are provided in Figures 61 through 63. Presuming that information was adequate to perform a load rating, referring to available load rating records in NDOT records (Figures 59 and 60), the procedure continued to Cell 4.

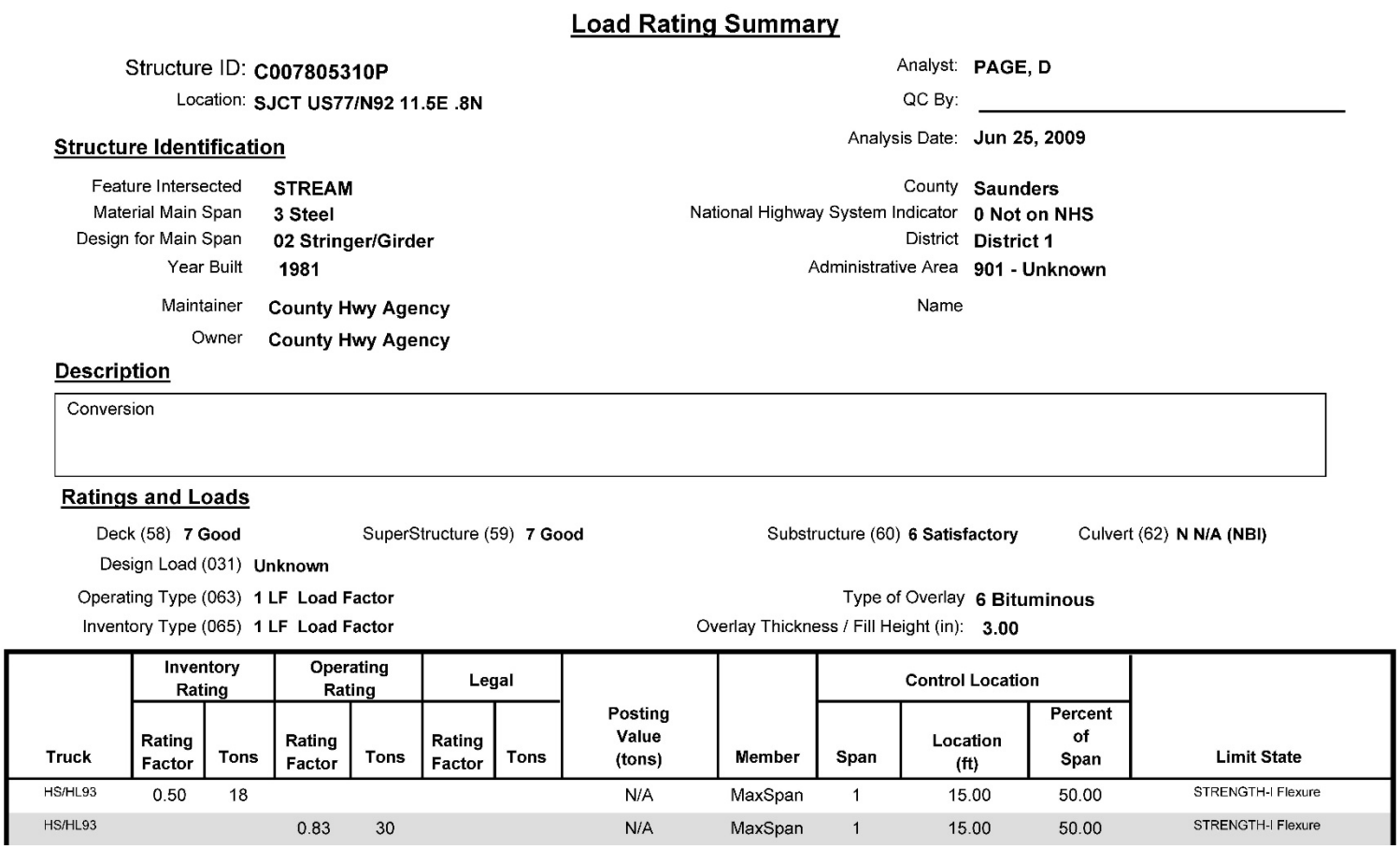

Load Rating Summary

Structure ID: **C007805310P**
Location: **SJCT US77/N92 11.5E .8N**

Analyst: **PAGE, D**
QC By: _____
Analysis Date: **Jun 25, 2009**

Structure Identification

Feature Intersected **STREAM**
Material Main Span **3 Steel**
Design for Main Span **02 Stringer/Girder**
Year Built **1981**
Maintainer **County Hwy Agency**
Owner **County Hwy Agency**

County **Saunders**
National Highway System Indicator **0 Not on NHS**
District **District 1**
Administrative Area **901 - Unknown**
Name

Description

Conversion

Ratings and Loads

Deck (58) **7 Good**
SuperStructure (59) **7 Good**
Substructure (60) **6 Satisfactory**
Culvert (62) **N N/A (NBI)**
Design Load (031) **Unknown**
Operating Type (063) **1 LF Load Factor**
Inventory Type (065) **1 LF Load Factor**
Type of Overlay **6 Bituminous**
Overlay Thickness / Fill Height (in): **3.00**

Truck	Inventory Rating		Operating Rating		Legal		Posting Value (tons)	Member	Control Location			Limit State
	Rating Factor	Tons	Rating Factor	Tons	Rating Factor	Tons			Span	Location (ft)	Percent of Span	
HS/HL93	0.50	18					N/A	MaxSpan	1	15.00	50.00	STRENGTH-I Flexure
HS/HL93			0.83	30			N/A	MaxSpan	1	15.00	50.00	STRENGTH-I Flexure

Figure 59. Excerpt from Yutan Bridge October 2017 Load Rating Summary Sheet

Load Rating Summary

Structure Id: C007805310P

Location: SJCT77 / 92 11.5E 0.8 N

Analyst:DPage
QC By: [signature] 7/11/19
Analysis Date:**November 26, 2018**

Structure Identification

Feature Intersected: **Stream**
Material Main Span. (43A) : 3 Steel
Design for the Main Span. (43B) : 02 Stringer/Girder
Year Built: **1981**
Maintainer : **County Hwy Agency**
Owner : **County Hwy Agency**

County : **Saunders**
National Highway System Indicator : **0 Not on NHS**
District : **District 1**
Administrative Area : **901 - Unknown**

Name : **Simple span 30.5 ft**
Emergency Route : Off

Description:
Girders appear salvaged . 33 ksi used for girder steel

Ratings and Loads

Deck (058) : 7 Good
Superstructure (059) : 7 Good
Substructure (060) : 6 Satisfactory
Culvert (062) : N N/A (NBI)
Design Load (031) : 0 Unknown
Depth & Type of Overlay : Asphalt
Operating Type (063) : 1 LF Load Factor
Wearing Surface Thickness / Fill Height (in) :3
Inventory Type (065) : 1 LF Load Factor

Truck	Inventory Rating		Operating Rating		Legal		Posting Value (tons)	Member	Control Location			Limit State
	Rating Factor	Tons	Rating Factor	Tons	Rating Factor	Tons			Span	Location (ft)	Percent of Span	
HS 20-44	0.536	19.30					N/A	G2	1	18.30	60.0	Design Flexure - Steel
HS 20-44			0.896	32.24			N/A	G2	1	18.30	60.0	Design Flexure - Steel

Figure 60. Excerpt from Yutan Bridge July 2019 Load Rating Summary Sheet

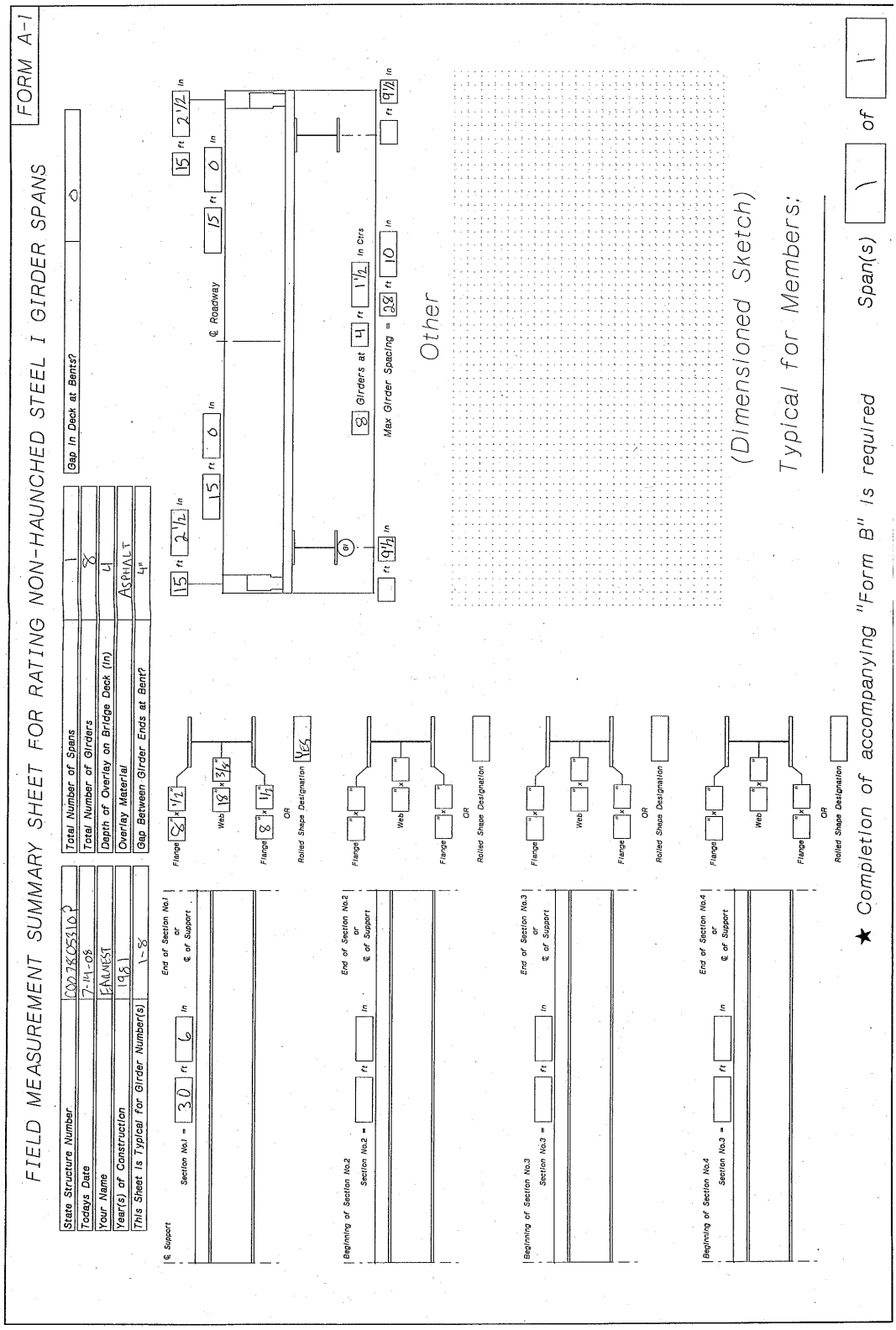

Figure 61. Yutan Bridge Documentation, Page 1 of 3

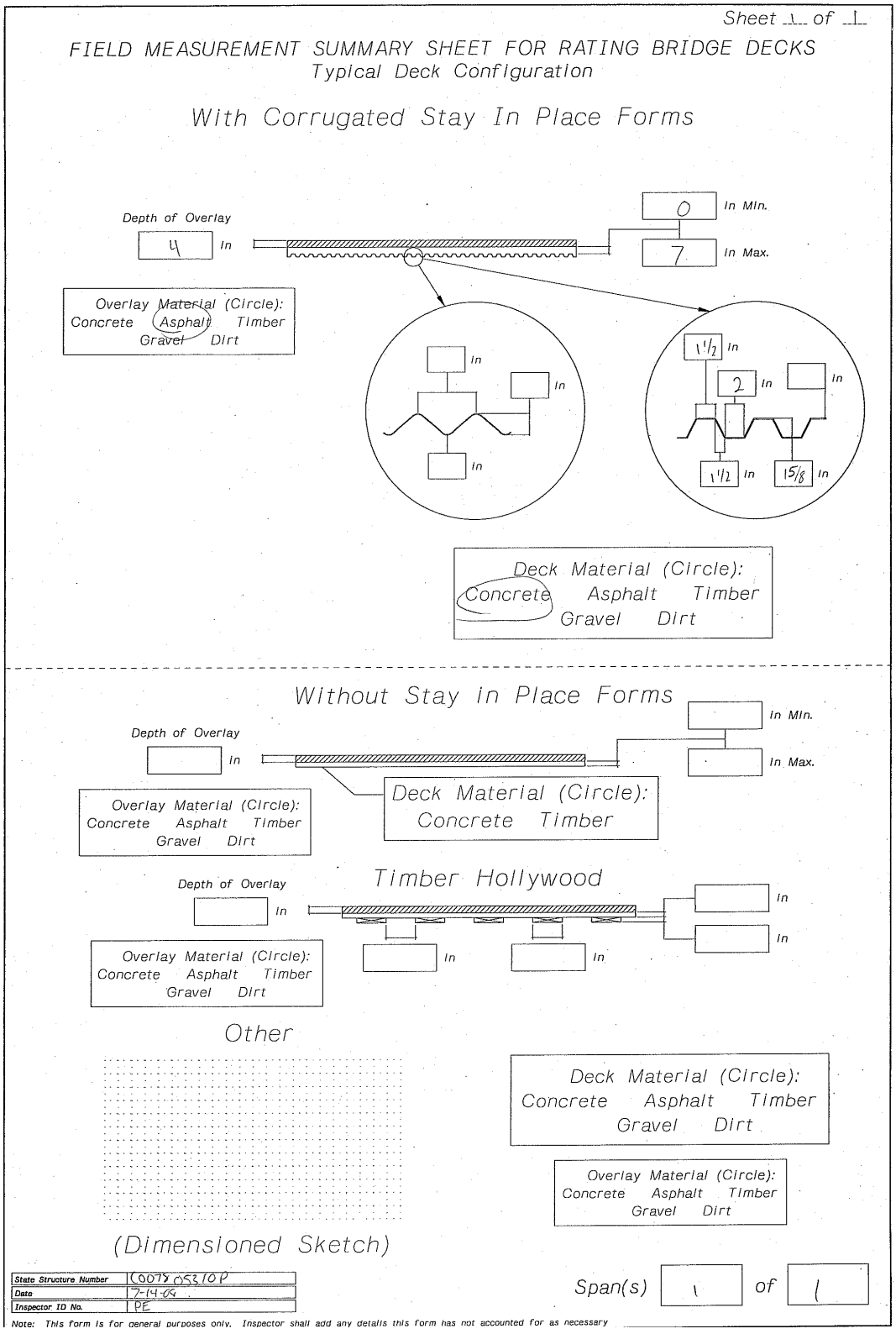

Figure 62. Yutan Bridge Documentation, Page 2 of 3

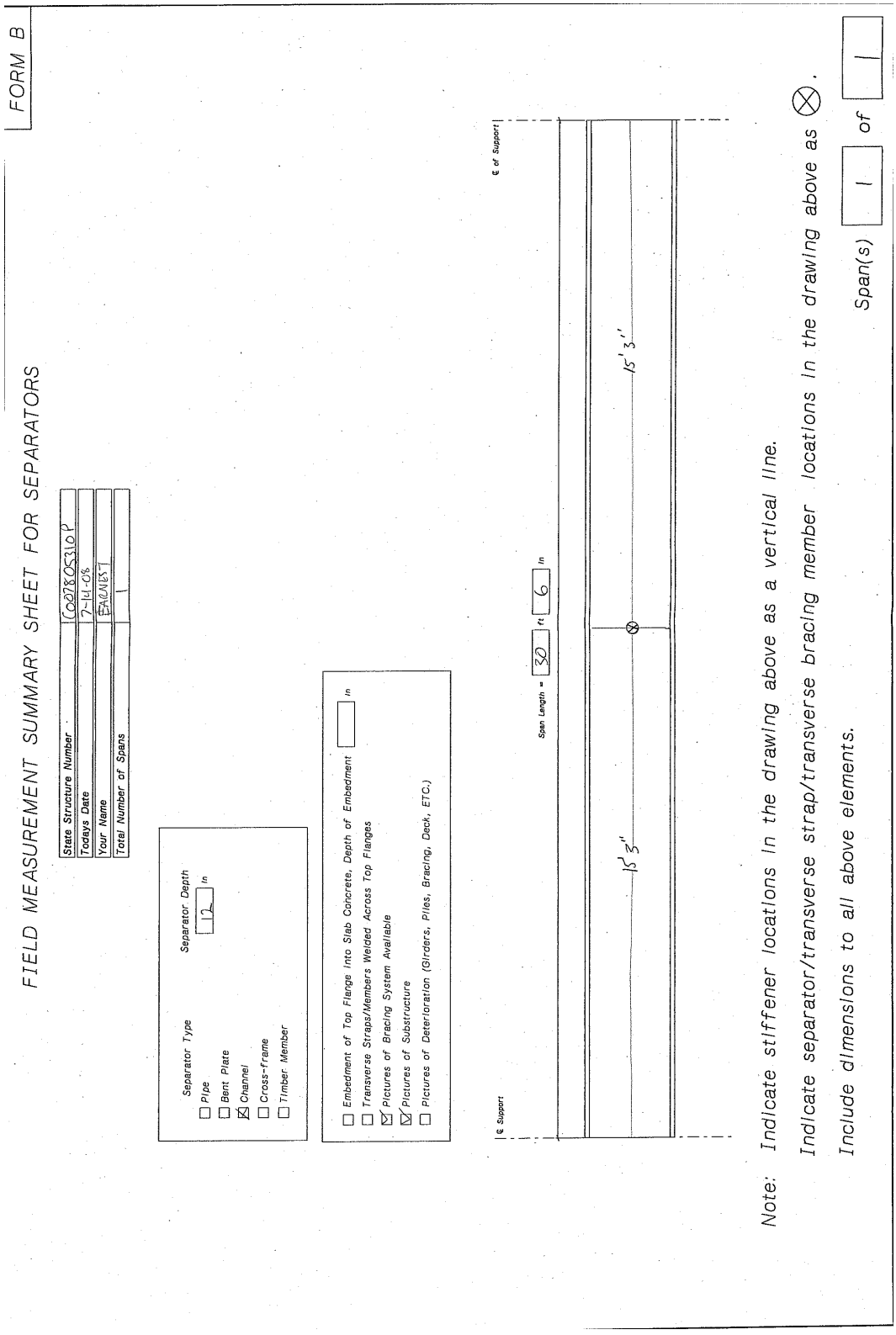

Figure 63. Yutan Bridge Documentation, Page 3 of 3

8.2 AASHTO Load Rating

This project has focused on reliability-calibrated, ANN-based girder distribution factors (GDFs) for use in determining live load effects. Load Factor Design and Rating (LFD/R) are not reliability-targeted, as Load and Resistance Factor Design and Rating (LRFD/R) are. Accordingly, this project has focused on LRFR, and the discussion presented here will focus primarily on LRFR. Additional discussion related to LFR is available at the end of this chapter. Equations applied from AASHTO documents are noted with an acronym to identify the particular source. Most commonly, the reference will be to the Manual for Bridge Evaluation, 3rd ed. (MBE) or the LFRD Bridge Design Specifications, 8th ed. (BDS).

The bridge girders are noted to be rolled sections, although the NDOT documentation did not note the specific designation. Consulting rolled section data available from the American Institute of Steel Construction (AISC), and considering the dimensions noted in the NDOT documentation to be only approximate and obtained from field measurements by hand, the rolled shape designation closest to the recorded dimensions is a W18x50. Pertinent parameters for this shape are provided in Table 18.

Section parameters correspond to AISC data, and dimensions are therefore slightly different than shown in Figure 61. The span length and unbraced length values correspond to information noted in Figure 63. The Load Rating Summary Sheets noted the year built as 1981. Therefore, referring to MBE Table 6A.6.2.1-1, the yield strength was assumed to be 36 ksi for a steel structure constructed after 1963. NDOT records note that the steel appears to have been repurposed, and was therefore assumed to have been manufactured prior to 1963 and penalized

to an assumed yield strength of 33 ksi instead of 36 ksi. The calculations that follow presume 36 ksi, but additional discussion related to steel strength is provided at the end of the chapter.

Table 18. Yutan Bridge Girder Parameters

Parameter	Value	Units
Rolled Shape	W18x50	
Depth, d	18	in
Flange width, b_f	7.5	in
Flange thickness, t_f	0.570	in
Web thickness, t_w	0.355	in
Area, A	14.7	in^2
Elastic section modulus, S_x	88.9	in^3
Plastic section modulus, Z_x	101	in^3
Span length, L	30.5	ft
Unbraced length, L_b	15.25	ft
Number of girders, n_{girder}	8	
Yield stress, F_y	36	ksi

Deck parameters are provided in Table 19. Maximum concrete thickness is presumed to represent the dimension from top of concrete to bottom of corrugated steel deck ribs. Minimum concrete thickness is presumed to measure from top of concrete to top of steel deck ribs. The available bridge documentation indicated that the wearing surface measured 4 inches thick. However, the Load Rating Summary Sheets indicated an assumed thickness of 3 inches, and this

value is used for the purposes of this report. The compression strength was estimated similarly to the steel yield strength. MBE Article 6A.5.2 and Table 6A.5.2.1-1 indicate that compression strength may be assumed to be 3.0 ksi for construction in 1959 or later, which applies to the Yutan Bridge constructed in 1981.

Table 19. Yutan Bridge Deck Parameters

Parameter	Value	Units
Max concrete thickness, $t_{slab,max}$	7	in
Min concrete thickness, $t_{slab,min}$	5.375	in
Wearing surface thickness, t_{wear}	3	in
Girder Spacing, S	4.125	ft
Deck total width, W_{deck}	30.42	ft
Deck overhang, W_{oh}	9.5	in
Guardrail width, W_{guard}	2.5	in
Concrete unit weight, γ_{conc}	150	lb/ft^3
Asphalt unit weight, γ_{wear}	140	lb/ft^3
Compression strength, f'_c	3	ksi

Rating Factor

LRFR Operating Rating Factors for flexural strength were determined from Eqn. 6:

$$RF = \frac{C - (\gamma_{DC})(DC) - (\gamma_{DW})(DW) \pm (\gamma_P)(P)}{(\gamma_{LL})(LL + IM)}$$ Eqn. 73

MBE (6A.4.2.1-1)

Permanent load effects, P, were taken as zero. Accordingly, load and resistance needed to be quantified for capacity, C, dead load of components, DC, dead load from the wearing surface, DW, and static live load, LL.

Capacity

Capacity, C, for strength limit states is:

$$C = \phi_c \phi_s \phi R_n$$ Eqn. 74

MBE (6A.4.2.1-2)

The superstructure is in Good condition, according to both the 2017 and 2019 Load Rating Summary Sheets shown previously. Therefore, the condition factor, ϕ_c, can be taken as 1 according to MBE Table 6A.4.2.3-1. Furthermore, this eight-girder bridge qualifies for a system factor, ϕ_s, of 1, according to MBE Table 6A.4.2.4-1. Lastly, MBE Article 6A.6.3 refers the reader to BDS Article 6.5.4.2 for resistance factors, ϕ. There, for flexure, $\phi = \phi_f = 1.00$. Ultimately, the capacity is equal to the nominal resistance, $C = R_n$ with all ϕ factors taken as unity.

MBE Article 6A.6.9.1 refers to the reader to BDS Article 6.10.6.2 for determination of flexural resistance. BDS Article 6.10.6.2.3 indicates that this bridge may be evaluated using BDS Appendix A6. The flange lateral bending stress term, f_l, was considered negligible (as

permitted in MBE Article 6A.6.9.1 for straight girder bridges). This shape, as typical for AISC rolled shapes, can be readily shown to be compact for both the web and flange, according to BDS Article A6.2.1 and BDS Article A6.3.2, respectively.

Flexural capacity will be limited either by plastic moment, Mp, or by lateral torsional buckling. MBE Article 6A.6.9.3 notes that compression flanges may be assumed adequately braced by the deck "where the top flange of the girder is fully in contact with the deck and no sign of cracking, rust, or separation along the steel-concrete interface is evident." While it is likely that even very minimal connections between the corrugated steel deck and girder top flange will be adequate to achieve continuously braced behavior, the construction for the Yutan Bridge is not technically recognized and addressed by this MBE Article. Therefore, to be conservative, the Yutan Bridge was evaluated assuming that the compression flange is braced only discretely at the transverse separator line at midspan.

According to BDS Article A6.1.1 for sections with discretely braced compression flanges, M_{nc} is to be determined according to BDS Article A6.3. Plastic moment is governed by:

$$M_{nc} = R_{pc} M_{yc} = \frac{M_p}{M_{yc}} M_{yc} = M_p \qquad \text{Eqn. 75}$$

BDS (A6.3.2-1)

According to BDS Article A6.2.1, M_p is to be determined from BDS Article D6.1. The formulations presented in BDS Article D6 are unnecessarily complicated for a noncomposite girder, and the plastic moment capacity can be determined simply from:

$$M_p = F_y Z_x = \frac{(36\,ksi)\left(101\,in^3\right)}{12\,\frac{in}{ft}} = 303\,k-ft \qquad \text{Eqn. 76}$$

The unbraced length, L_b, is 15.25 ft = 183 in. L_p can be determined to be 55.3 in. from BDS (A6.3.3-4), and L_r can be determined to be 244 in. from BDS (A6.3.3-5). If the beneficial effect of moment gradient is neglected (i.e., assume $C_b = 1$), the girder capacity will be limited by inelastic lateral torsional buckling with $L_p < L_b < L_r$. However, taking account of moment gradient effects for the longitudinal moment distribution from an HS-20 load at positioned to induce critical loading:

$M_0 = 0\,k-ft$ By analysis

$M_2 = 264\,k-ft$ By analysis

$M_{mid} = 169\,k-ft$ By analysis

$$M_1 = 2M_{mid} - M_2 = 2\left(169\,k-ft\right) - \left(264\,k-ft\right) = 74\,k-ft$$ Eqn. 77 BDS (A6.3.3-12)

The moment gradient factor is then:

$$C_b = 1.75 - 1.05\left(\frac{M_1}{M_2}\right) + 0.3\left(\frac{M_1}{M_2}\right)^2 \le 2.3$$ Eqn. 78

$$C_b = \left[1.75 - 1.05\left(\frac{74\,k-ft}{264\,k-ft}\right) + 0.3\left(\frac{74\,k-ft}{264\,k-ft}\right)^2 \le 2.3\right] = 1.48$$ BDS (A6.3.3-7)

Evaluating lateral torsional buckling capacity:

$$M_{nc} = C_b \left[1 - \left(1 - \frac{F_{yr} S_{xc}}{R_{pc} M_{yc}} \right) \left(\frac{L_b - L_p}{L_r - L_p} \right) \right] R_{pc} M_{yc} \le R_{pc} M_{yc}$$

$$M_{nc} = C_b \left[1 - \left(1 - \frac{0.7 F_y S_x}{M_p} \right) \left(\frac{L_b - L_p}{L_r - L_p} \right) \right] M_p \le M_p \qquad \text{Eqn. 79}$$

$$M_{nc} = 1.48 \left[1 - \left(1 - \frac{0.7(36\,ksi)(88.9\,in^3)}{303\,k-ft} \frac{1\,ft}{12\,in} \right) \left(\frac{183\,in - 55.3\,in}{244\,in - 55.3\,in} \right) \right] 303\,k-ft \qquad \text{BDS (A6.3.3-2)}$$

$$\le 303\,k-ft$$

$$M_{nc} = \left[332\,k-ft \le 303\,k-ft \right] = 303\,k-ft$$

So, flexural capacity will be limited by plastic moment, M_p.

$$C = R_n = M_{nc} = M_p = 303\,k-ft \qquad \text{Eqn. 80}$$

Dead Load of Components

DC loads are induced by the self-weight of the girders and the concrete deck. The guardrail is a light W-beam mounted to small steel posts. The weight of the guardrail and corrugated steel deck were neglected. The concrete deck was assumed to be a constant 7 inches thick, which overestimates the actual weight by neglecting mass reduction at steel deck corrugations. This overestimation of concrete weight is believed to more than compensate for neglecting the steel deck and guardrail weight. Deck weight was distributed uniformly to all girders, as recommended in BDS Article 4.6.2.2.1. Accordingly, the distributed dead load of components was estimated to be:

$$w_{DC} = \gamma_{steel} A + \gamma_{conc} \left(\frac{W_{deck}}{n_{girder}} \right) t_{slab,\max}$$

$$w_{DC} = \left(\begin{array}{c} \left(\frac{490\,lb}{ft^3} \right) \left(14.7\,in^2 \right) \left(\frac{1\,ft}{12\,in} \right)^2 \\ + \left(\frac{150\,lb}{ft^3} \right) \left(\frac{30.42\,ft}{8\,girders} \right) \left(7\,in \right) \frac{1\,ft}{12\,in} \end{array} \right) \frac{1\,kip}{1000\,lb} \qquad \text{Eqn. 81}$$

$$w_{DC} = 0.383 \frac{k}{ft}$$

Assuming the bridge to be simply supported, and the critical moment location to be at midspan:

$$DC = M_{DC} = \frac{w_{DC} L^2}{8} = \frac{\left(0.383 \frac{k}{ft} \right) \left(30.5\,ft \right)^2}{8} = 44.5\,k - ft \qquad \text{Eqn. 82}$$

Dead Load of Wearing Surface

DW loads are induced by the weight of the wearing surface. The wearing surface was conservatively assumed to be placed across the full width of the concrete deck, and the wearing surface weight was distributed uniformly to all girders, similarly to the concrete deck in the determination of component dead load effects. The distributed dead load of the wearing surface was estimated to be:

$$w_{DW} = \gamma_{wear}\left(\frac{W_{deck}}{n_{girder}}\right)t_{wear}$$

$$w_{DW} = \left(\left(\frac{140\,lb}{ft^3}\right)\left(\frac{30.42\,ft}{8\,girders}\right)(3\,in)\frac{1\,ft}{12\,in}\right)\frac{1\,kip}{1000\,lb} \qquad \text{Eqn. 83}$$

$$w_{DW} = 0.133\frac{k}{ft}$$

Similar to dead load of components, assuming the bridge to be simply supported, and the critical moment location to be at midspan:

$$DW = M_{DW} = \frac{w_{DW}L^2}{8} = \frac{\left(0.133\frac{k}{ft}\right)(30.5\,ft)^2}{8} = 15.5\,k-ft \qquad \text{Eqn. 84}$$

Live Load

Live load was evaluated using an HL-93 load, as a combination of an HS-20 design truck and a distributed design lane load of 0.64 k/ft. The maximum moment effect from the HS-20 truck was 287 k-ft, determined from a moving load analysis of axle weights shown in BDS Figure 3.6.1.2.2-1, and using the minimum spacing between trailer axles of 14 ft. The lane load effect was calculated similarly to distributed dead load effects, as mentioned previously.

$$M_{Truck} = 287\,k - ft / lane \qquad \text{Eqn. 85}$$

$$M_{Lane} = \frac{w_{Lane} L^2}{8} = \frac{\left(0.640 \frac{k}{ft}\right)(30.5\,ft)^2}{8} = 74.4\,k - ft / lane \qquad \text{Eqn. 86}$$

MBE Article 6A.4.3.3 refers the reader to BDS Article 3.6.2 for dynamic load allowance, IM. Accordingly, IM was taken as 33% of the truck loading effects according to BDS Table 3.6.2.1-1 and BDS Article 3.6.2.1. The nominal dynamic load effects per lane were then:

$$\frac{(LL + IM)}{lane} = M_{Truck}(1 + IM) + M_{Lane}(1 + 0) \qquad \text{Eqn. 87}$$

$$\frac{(LL + IM)}{lane} = \frac{287\,k - ft}{lane}(1 + 0.33) + \frac{74.4\,k - ft}{lane} = \frac{456\,k - ft}{lane}$$

Critical live load per girder was determined by multiplying the dynamic design load per lane by girder distribution factors (GDFs), g, from BDS Article 4.6.2.2. BDS Article 4.6.2.2.1 notes that multiple presence factors, m, shall not be used with the approximate load assignment methods in that section, except when the lever rule is invoked. m values were therefore taken as 1 in all cases except for the exterior girder subjected to 1 lane of load, in which case m = 1.20 according to BDS Table 3.6.1.1.2-1.

The bridge cross-section corresponds to Type a in BDS Table 4.6.2.2.1-1. If the bridge is assumed noncomposite, the longitudinal stiffness, K_g, is technically outside the range of applicability. If the modulus of elasticity of the deck, E_D, is estimated using BDS Commentary equation (C5.4.2.4-3) and an assumed f'$_c$ of 3 ksi, the resulting value is 3150 ksi. Then, assuming the modulus of elasticity of the beam, E_B, is 29,000 ksi, the modular ratio from BDS Equation (4.6.2.2.1-2) is 9.2. For a noncomposite steel girder bridge, the longitudinal stiffness in BDS Equation (4.6.2.2.1-1) omits the Ae_g^2 term, so that K_g is taken as the product of n = 9.2 and I = 800 in^4, resulting in a value of 7360 in^4, which is less than the applicable range of 10,000 in^4. Substituting the lower bound value for K_g in the distribution factor equations in BDS Table 4.6.2.2.2b-1 for interior girders:

$$g_{\text{int},1lane} = 0.06 + \left(\frac{S}{14}\right)^{0.4}\left(\frac{S}{L}\right)^{0.3}\left(\frac{K_g}{12.0Lt_s^3}\right)^{0.1}$$

$$g_{\text{int},1lane} = 0.06 + \left(\frac{4.125\,ft}{14}\right)^{0.4}\left(\frac{4.125\,ft}{30.5\,ft}\right)^{0.3}\left(\frac{10{,}000\,in^4}{12.0(30.5\,ft)(7\,in)^3}\right)^{0.1} \qquad \text{Eqn. 88}$$

$$g_{\text{int},1lane} = 0.321$$

$$g_{\text{int},2lane} = 0.075 + \left(\frac{S}{9.5}\right)^{0.6}\left(\frac{S}{L}\right)^{0.2}\left(\frac{K_g}{12.0Lt_s^3}\right)^{0.1}$$

$$g_{\text{int},2lane} = 0.075 + \left(\frac{4.125\,ft}{9.5}\right)^{0.6}\left(\frac{4.125\,ft}{30.5\,ft}\right)^{0.2}\left(\frac{10{,}000\,in^4}{12.0(30.5\,ft)(7\,in)^3}\right)^{0.1} \qquad \text{Eqn. 89}$$

$$g_{\text{int},2lane} = 0.390$$

According to BDS Table 4.6.2.2.2d-1 for moment in exterior girders, the effect for 1 lane loaded is to be determined from the lever rule, and for 2 lanes loaded is to be determined as a scaled value of interior girder load effect. For 1 lane loaded, the deck overhang is 9.5 inches and the guardrail inset from the edge of the deck is 2.5 inches. Assuming a wheel line located 2 feet

from the face of the guardrail, the wheel location is 17 inches = 1.417 ft inset from the exterior girder centerline. With a 4.125 ft girder spacing from the exterior to first interior girder, the tributary contribution of a truck wheel line is:

$$g_{ext,wheel\,line} = \frac{4.125\,ft - 1.417\,ft}{4.125\,ft} = 0.657 \qquad \text{Eqn. 90}$$

According to the lever rule, the other wheel line does not contribute to exterior girder load. Therefore, also accounting for multiple presence, m:

$$g_{ext,1lane} = g_{ext,wheel\,line}\left(\frac{1\,lane}{2\,wheel\,lines}\right)m$$
$$g_{ext,1lane} = 0.657\left(\frac{1\,lane}{2\,wheel\,lines}\right)(1.2) = 0.394 \qquad \text{Eqn. 91}$$

Exterior girder loading with two lanes loaded is determined according to BDS Table 4.6.2.2.2d-1 as:

$$d_e = W_{oh} - W_{guard} = 9.5\,in. - 2.5\,in. = 7\,in. \qquad \text{Eqn. 92}$$

$$e = 0.77 + \frac{d_e}{9.1} = 0.77 + \frac{7}{9.1} = 0.834 \qquad \text{Eqn. 93}$$

$$g_{ext,2lane} = e\ g_{\text{int},2lane}$$
$$g_{ext,2lane} = (0.834)(0.390) = 0.326 \qquad \text{Eqn. 94}$$

Reviewing Eqn. 88, Eqn. 89, Eqn. 91, and Eqn. 94, the exterior girder is observed to control under 1 lane loading conditions.

$$g_{critical} = \max\left(g_{\text{int},1lane}, g_{\text{int},2lane}, g_{ext,1lane}, g_{ext,2lane}\right)$$
$$g_{critical} = \max(0.321,\ 0.390,\ 0.394,\ 0.326) = 0.394 \qquad \text{Eqn. 95}$$

The critical dynamic live load effect is then:

$$\left(LL+IM\right)=M_{LL,dyn}=\left(\frac{\left(LL+IM\right)}{lane}\right)g_{critical}$$
$$\left(LL+IM\right)=M_{LL,dyn}=\left(\frac{456\,k-ft}{lane}\right)\left(0.394\right)=180\,k-ft \qquad \text{Eqn. 96}$$

Rating Factor

The rating factor equation from Eqn. 6 can be rewritten as:

$$RF=\frac{M_{nc}-\left(\gamma_{DC}\right)\left(M_{DC}\right)-\left(\gamma_{DW}\right)\left(M_{DW}\right)}{\left(\gamma_{LL}\right)\left(M_{LL,dyn}\right)} \qquad \text{Eqn. 97}$$

Referring to MBE Table 6A.4.2.2-1, for a steel bridge, evaluating the Strength I limit state in flexure, at the Operating level, the rating factor equation becomes:

$$RF_{Operating}=\frac{M_{nc}-\left(1.25\right)\left(M_{DC}\right)-\left(1.5\right)\left(M_{DW}\right)}{\left(1.35\right)\left(M_{LL,dyn}\right)} \qquad \text{Eqn. 98}$$

Finally, substituting the nominal demand and capacity moments from Eqn. 80, Eqn. 82, Eqn. 84, and Eqn. 96:

$$RF_{Operating}=\frac{\left(303\,k-ft\right)-\left(1.25\right)\left(44.5\,k-ft\right)-\left(1.5\right)\left(15.5\,k-ft\right)}{\left(1.35\right)\left(180\,k-ft\right)} \qquad \text{Eqn. 99}$$
$$RF_{Operating}=0.92$$

8.3 ANN Load Rating Prediction

In the previous section, a load rating was calculated as directed in Cell 4. The result of the calculation suggests that Legal loads should now be investigated to determine whether posting is required, although this report is limited to performing Operating ratings for simplicity and brevity. Presuming that additional calculations with Legal loads in Cell 4 would result in load posting in Cell 5, as was the current condition from an NDOT load rating evaluation, the next step is to re-evaluate ratings with ANN-predicted GDFs in Cell 6.

ANN parameters for the Yutan Bridge are shown in Table 20. All parameters are within the appropriate ANN applicability ranges, although the longitudinal stiffness is very low and on the boundary. Inputting the parameters into the provided Excel tool for moment GDFs, the calculations described in the following chapter are performed automatically. ANN-based critical GDFs are determined to be 0.358 without reliability calibration, or 0.372 with a reliability calibration to effectively raise the live load factor from 1.35 to 1.40. Because the calibration is incorporated into the ANN tool output, the live load factor used in rating factor calculations does not need to be modified in other spreadsheets or software that a user may employ.

Table 20. Yutan Bridge ANN Parameters

Parameter	Value
Span Length (ft)	30.5
Girder Spacing (ft)	4.13
Number of Girders (#)	8
Skew Angle (°)	0
Deck Thickness (in)	7
Concrete Compressive Strength (ksi)	3
Steel Yield Stress (ksi)	36
Total Width (ft)	30.42
Roadway Width (ft)	30
Unbraced Length (ft)	0.56
Girder Shape	W18x50
Diaphragm / Cross Frames Presence	Present
Composite / Noncomposite Behavior	Noncomposite

Without reliability calibration, the ANN-based GDF results in a reduced live load effect:

$$\left(LL+IM\right)=M_{LL,dyn}=\left(\frac{\left(LL+IM\right)}{lane}\right)g_{critical}$$

$$\left(LL+IM\right)=M_{LL,dyn}=\left(\frac{456k-ft}{lane}\right)\left(0.358\right)=163.5k-ft$$

Eqn. 100

And corresponding rating factor:

$$RF_{Operating} = \frac{(303k-ft)-(1.25)(44.5k-ft)-(1.5)(15.5k-ft)}{(1.35)(163.5k-ft)} \quad \text{Eqn. 101}$$

$$RF_{Operating} = 1.02$$

Alternatively, with reliability calibration,

$$(LL+IM) = M_{LL,dyn} = \left(\frac{(LL+IM)}{lane}\right) g_{critical} \quad \text{Eqn. 102}$$

$$(LL+IM) = M_{LL,dyn} = \left(\frac{456k-ft}{lane}\right)(0.372) = 169.5k-ft$$

And corresponding rating factor:

$$RF_{Operating} = \frac{(303k-ft)-(1.25)(44.5k-ft)-(1.5)(15.5k-ft)}{(1.35)(169.5k-ft)} \quad \text{Eqn. 103}$$

$$RF_{Operating} = 0.98$$

In summary, the original analytical load rating of 0.92 in Cell 4 is now estimated to be approximately 0.98 to 1.02 in Cell 6, with the lower value conservatively penalized to ensure an acceptably low probability of failure. Because this Operating rating factor is very close to 1 with the reliability-adjusted ANN GDF, it would be reasonable to consider this bridge for load testing and progress to Cell 7.

8.4 Load Rating by Detailed Analysis

8.4.1 CSiBridge Modeling and Rating Factor

Load rating engineers may wish to perform a detailed analysis prior to recommending a load test. A brief discussion of load ratings from detailed analyses for the Yutan Bridge are provided below. ANSYS is one of the most advanced modeling software packages available on the market. It is likely unavailable to DOT engineers because of its expense and it is more difficult to use. In exchange for a less user-friendly interface, particular ANSYS results are more easily interrogated to examine how results were obtained. Conversely, CSiBridge is a more broadly adopted software for use in practice, and provides a more streamlined interface. However, results may be difficult to interrogate, with less intermediate/detailed calculation data available to a user interested in examining how exactly loads were applied or mechanical components, connections, and interactions were mathematically represented.

8.4.2 Load Rating using ANSYS

The ANSYS modeling framework described in Chapter 5 was used to calculate an LRFR Operating load rating of the Yutan Bridge. As discussed in that chapter, the model directly connected deck and girder flange elements to simulate composite behavior, which was the assumption for typical bridge construction at the initiation of the project. ANSYS is a general purpose finite element continuum modeling software package, not specifically intended for use in structural or bridge engineering. Post-processing was therefore required to transform raw output into useful load rating results.

Analyses were performed with wheel loads modeled as pressure patches on the deck surface at the critical load position for a selected load effect (moment or shear), transverse position (exterior girder or interior girder), and number of lanes (one truck or two adjacent

trucks). A transverse section of the bridge was interrogated, extracting software output for the in-plane forces and edge moments of individual shell elements used to define the steel girder flanges and web, and for normal stresses on the faces of deck concrete brick elements. These results were transformed into resultant moments acting on the bridge cross-section, as described in detail in Sofi (2017). Moment GDFs were determined using the ratios of individual girder moments to the theoretical moment induced across the bridge cross-section by a single truck. Single-truck scenarios were also scaled by a multiple presence factor of 1.2.

These GDFs were then used to determine load ratings by substituting the maximum FEA-based GDF for $g_{critical}$ Eqn. 95, producing rating factors that reflected noncomposite capacity and AASHTO LRFR design lane loading, which had not been explicitly modeled in ANSYS. These modifications to extend ANSYS truck load modeling results to account for distributed lane loads and noncomposite behavior are described in the Appendix to this report.

The Operating moment rating factor for this bridge was determined to be 1.04, governed by the exterior girder. A longitudinal stress contour for the critical loading condition is shown in Figure 64. The units of stress are shown in Pascals, so the stress range in the figure is -2.9 ksi to +6.4 ksi induced by an HS-20 truck if the bridge acts with perfect composite behavior (i.e., no slip) between the deck and girders. Recalling that the unadjusted ANN rating factor was 1.02, these ANSYS analysis results reveal that the unadjusted ANN-based GDF prediction was, in the case of this particular bridge, slightly conservative by a margin of about 2%, and the reliability-calibrated ANN-based GDF provided an unnecessary margin of conservativism for this particular bridge.

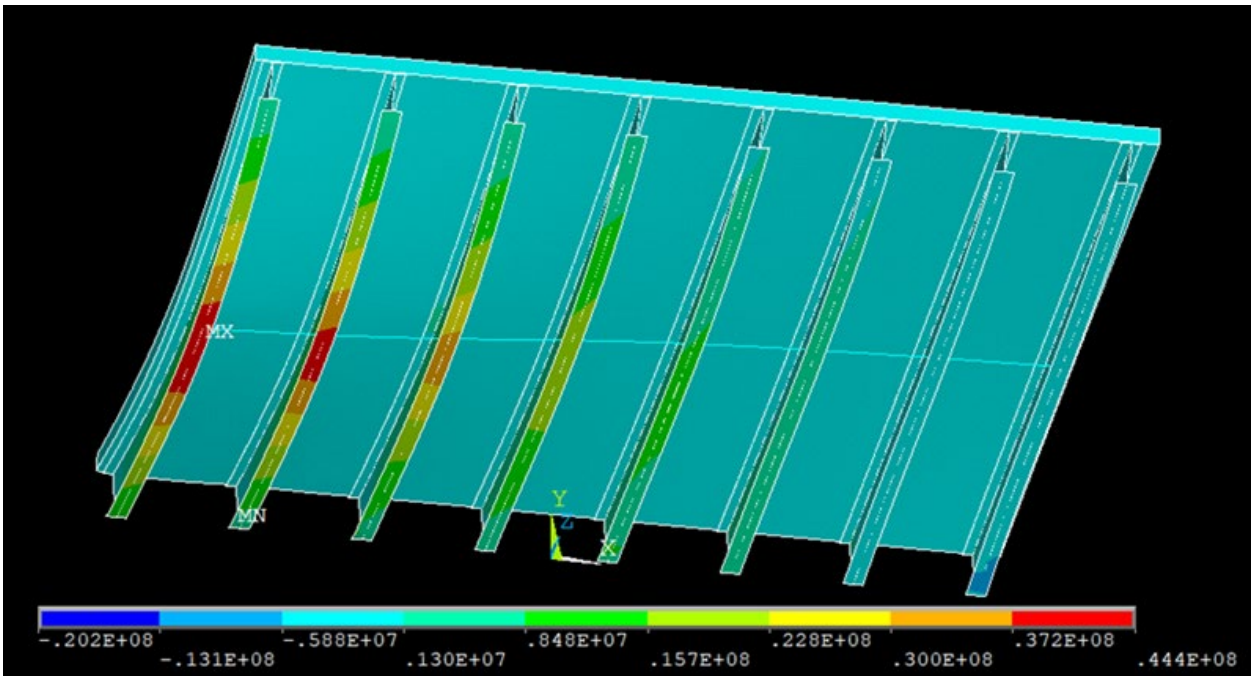

Figure 64. ANSYS Longitudinal Stress Contour for the Yutan Bridge (Pa)

8.4.3 CSiBridge Modeling and Rating Factor

The bridge was also modeled using CSiBridge according to the procedure described in Section 5.3. The LRFR Operating moment rating factor was determined to be 0.96, governed by flexure in the exterior girder. CSiBridge is a more appealing option for use in practice, because the user interface has been streamlined specifically to assist engineers performing bridge analysis and design, as opposed to the more generalized ANSYS modeling interface.

CSiBridge allows composite versus noncomposite action to be specified by the user. CSiBridge also allows users to specify lanes, for which it will perform moving load analyses with various live load models, rather than the specific location of discrete loading defined in ANSYS. A longitudinal stress contour of the Yutan Bridge under a single exterior lane of HL-93 nominal loading is shown in Figure 65. While this is generally simple and convenient, it also

obscures the clarity of exactly how loads were applied to the structural model in terms of locations and magnitudes of stresses or forces.

Intermediate calculations were not readily available from CSiBridge, so critical comparisons with ANSYS to identify specific aspects of deviations were therefore challenging. Differences in rating factors between CSiBridge and ANSYS are believed to arise from nuanced differences in modeling. For example, CSiBridge modeling used shell elements for both the girder and deck, whereas ANSYS likewise used shell elements for the girder, but brick elements for the deck. The fact that the CSiBridge rating factor was close to that obtained using ANSYS results, with both agreeing that the Operating rating is very close to 1, is encouraging. However, the inability to interrogate and examine intermediate calculations and assumptions in CSiBridge diminishes its reliability compared to the result from ANSYS.

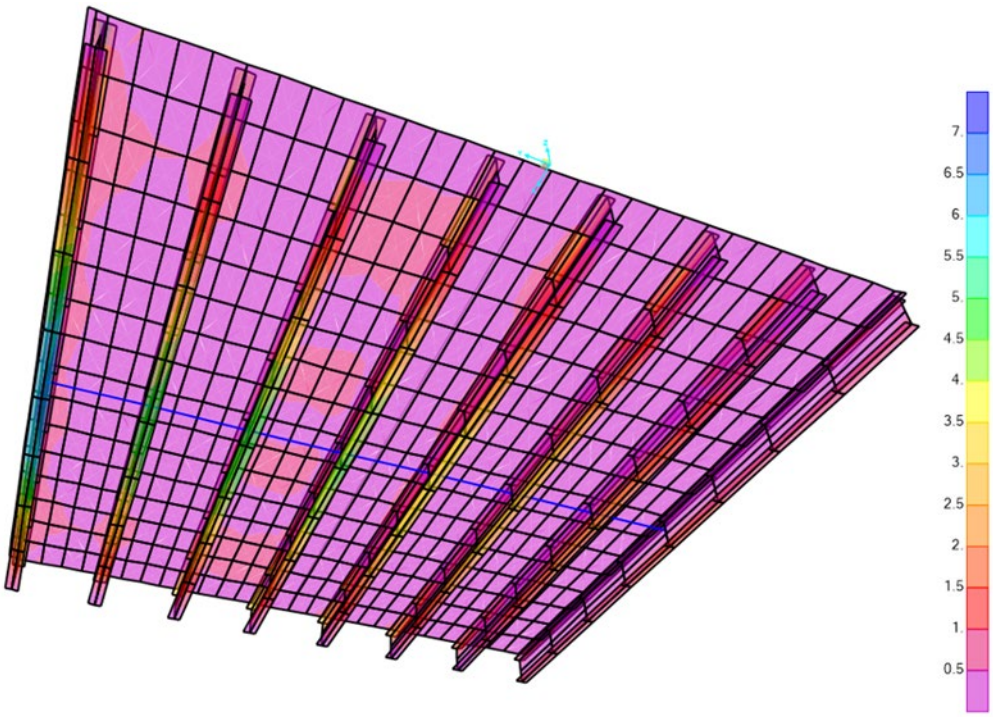

Figure 65. CSiBridge Longitudinal Stress Contour for the Yutan Bridge (ksi)

8.5 Diagnostic Field Testing Plans

Diagnostic load testing was performed for the Yutan Bridge on two occasions in 2019: April 19 and November 4. These tests are referred to herein as Test 1 and Test 2, respectively.

8.5.1 Instrumentation and Test Procedure for Test 1

Individual sensor dimensions provided by the manufacturer are shown in Figure 66. Sensors were installed near the abutments as well as at the center of the span to investigate both potential restraint and induced negative moments near supports, as well as anticipated critical positive moment.

The strain gauges were instrumented at girders 1-5 and girder 8 for the midspan and the South abutment. The same girders were instrumented for the North abutment with the exception of girder 8 due to safety concerns for the test team. For the instrumented girders, two strain gauges were installed at the bottom flange and one strain gauge was mounted on the web near the top flange. Two sensors were used at the bottom flange to investigate the potential presence of lateral bending. Additionally, girders 5 and 8 were instrumented to verify symmetric bridge behavior.

Strain gauges were placed about 6 inches to the South of the midspan to avoid a diaphragm. Instrumentation was placed near the abutments at about 8 inches from the ends. Instrumentation near the diaphragm at midspan is shown in Figure 67. The gauge near the North abutment for girder 4 and the gauge near the South abutment for girder 1 were placed about 12 inches from the abutments because there were small holes cut in the web at the typical instrumentation location.

Each strain gauge was installed along the longitudinal direction. Strain gauge installation locations can be seen in Figure 68 and Figure 69. Each individual strain gauge is identified by a

unique ID number as provided by the manufacturer. The strain gauge IDs and locations are provided in the appendix to this report.

The BDI software was tared to zero so that only live load strain is detected. The loading vehicle was driven across the bridge at a crawl speed to mitigate potential dynamic amplification effects. The vehicle was driven along three designated loading paths: critical loading for the exterior girder, critical loading for the interior girder, and along the bridge centerline to verify symmetric structural response to applied load. The vehicle was also driven along the three paths at the posted speed limit for the bridge to investigate dynamic amplification effects, although data from these runs was not deemed adequate upon review. A summary of the naming convention for the runs is shown in Table 21. Runs were performed for vehicle travel in both directions. The outsides of the tire load paths were painted on the pavement to guide the truck driver so that vehicle load distribution applied to the bridge would induce critical loading in the girders and would be reasonably similar to assumed loading in preliminary analyses. The load paths are shown in Figure 70 and the truck axle spacings are shown in Figure 71. Loads paths 1-3 correspond to center load placement, interior girder critical load location, and exterior girder critical load location, respectively.

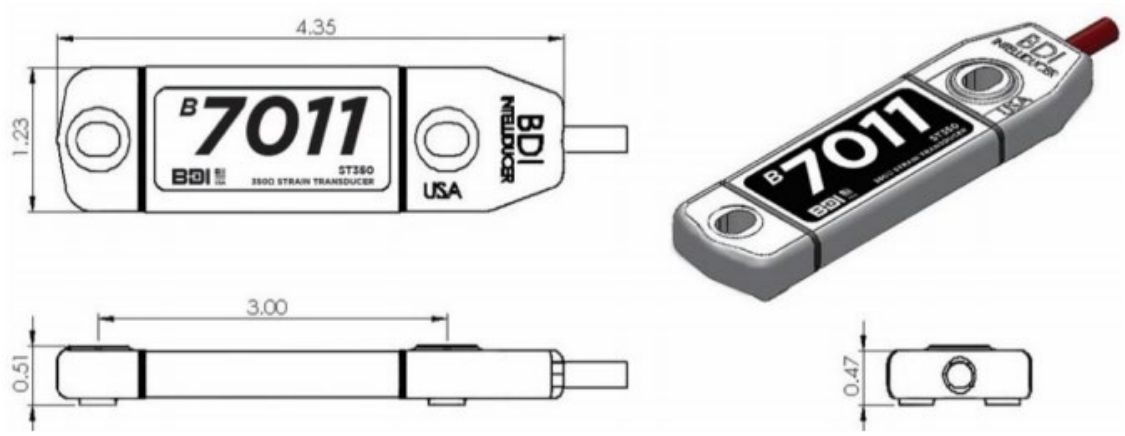

Figure 66. BDI Strain Transducer Dimensions in Inches

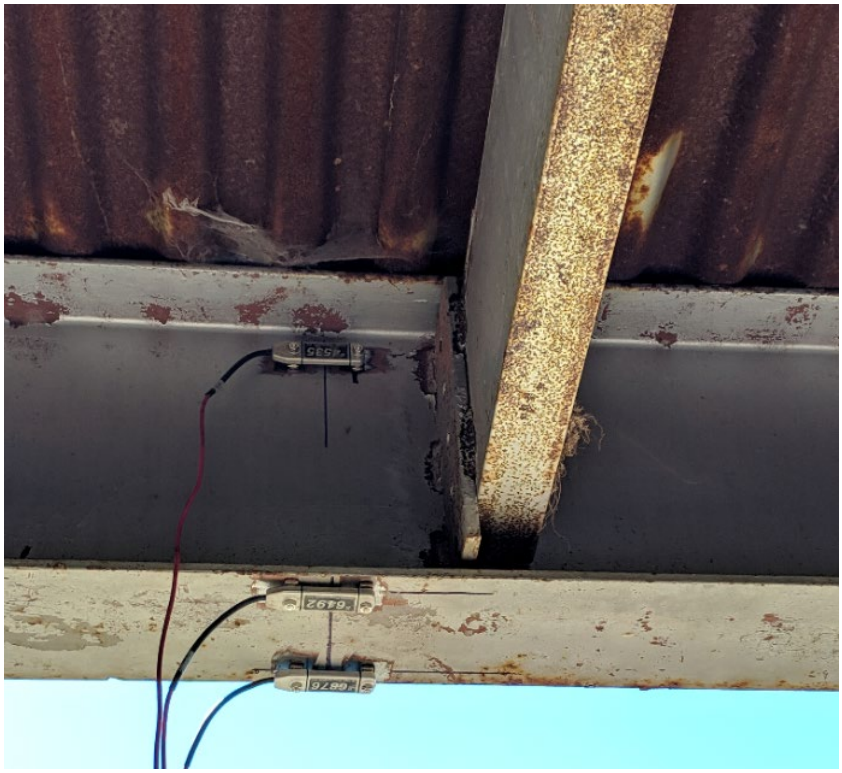

Figure 67. Instrumentation near Midspan for Yutan Bridge Load Test 1

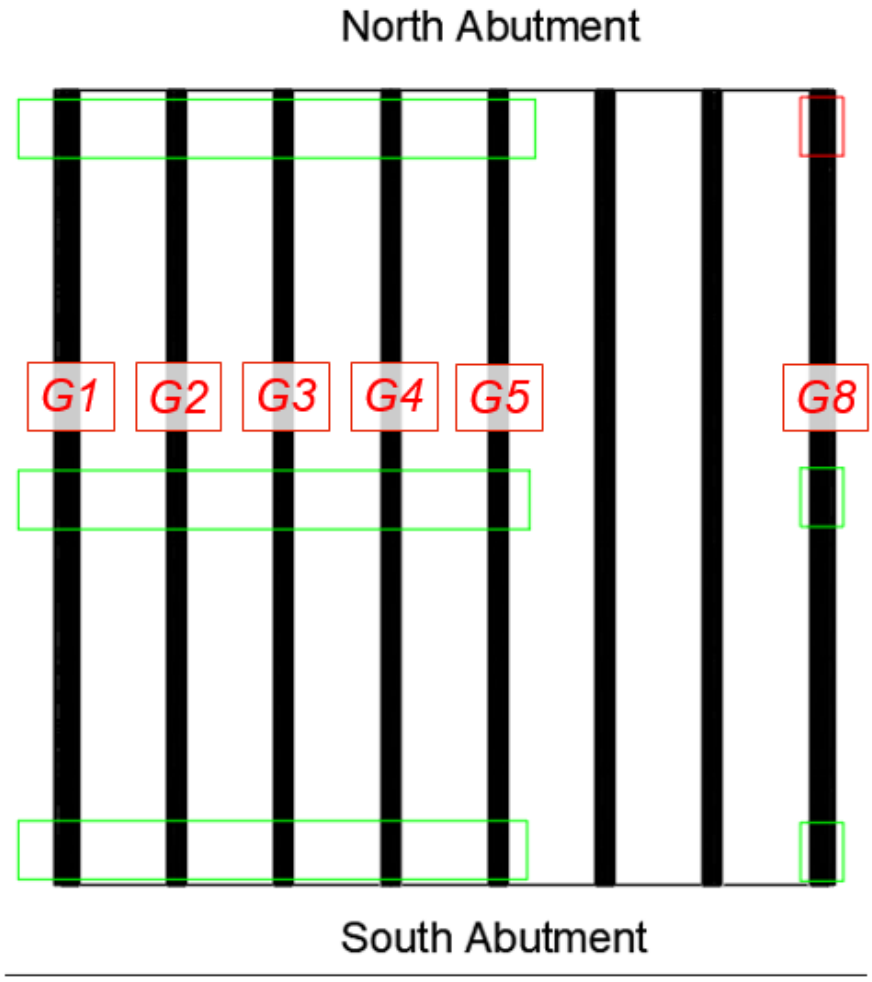

Figure 68. Plan View of Sensor Layout for Yutan Bridge Load Test 1

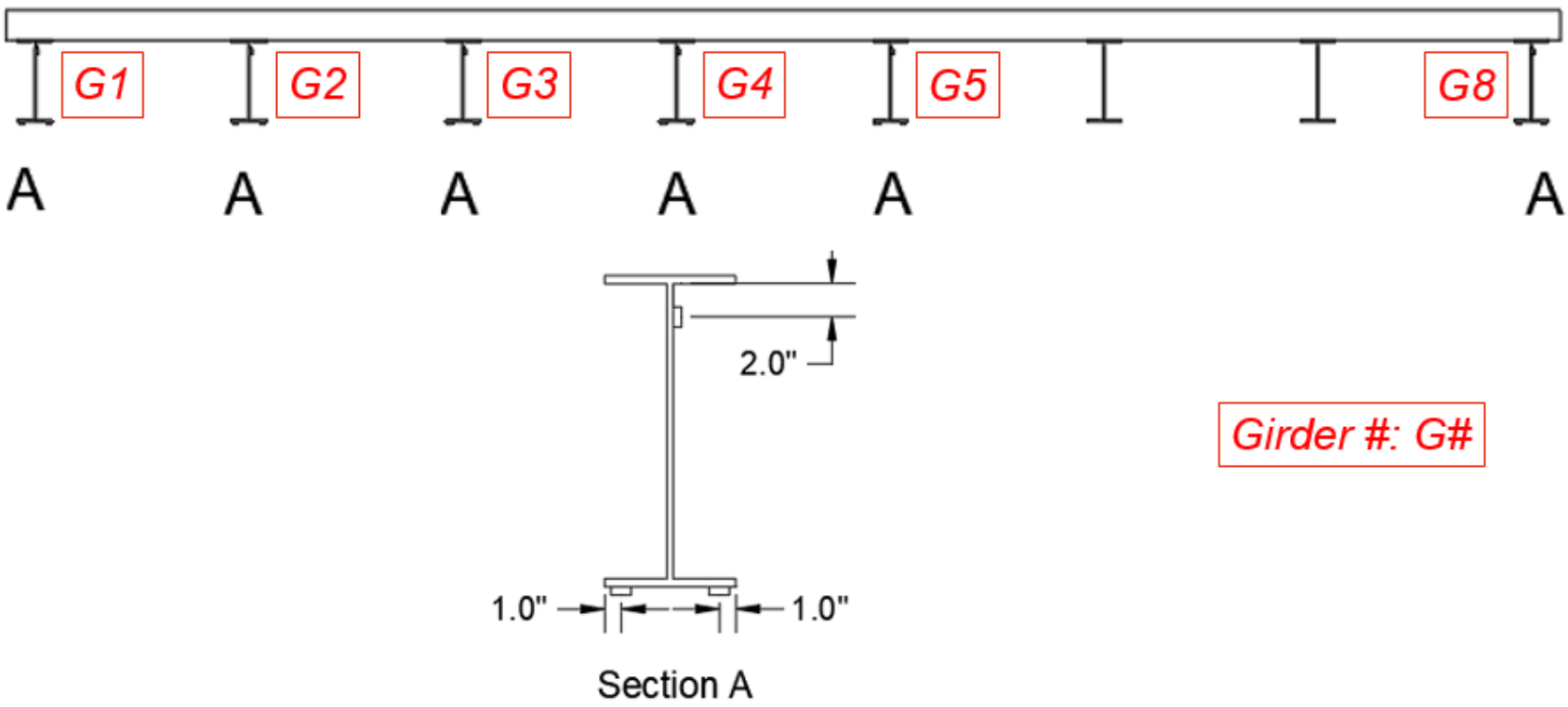

Figure 69. Cross-Section View of Sensor Layout (looking north) for Yutan Bridge Load Test 1

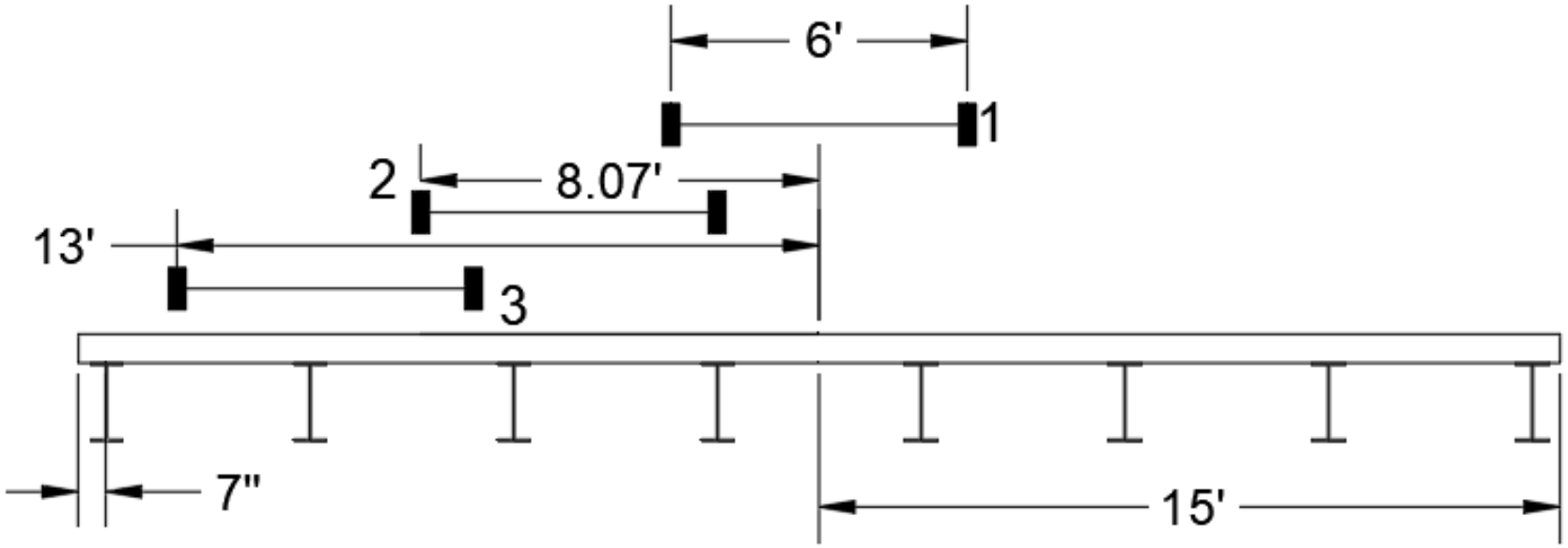

Figure 70. Load Test Plan for Yutan Bridge Load Test 1

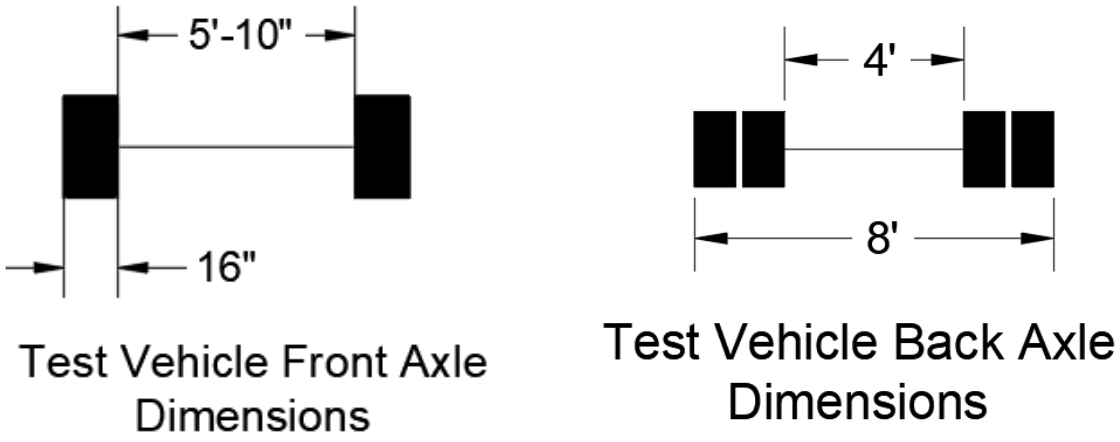

Figure 71. Load Test Vehicle Axle Dimensions for Yutan Bridge Load Test 1

Table 21. Truck Runs for Yutan Bridge Load Test 1

Run	Truck Position	Direction	Speed
1	1	N	Slow
2	1	S	Slow
3	1	N	Fast
4	1	S	Fast
5	2	N	Slow
6	2	S	Slow
7	2	N	Fast
8	2	S	Fast
9	3	N	Slow
10	3	S	Slow

8.5.2 Instrumentation and Test Procedure for Test 2

Instrumentation was modified for the second test so that behavior of all of the girders could be analyzed. Instrumentation was not installed at the north abutment ends of girders 7 and 8, as noted in Figure 72, due to hazards introduced by wet conditions and unstable footing. Instrumentation was installed farther from abutments than in the first

test to avoid the influence of localized connection stress effects. Since weak axis flexure effects were observed to be negligible in the first load test, the research team decided to instrument the bottom flanges with only one strain gauge, as shown in Figure 73. Since additional instrumentation was placed on the East side of the bridge, additional runs were performed over the now instrumented girders. Figure 74 outlines the designated load placements. Locations 1 and 5 correspond to exterior girder critical load placement, locations 2 and 4 correspond to interior girder critical load placement, and location 3 corresponds to geometrical center load placement. Table 22 summarizes the nomenclature of the runs performed for the 2nd load test.

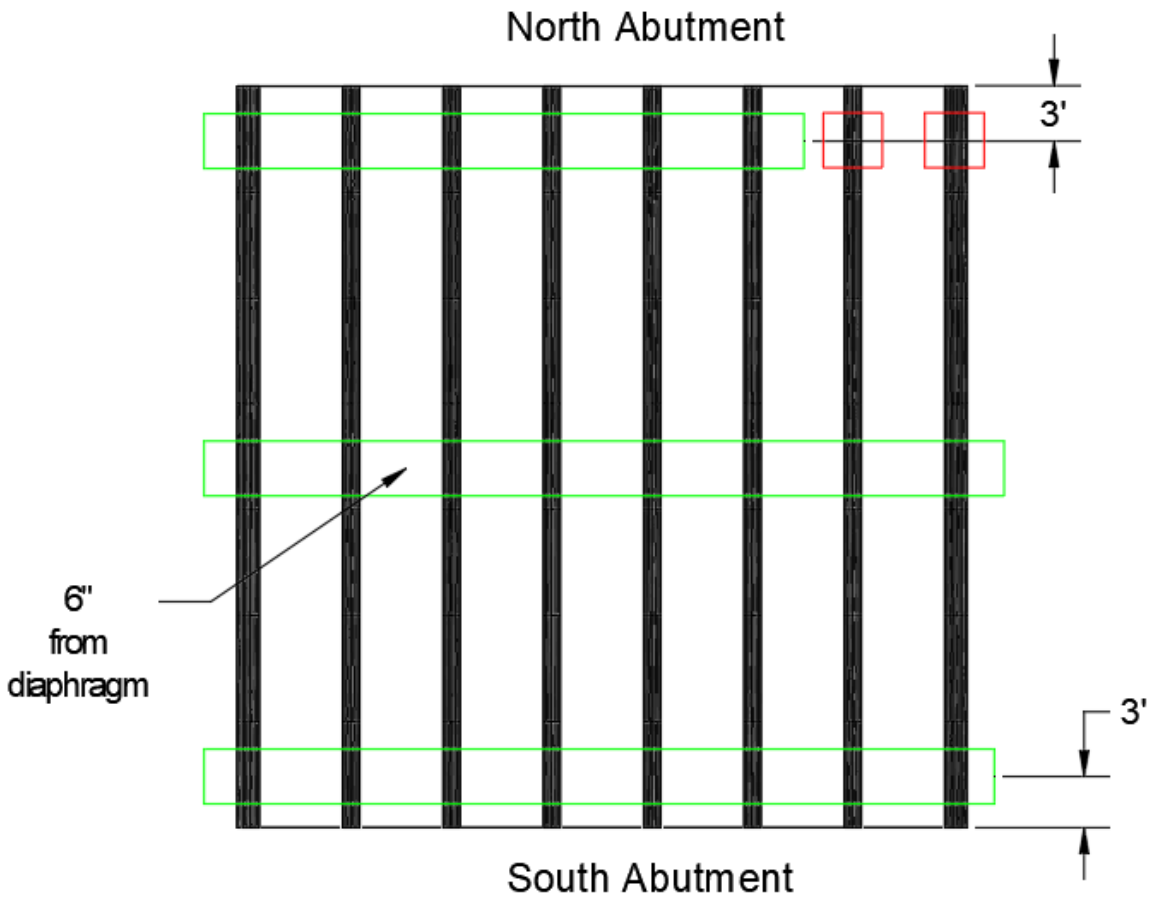

Figure 72. Plan View of Sensor Layout for Yutan Bridge Load Test 2

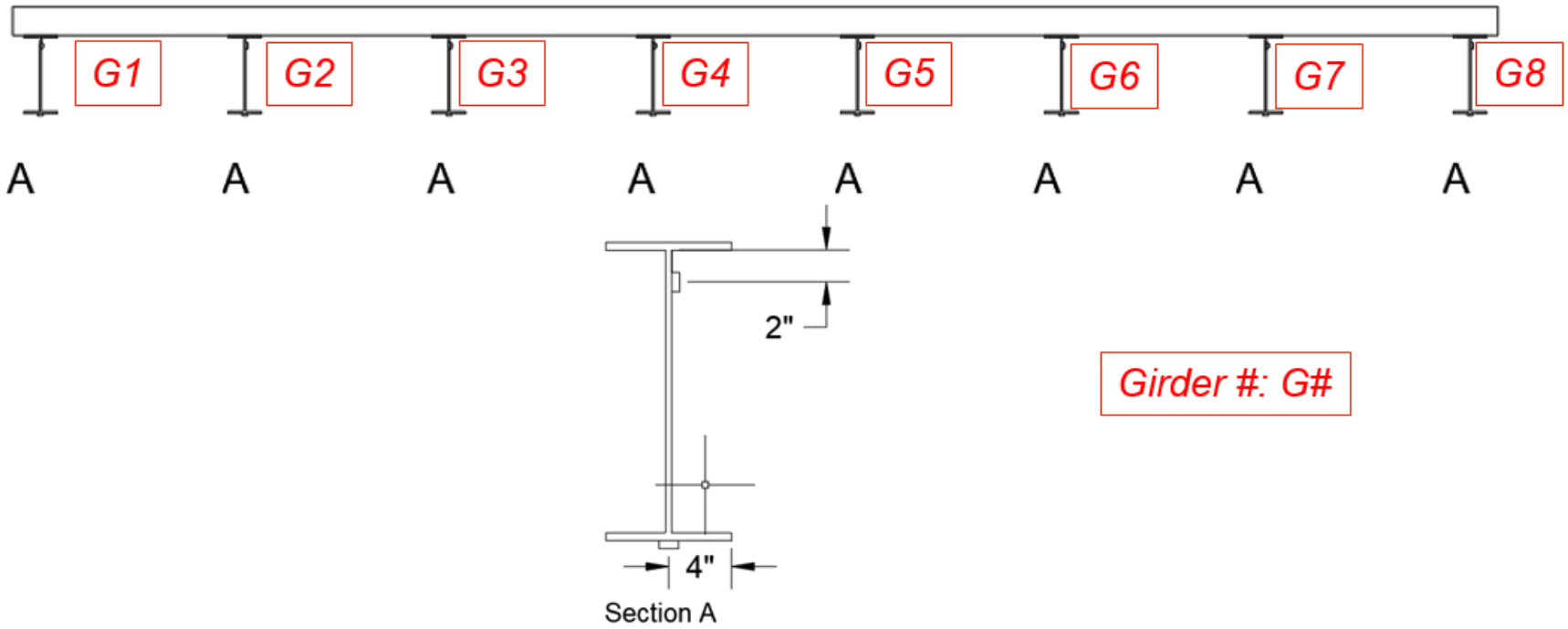

Figure 73. Cross-Section View of Sensor Layout (looking north) for Yutan Bridge Load Test 2

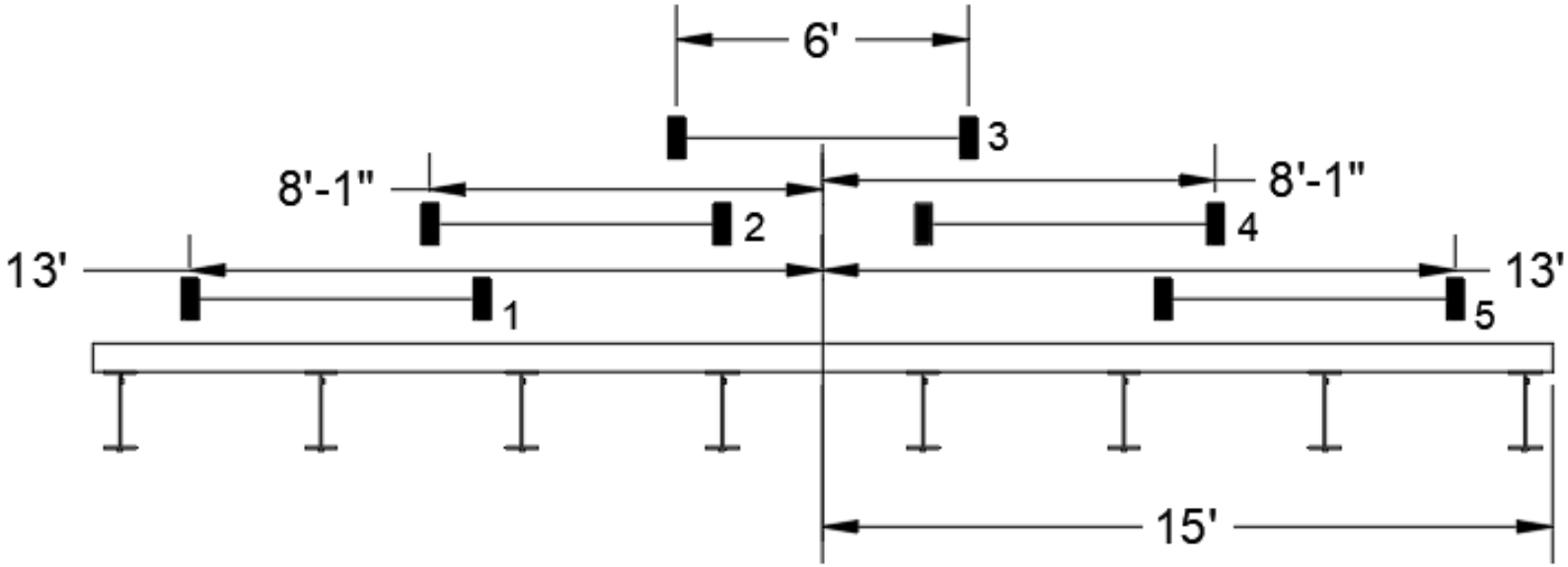

Figure 74. Load Test Plan for Yutan Bridge Load Test 2

Table 22. Truck Runs for Yutan Bridge Load Test 2

Run	Truck Position	Direction	Speed
1	1	N	Slow
2	1	S	Slow
3	2	N	Slow
4	2	S	Slow
5	2	N	Fast
6	2	S	Fast
7	3	N	Slow
8	3	S	Slow
9	3	N	Fast
10	3	S	Fast
11	4	N	Slow
12	4	S	Slow
13	4	N	Fast
14	4	S	Fast
15	5	N	Slow
16	5	S	Slow

8.6 Diagnostic Field Testing Data Processing

8.6.1 Unintended Composite Action

The presence of composite behavior was determined by examining strain profiles across the depth of each instrumented steel girder. Girders exhibiting composite behavior may potentially be benefited by accounting for enhanced capacity in load ratings, provided that interface shear transfer between the girder and deck is expected to be reliable under heavy loading. Theoretically, noncomposite sections have an elastic neutral axis, ENA, at the mid-depth of a rolled steel section, given that rolled steel sections are geometrically symmetric about their horizontal centroidal axis. Since there were strain gauges at the bottom flange and near the top web, the absolute value of the strain measurements should be similar upon a cursory inspection even without performing calculations, with only a minor differential attributed to the top gauge placement on the web instead of the flange.

A girder loaded in positive flexure experiences tension in the bottom flange, and compression in the web above the neutral axis. Tension and compression strain measurements are expressed as positive and negative microstrains (με), respectively, by the BDI testing system. Of the girders instrumented in the first load test, girder 2 appears to be noncomposite for all of the runs performed, as shown in Figure 75. A composite section, shown in Figure 76, exhibits top strain gauge readings closer to zero, reflecting the upward shift of the ENA for composite sections with the concrete deck participating through flexural compression resistance.

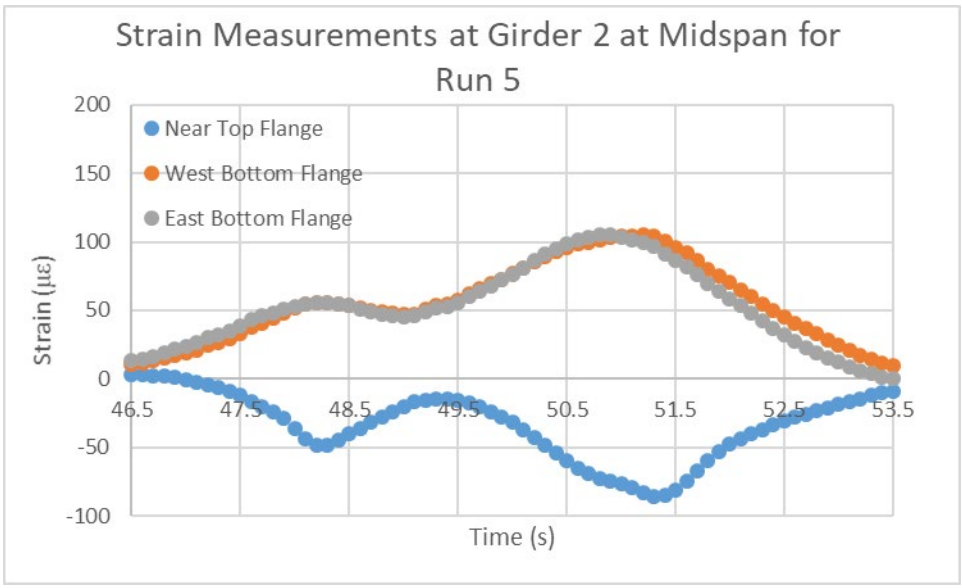

Figure 75. Example Noncomposite Strain Measurements

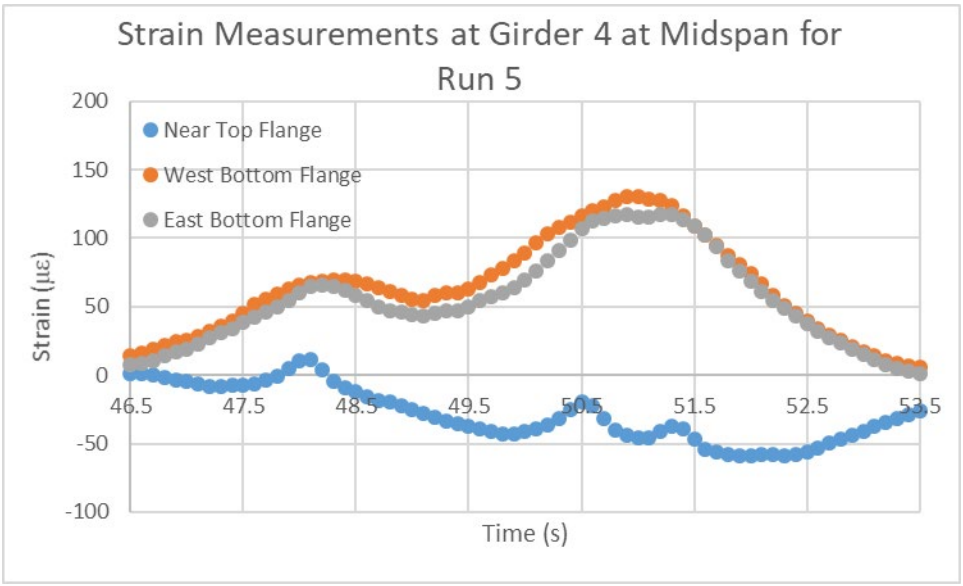

Figure 76. Example Composite Strain Measurements

The expected ENA for a noncomposite and composite section of an interior girder are shown below in Figure 77. The ENA for the composite section is based on AASHTO short-term section properties with the modular ratio, n, taken as 9.2.

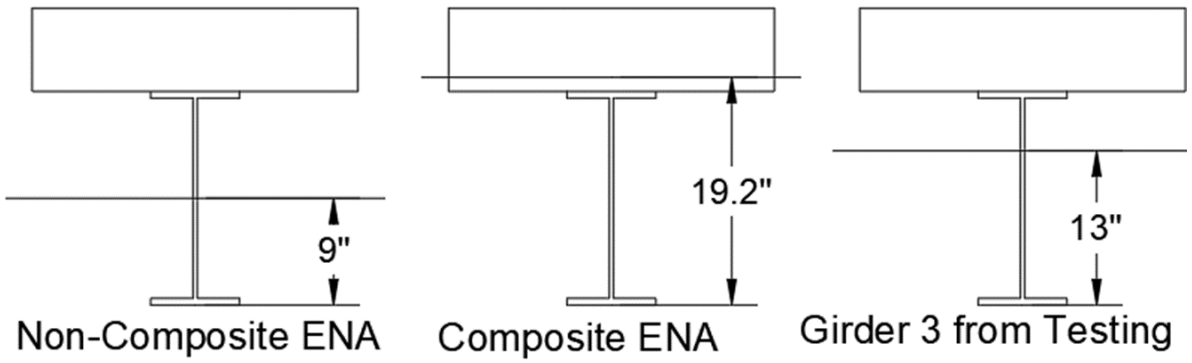

Figure 77. Theoretical and Measured ENA Locations

ENA values for the midspan were determined by assuming a linear strain variation across the entire steel section. This method, shown in Eqn. 104 and Eqn. 105, is consistent with the method used by Jeffrey et al. (2009). For Test 1, the bottom flange strain, ε_{bottom}, was taken as an average of the two bottom flange strains. The curvature, denoted as m (in^{-1}), is determined by dividing the difference in top and bottom strains by the vertical separation distance between instrument locations. The ENA height from the bottom flange, y (in), is then determined from Eqn. 105.

$$m = \frac{\varepsilon_{top} - \varepsilon_{bottom}}{height\ of\ top\ strain\ gauge} \quad \text{Eqn. 104}$$

$$y = \frac{-\varepsilon_{bottom}}{m} \quad \text{Eqn. 105}$$

Only Girder 2 exhibited noncomposite behavior in Test 1. All other girders exhibited partial composite behavior. The instrumentation plan assumed identical behavior across girders and did not include instrumentation on Girders 6 or 7 in Test 1. Test 2 confirmed noncomposite behavior at Girder 2 and also found that Girder 6 exhibited noncomposite behavior. All other girders exhibited partial composite behavior in Test 2.

8.6.2 Post-Processing for Positive Flexure Load Effects

Composite effectiveness varied across the bridge section. Most, but not all, girders exhibited significant influence on measured steel girder strains from composite deck participation. Typical methods to characterize load distribution using ratios of measured values, such as bottom flange strains, were therefore unrepresentative of the actual load acting at each individual girder. To obtain a legitimate and rational characterization of load distribution, the measured strains were post-processed to estimate positive moments at each girder. Load testing GDFs could then be established as moment fractions.

The AASHTO BDS does not explicitly recognize partially composite construction. All provisions for I-section flexure address either noncomposite or composite construction, and BDS Article 6.10.10.4 implicitly requires design for full composite strength. AASHTO BDS may be considered to implicitly acknowledge partial composite behavior, through SF or Ka terms or both. Additional discussion related to these points is provided in the next section of this chapter.

Partial composite behavior for service conditions is typically represented in applications outside of bridge engineering as slip between the concrete deck and steel girder. A similar approach was used to evaluate test results for the Yutan Bridge. The general strain profile for partially composite behavior and definitions of the strain terms are provided in Figure 78 and Table 23.

This approach uses a notional slip effect to represent partially composite behavior. The effect is notional in that it is phenomenologically similar to the aggregate resultant influence of deck-to-girder shear transfer flexibility. Flexibility is believed to have been introduced through (1) shear lag through the steel deck in the vicinity of presumed puddle welds, and (2) in-plan flexure of the corrugated deck as inclined corrugation surfaces develop compression against deck

concrete. Relative longitudinal motion at deck-to-girder connections is not necessarily large or significant, but no measured data is available to clearly establish the true stress states in the deck and shear transfer connections.

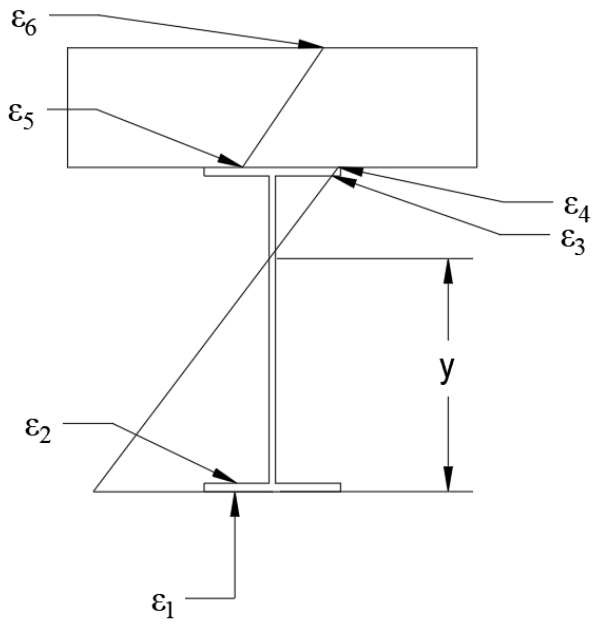

Figure 78. General Partial Composite Strain Profile

Table 23. Strain Locations

Subscript	Location
1	Bottom of Bottom Flange
2	Top of Bottom Flange
3	Bottom of Top Flange
4	Top of Top Flange
5	Bottom of Concrete
6	Top of Concrete

Using the strain profile, m, and ENA height, y, from Eqn. 104 and Eqn. 105, respectively, strains at other key points in the steel section were calculated using linear interpolation and extrapolation, as shown in Eqn. 106 to Eqn. 108. The tensile strains below the ENA are taken as positive values and the compressive strains above the ENA are taken as negative values.

$$\varepsilon_2 = (y - t_f) * m \quad \text{Eqn. 106}$$

$$\varepsilon_3 = (y - d + t_f) * m \quad \text{Eqn. 107}$$

$$\varepsilon_4 = (y - d) * m \quad \text{Eqn. 108}$$

Strains were converted to stresses, sigma (ksi), by multiplying the strain by the modulus of elasticity, E (ksi), at each key steel location. Steel forces were calculated by integrating stresses over areas. With a linear strain and stress diagram, stress profiles were simply triangular or trapezoidal areas acting over either a flange width or the web thickness, as shown in Eqn. 109 through Eqn. 112.

$$P_{s,tensionweb} = \sigma_2 * A = \sigma_2 \frac{(y - t_f) * t_w}{2} \quad \text{Eqn. 109}$$

$$P_{s,tensionflange} = \sigma_{avg,tension\,flange} * A = \frac{(\sigma_2 + \sigma_1)}{2} * t_f * b_f \quad \text{Eqn. 110}$$

$$P_{s,compressionweb} = \sigma_3 * A = \frac{\sigma_3 * (d - y - t_f) * t_w}{2} \quad \text{Eqn. 111}$$

$$P_{s,compressionflange} = \sigma_{avg,compression\,flange} * A = \frac{(\sigma_3 + \sigma_{4,steel})}{2} * t_f * b_f \quad \text{Eqn. 112}$$

The subscript "s" denotes that the force under consideration exists in the steel girder. Determining the net force in the steel section:

$$P_{s,net} = P_{s,tensionweb} + P_{s,tensionflange} + P_{s,compressionweb} + P_{s,compressionflange} \quad \text{Eqn. 113}$$

Test results indicated that support restraint was minor and induced negligible bridge axial load from thrust against supports. To satisfy beam theory with no net axial load, then:

$$P_c = -P_{s,net}$$ Eqn. 114

A "c" subscript indicates that the force exists in the concrete. To satisfy compatibility, the deck curvature, m, must match the steel girder. Using the notional slip effect to approximate the concrete strain profile, short-term elastic stress-strain in the concrete, and ignoring concrete tension, the concrete is quadratically related to the maximum concrete strain. The depth of the concrete compression region can then be determined from the concrete strain. Lastly, partially composite girder moment was determined by summing individual forces multiplied by moment arms from an arbitrary horizontal axis.

8.6.3 Repeatability of Load Tests

Results of the first and second load test were compared to evaluate the repeatability of load testing results. Figure 79 shows a sample of data used to compare midspan moment-fraction GDFs (the ratio of each girder moment to the total bridge moment under the applied load) for the maximum moment condition when the vehicle traveled along the interior girder critical loading path. Girders 1 through 5 are most useful for this comparison. Girders 6 and 7 were not instrumented in Test 1, and vehicle paths concentrated loads on the instrumented girders in Test 1, resulting in only very small strains at Girder 8. As shown in Figure 79, the load tests generally show close agreement. As noted previously, Girder 2 exhibited noncomposite behavior. The research team perceives the relatively low moment distribution participation in this girder as reflecting a significantly lower flexural stiffness in the absence of composite action. Girder 2 was the only location with significant differences between Test 1 and Test 2. This difference is attributed to performing the test with different field testing team members. A limited number of strain gauge attachments were detached with surprisingly little effort following Test 2, suggesting an inadequate bond between the sensor and girder.

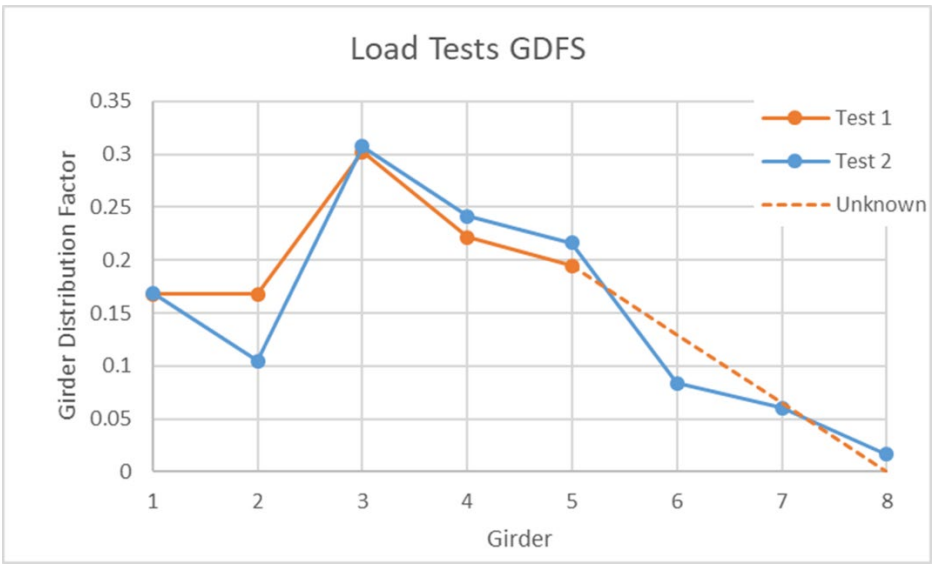

Figure 79. Moment-Fraction GDF Comparison between Tests 1 and 2 for the Critical Interior Girder Load Path

8.7 Diagnostic Field Testing Load Rating

The research team referred to MBE Section 8, particularly Article 8.8.2, for guidance to obtain an updated load rating using diagnostic load testing. A rating factor obtained from diagnostic load testing, RF_T, is determined from the product of a reference rating factor obtained from calculations, RF_C, and an adjustment factor, K, as shown in Eqn. 115.

$$RF_T = RF_C * K \qquad \text{Eqn. 115}$$

MBE (8.8.2.3-1)

The overall benefit from the diagnostic load test, K, is a result of two factors, K_a and K_b, as shown in Eqn. 116.

$$K = 1 + K_a K_b \qquad \text{Eqn. 116}$$

MBE (8.8.2.3.1-1)

K_a is the direct comparison between theoretical and measured field test results, as shown in Eqn. 117.

$$K_a = \frac{\varepsilon_C}{\varepsilon_T} - 1$$ Eqn. 117
MBE (8.8.2.3.1-2)

Theoretical strain determined from calculations, ε_C, is to be determined according to Eqn. 118 from the theoretical load effect acting in a girder, L_T, a section factor, SF, and the modulus of elasticity of steel, E.

$$\varepsilon_C = \frac{L_T}{(SF)E}$$ Eqn. 118
MBE (8.8.2.3.1-3)

K_b reflects the confidence that the load rating engineer has, or lack thereof, in the ability of the field test to represent expected bridge behavior under heavy truck loads. MBE leaves the exact determination of the appropriate K_b to the discretion of the load rating engineer, but does provide recommended values in MBE Table 8.8.2.3.1-1, which are replicated below in Table 24. In the Table, T represents the actual test vehicle effect, and W represents the nominal gross rating load effect.

Table 24. Recommended Values for K_b

Can member behavior be extrapolated to 1.33W?		**Magnitude of test load**			**K_b**
Yes	**No**	$\frac{T}{W} < 0.4$	$0.4 \leq \frac{T}{W} \leq 0.7$	$\frac{T}{W} > 0.7$	
✓		✓			0
✓			✓		0.8
✓				✓	1
	✓	✓			0
	✓		✓		0
	✓			✓	0.5

The proper method to consider unintended composite action in this methodology is not immediately obvious. MBE Article 8.8.2.3.1 states that "the theoretical strain ε_C resulting from

the test load should be calculated using a section factor which most closely approximates the member's actual resistance during the test." The Article then refers the reader to NCHRP Research Results Digest (RRD) 234. The specific RRD 234 pages referenced in the MBE use very similar language to that already found in the main article and associated Commentary in the MBE. However, exploring further to review the Illustrative Examples provided in RRD 234 Chapter 9 provides informative supplementary information and application guidance.

The RRD 234 Illustrative Examples include a composite steel girder example in Section 9.1.1 and a corresponding alternative approach for the same bridge in Section 9.1.2 assuming that the bridge is noncomposite. The noncomposite example calculations indicate that the "apparent section modulus" should be used to determine Ka and K. This initially results in a marginal benefit for the noncomposite bridge. However, the example continues with additional calculations wherein the RF_C is recalculated assuming composite capacity. This procedure results in an identical rating factor to the bridge in Section 9.1.1 which had been assumed composite throughout the example calculations. However, additional calculations are required in Section 9.1.2 to justify the expectation that interface shear strength can be reasonably expected to provide adequate composite capacity and maintain composite behavior under load at 1.33W.

The exterior girder was the critical member, and results presented here will focus exclusively on that structural element. Six cases were considered to examine the implications of various evaluation selection, as summarized in Table 25. Intermediate K calculations are provided in Table 26, and updated rating factors, RF_T, are provided in Table 27. The theoretical live load effect during the test, L_T, was consistent for all Cases. The test vehicle created a critical

moment across the bridge of 234 k-ft by determinate structural analysis with a moving load. The theoretical load effect in the exterior girder was (recall Eqn. 91 for the GDF):

$$L_T = \left(\frac{g_{ext,1lane}}{m}\right) M_{test\,truck} = \left(\frac{0.394}{1.2}\right)(234\,k-ft)\frac{12\,in.}{1\,ft} = 922\,k-in \qquad \text{Eqn. 119}$$

The theoretical GDF used previously for an analytical load rating included a multiple presence adjustment, as required by the AASHTO BDS. To characterize the theoretical predicted mechanical response, the multiple presence factor should be removed from the GDF when determining L_T. The maximum bottom flange strains for the exterior critical lane path were 234 and 216 με during the two runs performed to induce critical load in Girder 1. The average of these two bottom flange strain measurements, 225 με, was used for ε_T in Eqn. 117 for K_a when comparing to theoretical expected strains, ε_C.

The objective of this rating is to evaluate the Operating level for AASHTO LRFR. Therefore, W in Table 24 corresponds to the static effect of the nominal HL-93 effect. Recalling Eqn. 85 and Eqn. 86, the moment effects of an HS-20 truck and the design lane were 287 k-ft and 74 k-ft, respectively, resulting in W equal to 361 k-ft. With T equal to 234 k-ft for the Type 3 vehicle used in the load tests, T/W = 0.64. The MBE therefore recommends that K_b should be taken as 0.8 when load test behavior can be extrapolated to 1.33W, or 0 otherwise. Cases 1, 3, and 5 consider a K_b of 0.8. Cases 2, 4, and 6 consider a K_b of 0.

Table 25. Diagnostic Load Test Rating Options

Case	SF for K_a	K_b	Capacity for RF_C
1	Noncomposite	0.8	Noncomposite
2	Noncomposite	0	Noncomposite
3	Composite	0.8	Noncomposite
4	Composite	0	Noncomposite
5	Composite	0.8	Composite
6	Composite	0	Composite

In Cases 1 and 2, the noncomposite bare steel section modulus was used for SF in Eqn. 118, and the girder capacity was determined by assuming a noncomposite section. In Cases 3 and 4, the SF is taken as the composite section modulus in Eqn. 118, but the girder capacity continued to be taken as the noncomposite capacity. Lastly, in Cases 5 and 6, a composite section modulus is used for SF, and the girder capacity was also determined by assuming a composite section.

Cases 1, 2, 5, and 6 use consistent section assumptions for both stiffness when determining K from the ratio of ε_C and ε_T, and also capacity when determining RF_C. This internal consistency is intuitively appealing. Cases 1 and 2 may be the initial inclination of a rating engineer evaluating load test results. The bridge girder capacities were presumed to be noncomposite, so it would seem reasonable to also use the noncomposite section properties for SF. However, RRD 234 Section 9.1.2 indicates that the default approach should be Cases 3 and 4 for a noncomposite bridge. The RRD 234 example progressed onward to consider a modified result according to Cases 5 and 6. Adequate composite interface shear transfer was demonstrated by calculations in the RRD example to substantiate use of composite capacity.

Table 26. Diagnostic Load Test Rating Options – K Calculations

Case	SF (in^3)	ε_C $(\mu in.)$	K_a	K_b	K
1	88.9	358	0.59	0.8	1.47
2	88.9	358	0.59	0	1
3	139	228	0.01	0.8	1.01
4	139	228	0.01	0	1
5	139	228	0.01	0.8	1.01
6	139	228	0.01	0	1

Table 27. Diagnostic Load Test Rating Options – RF_T Calculations

Case	C (k-ft)	RF_C	K	RF_T
1	303	0.92	1.47	1.36
2	303	0.92	1	0.92
3	303	0.92	1.01	0.93
4	303	0.92	1	0.92
5	565	2.01	1.01	2.03
6	565	2.01	1	2.01

Cases 5 and 6 result in very large increases in rating factors, but the lack of any information to define the shear transfer mechanism prevents these results from being used. The bridge may potentially possess a very high rating factor similar to those in Cases 5 and 6, but the bridge would need to be subjected to a proof test to justify such rating factors.

Similar to the result in RRD 234 Section 9.1.2, when noncomposite capacity is coupled with composite stiffness in the evaluation of test results, the perceived benefit is very small. In this case, the results suggest negligible benefit from the load test. Although the results of Cases 5 and 6 appear unreasonably unconservative, the results for Cases 3 and 4 conversely appear unreasonably conservative. If composite behavior is present and affects the perceived benefit in K_a, then it seems at least possible that a benefit could be realized in the rating factor.

Cases 1 and 2 then appear to reasonably bound the potential rating factors, although using these results is inconsistent with RRD 234 and the current guidance in MBE. The load rating engineer must also determine how to map the elastic behavior observed during the test to anticipated strength under heavy loads, which may include partial plasticity. Even using the maximum RF_T value of 1.36 would not require the girder to achieve full plastic composite strength, which would provide an RF_T of about 2, referring to Cases 5 and 6. The MBE offers no assistance in addressing this consideration, other than to recommend K_b equal to zero unless the engineer can characterize and justify their assignment of an RF that can be reasonably and safely expected when loaded at 1.33W.

An alternative, rational procedure is recommended herein. MBE does not require that load testing data processing include determination of aggregate load effects, instead relying on the ratio of ε_C and ε_T to represent load testing benefits. As noted in the previous section, the load testing post-processing performed for the field tests in this project included determination of noncomposite and partially composite girder moments, as appropriate to each girder upon review of recorded response. The post-processed moments could then be used to establish load testing GDFs as moment-fractions relative to the total moment induced by the applied load across the entire bridge cross-section. An updated RF_T could then be determined for the critical exterior girder as:

$$RF_T = RF_C \frac{\left(\frac{g_{ext,1lane}}{m}\right)}{g_{ext,test}} = (0.92)\frac{\left(\frac{0.394}{1.2}\right)}{0.307} = 0.99 \qquad \text{Eqn. 120}$$

8.8 Summary and Recommendations

This section illustrated the application of a methodology to remove or raise load posting, taking advantage of improved analytical predictions from ANN-based girder distribution factors to aid in selection of appropriate candidates for refined analyses and/or load testing. The Yutan Bridge was load posted according to standard AASHTO analytical rating methods. However, ANNs indicated that an improved rating factor is expected for this bridge and that the load posting could likely be relaxed or removed. During a load test, the bridge exhibited unintended partial composite behavior, which posed complicated implications for rating evaluation. Calculated rating factors obtained from various methods for the Yutan Bridge are shown in Table 28. These rating factors do *not* include an improved dynamic load effect.

Table 28. Yutan Bridge Rating Factor Comparison

Method	**Rating Factor**
AASHTO Line Girder	0.92
Unadjusted ANN	1.02
Calibration-Adjusted ANN	0.98
ANSYS	1.04
CSiBridge	0.96
Load Test GDFs (noncomposite)	**0.99**
AASHTO MBE Minimum	0.92
AASHTO MBE Maximum	2.03

The highlighted result is proposed as the updated RF_T. The value is close to the rating factors produced with detailed analysis in ANSYS and CSiBridge, and is believed to be a slightly conservative estimate of the true rating factor. Recalling that Girder 2 exhibited noncomposite behavior and a relatively low GDF compared to the partially composite girders, it is likely that Girders 1 and 3 supported an increased amount of load due to load shedding by the relatively flexible Girder 2 through transverse deck flexure. Under heavy loads, either the girders will maintain composite strength, in which case RF_C and RF_T were significantly underestimated, or composite effectiveness will degrade and load distribution will more closely resemble that predicted by ANSYS, resulting in a slightly higher actual RF than that highlighted in Table 28.

Ideally, a computational model would be developed to accurately reflect the bridge behavior at the testing level and also up to at least 1.33W. Such a model could then be calibrated and validated using field testing data such that K_a effectively equals 1, and then used directly to predict rating factors with comparable accuracy and reliability to load testing. Some degree of judgement would still be required to establish K_b at extrapolated load levels. In the case of the Yutan Bridge, creating such a model would be difficult to achieve at the testing level, and infeasible due to lack of composite connector information for the 1.33W load level. At the testing level, Girders 2 and 6 would need to be modeled such that longitudinal slip occurs and composite behavior is negligible. Meanwhile, all other girders would need to reflect not simply composite behavior, but the relatively flexible, partially composite behavior exhibited during the test. This level of modeling effort was outside the scope of the project, and the RF highlighted in Table 28 is recommended as a reasonable and slightly conservative characterization of the AASHTO LRFR Operating rating for Strength I.

8.9 Other Considerations

8.9.1 Dynamic Load Amplification

MBE Article 6A.4.4.3 Dynamic Load Allowance specifies the typical amplification applied to static load effects of trucks to account for vertical vibrations of trucks moving across a bridge, and was referenced previously when discussing an analytical LRFR rating using typical assumptions and tools in the AASHTO BDS. The accompanying Commentary C6A.4.4.3 notes that "dynamic response of a bridge to a crossing vehicle is a complex problem affected by the pavement surface conditions and by the dynamic characteristics of both the bridge and vehicle." The commentary continues to discuss that roadway conditions are believed to be the dominant influence rather than vehicle characteristics. Table C6A.4.4.3-1 allows IM to be reduced from the standard value of 33% down to 20% or 10%, depending on a bridge inspectors observations. However, the Commentary Article also notes that "the riding surface conditions used in Table C6A.4.4.3-1 are not tied to any measured surface profiles, but are to be selected based on field observations and judgement of the evaluator." This is remarkably ambiguous guidance for selection of a parameter that can potentially increase a load rating by up to about 20%.

It would seem preferable to measure dynamic amplification in the field, rather than relying on an Inspector's personal judgement to arbitrarily sway a key parameter in a bridge load rating. This sentiment is found in MBE Article 8.3.5, which states "the use of full-scale dynamic testing under controlled or normal traffic conditions remains the most reliable and cost-effective way of obtaining the dynamic load allowance for a specific bridge." This project included a limited investigation of bridge dynamic response, as a marginal cost value-added activity to accompany quasi-static dynamic bridge tests. Data collected during Test 2 for runs performed at

highway speeds revealed that the maximum dynamic amplification of strains was approximately 3% relative to crawl speeds results for the same truck travel paths.

Dynamic tests are discussed in MBE Article 8.4.2. The primary subsections of interest and likely use to most bridge owners are MBE Articles 8.4.2.1—Weigh-In-Motion Testing and 8.4.2.2—Dynamic Response Tests. WIM testing is typically performed at a site by recording data over a period of time from days to years to characterize probabilistic expectations of dynamic response. MBE Article 8.4.2.2 for dynamic response tests states that "a variety of vehicle types, speeds, weights, and positions should be considered in estimating the appropriate dynamic load allowance." The testing for this project was limited to a single truck and a single speed, with a limited number of passes, and therefore could not be considered to satisfy the requirements stated in MBE to allow adjustment of IM, although they do suggest that use of the typical IM is likely unnecessarily conservative and could be reduced with an additional investment to satisfy MBE Article 8.4.2.

If adequate dynamic testing data was available, MBE Article 8.3.5 states that "measured dynamic load allowance may be used in place of code-specified value in load-rating calculations." This statement suggests that the measured 3% might be substituted for the typical 33% value. It is unfortunate that the MBE is silent regarding the rational basis for this approach, which may lead to unconservative evaluations. Engineers should bear in mind that all coefficients in deterministic LRFD/R limit state and rating factor equations were influenced by probabilistic variables.

AASHTO calibration studies for LRFD (NCHRP 20-07/Task 186 in 2007) and LRFR (NCHRP 20-07/Task 285 in 2011) note that 30% is near the upper bound of previously measured

dynamic amplifications, and a significantly lower mean dynamic amplification of 10% was used during AASHTO LRFD calibration (Kulicki et al., 2007). The coefficient of variation of dynamic amplification has been estimated at 80%, and contributed appreciably to dynamic live load variability during LRFD/R calibration. With limited data, a more rational approach would be to scale dynamic live load effects by 1.03 / 1.10 which would correspond to an approximate 7% amplification to the load rating, rather than substituting 3% for 33% IM which would correspond to an approximate 30% amplification to the load rating. As more data becomes available to justify a reduced variability (lower than 80% assumed in LRFD/R calibration), further reliability calibrations could rationally justify further reducing dynamic live load effects. Current MBE guidance to substitute measured dynamic amplification for the code-specified value would seem to imply that variability was reduced, but this is not clearly stated or qualified.

8.9.2 AASHTO LFR Rating with ANN GDFs

AASHTO Load Factor Rating (LFR) was used by NDOT to establish the posting for the Yutan Bridge. NDOT has expressed interest in continuing to rate bridges designed by LFD using LFR. The reliability calibration performed in this project cannot be arbitrarily applied to LFR with an expectation of similar reliability, because LFR is not fundamentally a reliability-calibrated load rating basis. However, the ANN-based GDF without reliability calibration was developed from detailed analytical models, and these analytical models are applicable to either LFR or LRFR. This section will provide an example of how the ANN-based GDFs might be applied to LFR. LFR references the AASHTO Standard Specifications (SS), so the following calculations will use guidance from the Standard Specifications, together with communication from personnel responsible for performing and overseeing bridge load ratings at NDOT.

First, an analytical rating performed using what are believed to be typical assumptions will be developed as a baseline. LFR Operating Rating Factors for flexural strength were determined from Eqn. 121:

$$RF = \frac{C - A_1 D}{A_2 L(1+I)} \qquad \text{Eqn. 121}$$

MBE (6B.4.1-1)

According to MBE Article 6B.4.3, A_1 = 1.3, and A_2 = 1.3 for the Operating level.

Nominal dead loads from concrete deck weight (LRFR DC) and asphalt topping weight (LRFR DW) were combined into a single D term for LFR. SS 3.23.2.3.1.1 indicates deck weight should be distributed by tributary width, whereas the BDS allows all dead loads to be distributed uniformly to girders. SS 3.23.2.3 applies to "Outside Roadway Stringers and Beams", but adjusting the deck weight applied to the exterior girder results in a reduction for the Yutan Bridge with a tributary width equal to the overhang (9.5 in.) width plus one-half of a girder spacing (2.06 ft). Although SS 3.23.2.2 for "Interior Stringers and Beams" does not explicitly address dead loads, the interior girder dead load was increased for the LFR analysis presented here by using a girder spacing tributary width (4.125 ft) for deck load to ensure that the full dead load of the deck was accounted for. The D moment effects for exterior and interior girders were:

$$w_{D,ext} = 0.433\frac{k}{ft} \qquad \text{Eqn. 122}$$

$$D_{ext} = M_{D,ext} = \frac{w_{D,ext} L^2}{8} = \frac{\left(0.433\frac{k}{ft}\right)(30.5\,ft)^2}{8} = 50.3\,k-ft \qquad \text{Eqn. 123}$$

$$w_{D,int} = 0.544\frac{k}{ft} \qquad \text{Eqn. 124}$$

$$D_{int} = M_{D,int} = \frac{w_{D,int}L^2}{8} = \frac{\left(0.544\frac{k}{ft}\right)(30.5\,ft)^2}{8} = 63.3\,k-ft \qquad \text{Eqn. 125}$$

For live loads, the nominal moment effect of an HS-20 truck was 287 k-ft, as noted previously in Eqn. 85. LFD/R considers wheel loads rather than lanes, so the HS-20 truck was factored by ½ for the LFR evaluation. For the interior girder, according to SS Table 3.23.1, the wheel line GDFs are:

$$g_{\text{int},1lane} = \left(\frac{S}{7}\right) = \left(\frac{4.125\,ft}{7}\right) = 0.589 \qquad \text{Eqn. 126}$$

$$g_{\text{int},2lane} = \left(\frac{S}{5.5}\right) = \left(\frac{4.125\,ft}{5.5}\right) = 0.750 \qquad \text{Eqn. 127}$$

The wheel line GDF for the exterior girder is determined by the lever rule according to SS 3.23.2.3.1.2, which was calculated previously:

$$g_{ext,lever\,rule} = \frac{4.125\,ft - 1.417\,ft}{4.125\,ft} = 0.657 \qquad \text{Eqn. 90}$$

However, SS 3.23.2.3.1.5 requires a minimum wheel line GDF identical to Eqn. 127. The critical wheel line GDF, then, is:

$$g_{critical} = \max\left(g_{\text{int},1lane}, g_{\text{int},2lane}, g_{ext,lever\,rule}, g_{ext,\min}\right)$$
$$g_{critical} = \max\left(0.589,\ 0.750,\ 0.657,\ 0.750\right) = 0.750 \qquad \text{Eqn. 128}$$

The live load required for interior and exterior girders is identical, and the dead load is higher for the interior girder, so the interior girder will control.

MBE Article 6B.6.4 notes that impact, I, should be considered in accordance with the SS, for which:

$$I = \left[\frac{50}{(L+125)} \le 0.3\right] = \left[\frac{50}{(30.5\,ft+125)} \le 0.3\right] = [0.32 \le 0.3] = 0.3 \qquad \text{Eqn. 129}$$

And

$$L(1+I) = \left(\frac{287\,k-ft}{truck}\right)\left(\frac{1\,truck}{2\,wheel\,lines}\right)(0.750)(1+0.3) = 140\,k-ft \qquad \text{Eqn. 130}$$

As noted previously, the girders are compact AISC rolled shapes. Therefore, the capacity, C, for each noncomposite girder is determined according to SS Article 10.48.1 as:

$$M_u = F_y Z = \frac{(36\,ksi)(101\,in^3)}{12\frac{in}{ft}} = 303\,k-ft \qquad \text{Eqn. 131}$$

SS (10-92)

Provided that the requirement of SS Article 10.48.1.1(c) is satisfied to avoid lateral instability:

$$\frac{L_b}{r_y} \le \frac{\left[3.6-2.2(M_1/M_u)\right]x10^6}{F_y} \qquad \text{Eqn. 132}$$

$$L_b \le \left(\frac{\left[3.6-2.2(M_1/M_u)\right]x10^6}{F_y}\right) r_y \qquad \text{SS (10-96)}$$

Here, the yield stress, Fy, is in units of psi rather than ksi. M1 is 0 for a simply supported girder braced at midspan. Substituting the weak axis radius of gyration, r_y, obtained from the AISC shapes database:

$$L_b \le \left(\frac{3.6x10^6}{36{,}000\,psi}\right)(1.65\,in.) = 165\,in. = 13.75\,ft \qquad \text{Eqn. 133}$$

The unbraced length for the Yutan Bridge is one-half of the span length: 15.25 ft or 183 in. This braced length would be adequate to develop:

$$F_{y,eff} \le \left(\left[3.6 - 2.2\left(M_1 / M_u\right)\right] x10^6\right)\frac{r_y}{L_b}$$
$$F_{y,eff} \le \frac{\left(3.6x10^6\ psi\right)}{1000\ psi/1ksi}\frac{1.65in.}{183in.} = 32.5\,ksi$$ Eqn. 134

So that

$$C = M_{u,eff} = F_{y,eff}Z = \frac{\left(32.5\,ksi\right)\left(101in^3\right)}{12\frac{in}{ft}} = 273\,k-ft$$ Eqn. 135

And finally:

$$RF = \frac{C - A_1 D}{A_2 L\left(1+I\right)} = \frac{\left(273\,k-ft\right)-\left(1.3\right)\left(63.3\,k-ft\right)}{\left(1.3\right)\left(140\,k-ft\right)} = 1.05$$ Eqn. 136

This value is noticeably higher than those recorded on the NDOT LRSS in Figure 59 and Figure 60, which were 0.83 and 0.896, respectively. Consulting with NDOT personnel, this bridge was presumed to be constructed of steel with F_y = 33 ksi steel, rather than 36 ksi. Furthermore, NDOT policy limited 33 ksi steel capacity to the theoretical yield strength, rather than the plastic strength. Therefore:

$$C_{yield} = M_{yield} = F_y S = \frac{\left(33\,ksi\right)\left(88.9\,in^3\right)}{12\frac{in}{ft}} = 245\,k-ft$$ Eqn. 137

And

$$RF_{yield} = \frac{C_{yield} - A_1 D}{A_2 L\left(1+I\right)} = \frac{\left(245\,k-ft\right)-\left(1.3\right)\left(63.3\,k-ft\right)}{\left(1.3\right)\left(140\,k-ft\right)} = 0.892$$ Eqn. 138

This calculated value is now within 0.5% of the value currently listed in NDOT records.

The ANN-predicted GDF can be used to obtain a modified RF by substituting the ANN-predicted GDF for the S-over GDF specified by the AASHTO Standard Specifications. The ANN-predicted GDF was developed for application to a lane load, so the value should be scaled by a factor of 2 before applying to wheel line effects. Without applying the reliability calibration:

$$RF_{yield,ANN\,non-cal} = \left(RF_{yield}\right)\left(\frac{S-over\,GDF}{\left(\frac{ANN\,GDF}{\left(\frac{2\,wheel\,lines}{1\,lane}\right)}\right)}\right) \qquad \text{Eqn. 139}$$

$$RF_{yield,ANN\,non-cal} = \left(0.892\right)\left(\frac{0.75}{\left(\frac{0.358}{\left(\frac{2\,wheel\,lines}{1\,lane}\right)}\right)}\right) = 0.933$$

Alternatively, with the LRFR reliability calibration:

$$RF_{yield,ANN\,cal} = (0.892)\left(\frac{0.75}{\left(\frac{0.372}{\left(\frac{2\,wheel\,lines}{1\,lane}\right)}\right)}\right) = 0.900 \qquad \text{Eqn. 140}$$

ANN-based GDFs increase the LFR rating by 4.6% when using the direct ANN prediction and 0.9% when using the penalized GDF reliability-calibrated for use in LRFR. The non-calibrated GDF may be conservative even without the reliability calibration penalty when used with LFR. The ANN-based GDFs are the critical GDFs determined according to the HL-93 notional load model, and in the case of the Yutan Bridge were governed by the exterior girder supporting one lane of load. One lane-loaded FEA results were scaled by a multiple presence factor of 1.2 according to the AASHTO LRFD BDS. If multiple presence is not required to be considered in LFR, then the ANN-based GDF has been unnecessarily amplified for use in LFR. The factor cannot simply be scaled to remove the 1.2 multiple presence factor, however, because the resulting factor for the exterior girder may then be lower than the two-lane loaded interior girder GDF, which was expected to govern according to the SS and LFR with S-over GDFs.

8.9.3 Material Strength NDOT Policy Implications

As noted in the previous section, NDOT policy specified that steel girders manufactured with 33 ksi material are not permitted to rely on capacity greater than the theoretical yield strength. However, MBE Appendix L6B, Article L6B.2.1 indicates that compact, noncomposite

steel girders are permitted to rely on the full plastic capacity (Eqn. 131, SS (10-92)) for "steels with a specified minimum yield strength between 33,000 and 50,000 psi." For the Yutan Bridge girders, the capacity would still be slightly influenced by the unbraced length and limited to the value in Eqn. 135. With this adjustment to capacity, C, the bridge would rate to an LFR Operating factor of 1.05 as noted in Eqn. 136, even without considering available benefits from ANN-based GDFs.

8.9.4 Rating to Minimize Steel Yielding

The preceding evaluations have focused exclusively on rating for Strength limit states. However, MBE Article 6A.4.2.2 and Table 6A.4.2.2-1 indicate that Steel bridges should be checked for the Service II with LRFR. According to MBE Article 6A.4.2.1:

$$C = f_r \qquad \text{Eqn. 141}$$

MBE (6A.4.2.1-4)

Then, according to Article 6A.6.4.2.2, with F_y = 36 ksi:

$$C = f_r = 0.80 R_h F_{yf} = (0.8)(1)(36\,ksi) = 28.8\,ksi \qquad \text{Eqn. 142}$$

Or with F_y = 33 ksi:

$$C = f_r = 0.80 R_h F_{yf} = (0.8)(1)(33\,ksi) = 26.4\,ksi \qquad \text{Eqn. 143}$$

The LRFD Service check is presented in terms of stresses so that pre-composite, long-term post-composite, and short-term post-composite load effects can be differentiated and induced stresses can be determined with appropriate section moduli. For a noncomposite steel girder, there is no variation in section modulus with any of these stages of load effects, and the evaluation will be carried out similarly to a Strength check format, in terms of aggregate load effects instead of stresses. In this format, with F_y = 36 ksi:

$$C = f_r S = (28.8\,ksi)\left(\frac{88.9\,in^3}{12\,in./1\,ft}\right) = 213\,k-ft \quad \text{Eqn. 144}$$

Or with F_y = 33 ksi:

$$C = f_r S = (26.4\,ksi)\left(\frac{88.9\,in^3}{12\,in./1\,ft}\right) = 196\,k-ft \quad \text{Eqn. 145}$$

Recalling the rating factor equation for LRFR (slightly modifying by substituting C for M_{nc}):

$$RF = \frac{C-(\gamma_{DC})(M_{DC})-(\gamma_{DW})(M_{DW})}{(\gamma_{LL})(M_{LL,dyn})} \quad \text{Eqn. 97}$$

According to MBE Table 6A.4.2.2-1 for Steel Service II, $\gamma_{DC} = 1$, $\gamma_{DW} = 1$, and $\gamma_{LL} = 1$. So, evaluating the rating factor with the ANN-based GDF without reliability calibration and with F_y = 36 ksi:

$$RF = \frac{(213\,k-ft)-(1.00)(44.5\,k-ft)-(1.00)(15.5\,k-ft)}{(1.00)(163.5\,k-ft)} = 0.94 \quad \text{Eqn. 146}$$

Or with the ANN-based GDF reliability-calibrated relative to the LRFR Strength I limit state and with F_y = 36 ksi:

$$RF = \frac{(213\,k-ft)-(1.00)(44.5\,k-ft)-(1.00)(15.5\,k-ft)}{(1.00)(169.5\,k-ft)} = 0.90 \quad \text{Eqn. 147}$$

Alternatively, evaluating the rating factor with the ANN-based GDF without reliability calibration and with F_y = 33 ksi:

$$RF = \frac{(196\,k-ft)-(1.00)(44.5\,k-ft)-(1.00)(15.5\,k-ft)}{(1.00)(163.5\,k-ft)} = 0.83 \quad \text{Eqn. 148}$$

Or with the ANN-based GDF reliability-calibrated relative to the LRFR Strength I limit state and with F_y = 36 ksi:

$$RF = \frac{(196k-ft)-(1.00)(44.5k-ft)-(1.00)(15.5k-ft)}{(1.00)(169.5k-ft)} = 0.80 \qquad \text{Eqn. 149}$$

Service II rating factors are approximately 8% lower than Strength I rating factors when comparing with otherwise identical parameters (yield strength, GDF reliability calibration). Calculations were provided for cases with Strength-based reliability-calibrated ANN GDFs, but there is not a rational foundation for performing this or any other reliability calibration for Service limit state evaluations. MBE Commentary C6A.6.4.2.2 states "it is important to note that the live load factors for the Service II limit state were not established through reliability-based calibration, but were selected based on engineering judgement and expert opinion. The level of reliability represented by this serviceability check is unknown." Therefore, the research team proposes that using the GDFs without a reliability calibration would be reasonable, or the GDFs with the reliability calibration could be used to provide some degree of assurance of a conservative result, albeit an unknown and unquantified degree.

Service limit states in LRFD/R are intended to minimize inelastic behavior and permanent deformation due to periodic overloads. MBE Commentary C6A.6.4.2.2 notes that "Load Factor design and evaluation procedures require the service behavior of steel bridges to be checked for an overload taken as 5/3 times the design load." MBE Appendix L6B, Article L6B.2.5 notes that A_1 = 1.0, and A_2 = 1.67 when checking the Overload Provisions of Article 10.57. Article L6B.2.5.1 notes that the capacity, C, according to SS Article 10.57.1 for noncomposite steel beams is identical to the values currently shown in Eqn. 144 and Eqn. 145.

The LFR Overload evaluation without considering ANN-based GDFs and with F_y = 36 ksi is:

$$RF = \frac{C - A_1 D}{A_2 L(1+I)} = \frac{(213k-ft)-(1.0)(63.3k-ft)}{(1.67)(140k-ft)} = 0.642 \quad \text{Eqn. 150}$$

Or with F_y = 33 ksi:

$$RF = \frac{C - A_1 D}{A_2 L(1+I)} = \frac{(196k-ft)-(1.0)(63.3k-ft)}{(1.67)(140k-ft)} = 0.566 \quad \text{Eqn. 151}$$

Evaluating the rating factor with the ANN-based GDF without reliability calibration and with F_y = 36 ksi:

$$RF = \frac{(213k-ft)-(1.0)(63.3k-ft)}{(1.67)(134k-ft)} = 0.672 \quad \text{Eqn. 152}$$

Or with the ANN-based GDF reliability-calibrated relative to the LRFR Strength I limit state and with F_y = 36 ksi:

$$RF = \frac{(213k-ft)-(1.0)(63.3k-ft)}{(1.67)(139k-ft)} = 0.648 \quad \text{Eqn. 153}$$

Alternatively, evaluating the rating factor with the ANN-based GDF without reliability calibration and with F_y = 33 ksi:

$$RF = \frac{(196k-ft)-(1.0)(63.3k-ft)}{(1.67)(134k-ft)} = 0.566 \quad \text{Eqn. 154}$$

Or with the ANN-based GDF reliability-calibrated relative to the LRFR Strength I limit state and with F_y = 36 ksi:

$$RF = \frac{(196k-ft)-(1.0)(63.3k-ft)}{(1.67)(139k-ft)} = 0.566 \quad \text{Eqn. 155}$$

The LFR Overload evaluation indicates that the Yutan Bridge is severely vulnerable to periodic overloads, regardless of the use of the most favorable conditions of highest yield strength steel and ANN-based GDF without reliability calibration. From the perspective of Service behavior and performance, LRFR provides a significantly more favorable evaluation than LFR. Although none of the Service or Overload evaluations indicated that the Yutan Bridge is adequate at Operating for design loads, it should be noted that all evaluations retained code-specified dynamic allowances. If sufficient dynamic testing was performed to justify substituting a measured dynamic allowance of about 3%, which was measured in a limited set of test runs during Test 2, then the Service Operating LRFR rating could increase to 0.99 with 33 ksi steel or 1.12 with 36 ksi steel.

8.9.5 Composite Interface Mechanism and Capacity

The Yutan Bridge was assumed to have no shear connectors because NDOT rating records indicated the bridge was noncomposite. When consulted, the County Engineer for Saunders County noted that puddle welds were commonly used during bridge construction to attach stay-in-place forms to steel girders prior to pouring concrete. However, exact sizes, spacings, and weld material, were not specified in available documentation, nor were typical expectations for these characteristics offered by the County Engineer. The actual source of composite behavior is not known, but is significantly higher than could be provided by steel-on-steel friction alone, and therefore strongly suggests that puddle welds were in fact installed, although with unknown sizes, at unknown locations or frequencies along the spans, and with unknown welding material.

A limited study was conducted by Mr. Juan Pablo Perez Garfias to examine potential puddle weld sizes and distributions required to achieve composite behavior. First a simple beam model was created to approximate the shear and bending moment of the truck. The loading scenario and shear diagram are shown below in Figures 80 and 81. The maximum shear scenario corresponds to the back axle being directly over one of the supports. The truck was offset by one section depth and one AASHTO tire width to avoid strut behavior.

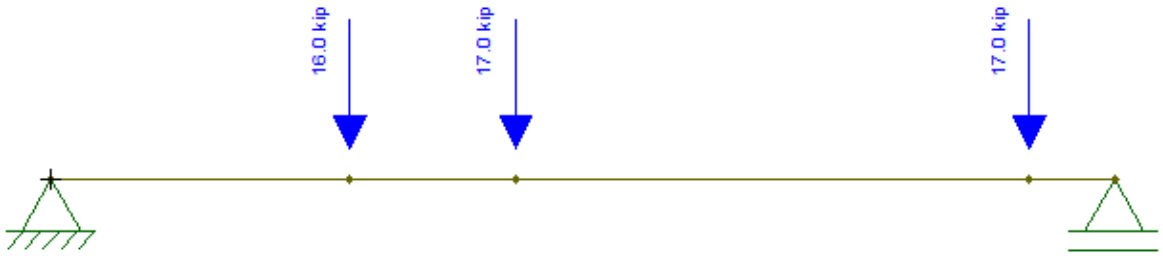

Figure 80. Critical Shear Loading

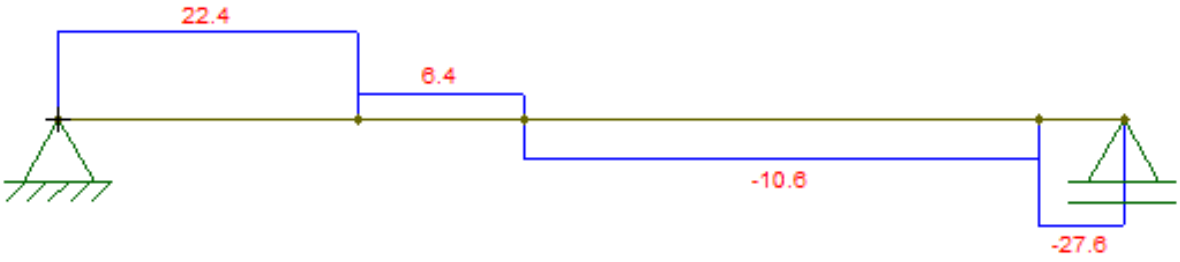

Figure 81. Shear Diagram (kips)

In the following calculations, the live load shear distribution was assumed to be the same as the moment distribution. The maximum moment GDF was approximated to be 0.29 from the second load test. The transverse shear flow is given by Eqn. 75-77.

$$V_{girder} = GDF * V_{theoretical}$$ Eqn. 75

$$q = \frac{VQ}{I}$$ Eqn. 76

$$Q = A' * y_{bar}$$ Eqn. 77

Y_{bar} is the distance of the neutral axis of the composite section to the centroidal axis of the concrete. A' is taken as the product of the transformed width of the concrete and the concrete thickness including the rib concrete. Once q is determined, the shear force at the interface, P, is calculated in Eqn. 78.

$$P = q * Puddle\ Weld\ Spacing$$ Eqn. 78

AISC Design Guide 21 (2017) was used to relate the interface shear force to the effective diameter, d_e, of the puddle weld, shown in Eqn. 79. This equation represents the area of the puddle weld multiplied by the weld strength, including a safety factor of 3. The expression provided by Design Guide 21 omits the π term in the calculation of circular area, assuming it to be approximately cancelled by the safety factor. The effective diameter of the puddle weld is related to the visible diameter, *d*, for a single sheet of steel decking with a thickness of, *t*.

$$P = \frac{{d_e}^2 F_{EXX}}{4}$$ Eqn. 79

$$d_e = \sqrt{\frac{P * F_{EXX}}{4}}$$ Eqn. 80

$$d_e = 0.7d - 1.5t$$ Eqn. 81

$$d = \frac{d_e + 1.5t}{0.7}$$ Eqn. 82

Figure 82 shows a diagram of the effective diameter and visible diameter parameters used in the previous equations.

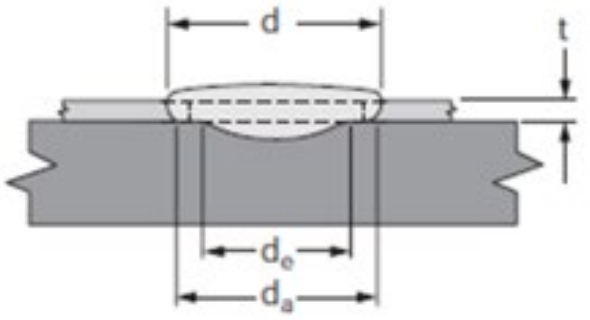

Figure 82. Puddle Weld Dimensions (from AISC Design Guide 21)

The minimum required puddle weld spacings to provide adequate shear transfer according to the AISC equations were computed. Since parameters such as the thickness of the corrugated steel decking and the puddle weld spacings are unknown, these parameters were varied to investigate a range of parameter combinations. Results are provided in Table 29 and Table 30.

Historically, Allowable Stress methods used reasonable upper bound service loads and compared these loads to capacities heavily penalized to achieve adequate safety. There is no guidance regarding whether or how the puddle weld strength including the safety factor should be used, either directly or modified, when considered in an evaluation other than an Allowable Stress or Allowable Strength method such as LFR or LRFR for which loading is amplified. Therefore, results are presented both including and excluding the puddle weld strength safety

factor. Additionally, MBE requires that structural behavior should be reliable if loading is extrapolated to 33% beyond the rating load. Tabulated Results are provided both at the tested legal load level and extrapolating this load by 33%.

The results indicate the high degree of uncertainty associated with consideration of puddle welds to provide composite shear transfer. In some lower bound cases, even when only carrying a Type 3 Legal load and also ignoring the safety factor assumed in AISC Design Guide 21, it should not be possible to achieve the required capacity to enable composite behavior. However, the bridge had been in service for nearly 40 years and under the legal load used during testing did in fact demonstrate composite behavior. Alternatively, at the upper bound, the results suggest that composite behavior could be achieved with only every 4^{th} or 6^{th} rib intactly connected. The results suggest that some degree of more frequent inspection may be required if composite behavior is accounted for in rating for this bridge or others similarly constructed.

Table 29. Puddle Weld Spacing based on Assumed Parameters for a Legal Load

	W											
Thickness of Sheet Metal (in)	0.02	0.02	0.02	0.02	0.04	0.04	0.04	0.04	0.06	0.06	0.06	0.06
F_{EXX} (ksi)	60	60	60	60	60	60	60	60	60	60	60	60
Puddle Weld Diameter	0.375	0.375	0.375	0.375	0.75	0.75	0.75	0.75	1	1	1	1
Required Puddle Weld Spacing with Safety Factor	Not Possible	Not Possible	Not Possible	Not Possible	Every Rib	Every Rib	Every Rib	Every Rib	Every 2nd Rib	Every 2nd Rib	Every 2nd Rib	Every 2nd Rib
Required Puddle Weld Spacing without Safety Factor	Not Possible	Not Possible	Not Possible	Not Possible	Every 3rd Rib	Every 3rd Rib	Every 3rd Rib	Every 3rd Rib	Every 6th Rib	Every 6th Rib	Every 6th Rib	Every 6th Rib

Table 30. Puddle Weld Spacing based on Assumed Parameters for 1.33 * Legal Load

	1.33W											
Thickness of Sheet Metal (in)	0.02	0.02	0.02	0.02	0.04	0.04	0.04	0.04	0.06	0.06	0.06	0.06
F_{EXX} (ksi)	60	60	60	60	60	60	60	60	60	60	60	60
Puddle Weld Diameter	0.375	0.375	0.375	0.375	0.75	0.75	0.75	0.75	1	1	1	1
Required Puddle Weld Spacing with Safety Factor	Not Possible	Not Possible	Not Possible	Not Possible	Not Possible	Not Possible	Not Possible	Not Possible	Every Rib	Every Rib	Every Rib	Every Rib
Required Puddle Weld Spacing without Safety Factor	Not Possible	Not Possible	Not Possible	Not Possible	Every 2nd Rib	Every 2nd Rib	Every 2nd Rib	Every 2nd Rib	Every 4th Rib	Every 4th Rib	Every 4th Rib	Every 4th Rib

9 Proposed Implementation

9.1 Overview

The intended use of the provided ANN tools is outlined in Figure 58, primarily influencing bridge management operations at Cell 5 when routine load rating for a steel girder bridge requires posting. The flowchart is a slightly modified version of the global decision tree presented in Szerszen et al. (2019). The provided moment and shear ANNs produce estimated refined modeling girder distribution factors (GDFs). These GDFs may be supplied as user input to other rating software, or the user may, at their discretion, consider rating factors provided through additional background spreadsheet calculations:

- calculation of HL-93 and Nebraska Legal (not including SHVs) live load moment and/or shear per lane,
- amplification of live load effects per AASHTO LRFR to account for dynamic effects,
- calculation of critical girder live load moment and/or shear by applying GDFs provided by ANNs,
- calculation of component and wearing dead loads per girder using a uniform distribution to all girders, as recommended by AASHTO LRFD,
- calculation of required critical girder factored loads according to the AASHTO LRFR Strength I limit state for Operating and/or Legal load ratings,
    - HL-93 loads are factored using an amplified AASHTO LRFR Operating live load factor to reflect ANN prediction uncertainty,

- Nebraska Legal loads are factored with standard AASHTO LRFR factors specified in the MBE,

- calculation of girder (composite or noncomposite, as specified by the user) moment and/or shear capacity according to AASHTO LRFR, and finally,
- calculation of Operating moment and/or shear rating factor(s) according to AASHTO LRFR for HL-93 loads, and/or Legal moment and/or shear rating factor(s) according to AASHTO LRFR for Nebraska Legal loads.

As stated in the Objective and Scope chapter, the primary objectives of the project were to:

(1) conduct detailed modeling of a representative sample of simple span, steel girder bridges in Nebraska,

(2) configure and train ANNs to predict critical girder static load effects, and

(3) calibrate load ratings according to a reliability-targeted paradigm to account for amplified live load uncertainty from ANN-based live load effect predictions.

The spreadsheets do not provide Serviceability load ratings. AASHTO MBE Commentary C6A.6.4.2.2 states: “It is important to note that the live load factors for Service II limit state were not established through reliability-calibration, but were selected based on engineering judgement and expert opinion. The level of reliability represented by this serviceability check is unknown.” Accordingly, it is not possible to calibrate to an objective AASHTO-specified reliability target for Serviceability, because none exists.

The ANN-predicted GDFs represent predictions of realistic mechanical phenomena and therefore could be used for Serviceability evaluations at the discretion of the load rating engineer. The spreadsheets accompanying this report provide unadjusted and adjusted GDFs. Unadjusted GDFs are the direct output of the ANN. Adjusted GDFs are scaled by the ratio of 1.40/1.35 to reflect the conservative margin of additional live load factor recommended in this study, based on a reliability calibration using the AASHTO Operating Strength I limit state. Therefore, use of adjusted GDFs effectively imparts an implicit live load factor of 1.037 instead of the factor of 1.00 specified in AASHTO MBE Table 6A.4.2.2-1 if used in a Service II evaluation.

The spreadsheets also provide LFR load ratings, but the user is cautioned that consideration of LFR was secondary and not fully developed within the scope of this project. The FEA performed on representative bridges directly modeled HS-20 loads and therefore applies identically to LFR evaluations. Similarly, the unadjusted ANN GDFs are expected to be reasonably representative of girder load distribution for LFR. The reliability calibration, however, is clearly not applicable to LFR, because LFR is not an objectively reliability-calibrated methodology. Users may elect to implement the adjusted GDFs to impart a small margin of conservativism, but this research cannot definitively state whether this margin is sufficient without additional investigation.

Furthermore, LFR guidelines follow the AASHTO Standard Specifications for Highway Bridges, rather than AASHTO LRFD Bridge Design Specifications, and various nuanced considerations are inconsistent between these documents. For instance, the treatment of dynamic

amplification varies with span in the Standard Specifications. The AASHTO MBE also notes particular special considerations applicable to Capacity determination for LFR, such as restrictions on the use of plastic moment for noncomposite steel girders when yield strength is less than 33 ksi under the provisions of AASHTO MBE L6B.2.1. The limitation on plastic moment applicability is uncommon in the Nebraska bridge inventory within sampling used for this study and was not incorporated into the provided spreadsheets for the approximate LFR ratings, but users should be aware of this consideration for bridges constructed in 1936 or earlier (according to AASHTO MBE Table 6A.6.2.1-1).

If use of the ANN tools indicates that posting is expected to be unnecessary, then it would be reasonable to prioritize the bridge in question for confirmation of adequate rating by analysis and/or load testing (Cell 7). Conversely, if the ANN initially indicates that the bridge is likely to require posting, then bridge management resources may be more effectively allocated elsewhere in the transportation network (Cell 8). However, the load rating engineer should bear in mind that a noncomposite bridge may realize benefits through a load test that are unavailable through analysis and neural network predictions, such as partially composite behavior.

The spreadsheets also assume a constant moment gradient ($C_b = 1$) for noncomposite girders, which can drastically underestimate girder capacity. Even ignoring the benefit of moment gradient on lateral-torsional buckling stability, AASHTO MBE 6A.6.9.3 indicates that the top compression flange may be considered braced even though not connected by shear connectors, provided that the deck is in contact with the girder. The accompanying Commentary notes that “bond between the deck slab and beam” provides adequate bracing to justify

considering the beam braced, so the engineer should consider whether steel stay-in-place forms are also likely to afford similar lateral restraint without the direct adhesive concrete-to-steel bond assumed by the MBE.

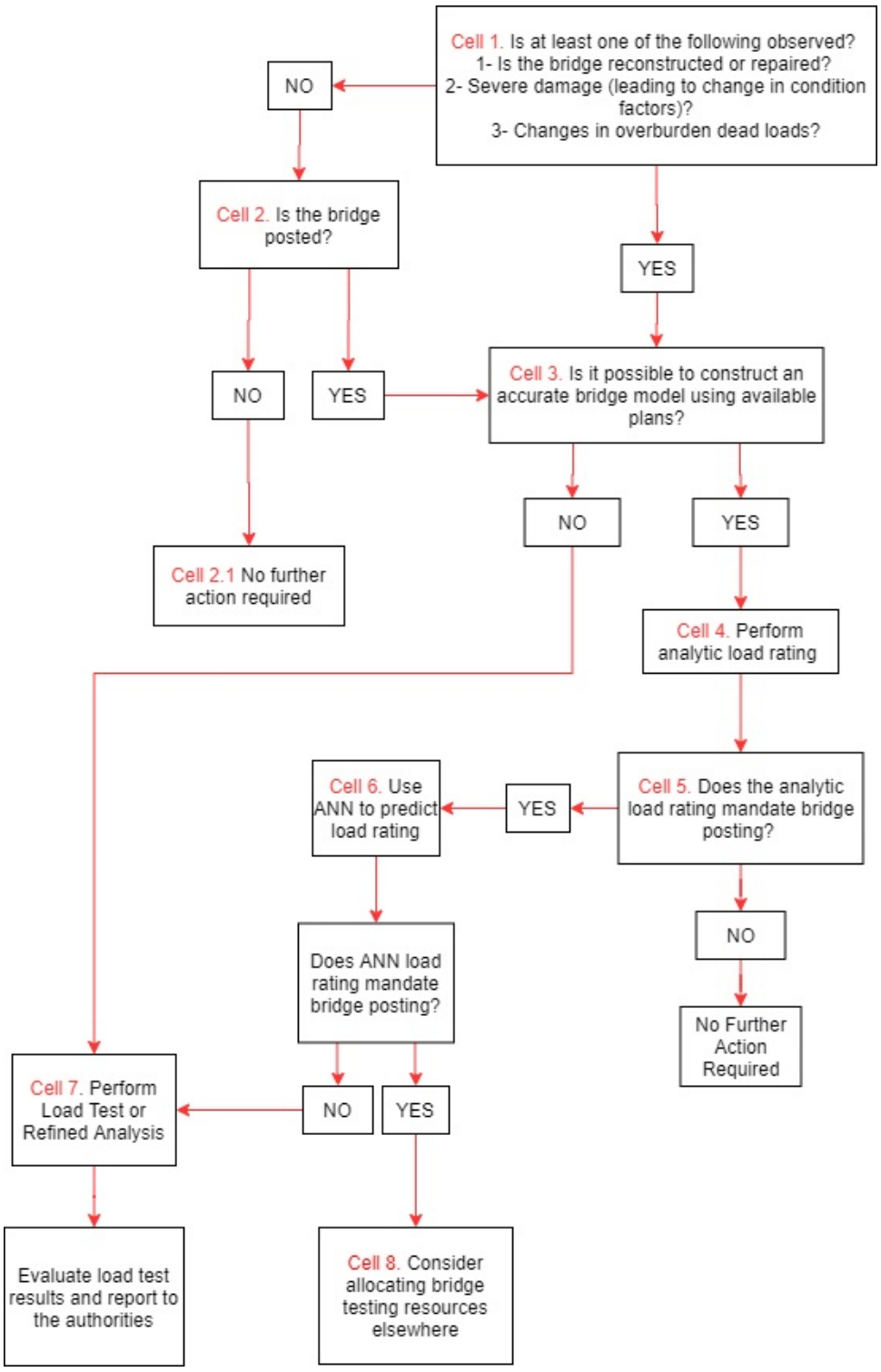

Figure 83. Proposed Methodology

9.2 User Application

Two spreadsheets have been configured to quickly and easily provide moment and shear ANN-based girder distribution factors (GDFs) closely estimating the results that would be obtained from detailed finite element analysis. The spreadsheets have been set up so that the user should not have to leave the "INPUT-OUTPUT" tab at any point in this procedure. This section of the report is provided as a reference, to explain the procedure carried out by the spreadsheets, and to enable the spreadsheets to be regenerated should they be lost in the future. The steps to obtain an ANN-based GDF are:

1) Input ANN parameters and additional bridge details such as bridge width and length. The spreadsheets require user input to indicate whether a bridge is composite or noncomposite. Longitudinal stiffness is automatically calculated within the spreadsheet according to Equation (4.6.2.2.1-1) of the AASHTO LRFD Bridge Design Specifications. The Ae^2 term is taken as zero for noncomposite bridges, as recommend in Zokaie (2000).
2) Verify that the bridge parameters are within the ANN ranges of applicability (refer to Section 9.3, below). If the ANN is outside of the scope of the ranges of applicability, then the ANN should not be used.
3) Perform calculations using the weights, biases, and transfer functions determined for the optimal trained ANN, as described in Sections 9.4 and 9.5 for moment and shear GDFs, respectively.
4) Verify that the calculated GDFs are within the "scatter" of the training data for all of the 10 input parameters. See Sections 9.6 and 9.7 for moment and shear, respectively.

9.3 Ranges of Applicability

The tables below are provided as reference templates for use with the ANNs provided by this study. Refer to step 2, above. The ranges of applicability can be checked for the moment and shear ANNs by using Table 31 and Table 32, respectively.

Table 31. Moment ANN Ranges of Applicability

Bridge Parameter	ANN Application Minimum	Bridge Being Evaluated	ANN Application Maximum
Span Length (L)	20 ft		81.6 ft
Girder Spacing (s)	32 in		99 in
Longitudinal Stiffness (K_g)	11,900 in^4		346,225 in^4
Cross Frames	No (0)		Yes (1)
Number of Girders (n_b)	4		11
Skew Angle (α)	0°		45°
Barrier Distance (d_e)	-4.5 in		31.25 in
Deck Thickness (t_s)	5 in		9 in
Concrete Compressive Strength (f_c')	2.5 ksi		4 ksi
Steel Yield Strength (f_y)	30 ksi		50 ksi

Table 32. Shear ANN Ranges of Applicability

Bridge Parameter	ANN Application Minimum	Bridge Being Evaluated	ANN Application Maximum
Span Length (L)	20 ft		81.6 ft
Girder Spacing (s)	32 in		92.5 in
Longitudinal Stiffness (K_g)	7,540.6 in^4		415,400.16 in^4
Cross Frames	No (0)		Yes (1)
Number of Girders (n_b)	4		11
Skew Angle (α)	0°		45°
Barrier Distance (d_e)	-4.5 in		32 in
Deck Thickness (t_s)	5 in		8 in
Concrete Compressive Strength (f_c')	2.5 ksi		4 ksi
Steel Yield Strength (f_y)	30 ksi		50 ksi

9.4 Moment ANN Calculations

ANN calculations are performed in the background of the provided spreadsheet. The moment and shear ANN calculations correspond to the best networks' architectures, weights, biases, which are provided below. For the moment ANNs, the best neural network corresponds to an architecture with two hidden layers with 5 nodes per hidden layer.

9.4.1 Calculation Step 1:

Scale inputs by using linear interpolation. The inputs are scaled between -1 and 1 relative to each individual parameter's minimum and maximum values used during ANN training, which were shown in Table 31 and Table 32. The equation for linear interpolation of input parameters is shown in Eqn. 6 where x is the unscaled input and x_{scaled} is the scaled value that will be used in ANN calculations.

$$x_{scaled} = \frac{2(x - x_{minimum)}}{x_{maximum} - x_{minimum}} - 1 \qquad \text{Eqn. 156}$$

9.4.2 Calculation Step 2a:

The general expression for ANN calculations produced by this study is a nested set of equations:

$$GDF_{scaled} = (W_3 f_2(W_2 f_1(W_1 x_{scaled} + b_1) + b_2) + b_3) \qquad \text{Eqn. 157}$$

Starting at the innermost layer and working outward, generate a 5x1 array, A_{1a}:

$$A_{1a} = [W_1]_{5x10}\{x_{scaled}\}_{10x1} + \{b_1\}_{5x1} \qquad \text{Eqn. 158}$$

Where W_1 is an array of weights as shown in Table 33, and b_1 is vector of biases as shown in Table 34.

Table 33. Moment ANN Weights to 1st Hidden Layer

$$W_1 = \begin{bmatrix} -0.792 & 0.309 & 0.227 & -0.312 & -0.284 & -0.146 & -0.106 & 0.079 & -0.180 & 0.146 \\ 0.569 & 0.069 & -0.131 & -0.022 & -0.353 & 0.247 & -0.030 & -0.371 & 0.246 & -0.323 \\ -0.098 & -0.145 & 0.258 & -0.029 & 0.516 & 0.048 & 1.014 & -0.361 & -0.137 & 0.063 \\ -0.093 & -0.368 & 0.224 & -0.229 & -0.042 & -0.081 & 0.308 & -0.389 & -0.124 & -0.248 \\ -0.153 & -0.351 & 0.055 & -0.118 & 0.316 & 0.376 & -0.086 & -0.082 & 0.092 & 0.178 \end{bmatrix}$$

Table 34. Moment ANN Biases of 1st Hidden Layer

$$b_1 = \begin{bmatrix} -0.481 \\ -0.413 \\ -0.403 \\ -0.303 \\ -0.124 \end{bmatrix}$$

9.4.3 Calculation Step 2b:

Pass each element of the array, A_{1a}, through a transfer function, f_1, to obtain a new array, A_{1b}.

$$A_{1b} = f_1(A_{1a}) \qquad \text{Eqn. 159}$$

The typical transfer function for the ANNs used in this study is a hyperbolic tangent function, shown in Eqn. 160.

$$A_{1b} = \tanh(A_{1a}) = \frac{2}{1 - e^{-2A_{1a}}} - 1 \qquad \text{Eqn. 160}$$

9.4.4 Calculation Step 2c:

Eqn. 157 has now been partially evaluated. For reference, the equation is now effectively:

$$GDF_{scaled} = (W_3 f_2(W_2 A_{1b} + b_2) + b_3) \quad \text{Eqn. 161}$$

Repeat the process in Calculation Step 2a to generate a 5x1 array, A_{2a}, using an array of weights W_2, shown in Table 35, and a vector of biases, b_2, shown in Table 36. Then, repeat the process in Calculation Step 2b, again passing the elements of A_{2a} through a hyperbolic tangent transfer function to produce A_{2b}.

Table 35. Moment ANN Weights to 2nd Hidden Layer

$$W_2 = \begin{bmatrix} -0.150 & -0.013 & -0.099 & 0.268 & 0.144 \\ -0.150 & -0.013 & -0.098 & 0.268 & 0.143 \\ -0.637 & -0.706 & -0.669 & 0.419 & 0.553 \\ -0.150 & -0.013 & -0.098 & 0.268 & 0.143 \\ -0.150 & -0.013 & -0.098 & 0.267 & 0.143 \end{bmatrix}$$

Table 36. Moment ANN Biases of 2nd Hidden Layer

$$b_2 = \begin{bmatrix} -0.040 \\ -0.040 \\ -0.266 \\ -0.040 \\ -0.040 \end{bmatrix}$$

9.4.5 Calculation Step 2d:

The equation has now been further evaluated and simplified to:

$$GDF_{scaled} = (W_3 A_{2b} + b_3) \quad \text{Eqn. 162}$$

Multiplying the 1x5 array W_3, shown in Table 37, by the 5x1 array A_{2b} and adding the scalar bias b_3, shown in Table 38, produces the a scaled value of the desired GDF.

Table 37. Moment ANN Weights to Output Layer

$$W_3 = \begin{bmatrix} -0.363 & -0.363 & -1.281 & -0.363 & -0.362 \end{bmatrix}$$

Table 38. Moment ANN Bias of Output Layer

$$b_3 = 0.100$$

9.4.6 Calculation Step 3:

The final step is to scale the ANN output relative to minimum and maximum GDF results produced by the ANN during training: 0.265 and 0.670. This final step produces the ANN-predicted GDF for moment effects, which can then be used in place of GDFs from AASHTO.

$$GDF = GDF_{min} + \frac{(GDF_{scaled} + 1)(GDF_{max} - GDF_{min})}{2} \quad \text{Eqn. 163}$$

9.5 Shear ANN Calculations

The mathematical procedure to find the shear GDF prediction is the same as shown in the previous section. However, the weight and bias arrays are different sizes and populated with different values to produce shear GDF predictions. The best shear ANN corresponds to two hidden layers with three nodes per hidden layer. The weights and biases of the best shear ANN are shown in Table 39-Table 44. The GDF_{scaled} output needs to be re-scaled between the minimum and maximum predictions from shear ANN training: 0.339 and 0.782.

Table 39. Shear ANN Weights to 1st Hidden Layer

$$W_1 = \begin{bmatrix} -0.008 & -0.106 & -0.192 & -0.501 & 0.277 & -1.011 & -0.127 & 0.376 & -0.051 & -0.421 \\ 0.058 & 0.915 & 0.001 & 0.023 & -0.039 & 0.260 & -0.745 & -0.001 & 0.106 & -0.007 \\ -0.015 & 0.165 & 0.067 & 0.049 & 0.088 & 0.247 & 0.720 & -0.092 & -0.201 & 0.252 \end{bmatrix}$$

Table 40. Shear ANN Biases to 1st Hidden Layer

$$b_1 = \begin{bmatrix} 0.467 \\ -0.280 \\ -0.104 \end{bmatrix}$$

Table 41. Shear ANN Weights to 2nd Hidden Layer

$$W_2 = \begin{bmatrix} 0.312 & 0.391 & 0.359 \\ 0.620 & 0.564 & 0.891 \\ -0.312 & -0.391 & -0.359 \end{bmatrix}$$

Table 42. Shear ANN Biases to 2nd Hidden Layer

$$b_2 = \begin{bmatrix} 0.035 \\ -0.040 \\ -0.035 \end{bmatrix}$$

Table 43. Shear ANN Weights to Output Layer

$$W_3 = \begin{bmatrix} 0.630 & 1.222 & -0.630 \end{bmatrix}$$

Table 44. Shear ANN Bias to 3rd Output Layer

$$b_3 = 0.077$$

9.6 Moment ANN Scatter Plots

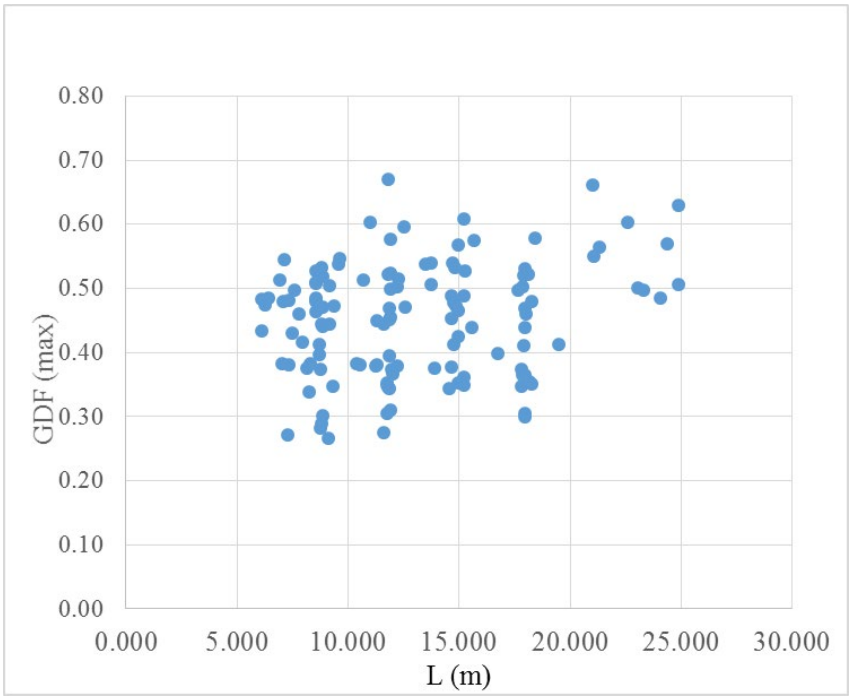

Figure 84. Moment GDFs vs. Length

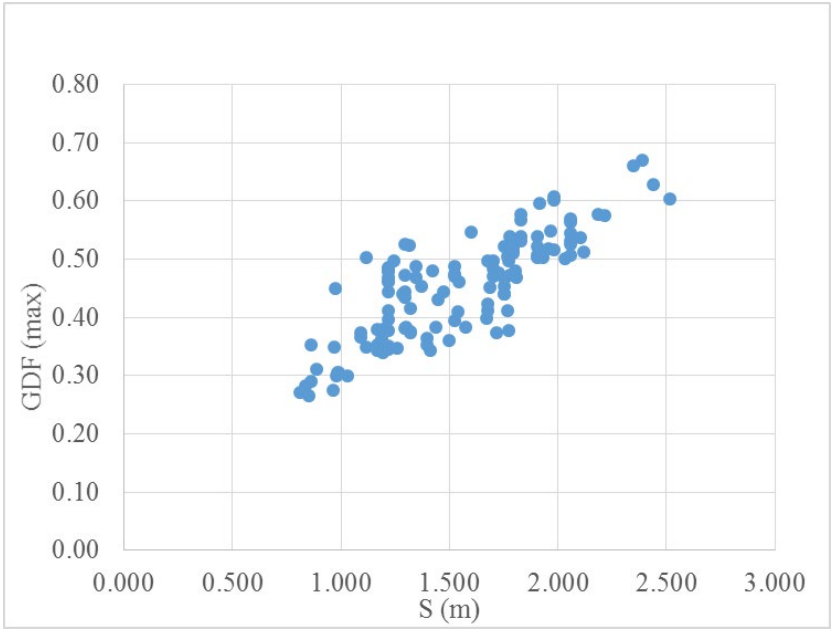

Figure 85. Moment GDFs vs. Girder Spacing

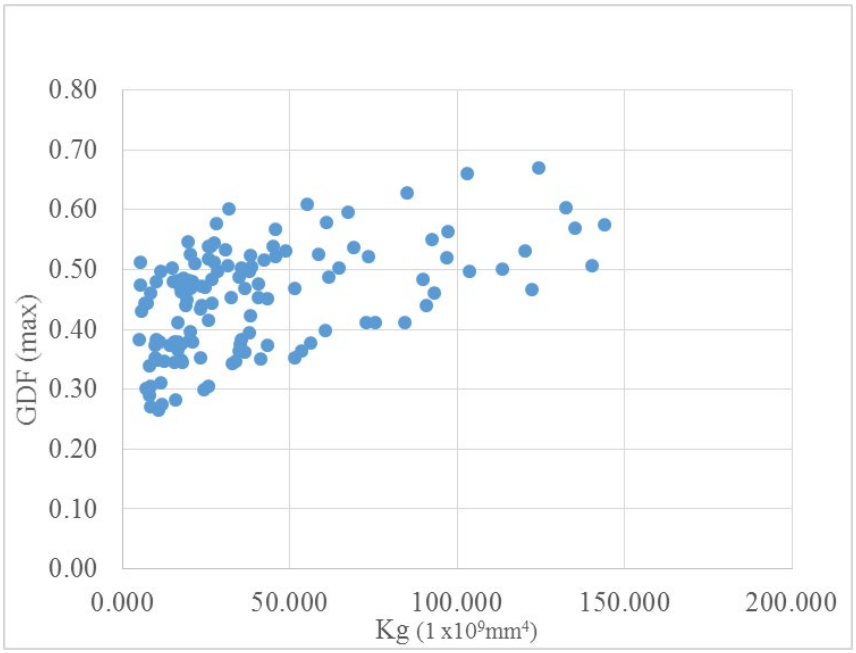

Figure 86. Moment GDFs vs. Longitudinal Stiffness

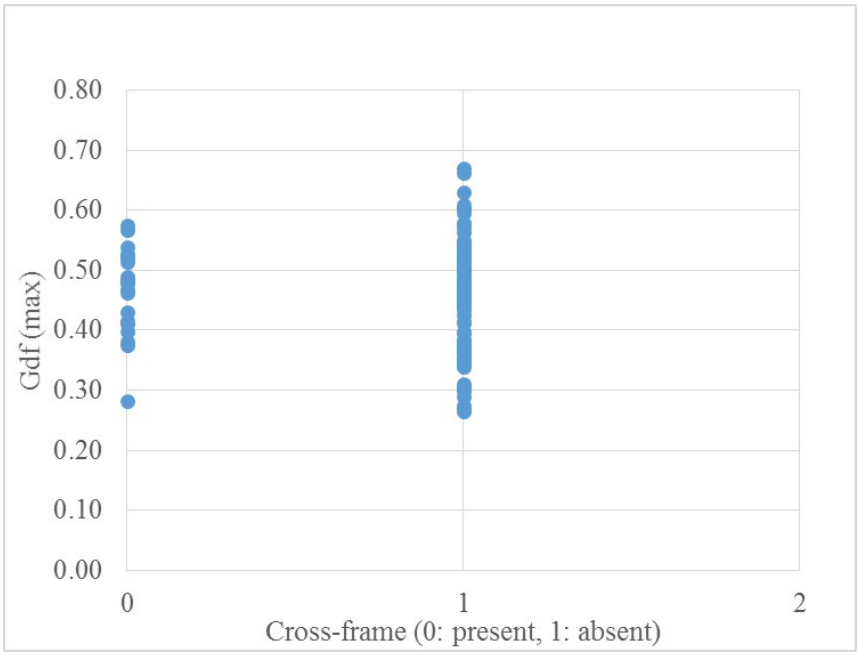

Figure 87. Moment GDFs vs. Cross Frame Presence

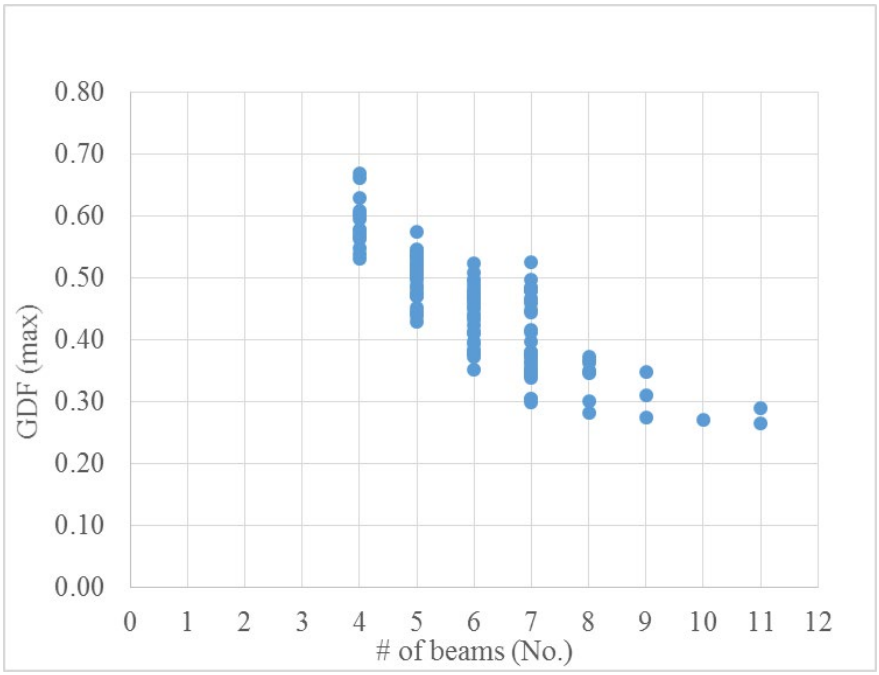

Figure 88. Moment GDFs vs. Number of Girders

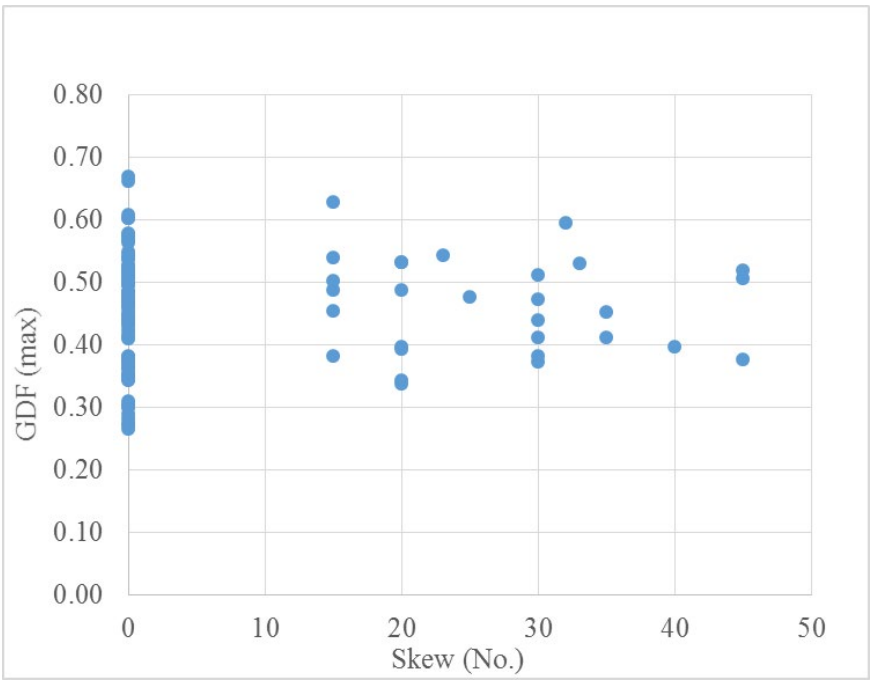

Figure 89. Moment GDFs vs. Skew

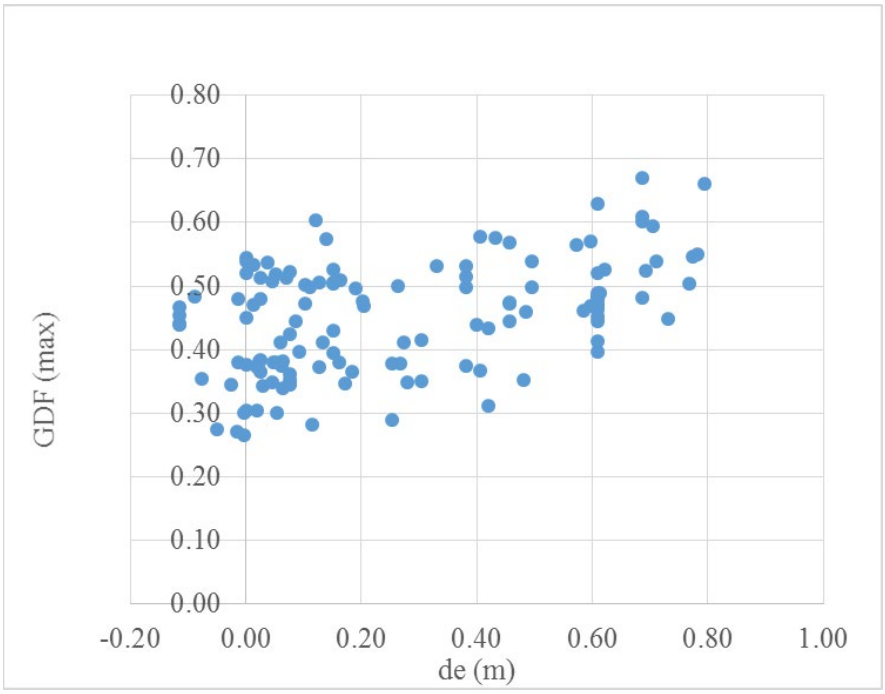

Figure 90. Moment GDFs vs. Edge Distance

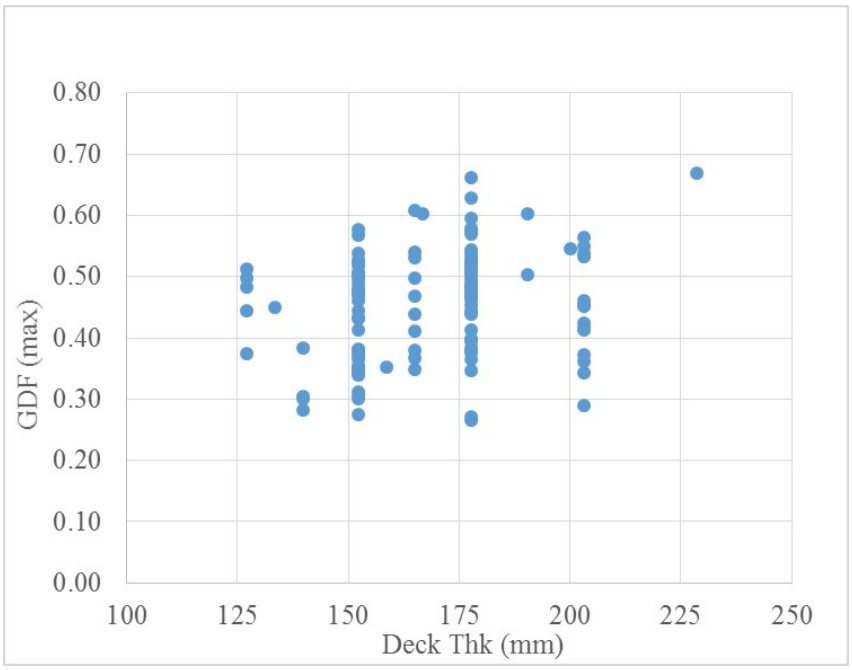

Figure 91. Moment GDFs vs. Deck Thickness

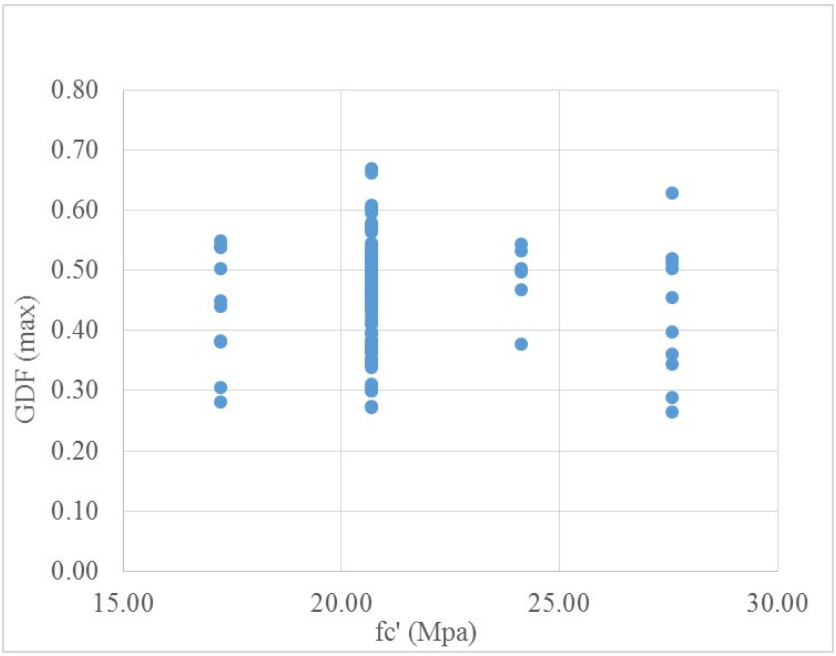

Figure 92. Moment GDFs vs. Concrete Compressive Strength

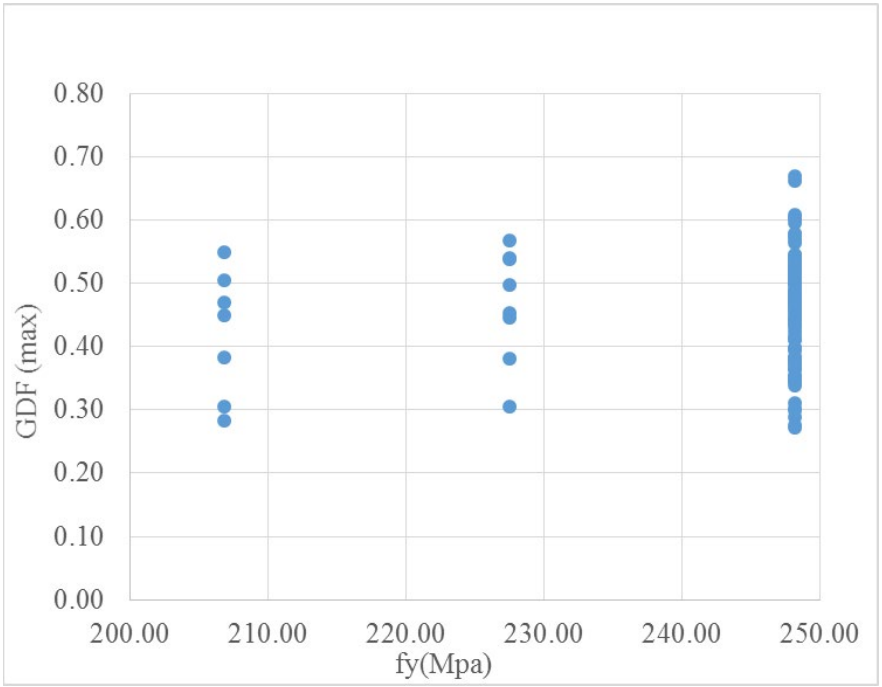

Figure 93. Moment GDFs vs. Steel Yield Strength

9.7 Shear ANN Scatter Plots

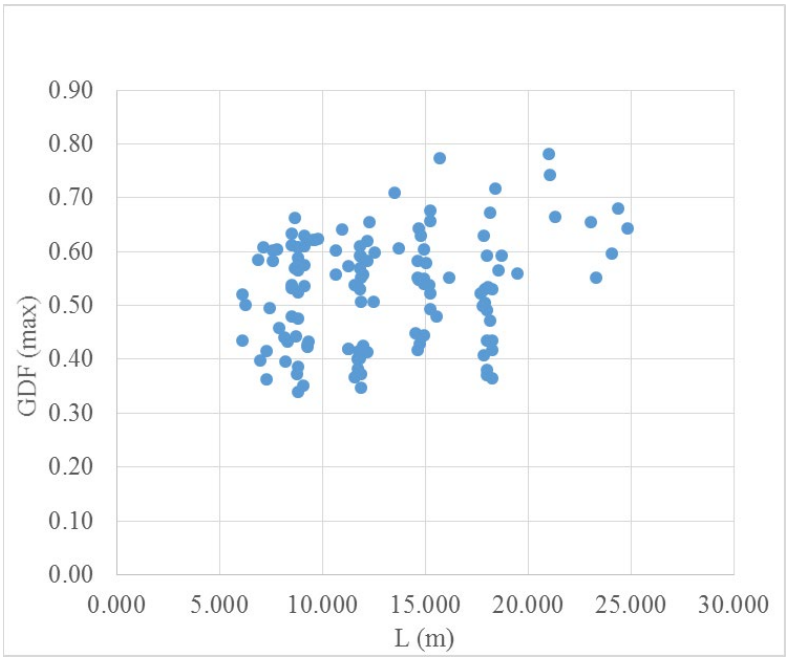

Figure 94. Shear GDFs vs. Length

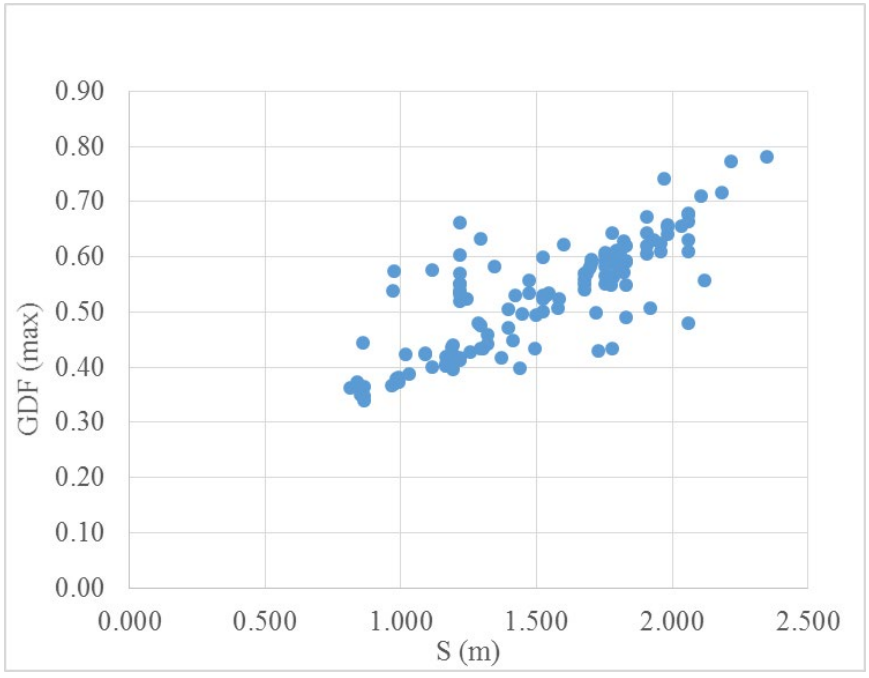

Figure 95. Shear GDFs vs. Girder Spacing

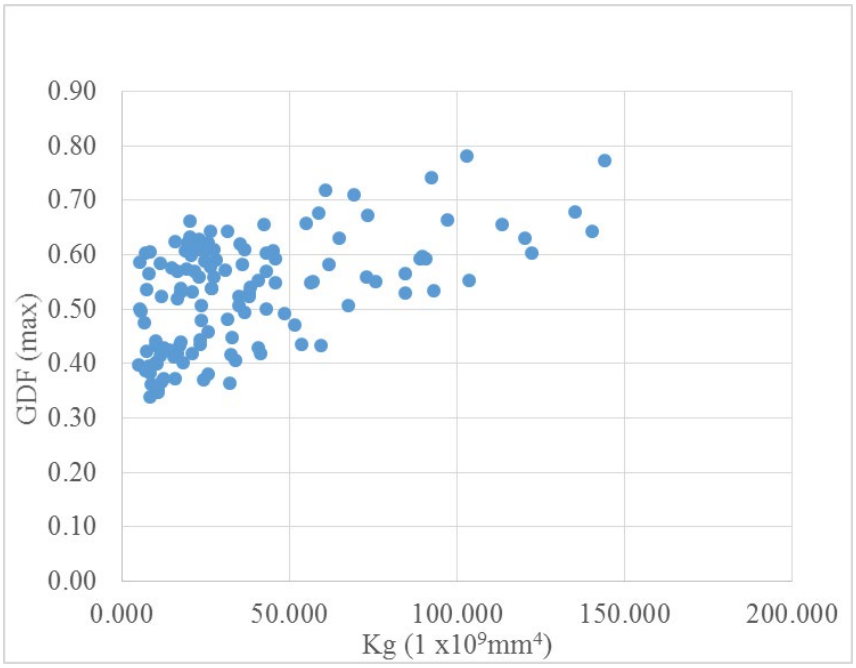

Figure 96. Shear GDFs vs. Longitudinal Stiffness

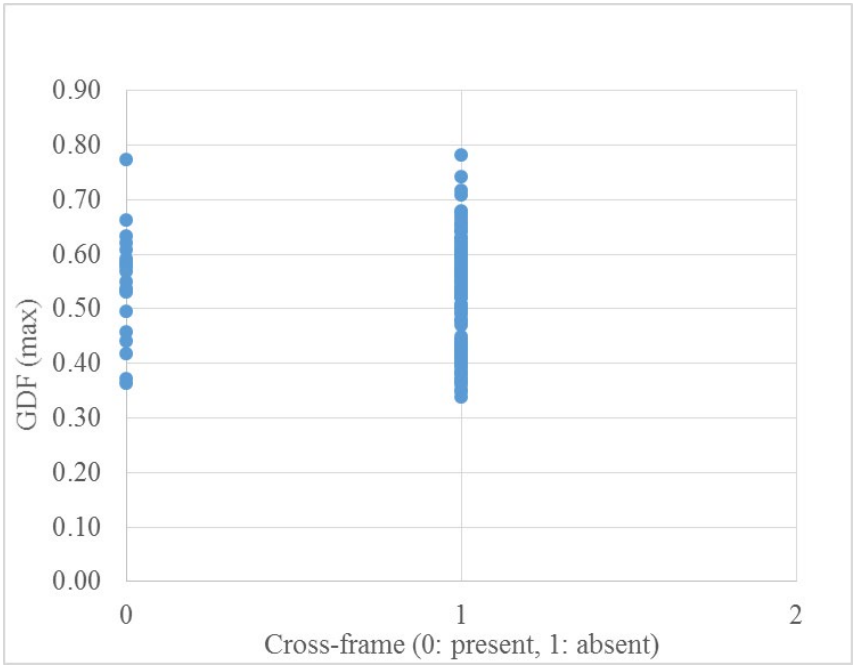

Figure 97. Shear GDFs vs. Cross Frame Presence

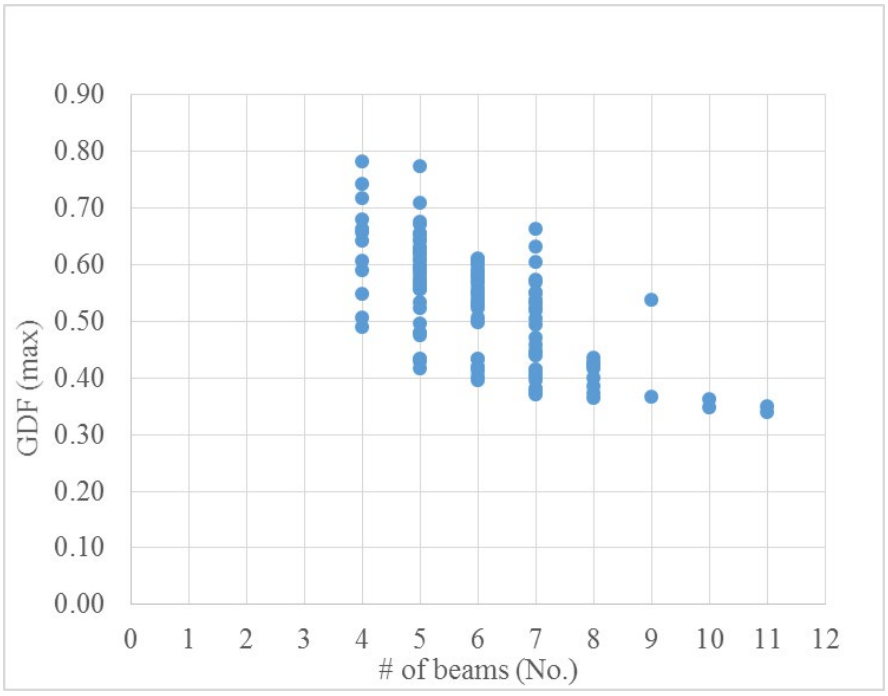

Figure 98. Shear GDFs vs. Number of Girders

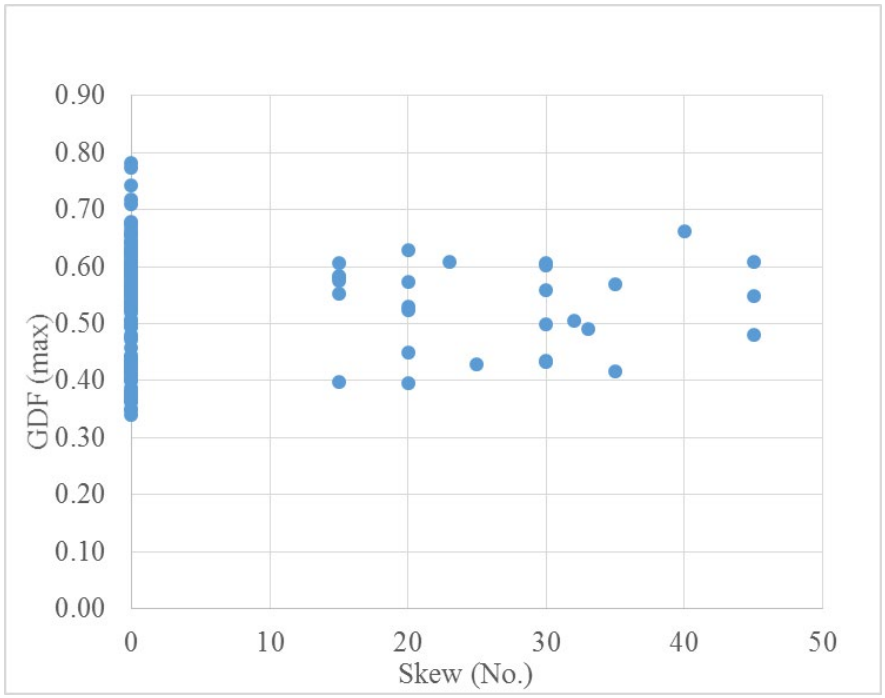

Figure 99. Shear GDFs vs. Skew

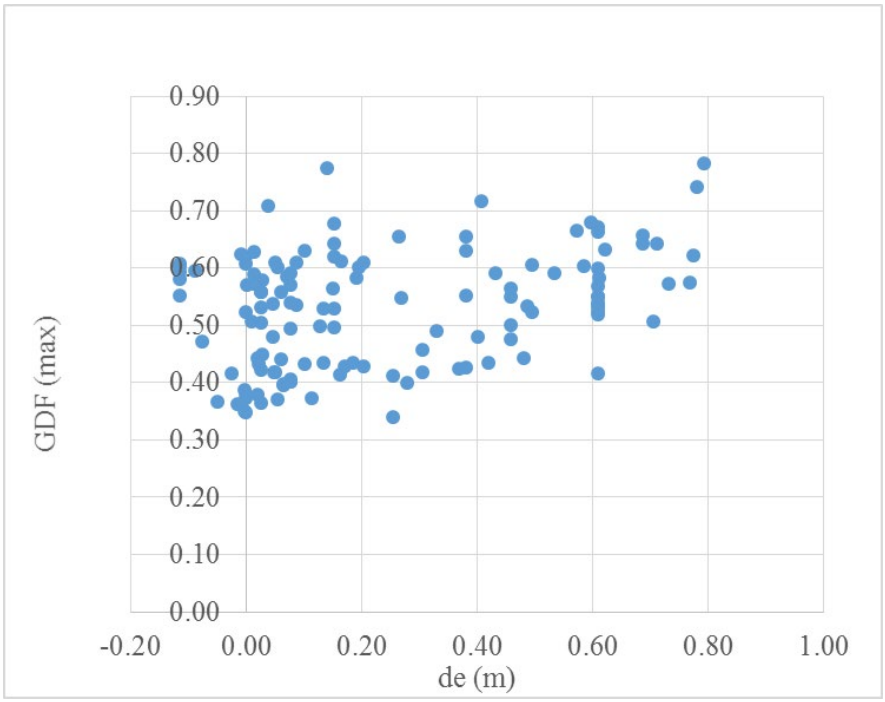

Figure 100. Shear GDFs vs. Edge Distance

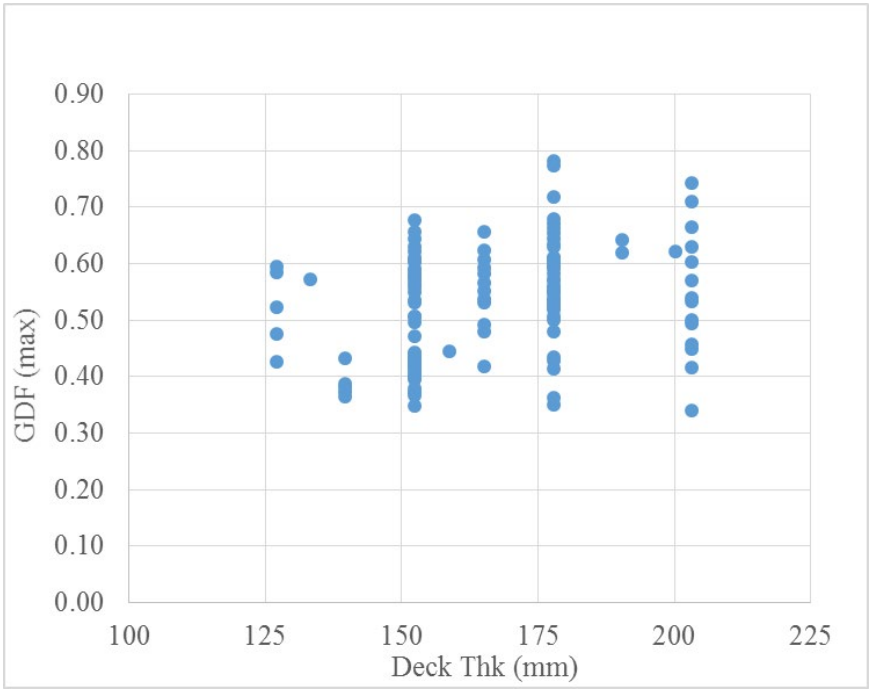

Figure 101. Shear GDFs vs. Deck Thickness

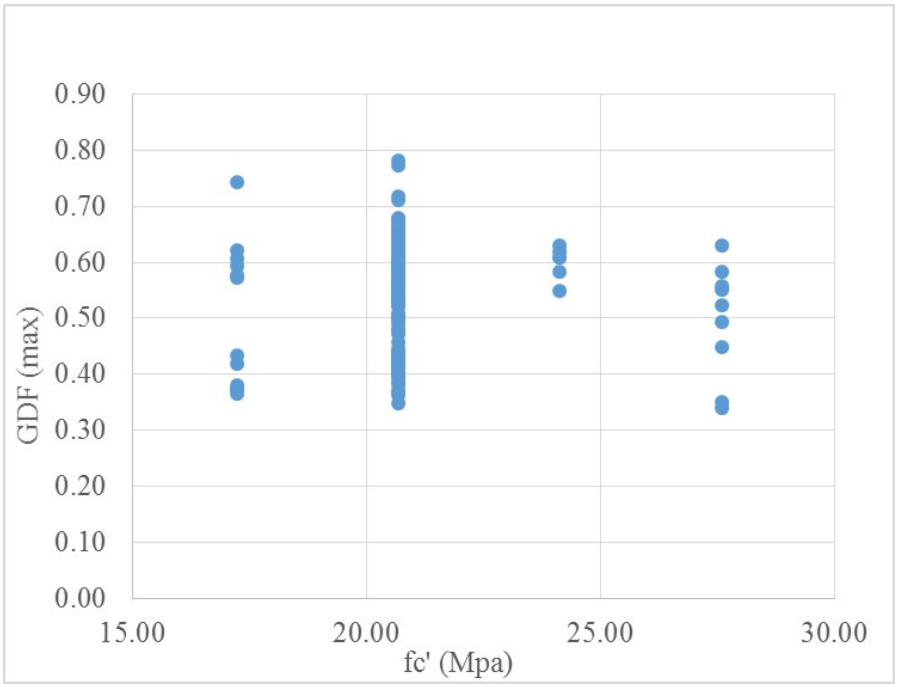

Figure 102. Shear GDFs vs. Concrete Compressive Strength

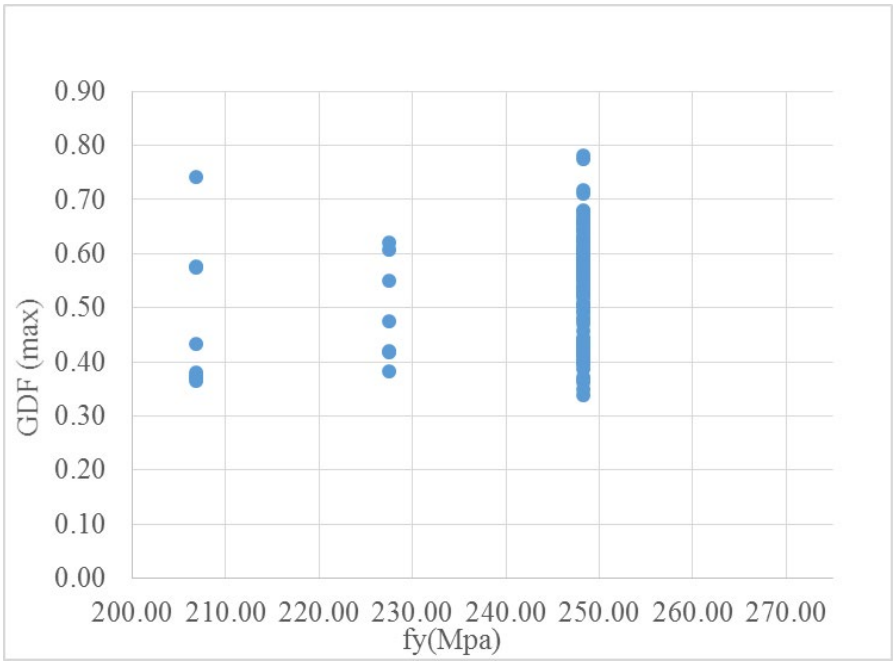

Figure 103. Shear GDFs vs. Steel Yield Strength

10 Summary, Conclusions, and Recommendations

This study expanded on a preliminary pilot study conducted by Sofi (2017), which produced an efficient parametric finite element steel girder bridge modeling framework for implementation in ANSYS, together with preliminary ANN development to directly predict bridge load rating factors. The objective of the present study was to enhance the ANN training data and integrate reliability calibration to develop an ANN-based tool, supplementing existing resources available to NDOT load rating engineers and facilitating more cost-effective bridge management decision-making.

This research project benefits NDOT load rating engineers by providing an easy-to-use Excel tool to calculate ANN-based, reliability-calibrated girder distribution factors (GDFs). These GDFs offer improved live load effect predictions, which result in moment and shear rating factors 16% and 17% higher on average, respectively, than rating factors obtained from line girder analyses. While various software packages, including AASHTOWare BrR, offer refined analysis options, the provided Excel tool greatly streamlines and simplifies the process to determine refined live load distributions, making refined analysis more easily accessible to load rating engineers.

Although this study focused on using ANNs to support bridge management and load rating, the resulting ANN tool could potentially be used at early design stages to optimally proportion bridge cross-sections for new construction, provided that the parameters of the new construction (e.g. simple span, length, number and spacing of girders) are consistent with the ANN training set.

ANSYS FEMs for a sample of the Nebraska bridge inventory provided refined moment and shear live load demands. Consistent with previous studies in literature, live load demands from FEMs tended to be lower than those typically obtained from AASHTO line girder analysis. ANSYS modeling results were expressed as moment and shear GDFs, which were used to train ANNs.

ANNs were trained to map 10 inputs (e.g., span length, steel yield strength, longitudinal stiffness) to the moment or shear GDFs. ANN architectures were optimized and design dataset sample sizes were compared. Finally, ANN GDF prediction error was incorporated into an updated live load statistical distribution with increased uncertainty, and the live load factor was calibrated using the modified Rackwitz-Fiessler and Monte Carlo Simulation methods to reflect the updated live load statistical distribution. The two reliability methods produced similar results. In addition to the development of an ANN, two load tests were conducted on a case study bridge in Yutan, NE. Load rating factors for the Yutan bridge were compared among AASHTO, ANSYS, CSiBridge, ANN, and field testing methods.

The following conclusions were drawn from the research presented herein:

1) Calibrated ANN-based rating factors provided a net benefit over those obtained from AASHTO line girder analysis, despite a penalty to account for additional ANN prediction error uncertainty. ANN rating factors with calibrated partial safety factors are on average 16% and 17% higher than AASHTO LRFR moment and shear rating factors, respectively.
2) A properly configured and trained ANN should introduce only marginal uncertainty compared to the inherent live load uncertainties routinely accounted for in bridge engineering, such as the vehicle weight, axle spacing, multiple presence in adjacent lanes, and dynamic load amplification. Because the uncertainties routinely attributed to live load effects are statistically independent from ANN-prediction errors, the live load coefficient of variation only increased slightly, from 18% to approximately 19%.
3) Accounting for the additional ANN uncertainty required only a marginally higher live load partial safety factor (corresponding to a marginally lower load rating factor). Moment and shear calibrated live load partial safety factors of 1.4 (vs. 1.35) were found to be adequate.
4) ANNs trained using a design sample set of 50 bridges were able to predict FEM GDFs with an average testing error of 4.56%. Increasing the design sample size to 130 bridges only reduced testing error to 3.65%.

Outliers were strategically identified and excluded from ANN design data to optimize ANN performance (prediction error minimization). The outliers could have been included and would have increased the range of bridge population applicability. However, broader applicability would be accompanied by higher errors on average, which would then require a higher live load partial safety factor penalty to the entire population.

The study found that ANN prediction errors had only a modest influence on live load factors to account for additional uncertainty. However, this outcome was achievable because the ANN training data was carefully selected to represent extreme cases of parameters in the space. While it is appealing to say that only a handful of bridges are sufficient to develop a reliable ANN, that statement must be coupled with careful review of available data to identify maximally representative training candidates.

While the study was originally limited in scope to composite bridges, discussions with the research sponsor indicated that noncomposite behavior was a significant consideration for older, off-system bridges such as those owned by counties. Transverse live load distribution is believed to be influenced by composite action only through the effect on longitudinal stiffness (as indicated by Zokaie (2000)), as long as all elements are uniformly either composite or noncomposite. Therefore, the ANN-based GDFs provided by this project are also believed to be applicable to noncomposite bridges, provided that longitudinal stiffness for a noncomposite structure is submitted to the ANN.

The study was also limited in scope to consider only bridges in fair or better condition, for which no penalties would be required to account for deterioration resulting in section loss and

reduced capacities. NDOT has previously sponsored research reported in Steelman and Shakya (2017) to address deterioration for steel girder bridges. The method to assign condition factors, ϕ_c, could be applied to capacities during LRFR load rating, together with the ANN-based, reliability-calibrated GDFs provided by the present research study. Deterioration and ANN error are likely statistically independent uncertain characteristics. Therefore, incorporating the products of both research studies simultaneously would likely result in a reasonably accurate, though potentially slightly conservative load rating result (i.e., greater reliability than strictly required).

Diagnostic field tests provide substantial additional load rating benefits, such as revealing unintended composite behavior and structure-specific (likely reduced) dynamic structural response to vehicle loading. These aspects were observed during two diagnostic load tests on the Yutan Bridge. However, the guidance available to address unintended composite action in the AASHTO Manual for Bridge Evaluation appeared potentially unconservative.

Based on the research presented herein, the following topics are recommended for future research:

1) Benefits from ANN-based design and rating tools could be extended to other bridge types, such as prestressed concrete girder bridges and multi-span continuous bridges.
2) Additional research should be performed to clarify appropriate load rating procedures influenced by partial and potentially unreliable composite behavior. Protocols stipulating complementary accelerometer instrumentation to facilitate future rapid and accessible structural health evaluation may enable questionable benefits from unreliable composite behavior to be considered in load ratings.

Investigating and evaluating NDOT load rating policy was not intended to be within the scope of this project. However, one point that emerged for consideration after discussions with NDOT personnel is to modify the rating policy with respect to steel girders having a yield strength of 33 ksi. The current policy restricts 33 ksi steel to a first yield limit for strength-based limit states. According to the AASHTO *Manual for Bridge Evaluation*, 3rd ed., Article L6B.2.1, plastic moment is permitted for steel with yield strength at least 33 ksi. Therefore, NDOT's policy is more conservative than required by MBE. This consideration has no effect on the ANN-based GDF predictions or reliability calibration, and so this point is incidental and anecdotal to the sponsored research effort. NDOT would be justified to revisit their current policy and allow plastic moment for strength-based evaluations of steel girders with 33 ksi yield strengths.

11 Appendices

11.1 Extended Literature Review

11.1.1 Studies of Bridge Analysis and Load Rating

Gheitasi, A. and Harris, D.K., 2015, Failure Characteristics and Ultimate Load-Carrying Capacity of Redundant Composite Steel Girder Bridges: Case Study

This investigation included comprehensive nonlinear FEAs of two representative intact composite steel girder bridges (Nebraska Laboratory Bridge Test and the Tennessee Field Bridge Test) that were tested to failure and provided sufficient details for model validation. Both bridges demonstrated additional reserve capacity over the theoretical nominal capacity according to AASHTO LRFD. The researchers categorized the bridges' behavior into four stages; I. flexural cracks in concrete deck II. plasticity initiated in steel girders III. Structural stiffness drops off significantly, and plastic hinges form at the location of the maximum moment IV. local failure after significant plastic deformation and load redistribution within the structural system. The bridges' behavior is shown below in Figure 104.

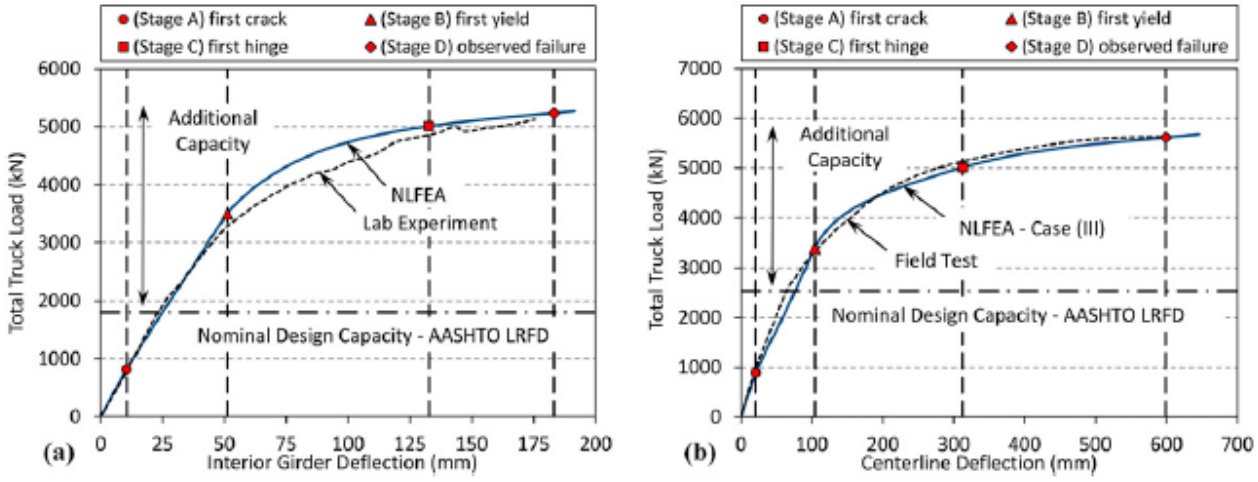

Figure 104. Behavioral Stages: (a) Nebraska Laboratory Test (b) Tennessee Field Test

Gheitasi, A. and Harris, D.K., 2015, Overload Flexural Distribution Behavior of Composite Steel Girder Bridges

A comprehensive study was performed on two in-service bridge superstructures in Michigan to investigate the impact of variations in boundary condition, loading position, and load configuration on the overall structural response and girder distribution behavior of bridges approaching their ultimate capacities. The three parameters were all found to be highly sensitive.

Variations in lateral distribution behavior occur once the structure passes the linear-elastic stage of behavior. GDFs published in AASHTO LRFD specifications are usually conservative in predicting superstructure ultimate capacities. GDFs' level of conservativeness is dependent on loading configuration. Also, AASTHTO GDFs were calibrated based on linear-elastic behavior. Once inelastic behavior is reached, lateral load distribution factors are governed by the geometry of the structure and the loading configuration. Adjustments made to AASHTO LRFD need validation through a parametric study on many geometrically different bridges and different loading configurations.

Bowman, M.D. and Chou, R., 2014, Review of Load Rating and Posting Procedures and Requirements

This report summarizes where load rating specifications can be found for LRFR, LFR, and ASR, as well as the Indiana Department of Transportation (INDOT) Bridge Inspection Manual. The report also summarizes findings from surveys that DOTs completed related to which specifications they use, which design methods (LRFR, LFR, or ASR) they use, and which method they prefer. At the time of the publication, LFR was the preferred method, although many DOTs did not specify a preferred method. The findings are shown below in Figure 105. After reviewing and performing load ratings with the different methods, it was recommended that INDOT follow AASHTO MBE (2011) with AASHTO legal loads for load ratings.

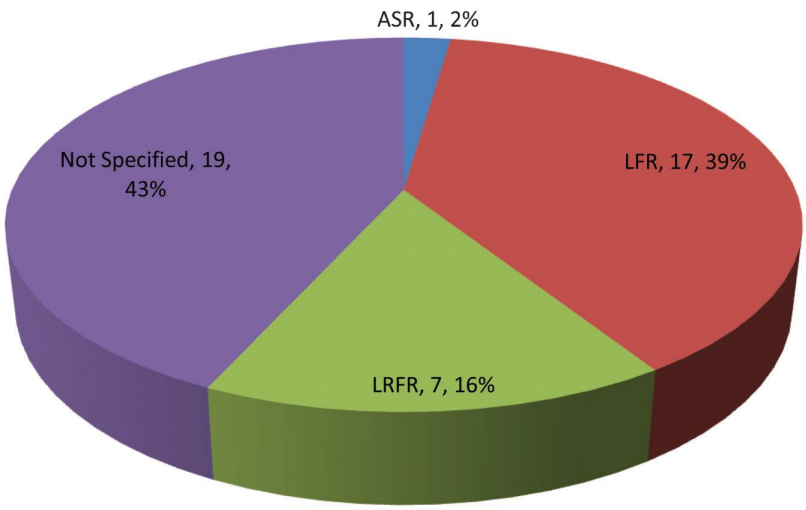

Figure 105. Preferred Method Used for Load Rating and Posting

Harris, D.K. and Gheitasi, A., 2013, Implementation of an Energy –Based Stiffened Plate Formulation for Lateral Distribution Characteristics of Girder-Type Bridges

An analytical approach called the stiffened plate model is presented for determining lateral load distribution characteristics of beam-slab bridges. The methodology was validated using FEM and

field investigation of three bridges. The stiffened plate model yielded a more flexible system response compared to upper bound FEM results. The stiffened plate model had lateral load distribution that is similar in the FEM and field measurements. The majority of DFs calculated from the stiffened plate method were within 15% of the measured DFs.

Kim, Y.J., Tanovic, R., and Wight, R.G., 2013, A Parametric Study and Rating of Steel I-Girder Bridges Subjected to Military Load Classification Trucks

The researchers analyzed six simply-supported bridges that were designed with varying span lengths, number of girders, girder spacings, and moments of inertia. The AASHTO LRFD provisions were conservatively rated between 2.46 and 3.87 while the unfactored FEA models yielded an average of 7.01. The geometric parameters influenced the load distribution of the MLC trucks on the superstructure, but none as much as the wheel-line spacing of the MLC trucks. Although the predictive models were conservative, when a bridge is rated higher than MLC50, the margin between FEA and predictive methods decreases considerably.

Razaqpur, A.G., Shedid, M., and Nofal, M., 2012, Inelastic Load Distribution in Multi-Girder Composite Bridges

The researchers used FEMs to analyze fifty bridge cases. Load distribution factors were obtained from the FEMs and compared to AASHTO LRFD. The researchers also analyzed the sensitivities of bridge parameters. For exterior girder load DFs at elastic state, AASHTO LRFD were on average 67% higher than FEA. For interior girders, this value was 73% higher for AASHTO LRFD. At ultimate state, AASHTO was on average 36% higher than FEA.

Bae, H.U. and Oliva, M.G., 2011, Moment and Shear Load Distribution Factors for Multigirder Bridges Subjected to Overloads

The researchers developed new moment and shear load distribution factor equations for oversize, overweight vehicles. 118 multi-girder bridges with 16 load cases of oversize overload vehicles were used to develop FEMs. Distribution factor equations were created and simulated. Furthermore, the researchers performed load tests, and results were found to be within 8% of the predicted deflection. The equations yield results more conservative than FEM, but less conservative than AASHTO equations. Sample moment and shear GDFs are provided in Figure 106.

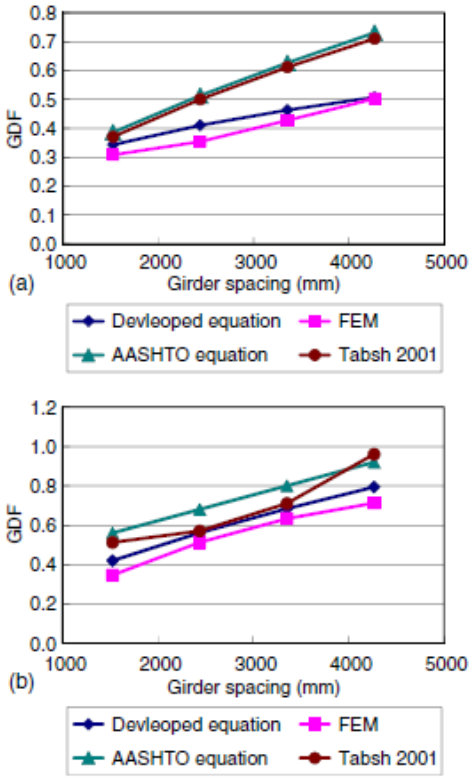

Figure 106. Moment (a) and Shear (b) GDFs based on Girder Spacing from Bae and Oliva (2011)

Harris, D.K., 2010, Assessment of Flexural Lateral Load Distribution Methodologies for Stringer Bridges

The goal of the study was to find the most appropriate analysis method for determining load DFs for slab-girder bridges. Harris validated FEMs for the study using documented field testing, and found that the beam-line method neglects contributions by secondary elements of bridges and concluded that that these contributions should be accounted for in load rating analyses. Furthermore, section response about the composite section neutral axis should be considered for bridges designed for composite action. Harris asserts that boundary conditions had little effect on the distribution factors in the load fraction method, but do affect member response in beam-line analysis.

Murdock, M., 2009, Comparative Load Rating Study Under LRFR and LFR Methodologies for Alabama Highway Bridges

This paper presents major differences between LRFR AND LFR in a comparative study. 95 bridges in Alabama were analyzed using LRFR and LFR rating methods. The researcher

concluded that LRFR rating factors correlated well to the estimated probability of failure for interior and exterior girders in moment and shear. LFR rating factors were found to not correlate well to this estimated probability of failure. Main differences between the two rating methodologies can be seen in.

Table 45. Differences between LRFR and LFR from Murdock (2009)

Rating Methodology	LRFR	LFR
Capcity	According to LRFD	According to LFD
Condition and System Factors	ϕ - Resistance ϕ_c - Condtion ϕ_s - System	- - -
Distribution Factors	LRFD Formulas	"S Over" Formulas
Dead Load Factors	λ_{DC} - 1.25 λ_{DW} - 1.5	A_1 - 1.3
Live Load Factors	λ_{LL} Inventory - 1.75 Operating - 1.35 Legal - 1.4 to 1.8 Permit - 1.15 to 1.8	A_2 Inventory - 2.17 Operating - 1.3
Dynamic Load Allowance / Impact Factor	Constant	Span Length Dependent

Kulicki, J.M., Prucz, Z., Clancy, C.M., Mertz, D.R., Nowak, A.S., 2007, Updating the Calibration Report for AASHTO LRFD Code/NCHRP 20-07/186

NCHRP 12-33 Report 368 provided a calibration procedure that did not correspond to a code. The goal of this project was to document calibration of strenght limit state for AASHTO LRFD Bridge Design Specifications. Reliability analyses were performed for representative bridges including beam-slab bridges, composite and noncomposite steel girder bridges, reinforced concrete T-beams, and prestressed concrete bridges. Several adjustments were made to the data used in Report 368, including increasing the ADTT from 1,000 to 5,000, using a lognormal distribution for resistance in reliability analyses, and using a representative bridge database. In this report, Monte Carlo was used and compared to results from the Rackwitz-Fiessler method. Monte Carlo sampling has become more widespread with the advancement in computing power in recent years. As a check, the Rackwitz-Fiessler method was performed and similar results were attained by using both methods. The reliability of the bridges in the dataset used are shown in Figure 107. An interesting observation noted by the researchers is that there is a general decrease in reliability as the length of the bridge increases, as noted by Figure 108. This suggests that there is a correlation between dead to live load ratio and reliability. Lastly, the researchers perturbed load effects to investigate the sensitivity of the reliability index of the bridges. One of their findings is that if they multiply all of the load effects by a scalar, they see a uniform parallel

offset in the reliabilities. Furthermore, an increased load effect produced the same results as a resistance that is reduced by the same percentage. Another observation made is that modifying the dead loads by a factor is more sensitive as the length of the bridge increases. This can be explained by the fact that bridges typically have higher dead to live load ratio as the span increases. When only the live load is modified by a scalar, the opposite effect was noted. As the span length increases, the sensitivity of reliability index decreases.

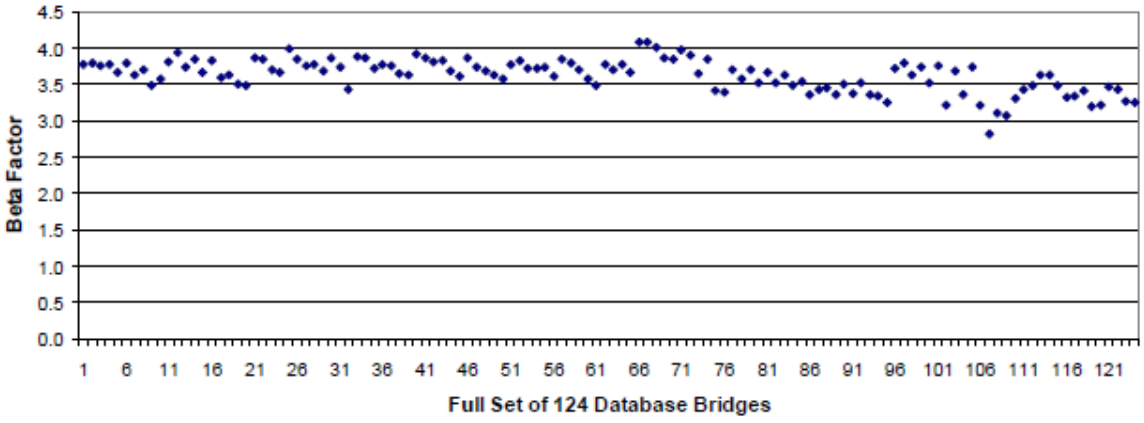

Figure 107. Beta Factors Using Monte Carlo Analysis for Bridge Database

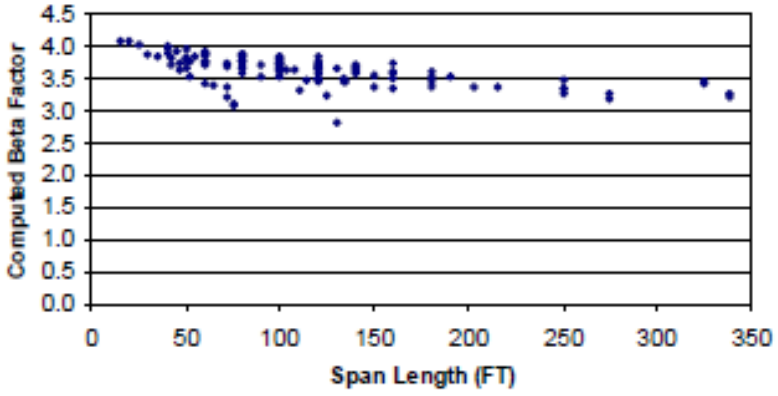

Figure 108. Reliability vs. Span Length

Yousif, Z. and Hindi, R., 2007, AASHTO-LRFD Live Load Distribution for Beam-and-Slab Bridges: Limitations and Applicability

The researchers compared AASHTO LRFD distribution factors to several types of FEM for simple span slab-on-girders concrete bridges. AASHTO LRFD overestimated the live load distribution when compared to FEM for a significant number of cases. AASHTO overestimated the live load distribution a maximum of about 55%. Despite this, AASHTO LRFD did underestimate the distribution factors when compared to FEM in some cases. The range of the limitations specified by AASHTO regarding span length, girder spacing, deck thickness, and longitudinal stiffness all have a significant effect on the live load distribution. Outside of these boundaries, deviations from AASHTO LRFD appear.

Zheng, L., 2007, Comparison of Load Factor Rating (LFR) to Load and Resistance Factor Rating (LRFR) of Prestressed Concrete I-Beam Bridges

This paper presents key differences between LFR and LRFR. Furthermore, the researcher analyzed seven prestressed concrete bridges including one straight, simple span Bulb Tee-girder bridge, three skewed simple span, I-girder, and three skewed continuous multi-span I-girder bridges. They found that the majority of load ratings using LRFR were governed by shear, not flexure. The governing failure mechanism is different from LFR, which has flexural ratings that typically govern.

Moses, J.P., Harries, K.A., Earls, C.J., and Yulismana, W., 2006, Evaluation of Effective Width and Distribution Factors for GFRP Bridge Decks Supported on Steel Girders

Glass fiber-reinforced polymers (GFRP) may be used for replacing concrete decks. Three of these types of bridges underwent situ load tests. Design standards treat GFRP decks similar to noncomposite concrete decks. The researchers found that this may result in nonconservative bridge girder designs. The effective width of the GFRP deck that may be engaged is lower than that of an equivalent concrete deck. This behavior is due to increased horizontal shear lag due to less stiff axial behavior in the GFRP deck and increased vertical shear lag due to the relatively soft in-plane shear stiffness of the GFRP deck. The engaged effective width shows some evidence of degradation with time, which the researchers attributed to the reduction of shear transfer efficiency required for composite behavior.

Chung, W., Liu, J., and Sotelino, E.D., 2006, Influence of Secondary Elements and Deck Cracking on the Lateral Load Distribution of Steel Girder Bridges

The researchers used FEMs to model secondary elements such as diaphragms and parapets. The researchers concluded that the presence of diaphragms and parapets could make girder distribution factors up to 40% lower than the AASHTO values. They also found that longitudinal cracking increased the load distribution factors by up to 17% higher than AASHTO. Transverse cracking was not attributed toimpact the transverse distribution of moment.

Chung, W. and Sotelino, E.D., 2006, Three-Dimensional Finite Element Modeling of Composite Girder Bridges

The researchers created four FEMs with varying modeling parameters. The FEMs' flexural behavior was analyzed and compared to a full–scale lab test and a field test. The first FEM used shell element webs and shell elements flanges. The second FEM used shell element webs and beam element flanges. The third FEM used beam element webs and shell element flanges. The last FEM modeled each girder cross section with a single beam element. All FEMs used shell elements to model the deck. The researchers compared the models' data to physical tests, and differences were attributed to element compatibility as well as geometric discrepancies. The researchers concluded that shell element girder modeling requires a higher level of mesh refinement to converge due to the displacement incompatibility between the drilling DOF of the web element and the rotational DOF of the flange element. The FEM that is the most economical is the fourth model since it is capable of accurately predicting the flexural behavior of the girder bridges including deflection, strain, and lateral load distribution.

Conner, S. and Huo, X.S., 2006, Influence of Parapets and Aspect Ratio on Live-Load Distribution

24 two–span continuous bridges with varying structural parameters were analyzed. FEMs were used to quantify distribution factors and compared to AASHTO distribution factors. The presence of parapets was found to reduce DFs by as much as 36% for exterior girders and 13% for interior girders. Increasing the overhang length decreased the effect of the parapet. AASHTO LRFD was found to be conservative compared to FEMs. Moment DFs were virtually unaffected until the aspect ratio surpassed 1.8. The effect beyond that point, however, was still quite small.

Jaramilla, B. and Huo, S., 2005, Looking to Load and Resistance Factor Rating

This short article describes the differences between LFR and LRFR. LRFR is noted to provide more uniform reliability with HL-93 instead of HS-20 loading. Benefits from nondestructive load testing are noted to be more easily incorporated with LRFR. According to NCHRP Project C12-46, "DOT rating engineers were able to perform the LRFR evaluations without undue difficulty and with relatively few errors." The implementation of LRFD reported at the time of publication is shown in Figure 109.

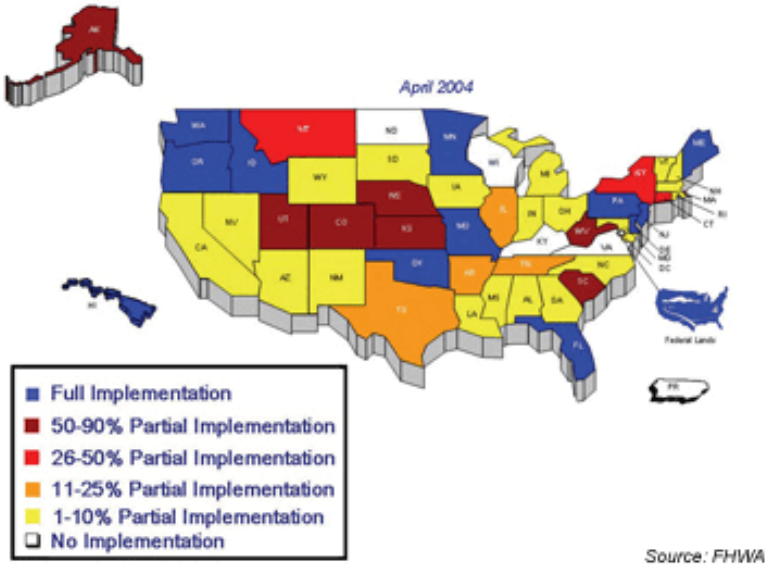

Figure 109. LRFD Implementation as of April of 2004

Sotelino, E.D., Liu, J., Chung, W., and Phuvoravan, K., 2004, Simplified Load Distribution Factor for Use in LRFD Design

AASHTO LDF equation presented in 1994 includes a longitudinal stiffness parameter that is not initially known which makes the procedure iterative. The researchers developed a simplified equation and used it to compare FEMs and AASHTO calculations of 43 steel girder and 17 prestressed concrete girder bridges. The simplified equation always produces conservative LDF values compared to FEA, but larger than the LDFs generated by using AASHTO LRFD. The researchers did improve the FEM by accounting for secondary elements. They found that the presence of secondary elements produced LDFs that were up to 40% less than AASHTO LRFD values.

F., 2003, Nonlinear Finite-Element Analysis for Highway Bridge Superstructures

Researchers compared the Transformed Area Method and FEM (on FORTRAN) to experimental data of a single concrete deck steel-girder bridge. The FEM process the researchers used for the concrete deck, reinforcement, and steel was discussed extensively. The FEM's deflection was closer to the experimental data than what the design method at the time would have predicted (AASHTO 1996).

Khaloo, A.R. and Mirzabozorg, H., 2003, Load Distribution Factors in Simply Supported Skew Bridges

Simply supported skew bridges were analyzed using FEA in ANSYS. The researchers found that AASHTO DFs are conservative in right bridges and even more conservative for skew bridges.

The researchers also concluded that internal transverse diaphragms perpendicular to the longitudinal girders are the best arrangement for load distribution in skew bridges.

Eamon, C.D. and Nowak, A.S., 2002, Effects of Edge-Stiffening Elements and Diaphragms on Bridge Resistance and Load Distribution

These researchers analyzed secondary effects for simple span, two-lane highway girder bridges with composite steel. The researchers also considered prestressed concrete girder bridges in this study. They performed elastic and inelastic analyses for nine bridges modeled in FEM. In the elastic range, secondary elements affected the location and magnitude of moment and were found to experience a 10-40% decrease in GDF, for a typical case. GDFs decrease by an additional 5-20% in inelastic analysis while the ultimate capacity increases 1.1-2.2 times that of the base bridge. Despite the positive influences these elements offer, the researchers seem reluctant to include these benefits in load ratings. “Although ignoring the effects of secondary elements on load distribution and ultimate capacity typically leads to conservative results, their effect varies greatly, depending on bridge geometry and element stiffness. Bridges designed according to the current LRFD code thus have varying levels of safety or reliability, a topic to be investigated in the future.”

Eom, J. and Nowak, A.S., 2001, Live Load Distribution for Steel Girder Bridges

The literature at the time of this publication indicated that GDFs appear to be conservative for long spans and large girder spacing, but too permissive for short spans and small girder spacing. The research program field tested 17 steel girder bridges, and the strains were used to calculate GDFs and compare to FEMs with either roller-hinge supports, hinge-hinge supports, or partially fixed supports. Examples of GDFs derived from strain are shown in Figure 110. The absolute value of measured strain was found to be less than that of the FEM. One important reason for this observation is the partial fixity of supports. Measured GDFs were consistently lower than those of the AASHTO code-specified values. FEM and GDFs agree more when the support condition is ideally simply supported. If the reduction of stress due to the partial fixity of supports is considered, then the code-specified girder distribution values are suitable for use in the rating equations. However, caution must be exercised when relying on partial fixity at supports because the theoretical support restraint may not always be fully available when extremely high loads are present, thereby diminishing the expected beneficial effects.

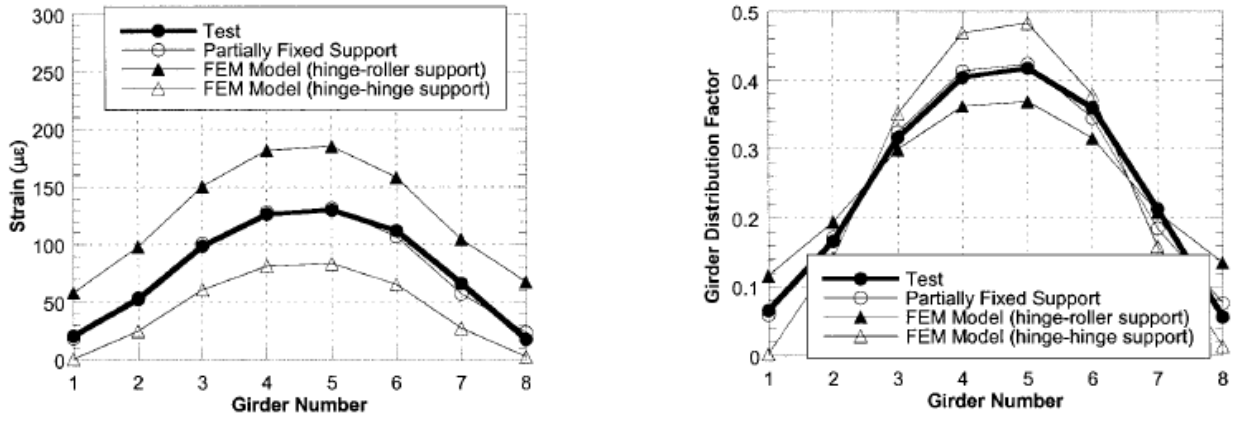

Figure 110. Strain and Resulting GDFs Derived from Strain for Two Lane Loading

Barker, M.G., 2001, Quantifying Field-Test Behavior for Rating Steel Girder Bridges

A systematic approach is presented to separate and quantify the contributions from various effects, such as bearing restraint forces and unintended composite action, in bridge field testing. Bearing restraint was found to increase the capacity by 3.6%. Non-composite sections exhibited composite behavior that increased the capacity an average of 32.3% at those sections. The critical section is composite, so the rating was raised only 4.2%. Load rating engineers should note that bearing restraint contributions may not be reliable over time. The procedure includes inspecting the bridge and determining dimensions and dead loads, determining the experimental impact factor, calculating the experimental distribution factors, determining the bearing restraint forces and moments, calculating the total measured moments, removing the bearing restraint moments, calculating the elastic moments, determining the section moduli, and calculating the elastic longitudinal adjustment moments.

Tabsh, S.W. and Tabatabai, M., 2001, Live Load Distribution in Girder Bridges Subject to Oversized Trucks

FEM was used to develop modification factors for the AASHTO flexure and shear GDFs to account for oversize trucks. Four loading cases were studied; HS20-44, PennDOT P-82 permit truck, Ontario Highway Bridge Design Code's load level 3 truck, and HTL-57 notional truck. The results showed that the modification factors with the specification-based GDFs could help increase the allowable loads on slab-on-girder bridges.

Sebastian, W.M. and McConnel, R.E., 2000, Nonlinear FE Analysis of Steel-Concrete Composite Structures

This paper describes the researchers' FEM process in detail. A verification study was done to assess the FEM's capabilities. The researchers used four structures, tested and published in literature, to validate the FEMs. The FEMs performed well, including those with ribbed

reinforced concrete slabs acting compositely with profiled steel sheeting. Internal deformations, crack patterns, and shear connector actions were shown to be modeled accurately.

Zokaie, T., 2000, AASHTO-LRFD Live Load Distribution Specifications

The AASHTO-LRFD Bridge Design Specifications live load distribution equation was only a function of girder spacing. Now, the equations are more complex to account for skew, slab thickness, and length. The researchers tested the accuracy of the new equations and they found that FEM works the best, but the new formulas were within 5% of FEMs' live load distribution. Limitations include that the formulas had uniform spacing, girder inertia, and skew. The researchers also did not include diaphragm effects in the model. Although the formulas are more accurate than S/D factors, they are most accurate when applied to bridges with similar restraints.

Mabsout, M.E., Tarhini, K.M., Frederick, G.R., and Kesserwan, A., 1998, Effect of Continuity on Wheel Load Distribution in Steel Girder Bridges

The researchers made FEMs for 78 two-equal-span, straight, composite, steel girder bridges. Results of the FEMs were used to predict wheel load distribution factors. They were found to generally be less than values obtained using the AASHTO formula (S/5.5). AASHTO overestimated the actual wheel load distribution by as much as 47% depending on the bridge geometry. As the span and girder spacing increases, AASHTO aligns more closely to FEA results.

Chajes, M.J., Mertz, D.R., and Commander, B., 1997, Experimental Load Rating of a Posted Bridge

A posted bridge with non-composite girders was found to have significant bearing restraint. Additionally, the girders were found to act compositely based on data from a diagnostic load test. An FE model was developed and calibrated using the measured response to obtain accurate analytical predictions of bridge structural response to applied live load. Load ratings for Delaware's seven load vehicles increased from the range of 0.72 to 1.39, to 1.38 to 2.55 which justified removing load posting. The authors discussed whether to include unintended composite action in load rating. For this specific case, the researchers recommended including unintended composite action in the load rating since, in the researchers' opinions, the observed structural behavior could be reliably expected for applicable loading patterns and magnitudes. However, they recommend relatively frequent inspection.

Mabsout, M.E., Tarhini, K.M., Frederick, G.R., and Kobrosly, M., 1997, Influence of Sidewalks and Railings on Wheel Load Distribution in Steel Girder Bridges

120 bridges were analyzed using FEMs in a parametric study. AASHTO LRFD wheel load distribution formulas correlated conservatively with the FEM results. Both were less than the AASHTO (S/5.5) formula. NCHRP 12-26 formulas were found to be conservative too, but not as much as AASHTO except for short spans. Sidewalks and railings were found to increase the load-carrying capacity by upwards of 30% if they are included in the strength evaluation. However, the researchers seemed reluctant to be able to count on the sidewalks and railings

when determining the bridge capacity. The researchers' recommendations include, "The results of this research can assist the bridge engineering in determining the actual load-carrying capacity of steel bridges when encountering sidewalks and/or railings in a bridge deck."

Ebeido, T. and Kennedy, J.B., 1996, Shear and Reaction Distributions in Continuous Skew Composite Bridges

AASHTO provisions at the time did not account for skew or continuity; therefore, load ratings could be conservative for continuous skew bridges. FEM was verified with test data and then used to conduct a parametric study on more than 600 prototype cases. The generated data was then used to find expressions for span and support moment DFs for truck loading as well as dead load. Parametric sensitivity was analyzed as well

Ebeido, T. and Kennedy, J.B., 1996, Girder Moments in Continuous Skew Composite Bridges

Six simply supported skew composite steel-concrete bridges were constructed and tested. The researchers included an additional 300+ prototype bridges for a parametric study using FEA. The study produced empirical formulas to evaluate moment DFs for exterior and interior girders. The authors concluded that skew is the most important parameter affecting girder moments in composite bridges. Girder spacing, intermediate transverse diaphragms, and aspect ratio all influence the moment DF as well. Ebeido and Kennedy concluded that, "in the design of continuous skew composite bridges, the exterior girder is the controlling girder in terms of both span and support moments." They found that the higher the skew, the more moment is placed on the exterior girders.

Chen, Y., 1995, Prediction of Lateral Distribution of Vehicular Live Loads on Bridges with Unequally Spaced Girders

Chen proposed an analysis method for predicting the lateral distribution of vehicular live loads on unequally spaced I-shaped bridges. The paper describes the bridge modeling process and verification as well as AASHTO methods of lateral load distribution. Live load distribution factors were obtained using a refined analysis method that uses FEM and compared with data from a parametric study of 13 bridges. The researcher performed nonlinear and linear analysis and found that nonlinear analysis yielded slightly lower DF values. Compared to the refined method presented, AASHTO gave unconvervative distribution factors for exterior girders that are spaced less than six feet.

Helba, A. and Kennedy, J.B., 1994, Parametric Study on Collapse Loads of Skew Composite Bridges

The researchers used FEMs in this parametric study to relate bridge parameters and geometries to failure patterns for the minimum collapse load of simply supported and continuous two-span skewed composite bridges. The analyzed parameters included eccentric and concentric critical loadings, skew, aspect ratio, number of girders, interaction between diaphragms and main girders, and the number of loaded lanes. For eccentric loading, the "critical crack length"

(meaning the transverse distance from the deck edge nearer the applied load to the longitudinal hinging line on the opposite side of the load) was found to be significantly affected by the bridge aspect ratio and slightly by skew. For concentric loading, the inclination of the positive transverse failure line was shown to be related to the number of loaded lanes and skew.

Galambos, T.V., Dishongh, B., Barker, M., Leon, R.T., and French, C.W., 1993, Inelastic Rating Procedures for Steel Beam and Girder Bridges

This project developed a rating methodology for existing bridges that included inelastic capacity available in most multi-girder bridges as well as the redistribution capacity due to composite action. The authors also investigated shakedown – the response of a structure after some initial plastic deformation. Shakedown happens when the structure adapts to prior inelastic excursions and responds in the elastic range to working loads. This study asserts that system-capacity is a more accurate load capacity method than typical element-based approaches. Field tests and experimental studies showed that composite and non-composite compact beams exceeded their theoretical plastic moment capacity and also showed excellent ductility and rotational capacity. The researchers recommended the shakedown method of load testing since bridges are loaded cyclically, which would make the ultimate strength limit state unconservative. One reason they make this assertion is the fact that the friction between slab and girders is overcome at ultimate and composite bridges act noncompositely. Furthermore, "Although the ultimate strength of the composite plate girders can be reached and exceeded by using stiffeners and tension field action, the question of available rotational ductility of the plate girders has not yet been thoroughly researched. It should also be pointed out that plate girders, because of the use of stiffeners and bracing, are very sensitive to fatigue problems." The report goes on to say, "Rather shakedown, or that load causing a set of residual moments throughout the structure such that the bridge responds to subsequent loads of the same magnitude or smaller in an elastic fashion, is the recommended limit state to be used when cyclic loads are present." Shakedown was still in early research phases at the time of this publication, but this article indicated that it will more adequately predict a global failure mechanism instead of local approaches.

Bishara, A.G, Liu, M.C., and El-Ali, N.D., 1993, Wheel Load Distribution on Simply Supported Skew I-Beam Composite Bridges

This paper presents distribution factor expressions for wheel-load distribution for the interior and exterior girders of multi-steel beam composite bridges of medium span length. The researchers used FEMs to determine the wheel load distributions. They also performed sensitivity analysis on parameters such as span lengths, widths, skew angle, and spacing and size of intermediate cross frames. AASHTO wheel-load distribution factors for interior and exterior girders were found to be 5-25% higher than those from FEA. The interior girder distribution factors developed in this study were 30-85% of the contemporary AASHTO distribution factors and exterior girder distribution factors were found to be 30-70% of AASHTO.

Tarhini, K.M. and Frederick, G.R., 1992, Wheel Load Distribution in I-Girder Highway Bridges

FEAs were used to model I-girder highway bridges. Researchers made a wheel load distribution formula by using the FEAs. They used a standard bridge design while they varied one parameter within a specified range while the remaining parameters were the same to measure sensitivity of the parameters. The parameters analyzed were girder size and spacing, cross bracing presence, slab thickness, span length, single or continuous spans, and composite and noncomposite behavior. The formula's DF was compared to AASHTO DFs and other researchers' work and can be seen in Table 46. The sensitivity of the parameters was also analyzed.

Table 46. Comparison of Wheel Load Distribution Factors from Tarhini and Frederick (1992)

Span L (ft) (1)	Beam spacing (ft) (2)	AASHTO $S/5.5$ (3)	S/D_d Bakht and Moses (4)	S/D_d (SALOD) (5)	Proposed DF formula (6)
20	7.5	1.364	1.44	1.85	1.61
50	7.5	1.364	1.33	1.28	1.25
50	6.0	1.09	1.07	1.08	1.04
75	6.0	1.09	1.01	0.96	0.92
75	5.0	0.91	0.84	0.83	0.75
77	8.8	1.60	1.313	—	1.28
100	5.0	0.91	0.82	0.77	0.80
110	8.5	1.545	1.29	—	1.36

Khaleel, M.K. and Itani, R.Y., 1990, Live-Load Moments for Continuous Skew Bridges

Khaleel and Itani modeled a total of 112 pretensioned concrete, 5-girder continuous bridges using FEMs. The researchers found that AASHTO underestimated positive bending moments by as much as 28% for skew bridges. The edge girders controlled the design for a combination of large skew angles, large spans, small girder spacings, and smaller girder-to-slab stiffness ratios. For a skew angle of 60 degrees, the maximum moment in the interior girder is 71% of the corresponding moment for a bridge with no skew. For the exterior girders, the reduction of the moment for the maximum girder is 20%.

Razaqpur, A.G. and Nofal, M., 1990, Analytical Modeling of Nonlinear Behavior of Composite Bridges

Details of modeling bridge deck, steel girders, and reinforcement are discussed. Experimental verification was done using results of the two beam tests and a multi-girder bridge test. FEM accurately determined complete cracking over interior support, bottom flange first yielding, first yielding in the web, and complete cracking with less than 3.5% error and failure load with less than 1% error for the beam test. FEM had similar results to the bridge test with less than 2% difference in failure load.

Bakht, B. and Jaeger, L.G., 1988, Bearing Restraint in Slab-on-Girder Bridges

Researchers found that girder restraint can reduce live load moments in existing single-span slab-on-girder bridges by up to 20%. This paper presents simple expressions for deflection reduction and stress reduction to account for additional girder support restraint. The researchers performed FEA and obtained similar results. The paper provides a procedure to account for additional support restraint. Researchers performed a case study of a short-span simply supported bridge having six rolled-steel girders and a non-composite deck slab that was statically tested. Bearing restraint forces reduced the bending moment at mid-span by at least 12%.

Marx, H.J., Khachaturnian, N., and Gamble, W.L., 1986, Development of Design Criteria for Simply Supported Skew Slab-on-Girder Bridges

Elastic analyses were performed using FEMs on 108 single span skew slab-and-girder bridges. The parametric study was performed to determine the most important bridge variables and to gain insight on how skew bridges respond. AASHTO wheel load (S/5.5) was found to be between 12% unsafe or 32% too large. AASHTO underestimated the actual exterior girder bending moments in most bridges considered – up to 23% too small. It was found that higher skew results in smaller interior girder moments. However, exterior girders are not affected as much as interior girders. Because of this, the exterior girders typically control the design of highly skewed bridges. The presence of end diaphragms can reduce maximum bending moments.

Hall, J.C. and Kostem, CN, 1981, Inelastic Overload Analysis of Continuous Steel Multi-Girder Highway Bridges by the Finite Element Method

This paper describes an analytical technique for predicting the response to overloads of simple-span and continuous multi-girder beam-slab type highway bridge superstructures made of steel beams and concrete slabs by employing a displacement based FEA. This paper was the first study to consider post-plastic stress-strain relationships for the steel girder, strain hardening of steel, buckling of beam compression flanges and plate girder webs, and post-buckling response of the flanges and webs in FEA. Researchers compared the stress and strain of two bridges, two bridge models, two composite beams, and eight plate girder tests to experimental results, and found that the analytical predictions were similar to observed physical responses. The researchers confidently assert that engineers can use the model for structural overload response, regarding stresses, deflections, and damage, for steel beam concrete slab highway bridges, composite beams, and plate girder structures. They also noted that the negative moment regions suffered the most damage.

11.1.2 Studies of Neural Networks in Engineering

Alipour, M., Harris, D.K., Barnes, L.E., Ozbulut, O.E., Carroll, J., 2007, Load-Capacity Rating of Bridge Populations through Machine Learning: Application of Decision Trees and Random Forests

Load rating bridges poses many challenges with limited resources for testing bridges and imcomplete plans. Researchers created neural network models in order to create a data-driven

approach to load rating bridges, rather than systematic procedures that are common at state departments of transportation. Data was collected for 47, 385 highway bridges from NBI (2014) and used to create and test the models. The C4.5 algorithm from Weka machine-learning software. In this project, researchers created decision trees that could predict whether the bridge is posted or not. In addition to decision trees, random forests were created. Random forests are a group of decision trees that are varied in random samples until the optimal number of trees is achieved. Then, the majority prediction between all of the trees is taken. Since the number of posted bridges was about 10% of the entire population, different sampling techniques were used to address class imbalance. Models were created using the original data, majority undersampling so that half of the bridges in the training set are posted, and majority undersampling so that a quarter of the bridges in the training set are posted. Synthetic minority oversampling technique (SMOTE), in conjunction with the two majority undersampling techniques mentioned, were used as alternative models too. The metrics used to evaluate the models are accuracy rate, false positive rate, and false negative rate. Furthemore, a scale factor was used to count false negatives (the model predicting the bridge is posted when it is not according to NBI) more severly. The best model was found to be a random forest made up of 200 trees. This method was found to be suitable for predicting load postings, as shown in Table 47. Comparison of Performance of the Proposed Approach with Contemporary Practices. Furthermore, the team suggests that this tool could be used to identify bridges that may need to be investigated based on false positives or false negatives.

Table 47. Comparison of Performance of the Proposed Approach with Contemporary Practices

Method	FNR (%)	FPR (%)	Accuracy (%)
Proposed method (M3)	9.9	13.5	86.8
Oregon, Washington, Idaho, Kentucky DOT methods	89.5	2.3	90.0
Using condition ratings of Texas DOT flowchart	45.8	14.1	83.1

Bandara, R.P., Chan, T.H.T., and Thambirathnam, D.P., 2014, Frequency Response Function Based Damage Identification Using Principal Component Analysis and Pattern Recognition Technique

Frequency response function (FRF), ANN, and principal component analysis are combined in a procedure for identifying damage to structures. First, FRF data is collected and used to train an ANN. The ANN is then able to predict damage location and severity. The procedure can filter out noise so that the accuracy is not jeopardized. The procedure seems to be adequate at predicting single and multiple damage cases.

Hasancebi, O. and Dumlupinar,T., 2013, Detailed Load Rating Analyses of Bridge Populations Using Nonlinear Finite Element Models and Artificial Neural Networks

T-beam bridges were analyzed using a feed-forward, multi-layer ANN in this study. Governing parameters were span length, skew, bridge width, number of T-beams, beam depth, beam web width, beam spacing, slab thickness, reinforcement detailing, boundary conditions, material properties, and secondary load carrying components such as parapets and diaphragms, as shown in Figure 111. The study had 90 bridges in the sample set, and it provided enough diversity for training (if 60 are used then the accuracy of the ANN compared to the FEM is reduced by 2-3%). The researchers found that the prediction improves by merely 0.5% if the number of training patterns is increased beyond a total of 200. Single layer architecture was found to be adequate for this study. Results were excellent for both moment and shear load ratings with R-values of 0.997 and 0.996 respectively.

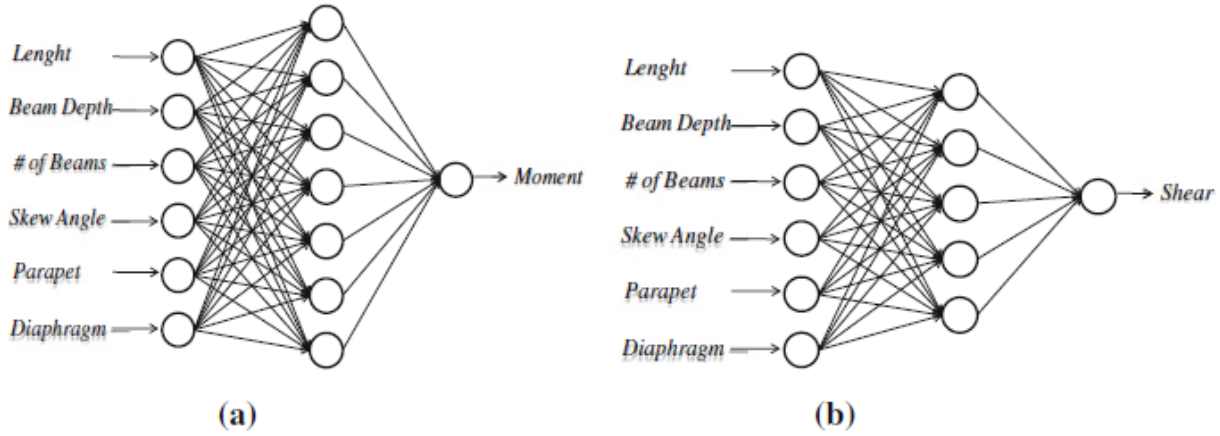

Figure 111. Network Architecture for Moment (a) and Shear (b) from Hasancebi and Dumlupinar (2013)

Shu, J., Zhang, Z., Gonzalez, I., and Karoumi, R., 2013, The Application of a Damage Detection Method Using Artificial Neural Network and Train-Induced Vibrations on a Simplified Railway Bridge Model

A backpropagation ANN was trained to predict damage for a one-span simply supported beam railway bridge. The bridge was modeled using an FEM program. The ANN was found to be able to predict the location and severity of damage. The researchers found that damage in the middle of the bridge is easier to detect than near the supports. Furthermore, the severity estimation depends heavily on an accurate damage location.

Tadesse, Z., Patel, K.A., Chaudhary, S., and Nagpal, A.K., 2012, Neural Networks for Prediction of Deflection in Composite Bridges

Three neural networks were developed to predict the mid-span deflections of simply supported bridges, two-span continuous bridges, and three-span continuous bridges. They made six FEMs for the bridges, and they compared the mid-span deflection to the outputs of the ANNs. The maximum error for any of the spans was 6.4%, and the root mean square error was 3.79%.

Hasancebi, O. and Dumlupinar, T., 2011, A Neural Network Approach for Approximate Force Response Analyses of a Bridge Population

An ANN was used to make an efficient method for approximate force response analyses of a concrete T-beam bridge population. Bridge input parameters were span length, skew, bridge width, number of T-beams, beam depth, beam web width, beam spacing, slab thickness, reinforcement detailing, boundary conditions, and secondary load carrying components such as parapets and end diaphragms, which can be visualized using Figure 113. The researchers also modeled the bridges with FEMs. Results of the ANN were compared to the FEM and found to be very reasonable. The researchers analyzed the parameters' sensitivities. Span length and beam depth were the most sensitive for moment output. Span length, skew angle, and beam depth were the most sensitive for shear output.

Sakr, M.A. and Sakla, S.S.S, 2008, Long-Term Deflection of Cracked Composite Beams with Nonlinear Partial Shear Interaction: Finite Element Modeling

The researchers presented a uniaxial nonlinear FE procedure for modeling the long-term behavior of composite beams at the serviceability limit state in this paper. They performed the procedure on four composite beams from literature. The deflections and stresses of the four beams were within an acceptable degree of accuracy. Neglecting the effect of concrete cracking leads to unrealistic deflection and stress deflections. A parametric study was done to study the effect of the nonlinearity of the load—slip relationship of shear connectors and the cracking the concrete deck on the long-term behavior of simply-supported composite beams. The effect of nonlinearity becomes more significant as the stiffness of the shear connection decreases.

Pendharkar, U., Chaudhary, S., and Nagpal, A.K., 2007, Neural Network for Bending Moment in Continuous Composite Beams Considering Cracking and Time Effects in Concrete

A methodology using an ANN was developed to predict the inelastic moments from the elastic moments while neglecting cracking in continuous composite beams. The eight parameters used as inputs are the age of loading, stiffness ratio of adjacent spans, cracking moment ratio at the support, load ratio of the adjacent spans, composite inertia ratio, cracking moment ratio at left and right adjacent support, and grade of concrete. Four networks with varying architecture details were produced that can all predict inelastic moments with reasonable accuracy.

Sheikh-Ahmad, J.S., Twomey, J., Kalla, D., and Lodhia, P., 2007, Multiple Regression and Committee Neural Network Force Prediction Models in Milling FRP

A tool is used to cut fiber-reinforced polymer chips. The goal of this research was to obtain a continuous specific cutting energy function for given material-cutting tool combination. The parameters were fiber orientation and uncut chip thickness. A committee neural network was used to predict the force of the tool to cut the chips. The neural network did an adequate job of predicting the force when compared to experimental data.

Guzelbey, I.H., Cevik, A., and Gogus, M.T., 2006, Prediction of Rotation Capacity of Wide Flange Beams Using Neural Networks

A backpropagation ANNs was trained to predict the rotation capacity of wide flange beams. The researchers compared its predictions to numerical results from literature at the time of the publication. The ANN inputs are half of the length of flange, the height of the web, the thickness of the flange, the thickness of the web, length of the beam, the yield strength of the flange, and yield strength of the web. The proposed ANN was found to be more accurate than numerical results as well as more practical and fast compared to FEM.

Sirca Jr., G.F. and Adeli, H., 2004, Counterpropagation Neural Network Model for Steel Girder Bridge Structures

The researchers developed a counter-propagation neural network for estimating detailed section properties of steel bridge girders needed in the LFD rating based on just cross-section area, moment of inertia, and section modulus. The motivation of this study was that many old bridges were rated by using working stress design that needed to be updated to LFD. Rating software used by state engineers at the time of the study required unavailable section properties, shown in Figure 112. The ANN used a training set made up of an AISC W-shape database and an additional 100 plate girder designs. The ANN did an adequate job at predicting the needed parameters. State engineers integrated the ANN into an intelligent decision support system that they used at the Ohio Department of Transportation at the time of the study's publication.

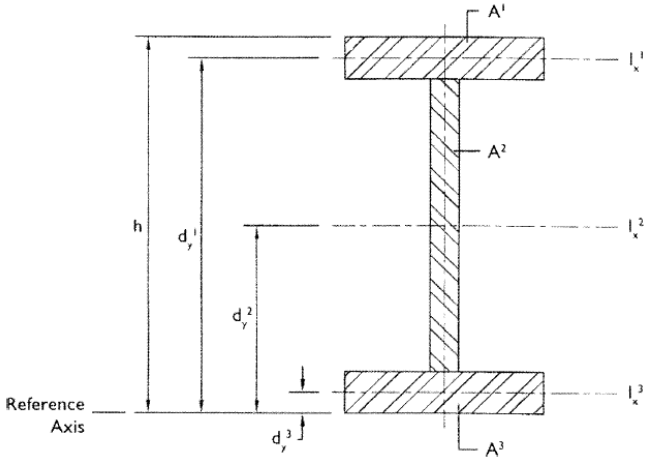

Figure 112. Detailed Description of Geometric Properties Sought After in Ohio

Hadi, M.N.S., 2003, Neural Networks Applications in Concrete Structures

A backpropagation, single-hidden layer ANN was trained to predict optimum beam designs and cost optimization of steel fibrous reinforced concrete beams. The researchers compared several types of backpropagation models and the Levenberg-Marquardt was found to have the least amount of epochs until results converge. The number of samples is a tradeoff: the more samples, the less error the model has, but the longer it takes to get the prediction. ANNs were found to be a powerful tool that are potentially superior to conventional methods (time spent on calculations, accuracy, ease of use).

Adeli, H., 2001, Neural Networks in Civil Engineering: 1989-2000

This review article sums up neural network implementations in civil engineering. A backpropagation training algorithm has been used in civil engineering because of its simplicity. Estimating a bridge rating is something that has been attempted since 1997 (Cattan and Mohammadi). Neural networks could be used to speed up FEA since linear equations take up a lot of time in large-scale structures. Consolazio (2000) proposed merging neural networks with iterative equation-solving techniques. The author mentions many other applications outside of structural engineering.

Huang, C.C. and Loh, C.H., 2001, Nonlinear Identification of Dynamic Systems Using Neural Networks

This paper discusses the technical details of ANNs. The proposed ANN methodology was put to the test when researchers attempted to find the seismic response of a bridge. The ANN was found to be effective. However, it cannot be applied solely for damage detection. It could be used as a tool for engineers to use before advanced structural analysis is done.

Masri, S.F., Smyth, A.W., Chassiakos, A.G., and Caughey, T.K., 2000, Application of Neural Networks for Detection of Changes in Nonlinear Systems

An ANN was used to try to detect damage in structures. By using vibration measurements from a non-damaged structure, the ANN can detect damage. The ANN was then fed comparable vibration measurements from the same structure but during different episodes. The ANN would then be able to indicate any changes in vibration measurements which would be inferred as damage to the structure. The ANN was successful in detecting changes. However, this was not done on a large, parametric scale.

Chuang, P.H., Anthony, T.C., and Wu, X., 1998, Modeling the Capacity of Pin-Ended Slender Reinforced Concrete Columns Using Neural Networks

A multilayer feedforward neural network was found to be reasonable in predicting concrete column behavior. It could be implemented as a tool to check routine designs since results are instantaneous after training and testing is completed. 54 experimental high strength concrete

column tests were adequately predicted using the neural network. The inputs used to train the neural network were b, h, d/h, ρ, f_y, f_{cu}, e/h, and L/h.

Mikami, I., Tanaka, S., and Hiwatashi, T., 1998, Neural Network System for reasoning Residual Axial Forces of High-Strength Bolts in Steel Bridges

An automatic looseness detector was developed to measure how loose high-strength bolts are in bridges. The detector, however, cannot determine the residual axial forces of the bolts. The ANN could reasonably predict looseness based on the reaction and acceleration waveforms collected by the new tool.

Hegazy, T., Tully, S., and Marzouk, H., 1998, A Neural Network Approach for Predicting the Structural Behavior of Concrete Slabs

ANNSs were developed to predict the load-deflection behavior of concrete slabs, the final crack-pattern formation, and the reinforcing steel and concrete strain distributions at failure. The researchers used a total of 19 parameters as inputs. They compared the ANN predictions for the four analysis cases to well-documented tests. Considerable amounts of error were found, but the researchers propose that this would decrease with a larger training set. A user-friendly structural engineering tool was formulated using excel to give the engineer the results upon submitting inputs. Input descriptions is shown below in Table 48.

Table 48. Description of Inputs from Hegazy et al. (1998)

Category	Input factor
Slab geometric properties	1. Slab thickness (mm)
	2. Slab depth (mm)
	3. Ratio of rebar depth to slab depth
	4. Slab span (mm)
Aggregate properties	5. Aggregate type (1, sandstone; 2, granite)
	6. Aggregate size (mm)
Concrete properties	7. Concrete compressive strength (MPa)
	8. Concrete tensile strength (MPa)
	9. Concrete modulus of elasticity (MPa)
Reinforcement steel properties	10. Reinforcing steel ratio
	11. Rebar size (1, M10; 2, M15)
	12. Rebar shape (0, smooth; 1, deformed)
	13. Rebar spacing (mm)
	14. Number of rebar layers
	15. Rebar yield strength (×10 000 MPa)
	16. Rebar modulus of elasticity (×10 000 MPa)
	17. Type of shear reinforcement (0, none; 1, hat; 2, U-shape; 3, W-shape)
Loading and boundary conditions	18. Load type (0, axial; 1, bending; 2, axial + bending; 3, cyclic)
	19. Boundary conditions (0, simply supported; 1, fixed; 2, partially fixed)

Anderson, D., Hines, E.L., Arthur, S.J., and Eiap, E.L., 1997, Application of Artificial Neural Networks to the Prediction of Minor Axis Steel Connections

Steel frame designs usually involve minor-axis beam-to-column connections that govern restraint to the columns against buckling. Predicting behavior of those connections has its difficulties. An ANN was trained to predict how these connections will behave. The inputs were column depth of section, column flange thickness, column web thickness, beam flange breadth, beam depth of section, connection number of bolts, and connection plate thickness. The training data was obtained from experiments summarized in the paper. The researchers compared ANN predictions to experimental data, and it suited it well. The researchers attributed the error in the ANN it to the values that were at the edge of the sample space.

Cattan, J. and Mohammadi, J., 1997, Analysis of Bridge Condition Rating Data Using Neural Networks

An ANN was used to predict ratings for Chicago metropolitan railroad bridges. Parameters varied in bridge type, span type, substructure type, deck type, bridge height/clearance, bridge length, number of tracks on the bridge, number of spans composing the bridge, span length, date the span was built, date substructure was built, and date the deck was built. ANNs compared to fuzzy logic and Cooper rating and found to be superior to them. No FEM was performed and compared to the ANN though. The appropriate sample size was determined by using Eqn. 96:

$$\Delta = \frac{K\delta}{\sqrt{n}} \qquad \text{Eqn. 96}$$

where n is sample size, Δ is the confidence interval for the mean as a percentage below and above the mean, and δ is the coefficient of variation. K is obtained based on a confidence level from the table of the normal probability values.

Kushida, M., Miyamoto, A., and Kinoshita, K., 1997, Development of Concrete Bridge Rating Prototype Expert System with Machine Learning

The objective of this study was to evaluate the structural serviceability of concrete bridges by the specifications of the bridges to be evaluated, environmental conditions, traffic volume, and other subjective information gained through visual inspection. The researchers trained the ANN with results of a questionnaire survey conducted with domain experts. The neural network used fuzzy logic. Reasonable agreement between the results attained from the original system and the new system confirmed that knowledge for the new system was successfully acquired from the original system.

Mukherjee, A., Deshpande, J.M., and Anmala, J., 1996, Prediction of Buckling Load of Columns Using Artificial Neural Networks

An ANN was produced to predict the buckling load of columns. The motivation of this study was that semi-empirical formulas typically follow a lower bound to experimental observations which leave a significant portion of the actual column strength unutilized. A total of 20 examples, tested five times each, were used to train the ANN. The researchers found that the ANN could accurately predict the buckling behavior of columns based on the learning based on slenderness ratio, modulus of elasticity, and buckling load. The adequacy of the ANN can be seen in Figure 113.

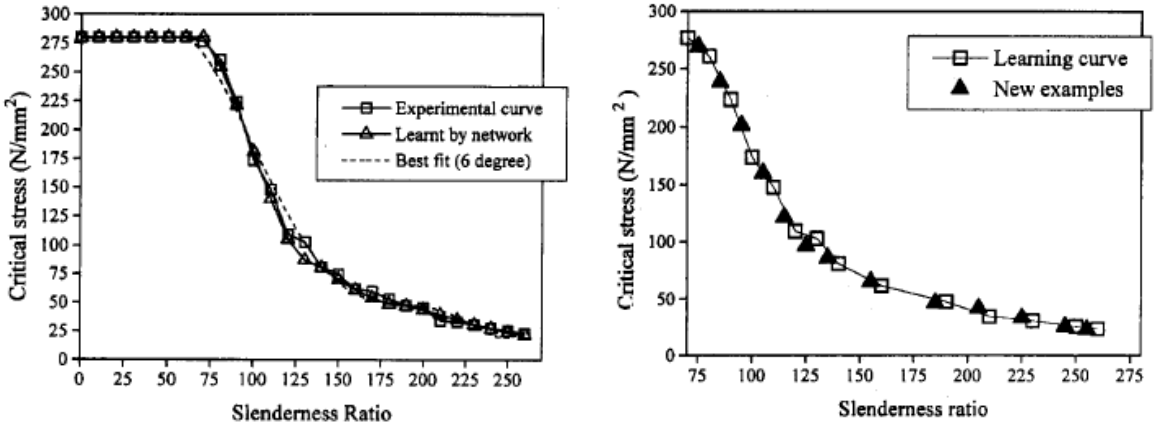

(a) Learning of Critical Stress for Columns (b) Performance Network

Figure 113. Critical column buckling stress by experiments and network predictions from Mukherjee et al. (1996)

Chen, H.M., Tsai, K. H., Qi, G.Z., Yang, J.C.S., and Amini, F., 1995, Neural Network for Structure Control

A backpropagation neural network was used to model the dynamic behavior of an apartment building during an earthquake. The data set used for training was the first 1,000 out of the total 2,000 points from the Morgan Hill earthquake (displacement, velocity, and acceleration). The neural network could then predict and nearly replicate the remaining points of the earthquake record.

Mukherjee, A. and Deshpande, J.M., 1995, Modeling Initial Design Process Using Artificial Neural Networks

It can take years of experience to develop intuition on formulating an initial design. A good initial design can reduce the time and money spent on analysis. The goal of this research project was to make an ANN that could make a preliminary design that includes the amount of tensile reinforcement required, depth of beam, width, cost per meter, and moment capacity. The input

parameters are span length, dead load, live load, concrete grade, and steel type. The ANN was suitable at providing a good initial design and could aid structural engineers in the preliminary design stage.

Pandey, P.C. and Barai, S.V., 1995, Multilayer Perceptron in Damage Detection of Bridge Structures

This paper presents an application of multilayer perceptron that learns through backpropagation, in damage detection of steel bridge structures. A total of 40 training patterns and 10 additional testing patterns for verification were used. The engineers used an FE software to design find target outputs. The ANN worked well in determining where the damage is in the bridge. The engineering significance of the investigation is that the measured data at only a few locations in the structure is needed to train the network for the damage identification.

Masri, S.F., Chassiakos, A.G., and Caughey, T.K., 1993, Identification of Nonlinear Dynamic Systems Using Neural Networks

An ANN was used to predict the internal forces of the same nonlinear oscillator under stochastic excitations of different magnitude. The model was simple, with two inputs and one output, and a total of 15 and 10 nodes in the first and second layers, respectively. This simple three-layer model was adequate to characterize internal forces of the damped Duffing oscillator.

Marquardt, D.W., 1963, An Algorithm for Least-Squares Estimation of Nonlinear Parameters

This paper describes an algorithm that determines the least-square. Like the Taylor series method, it converges rapidly once the vicinity of the converged values is reached. It is like the gradient methods in the way that it may converge from an initial guess which may be outside the region of convergence.

11.1.3 Studies of Static and Dynamic Load Testing

Yarnold, M., Golecki, T., Weidner, J., 2018, Identification of Composite Action Through Truck Load Testing

This paper describes methods that can be used to determine whether or not a slab on girder bridge is behaving compositely. Three cases studies are shown to illustrate the methods.

The first case study is a three span highway bridge in Tennessee. The two lane rural bridge has eight girders, two of which were instrumented for testing. Ambient traffic data was recorded over 10 days. The elastic neutral axis was determined by projecting the elastic strain profile over the entire girder depth. As shown in Figure 114, the elastic neutral axis projection near the top of this girder indicates that it was behaving compositely. Neutral axis projections for all load events were performed and nearly all were found to be around the elastic neutral axis of a truly composite section.

The second case study was carried out on a typical highway bridge with eight spans in Eastern United States. This bridge was selected for monitoring because it exhibited performance

problems. Four girder of a single span was tested at quarterspans and midspans. It was found that the exterior girder had an elastic neutral axis very close to a composite neutral axis anywhere along the longitudinal length of the girder. However, girder 3 showed an elastic neutral axis closer to the noncomposite neutral axis.

Finally, a third load test was done to see if the load test would provide an improved load distribution and load rating for a nine girder steel bridge. The bridge was instrumented on all girders at one quarter-span and near the midspan. Although the bridge was rated as noncomposite, it was found that the bridge exhibited substantial partial composite behavior.

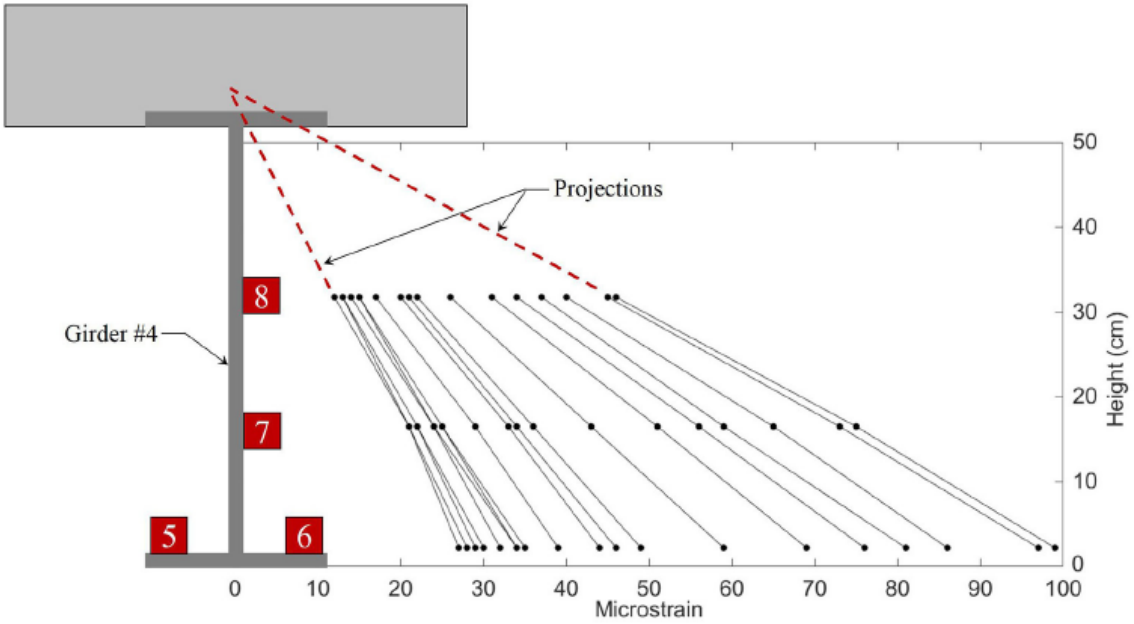

Figure 114. Strain Measurements at Girder #4 for Maximum Truck Events

The researchers recommended two instrumentation profiles for others investigating level of composite behavior in bridges. The two instrumentation profiles can be seen in Figure 115.

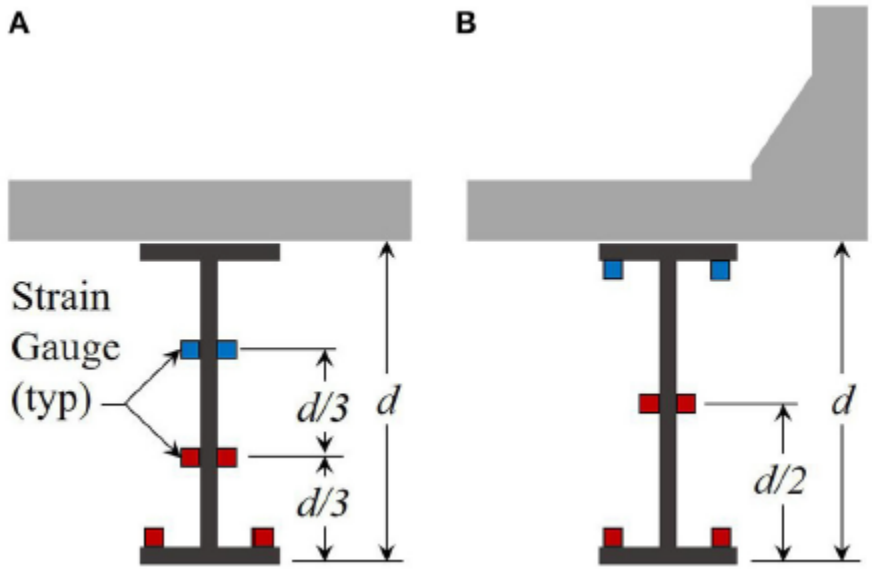

Figure 115. Recommended Strain Gauge Locations for (A) Interior Girder and (B) Exterior Girder with Symmetric Cross-Sections

Harris D.K., Civitillo, J.M., and G heitasi, A., 2016, Performance and Behavior of Hybrid Composite Beam Bridge in Virginia: Live Load Testing

A hybrid composite beam (HCB) was recently implemented in Colonial Beach, VA. The HCB system is made up of a glass fiber-reinforced polymer (FRP) box shell that encases a passively tied concrete arch. The tie reinforcement is an unstressed prestressing strand integrated into the FRP shell during production, and the arch is made up of self-consolidating concrete. This study was focused on evaluating and understanding the in-service performance of the bridge. A conclusion is that the FRP shell does not act compositely with the internal HCB components. The dynamic load allowance was found to be very different than AASHTO recommendations.

McConnell, J., Chajes, M., and Michaud, K., 2015. Field Testing of a Decommissioned Skewed Steel I-Girder Bridge: Analysis of System Effects

Researchers performed a decommissioned field test to calibrate and validate an FEM. The FEM was then used to apply much greater loads than the physical constraints allowed for in the field test. Higher strains in the FEA were attributed to partial fixity at the supports of the decommissioned bridge. The researchers determined that the AASHTO prediction is conservative because it determines load rating by using element-level capacity instead of system-level capacity. The researchers suggest that AASHTO should use a system-level rating system. The researchers also offer a simple upper-bound equation. AASHTO specifications had a capacity of 15 HS-20 trucks, the field test showed a strain that's equivalent to that induced by 17 trucks, and FEA showed that first flexural yielding of a single element was at 19 trucks.

Bell, E.D., Lefebvre, P.J., Sanayei, M., Brenner, B.R., Sipple, J.D., and Peddle, J., 2013, Objective Load Rating of a Steel-Girder Bridge Using Structural Modeling and Health Monitoring

The researchers analyzed and evaluated one bridge in this case study. SAP2000 enhanced designer's model (EDM) was calibrated using bridge data taken during a nondestructive load test and compared to AASHTO LRFR load ratings. EDM RFs were found to be higher than AASHTO in interior girders and nearly identical for exterior girders. They also determined load ratings for hypothetical damage. In a real world setting, load rating engineers would notice the damage during bridge inspection. The researchers analyzed a scenario on SAP2000 for when the section loss is in both an interior and exterior girder, and they found two damage rating factors. One was found assuming the section loss was over the entire length, and the other one assuming the section loss over the noted area only. Although the capacity decreases, system level capacity is still higher than what the LRFR rating would be. The figures shown in Figure 116 compare rating factors of LRFR, EDM, and EDM with the damage considered.

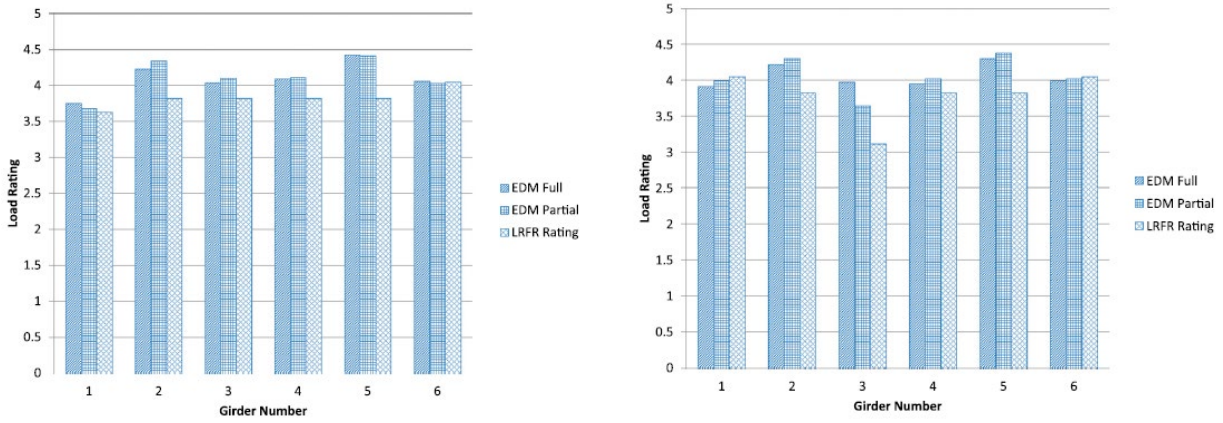

Girder 1 Girder 3

Figure 116. Comparison of RFs for Damage in Girders from Bell et al. (2013)

Hosteng, T., and Phares, B., 2013, Demonstration of Load Rating Capabilities Through Physical Load Testing: Ida County Bridge Case Study

Researchers performed load tests on a two-lane, three-span, continuous steel girder bridge built in 1949. Strain transducers were placed at the top and bottom flanges in locations specified in Figure 117. Trucks passed over the bridge at crawl speed in three locations: two feet away from one barrier, two feet away from the other barrier, and along the center of the roadway. Two runs were performed to verify the data. Distribution factors were estimated by taking the ratio of girder strains to the girder strains experienced by all of the girders. The researchers found distribution factors significantly lower than what AASHTO prescribes. By using the strain data, the researchers developed a two-dimensional finite element model to perform LFR load rating analyses on AASHTO rating vehicles. The operating load ratings for all of the analyses were

found to be greater than one despite the bridge being load posted. A summary of the bridge critical rating factors is shown in Table 49.

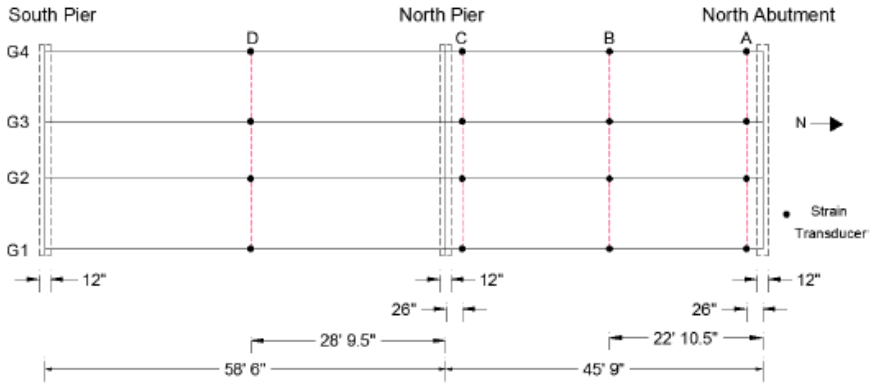

Figure 117. Ida County Bridge Plan View of Strain Transducer Locations

Table 49. Ida County Bridge Critical Rating Factors

Rating Vehicle	Location/Limiting Capacity	Inventory Rating Factor		Operating Rating Factor	
		Two Lane	One Lane	Two Lane	One Lane
HS-20(14)	Two Lane Interior, One Lane Exterior, Center Span, (+) Flexure	0.80	1.10	1.34	1.84
HS-20(22)	Two Lane Interior, One Lane Exterior, Center Span, (+) Flexure	0.96	1.31	1.60	2.19
HS-20(30)	Two Lane Interior, One Lane Exterior, Center Span, (+) Flexure	1.10	1.52	1.84	2.53
Type 4	Two Lane Interior, One Lane Exterior, Center Span, (+) Flexure	0.92	1.27	1.54	2.11
Type 3S3A	Two Lane Interior, One Lane Exterior, Center Span, (+) Flexure	0.98	1.35	1.64	2.26
Type 3-3	Two Lane Interior, One Lane Exterior, Center Span, (+) Flexure	1.00	1.35	1.67	2.26
Type 3S3B	Two Lane Interior, One Lane Exterior, Pier, (-) Flexure	1.01	1.39	1.69	2.32
Type 4S3	Two Lane Interior, One Lane Exterior, Pier, (-) Flexure	0.94	1.27	1.57	2.12
Type 3	Two Lane Interior, One Lane Exterior, Center Span, (+) Flexure	1.01	1.39	1.69	2.32
Type 3S2B	Two Lane Interior, One Lane Exterior, Pier, (-) Flexure	1.06	1.45	1.78	2.42
Type 3S2A	Two Lane Interior, One Lane Exterior, Center Span, (+) Flexure	1.05	1.44	1.75	2.40
Midspan and Endspan Lane Load	Two Lane Interior, One Lane Exterior, Pier, (-) Flexure	1.15	1.39	1.93	2.32
Both Endspans Lane Load	Two Lane Interior, One Lane Exterior, Pier, (-) Flexure	2.11	2.58	3.52	4.31
Midspan Lane Load	Two Lane Interior, One Lane Exterior, Pier, (-) Flexure	1.62	1.94	2.70	3.23
Single Endspan Lane Load	Two Lane Interior, One Lane Exterior, Pier, (-) Flexure	2.03	2.50	3.39	4.18

Sanayei, M., Phelps, J.E., Sipple, J.D., Bell, E.S., and Brenner, B.R., 2012, Instrumentation, Nondestructive Testing, and Finite-Element Model Updating for Bridge Evaluation Using Strain Measurements

An approach is introduced for the instrumentation of a bridge during construction, performing a nondestructive load test before the bridge is opened, creating a detailed FEM, calibrating the model using measured strains, and producing a load rating factor. Three load ratings calculated and compared. One was ASD in accordance to AASHTO load ratings using Virtis. Another was found by NDT strain data. The last one was found by using the calibrated baseline FEM. FEM typically had the highest load rating factors for all of the girders except for exterior girders. The benefits of the NDT are evident in all of the girders, except for the interior girders that govern the rating factor of the bridge. In this case, there is no benefit from testing the bridge. The findings can be seen in Figure 118.

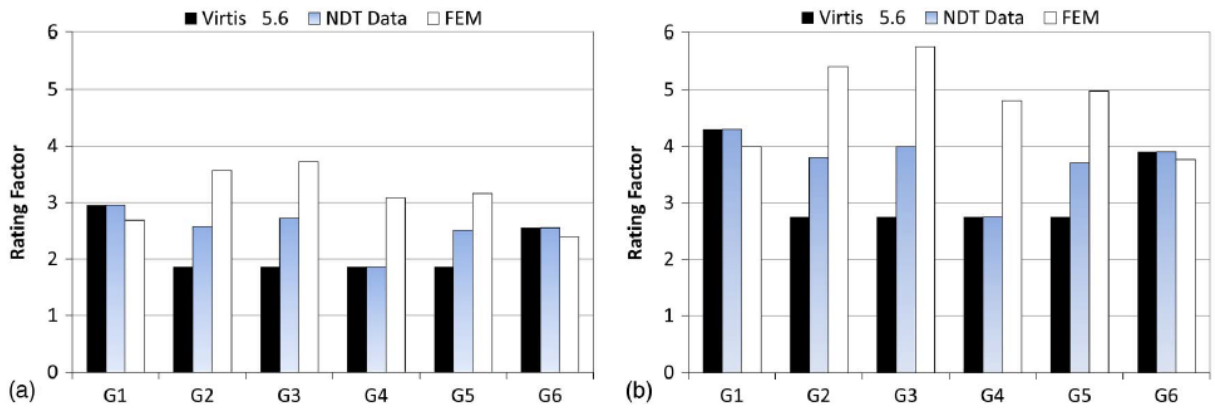

Figure 118. Vernon Avenue Bridge Rating Factors: (a) Inventory and (b) Operating from Sanayei et al. (2012)

Wipf, T.J. and Hosteng, T., 2010, Diagnostic Load Testing May Reduce Embargoes

Load rating engineers performed diagnostic load testing on 17 bridges in Iowa. Six of the 12 bridges were not posted after the test because the diagnostic test found the load rating to be too conservative. A summary of the diagnostic load tests is shown in Table 50.

Table 50. Effects of Diagnostic Test Results on Bridge Postings

Tested Bridges	Span (#, length)	Bridge Type	Data Analyzed*	Posting before Testing	Posting after Testing
IA-92 west of Massena	1, 40'	Girder	A,B	Yes	Yes
IA-57 in Butler County	1, 50'	Girder	A,B	Yes	Yes
IA-136 in Dubuque County	3, 210'	Girder	A,B	Yes	Yes
US-18 east of Hartley	2, 100'	Girder	A[1],B	Yes	Yes
IA-183 north of Pisgah	3, 96'	Girder	A,B	Yes	Yes
IA-60 near Sibley	1, 43'	Girder	A,B	Yes	Yes
IA-31 west of Quimby	1, 50'	Girder	A,B	Yes	No
US-30 near Wheatland	4, 368'	Girder	A,B,D	Yes	No
US-63 in Davis County	3, 210'	Girder	A,B	Yes	No
IA-78 in Keokuk County	4, 292'	Girder	A,B	Yes	No
IA-93 in Sumner	1, 61' 6"	Girder	A,B	Yes	No
IA-5 in Appanoose County	1, 51' 3"	Girder	A,B	Yes	No
I-80 in Jasper County	3, 100'	Slab	A,C	No	No
I-80 in Jasper County	5, 178'	Slab	A,C	No	No
I-80 in Poweshiek County	3, 114'	Slab	A,C	No	No
US-20 westbnd on-ramp no. Wellsburg	5, 198'	Slab	A,C	No	No

Bechtel, A.J., McConnell, J., and Chajes, M., 2010, Ultimate Capacity Destructive Testing and Finite-Element Analysis of Steel I-Girder Bridges

The problem with bridge evaluation codes is that bridges are rated with component-level capacities, not system-level capacities. A 1/5 scale slab-on-steel girder bridge was tested to ultimate capacity and then analytically modeled to see how different this is compared to bridge evaluation codes. The AASHTO ultimate capacity was found by dividing the plastic capacity of the governing girder by the AASHTO DF. The ultimate capacity of the tested bridge was approximately 9% higher than the AASHTO prediction. The researchers used FEA by using ABAQUS. Strains, deflections, and load distributions were compared between FEA and the physical test and found to be similar. Researchers concluded that FEA is an excellent tool if initial conditions can be properly identified. The testing matched up with the controlling deck failure case for FEA. They found that the deck failed at a load equivalent to 22 scaled AASHTO trucks. Only 30% of the steel in the critical cross section had yielded at the time of deck failure. The concrete deck strengthed also governed for the FEA.

Bechtel, A.J., McConnell, J.R., Chajes, M.J., 2009, Destructive Testing and Finite Element Analysis to Determine Ultimate Capacity of Skewed Steel I-Girder Bridges

The researchers tested a four-girder, simple-span bridge with varying levels of skew and tested it until failure. They compared the bridges' ultimate capacity to AASHTO capacities and FEM produced by Abaqus. The purpose of the study was to investigate how system-level analyses and

how it corresponds with skew. The researchers found that the FEA modeled the behavior adequately. Conclusions from the modeling include that tension softening of the concrete and the internal forces and boundary conditions have to be modeled carefully to get accurate results. The capacities from the destructive tests were higher than AASHTO predictions, as expected. They also found that bridges with higher skews had higher capacities because of the changes in effective length and relative stiffness of the beams running perpendicular to the girders that intersect the support at the obtuse corners of the bridge.

Jeffrey, A., Breña, S.F., Civjan, S.A., 2009, Evaluation of Bridge Performance and Rating through Non-destructive Load Testing

A report was prepared for the Vermont Agency of Transportation which included a literature review and two case study load tests on a 1920's reinforced concrete bridge and an interstate non-composite steel girder bridge that was damaged in three girders from getting hit by trucks passing underneath it. Load ratings were determined for the two bridges based on the load tests. Due to the scope of this project, the steel girder bridge will be described in greater detail.

Two identical and adjacent, three-span continuous steel girder bridges were tested with the goal of removing the load posting. The negative moments over the piers control the rating factor of these bridges. The piers are skewed at just under 42°. The bridges are made up of five A36 rolled shapes that are spaced at 7.5'.

The middle span was instrumented with 30 BDI strain gauges, as shown in Figure 119. One strain gauge was placed at the bottom of the top flange and bottom of the bottom flange for each instrumented location. Three lanes were used for crawl speed tests that correspond to East and West traffic lanes and a lane at the geometric center of the bridge.

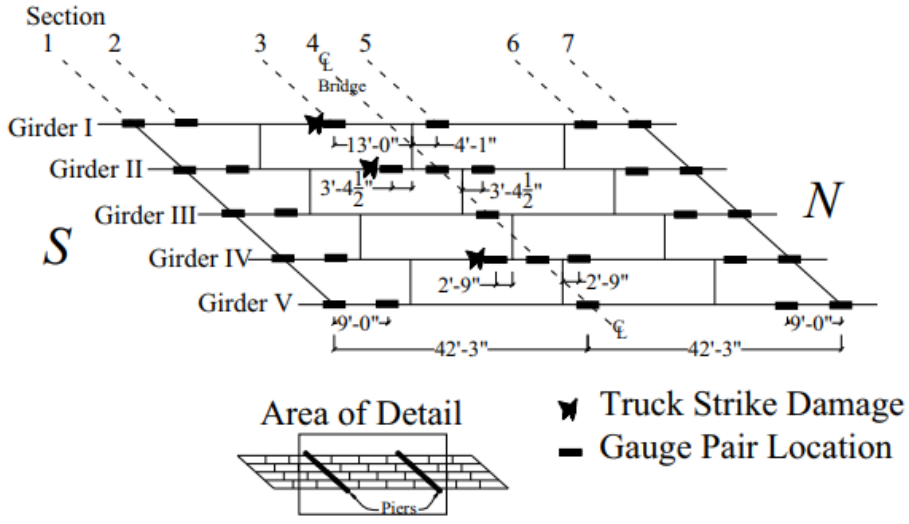

Figure 119. Diagram of Weathersfield Bridge Gauge Locations

Methods were described for deriving positive and negative moment effects and elastic neutral axis locations. To evaluate the performance of the girder with the damaged bottom flange, the same load trucks were placed on the mirrored side of the bridge and traveling in the opposite direction. Since the bridge is symmetrical, the responses should be the same. Interestingly enough, it appears as though the girder damage is not noticeable in positive bending. However, when the girders' negative bending values were compared, discrepencies were noted.

It was found that neutral axis depths suggest that the bridge was behaving composite and midspan and partially composite at negative moment regions. The researchers noted that neutral axis varied due to multiple reasons. One reason it that error is introduced when the top strain gauge is near the neutral axis. Another reason that error was introduced is because the wheels ran near some of the instrumented girders. This caused for there to be spikes at some locations. Lastly, minimal errors in strain values that are small result in large neutral axis errors. Because of this, the researchers did not use strain measurements less than 20 με for neutral axis calculations.

Rating factors were determined by using AASHTO MBE adjustment factors. Rating factor benefits were observed from the load test. A noncalibrated finite element model was set up to compare to the load test data. The load test data did not match up perfectly with the finite element model, but it was a reasonable uncalibrated model that also yields benefits when compared to line girder analysis. Calibrating it to match up with the load test would yield better results.

Harris, D.K., Cousins, T., Murray, T.M., and Sotelino, E.D., 2008, Field Investigation of a Sandwich Plate System Bridge Deck

The research presented is on the results of a live-load test of the Shenley Bridge – the first bridge to employ the sandwich plate system in North America. The sandwich plate system is made up of a polyurethane core surrounded by two steel plates on the top and bottom. The researchers performed a field test and made an FEM. They compared measured GDFs to AASHTO LRFD, AASHTO standard, and CHBDC. The codes were found to be conservative except for CHBDC for the exterior girder subjected to multiple trucks. The dynamic response from AASHTO LRFD, AASHTO standard, and CHBDC was conservative in two out of three loading configurations (where the truck was positioned to straddle the interior girder).

Barth, K.E. and Wu, H., 2006, Efficient Nonlinear Finite Element Modeling of Slab on Steel Stringer Bridges

ABAQUS was used to capture the behavior of two composite steel girder with high-performance steel and one four-span continuous composite steel bridge that were also tested to failure. FEA matched up well with the testing data. The paper describes two modeling techniques in detail. The smeared crack model captures ultimate behavior well for simple span bridge superstructures. The concrete damage plasticity model is suggested to model continuous span bridges more reasonably than the smeared crack model.

Huang, H., Shenton, H.W., and Chajes, M.J., 2004, Load Distribution for a Highly Skewed Bridge: Testing and Analysis

A highly skewed bridge was tested and modeled using FEM to investigate the influences of model mesh, transverse stiffness, diaphragms, and modeling of the supports. The AASHTO LRFD formulas for transverse load distribution appear to be conservative for positive bending for the two-span, continuous, slab-on-steel, 60-degree skew bridge. They found that the code is accurate but not conservative for negative bending.

Phares, B.M., Wipf, T.J., Klaiber, F.W., and Abu-Hawash, A., 2003, Bridge Load Rating Using Physical Testing

The researchers tested Boone Country Bridge #11 using Bridge Diagnostic, Inc. (BDI) with three different load vehicles. They found that the BDI found an average of 42% higher flexure capacity and 55% higher shear capacity than that derived from AASHTO LFD. The instrumentation plan can be seen in Figure 120.

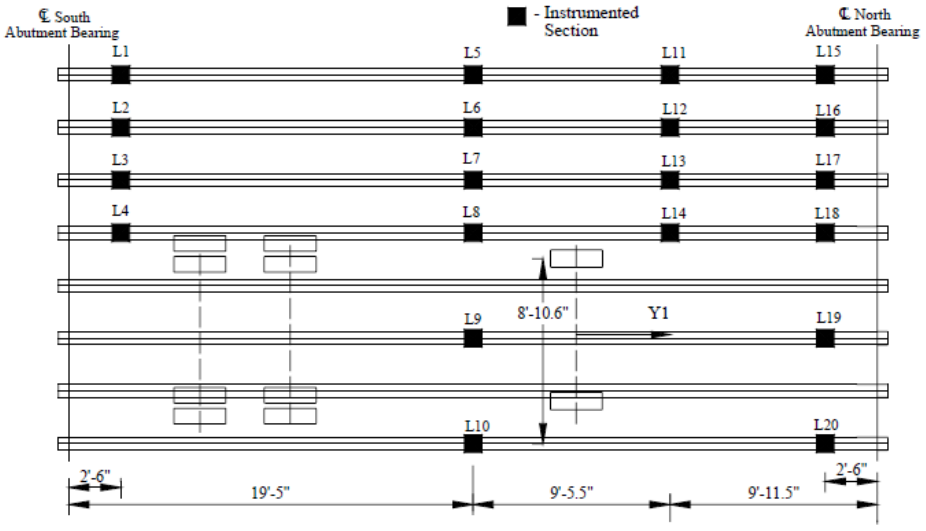

Figure 120. Boone County Bridge #11 Instrumentation Plan

Wipf, T.J., Phares, B.M., Klaiber, F.W., Wood, D.L., Mellingen, E., and Samuelson, A., 2003, Development of Bridge Load Testing Process for Load Evaluation

Bridge Diagnostics, Inc. (BDI) is a software and hardware that engineers developed to perform bridge rating systems based on field data. BDI was used to test three steel-girder bridges with concrete decks, two concrete slab bridges, and two steel-girder bridges with timber decks. The researchers determined that BDI produced accurate models with relative ease. The BDI load ratings were generally greater than AASHTO LFD ratings.

Cai, C.S. and Shahawy, M., 2003, Understanding Capacity Rating of Bridges from Load Tests

Field tests yield different results than analytical methods due to the difference in live load stresses and material conditions. In analytical analyses, some of these parameters are difficult to quantify. A proof load test (lower bound) is done by testing a bridge up to a target load or once the bridge shows any sign of distress. Proof load tests do not require complicated bridge analysis since the target load or a smaller load is reached. However, the risk of damaging the bridge is higher than in other testing methods. A rating with a diagnosticdiagnostic load test (upper bound) uses a much lower load for testing. This method is preferred if analysis shows that a target load for a proof load test cannot be achieved safely or if the load capacity of the proof load test can't be performed. Reasons for not being able to perform the test include test vehicles not being heavy enough or traffic conditions prohibiting the proof load test. Results of diagnostic tests are used to calibrate a theoretical prediction of live load effects. Load rating using this method is identical to the linear extrapolation method which is the upper bound of the load rating. The total internal moment may be significantly different from applied total external moment due to many field factors that are usually ignored in calculations. Different test interpretations can yield different capacity ratings.

Nowak, A.S., Kim., S., and Stankiewicz, P.R., 2000, Analysis and Diagnostic Testing of a Bridge

The purpose of this study was to find the reasons why transverse crack patterns formed on a seven-span haunched steel-girder bridge built in 1968. As part of the methodology, field tests were performed to investigate what the bridge's actual stresses are under a test truck, and to see what the load distribution and impact factors are. Strain transducers were placed at the top and bottom flanges or near flanges on web. The instrumentation plan is shown below in Figure 121. Strains were collected at crawling-speed and high-speed with single truck and side-by-side trucks. The concrete from the deck was also tested and the water/cement ratio was higher than what AASHTO specifies.

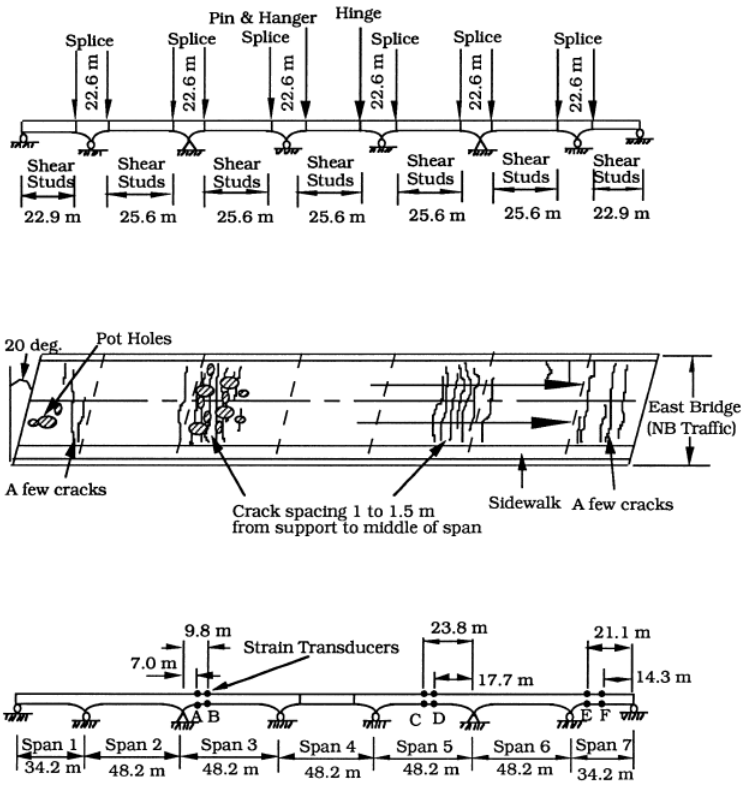

Figure 121. Elevation View of the Bridge, Major Crack Pattern, and Strain Transducer Locations

Distribution factors were determined in two ways: (1) the ratio of girder strains to the sum of all bottom-flange strains and (2) the ratio considering the differences in section modulus between girders because of the sidewalk and parapets. The researchers found that the distribution factors, found by either of the two methods, were much lower than contemporary AASHTO values. Furthermore, the distribution is more uniform when the second method is used.

Impact factors were found to be smaller than the contemporary AASHTO-specified value for all of the girders except for one exterior girder that has “no practical significance since the stress in girder 4 is small compared with stresses in other girders.”

Finally, a FEM was made and used to find the causes of the transverse deck cracking. The results of the field test matched well with analyses performed on the FEM. However, the FEA live load stresses do not correspond to the observed crack patterns. Because of this inconsistency, the researchers have attributed the transverse deck cracking to deck pouring sequence and concrete shrinkage due to the high water/cement ratio.

Lichtenstein, A.G., Moses, F., Bakht, B., 1998., Manual for Bridge Rating Through Load Testing

Nondestructive load test applications, considerations and benefits are briefly summarized. The general considerations of bridge load tests, such as dead loads, dynamic and static live loads, fatigue, impact, and the types of bridges are summarized. The researchers advise the reader to avoid load tests for the following reasons:

- The cost of testing reaches or exceeds the cost of bridge rehabilitation.
- The bridge, according to calculations, cannot sustain even the lowest level of load.
- Calculations of weak components of the bridge indicate that a field test is unlikely to show the prospect of improvement in load-carrying capacity.
- In the case of concrete beam bridges, there is the possibility of sudden shear type of failure.
- The forces due to restrained volume changes from temperature induced stresses may not be accounted for by load tests. Note that significant strains and corresponding stresses induced by temperature changes could invalidate load test results especially when end bearings are frozen.
- There are frozen joints and bearing which could cause sudden release of energy during a load test.
- Load tests may be impractical because of inadequate access to the span.
- Soil and foundation conditions are suspect. The bridge has severely deteriorated piers and pier caps, especially at expansion joints where water and salt have caused severe corrosion of reinforcement.

According to the manual, unintended composite action is a result of noncomposite steel girder bridges acting compositely. However, the composite behavior can be compromised as the load is increased. The researchers propose a limiting bond stress between the concrete slab and steel girders of 70 psi for concrete decks with a compressive strength of 3 ksi. For partially or fully embedded flanges, 100 psi for the limiting bond stress is recommended. Other effects, such as end bearing restraint, additional parapet and sidewalk stiffness, secondary member participation can potentially appear in load test data.

Recommended procedures for planning a load test are outlined in this report. Various data acquisition methods are presented as well. Illustrative diagnostic and proof load test examples are presented for multiple kinds of bridges. This report was cited in the AASHTO MBE in the diagnostic load test section for its walk-through example.

Ghosn, A., Moses, F., 1998, NCHRP Report 406: Redundancy in Highway Bridge Superstructures

In this report, researchers investigate redundancy and they present a methodology on how to consider redundancy in design and load capacity evaluation. The methodology is made up of

tables of system factors that can be used to modify AASHTO predictions of ultimate capacities. For bridges outside of the tables' scope, they also present a direct analysis procedure.

Kim, S. and Nowak, A.S., 1997, Load Distribution and Impact Factors for I-Girder Bridges

The researchers monitored two simply supported I-girder bridges for two consecutive days under normal traffic, and captured strain data from the girders. They processed the data, and obtained the statistical parameters for the girder distribution and impact factors. They found that both the load distribution and impact factors are lower than AASHTO values.

Kathol, S., Azizinamini, A., and Luedke, J., 1995, Strength Capacity of Steel Girder Bridges

Four destructive tests were performed to investigate the global and local behavior of steel girder bridges with and without diaphragms. The study compares the destructive test data to AASHTO LRFD empirical methods of the time. The researchers found that the contributions of diaphragms to capacity was minimal. The deflection of the steel bridge due to shrinkage was found to be less than that predicted by AASHTO. The researchers were also able to make an FEM, that had been validated with test data, which would eliminate specifying distribution factors.

Stallings, J.M. and Yoo, C.H., 1993, Tests and Ratings of Short-Span Steel Bridges

The researchers performed static and dynamic diagnostic tests on three short-span, two-lane, steel-girder bridges. Some of the tests exhibited unintended composite action through friction and bond between the deck and girders. Girder strains calculated using the measured wheel-load distribution factors were consistently larger than the measured strains. They calculated impact factors using various methods. Impact factors based on the combined response of all girders were larger than those values calculated for the most critically loaded girder.

Bakht, B. and Jaeger, L.G. 1990, Bridge Testing – A Surprise Every Time

This paper lists some of the various surprises encountered in bridge testing that may have a significant influence on the load-carrying capacities of bridges. Some surprises include enhanced flexural stiffness of slab-on-girder bridges, composite action in non-composite bridges, the failure mode of cracking deck slab, as well as many others.

Cheung, M.S., Gardner, N.J., NG, S.F., 1987, Load Distribution Characteristics of Slab-on-Girder Bridges at Ultimate

In this study, researchers made a scaled bridge for testing purposes, and strains and deflections were found to be similar to FEA. The values determined from resistant bending moments of the steel girders indicate that there is a significant reduction in load distribution factors between linear elastic and post yielding stages. The shape factor of the girder section can be the reduction factor. The researchers claim that load redistribution and residual stresses are insignificant before the formation of a plastic hinge and can be ignored up until then.

Ghosn, A., Moses, F., and Gobieski, J., 1986, Evaluation of Steel Bridges Using In-Service Testing

This evaluation discusses the benefit of testing bridges to incorporate into rating process. The researchers tested five bridges, and the maximum stresses were below what the conventional procedures would predict. The difference in results are attributed to unintended composite action, secondary elements adding stiffness, girder distributions being more conservative than AASHTO predictions, and impact values being different.

Burdette, E.G., Goodpasture, D.W., 1971, Full-Scale Bridge Testing: An Evaluation of Bridge Design Criteria

The researchers tested girder deck bridges in Tennessee to evaluate bridge design topics such as the lateral distribution of load, dynamic response, ultimate strength, and mode of failure. They found that the load distribution factors are similar to that of other studies. An analytical method based on strain compatibility predicted the ultimate capacity within 9% for three out of the four bridges tested. They also found the AASHTO ultimate loads to be somewhat conservative compared to the load tests.

11.2 Rating Factor Modification Equations

The FEMs' loads were an AASHTO HS-20 load with LRFR load factors. This is inconsistent with LRFR since the load vehicle omits the lane load that the AASHTO HL-93 uses. Because of this inconsistency, two calibration equations were developed to get load ratings consistent with LRFR load ratings and LFR load ratings. Eqn. 97 is the standard load rating equation. In the preexisting model, the equation used a live load induced by an HS-20 (LL), and used LRFR factors. Eqn. 98 is the calibration equation to get a rating factor that is consistent with LFR specifications. Eqn. 99 is the calibration equation to get a rating factor that corresponds to LRFR. The calibration equations were derived by multiplying by the ratio of LRFR to LFR factors and live load effects.

$$RF = \frac{C - \gamma_{DL} * DL}{\gamma_{LL}(LL + IM)} \quad \text{Eqn. 97}$$

$$RF_{LFR} = RF * (\frac{\gamma_{LL,LRFR}}{\gamma_{LL,LFR}}) * (\frac{IM_{LRFR}}{IM_{LFR}}) * (\frac{C - \gamma_{DL,LFR} * DL}{C - \gamma_{DL,LRFR} * DL}) \quad \text{Eqn. 98}$$

$$RF_{LRFR} = RF * (\frac{M_{HS-20}}{M_{HL-93}}) \quad \text{Eqn. 99}$$

The FEM was performed assuming composite action. However, it became apparent that a load rating factor based on noncomposite behavior is desirable to correspond to state load rating summary sheets. Equation 100 shows another calibration to get the noncomposite load rating.

$$RF_{nc} = RF_c * \frac{(C_{nc} - D)}{(C_c - D)} \quad \text{Eqn. 100}$$

11.3 ANN Data

11.3.1 Moment ANN Training and Testing Data

The manila-colored cells designate bridges that were used in the design set. The green-colored cells designate bridges that were used in the design-set size for some ANNs and additional testing bridges in reduced size ANNs. The aqua-colored cells designate bridges that were used in the independent testing set.

Bridge	L (m)	s (m)	Kg (Gmm^4)	CF (1 or 0)	#girders	Skew (deg.)	de (m)	Deck ts(mm)	fc' (MPa)	fy (MPa)	Moment $GDF_{maximum}$
C000621615	11.786	2.388	124.295	1	4	0	0.69	229	20.69	248.22	0.654
C003403910	15.240	1.981	55.171	1	4	0	0.69	165	20.69	248.22	0.601
C007802440	18.440	2.184	60.850	1	4	0	0.41	178	20.69	248.22	0.573
C006500230	9.093	0.854	10.914	1	11	0	0.00	178	27.58	344.75	0.246
C007203715	9.144	1.473	7.518	1	5	0	0.09	152	20.69	248.22	0.414
C006341615	17.983	0.978	24.279	1	7	0	0.05	152	20.69	248.22	0.298
C006301204P	17.983	0.984	25.870	1	7	0	0.02	152	17.24	206.85	0.302
C006313310P	7.010	1.438	4.954	1	6	15	0.06	152	20.69	248.22	0.382
C009202210	12.192	1.219	15.479	1	6	0	0.25	152	20.69	248.22	0.370
C008101013P	6.096	1.295	23.279	1	6	0	0.42	152	20.69	248.22	0.434
C001111430	10.973	1.981	31.674	1	4	0	0.69	191	20.69	248.22	0.585
C007904705	7.141	2.057	27.549	1	5	23	0.00	178	24.13	248.22	0.544
C004702203	6.909	1.791	5.314	0	5	0	0.07	127	20.69	248.22	0.513
C002014017	6.096	1.219	16.448	1	7	0	0.61	178	20.69	248.22	0.482
C005913903	11.735	1.118	10.396	1	8	0	0.28	152	20.69	248.22	0.341
C000602505	9.144	1.118	15.005	1	5	15	0.77	152	17.24	206.85	0.469
C007424540	24.854	2.438	85.164	1	4	15	0.61	178	27.58	344.75	0.626
C009111705	9.626	1.600	19.540	1	5	0	0.77	200	20.69	248.22	0.519

C002001505	8.534	1.295	20.192	0	7	0	0.62	178	20.69	248.22	0.474
C009103005	22.600	2.515	132.446	1	4	0	0.12	167	20.69	248.22	0.600
C007815273	12.497	1.918	67.504	1	4	32	0.70	178	20.69	248.22	0.583
C005463410	7.283	0.813	8.579	1	10	0	-0.02	178	20.69	248.22	0.271
C007603710	11.887	1.829	28.183	1	4	0	0.43	152	20.69	248.22	0.563
C001716105	14.675	1.775	56.245	1	6	45	0.27	178	24.13	344.75	0.373
C006607105P	21.031	2.350	103.109	1	4	0	0.79	178	20.69	248.22	0.657
C007302705P	17.805	1.718	43.257	1	6	30	0.13	203	20.69	344.75	0.370
C000102115	14.561	1.413	32.764	1	7	20	0.03	203	27.58	344.75	0.339
C007010905	11.278	0.975	19.264	1	7	0	0.73	133	17.24	206.85	0.437
C006710205	24.384	2.057	135.193	1	4	0	0.60	178	20.69	248.22	0.568
C007025010	24.866	1.905	140.400	1	5	0	0.15	152	20.69	248.22	0.505
C001403305P	24.079	1.702	89.674	1	5	0	-0.09	127	20.69	248.22	0.482
C007805310P	9.296	1.257	12.586	1	8	0	0.17	178	20.69	248.22	0.325
C007102605	15.240	1.499	36.481	1	7	0	0.08	203	27.58	344.75	0.357
C001401535	10.668	2.121	27.515	1	5	30	0.03	178	27.58	248.22	0.497
C006305115	8.230	1.194	8.161	1	7	20	0.06	152	20.69	248.22	0.313
C000102908	23.063	2.032	113.440	1	5	0	0.26	152	20.69	248.22	0.498
C001712925	11.855	1.808	36.552	1	6	0	0.20	178	24.13	344.75	0.457
C007000515	11.887	0.889	11.428	1	9	0	0.42	152	20.69	248.22	0.304
C007103415	8.807	0.864	8.264	1	11	0	0.25	203	27.58	248.22	0.265
C004803915	8.763	0.838	16.033	0	8	0	0.11	140	17.24	206.85	0.258
C005901825	8.839	1.956	25.751	0	5	45	0.05	152	20.69	248.22	0.476
C001424750	15.697	2.216	144.110	0	5	0	0.14	178	20.69	248.22	0.568
C001210930	14.935	1.753	122.459	1	6	0	-0.11	178	20.69	248.22	0.460
C006311110	17.907	1.537	84.547	0	6	0	0.13	165	20.69	248.22	0.407
C005903110	11.582	0.965	11.722	1	9	0	-0.05	152	20.69	248.22	0.268
C006924230	6.248	1.524	5.333	1	6	0	0.46	178	20.69	248.22	0.474

C005901805	18.161	1.397	51.664	1	7	0	-0.08	152	20.69	248.22	0.351
C001400730	19.507	1.676	72.955	1	6	0	0.06	178	20.69	344.75	0.410
C002003405	8.534	1.219	18.908	0	7	0	0.61	178	20.69	248.22	0.432
C001823610	11.976	1.092	14.176	1	8	0	0.38	127	20.69	248.22	0.365
C009133625	14.935	0.861	23.405	1	7	0	0.48	159	20.69	248.22	0.348
C002602910	17.983	1.188	53.629	1	8	0	0.18	178	20.69	248.22	0.362
C003303710	18.288	1.219	41.497	1	8	0	0.30	152	20.69	248.22	0.348
C001411615P	16.764	1.670	60.705	1	6	20	0.09	178	27.58	248.22	0.394
C007101130	14.780	1.770	75.551	1	6	30	0.27	203	20.69	344.75	0.407
C001224325	17.983	1.753	90.872	1	6	0	-0.11	178	17.24	248.22	0.436
C003413410	21.056	1.969	92.415	1	4	0	0.78	203	17.24	206.85	0.546
C007602705	14.935	1.829	45.661	0	4	0	0.46	152	20.69	227.54	0.561
C005900525	11.735	0.991	8.455	1	7	0	0.00	140	20.69	227.54	0.298
C008803505	8.814	1.295	6.782	1	5	0	0.46	127	20.69	227.54	0.407
C002001220	8.687	1.219	20.175	0	7	40	0.61	178	20.69	248.22	0.361
C001401710	13.503	2.105	69.179	1	5	0	0.04	203	20.69	248.22	0.529
C002001215	8.687	1.219	16.602	0	7	35	0.61	152	20.69	248.22	0.375
C000103420	15.215	0.972	17.697	1	9	0	0.05	165	20.69	248.22	0.345
C005922330	11.735	1.168	9.940	1	6	0	0.08	152	20.69	248.22	0.343
C008722020	11.887	1.753	40.644	1	6	15	-0.11	178	27.58	248.22	0.443
C001202005	11.918	1.314	38.333	0	6	0	0.69	152	20.69	248.22	0.512
C006300825P	8.839	1.029	6.933	1	8	0	0.00	140	20.69	248.22	0.275
C001103815	23.311	1.676	103.774	1	6	0	0.38	165	20.69	248.22	0.496
C000604715	18.034	1.543	93.067	1	6	0	0.49	203	20.69	248.22	0.456
C006602010	21.336	2.057	97.171	1	4	0	0.57	203	20.69	248.22	0.561
C001201410	8.839	1.753	18.992	1	6	30	-0.11	178	20.69	248.22	0.404
C007824260	18.136	1.905	73.369	1	5	0	0.61	178	20.69	248.22	0.517

C002012435	17.678	1.245	38.011	1	7	0	0.50	127	20.69	248.22	0.493
C007932415	14.630	1.372	32.621	1	5	35	0.61	203	20.69	227.54	0.447
C002004730	8.534	1.219	20.044	0	7	0	0.69	178	20.69	248.22	0.433
C002702510	14.732	1.727	40.802	1	5	25	0.20	152	20.69	248.22	0.470
C001205010	14.630	1.346	61.658	0	6	15	0.61	152	20.69	248.22	0.482
C002004725	11.582	1.219	26.896	1	7	0	0.61	178	20.69	248.22	0.433
C001234905	17.983	1.829	48.628	1	4	33	0.33	165	20.69	248.22	0.527
C005900505	11.811	1.753	45.724	0	5	0	0.08	178	20.69	248.22	0.510
C005901410	17.882	1.397	35.029	1	7	0	0.03	152	20.69	248.22	0.362
C002701945	14.707	1.778	26.389	1	5	0	0.71	178	20.69	248.22	0.532
C007910405	8.534	1.794	21.569	1	6	0	0.16	178	20.69	248.22	0.459
C008404020	9.550	1.829	25.698	0	5	0	0.00	152	17.24	227.54	0.510
C003416235	10.541	1.295	20.054	1	7	0	-0.01	178	20.69	248.22	0.368
C004712915	7.588	1.699	11.473	1	6	0	0.19	178	24.13	344.75	0.489
C005901502	7.315	1.803	10.254	1	6	0	-0.01	178	20.69	248.22	0.481
C002004730	8.712	1.219	20.175	0	7	0	0.60	178	20.69	248.22	0.426
C004507603	8.153	1.194	17.564	0	7	0	0.06	152	20.69	248.22	0.349
C003704805P	15.278	2.057	58.662	1	5	0	0.15	152	20.69	248.22	0.520
C002012040	8.534	1.219	26.669	0	7	0	0.61	178	20.69	248.22	0.436
C005914820	11.836	1.524	37.880	1	6	20	0.15	178	20.69	248.22	0.385
C000134022	8.839	1.702	24.582	1	6	0	0.01	152	20.69	248.22	0.431
C004513915	13.884	1.321	35.222	1	7	0	0.00	178	20.69	248.22	0.370
C001705805	7.798	1.219	8.479	1	7	0	0.58	152	20.69	248.22	0.444
C009143435	15.570	1.286	23.607	1	5	0	0.40	165	20.69	248.22	0.434
C007443235	9.347	1.778	17.229	1	5	30	0.10	152	20.69	248.22	0.444
C002001627	6.401	1.219	18.400	0	7	0	0.61	178	20.69	248.22	0.485
C005900915	10.363	1.575	35.508	1	6	30	0.03	178	20.69	248.22	0.370

C005902215	17.831	1.168	34.034	1	7	0	0.08	152	20.69	248.22	0.345
C000602310	11.278	1.168	21.091	0	6	0	0.05	165	17.24	227.54	0.370
C001902340	8.738	1.321	9.940	1	7	0	0.02	152	20.69	248.22	0.340
C009114505	8.306	1.302	9.989	1	6	0	0.02	140	17.24	206.85	0.351
C008511515	7.925	1.321	25.798	0	7	0	0.30	203	20.69	248.22	0.395
C008002310	12.268	1.981	42.313	1	5	0	0.38	178	20.69	248.22	0.504
C005901925	14.834	1.295	23.570	1	5	0	0.46	152	20.69	248.22	0.466
C009314130	11.855	1.686	43.257	1	6	0	0.00	203	20.69	248.22	0.441
C004903005	11.252	1.200	16.496	1	6	0	0.05	152	20.69	248.22	0.370
C002000707P	8.534	1.219	17.487	0	7	0	0.61	178	20.69	248.22	0.417
C005913505	18.288	1.422	20.935	1	6	0	0.03	152	20.69	248.22	0.475
C008602105P	17.888	1.791	96.927	1	5	0	0.00	178	27.58	248.22	0.516
C003302510	13.716	1.765	38.757	1	5	0	0.13	152	20.69	248.22	0.497
C004802905	8.534	2.057	31.555	1	5	45	0.05	178	20.69	248.22	0.456
C007001220	17.983	1.346	51.539	1	6	0	0.61	165	20.69	206.85	0.465
C007213110	11.887	1.773	28.497	1	5	0	0.11	152	20.69	227.54	0.487
C007911205	14.808	2.057	120.415	1	5	20	0.38	203	24.13	248.22	0.525
C005913020	11.836	1.168	18.100	1	7	0	0.08	152	20.69	248.22	0.336
C005901830	14.935	1.676	38.359	1	6	0	0.08	203	20.69	248.22	0.418
C000226205	12.192	1.905	35.412	1	5	0	0.15	191	24.13	248.22	0.492
C001526720	8.785	1.822	30.955	1	5	20	0.01	178	20.69	248.22	0.487
C001800605	11.989	1.092	16.517	1	8	0	0.41	165	20.69	248.22	0.358
C002704210P	15.240	1.524	34.988	1	5	20	0.61	178	20.69	248.22	0.482
C004720810	7.468	1.448	5.617	0	5	0	0.15	152	20.69	248.22	0.430
C009102805	17.856	1.930	64.849	1	5	0	0.10	178	27.58	344.75	0.498
C005900730	11.786	1.219	15.614	1	7	0	-0.03	152	20.69	248.22	0.337
C003406020	12.573	1.524	20.712	1	5	0	0.61	178	20.69	248.22	0.461
C002013720	7.087	1.219	15.218	0	7	0	0.61	178	20.69	248.22	0.480

C000805510P	7.315	1.191	11.320	1	7	0	0.16	178	20.69	248.22	0.380
C001301620	13.716	1.905	45.147	1	4	15	0.50	165	17.24	227.54	0.531
C002000823	7.010	1.219	14.137	0	7	0	0.61	178	20.69	248.22	0.460
C001900130	9.144	1.791	22.898	1	6	0	0.09	152	20.69	248.22	0.451
C004529620	9.601	1.181	19.195	0	7	0	0.05	152	20.69	248.22	0.360
C007202710	11.887	1.581	23.774	1	6	0	0.01	152	20.69	248.22	0.393
C001101705	14.935	1.753	39.173	1	5	0	0.15	165	20.69	248.22	0.482
C004800415	18.745	1.829	88.995	1	5	0	0.53	165	20.69	248.22	0.526
C007602610	11.735	1.524	44.889	0	6	20	0.08	152	17.24	206.85	0.397
C008402410	11.963	1.473	23.128	1	5	0	0.03	152	20.69	248.22	0.439
C005121315P	9.144	1.822	22.898	1	5	0	0.01	152	20.69	248.22	0.480
C001201210	7.620	1.794	7.188	1	6	0	0.05	152	20.69	248.22	0.494
C007012235	11.887	1.339	29.265	1	6	0	0.63	165	17.24	206.85	0.468
C002705115	8.809	1.499	12.300	1	6	0	0.55	152	20.69	248.22	0.441
C006313105	11.887	0.991	12.518	1	7	0	0.00	152	17.24	206.85	0.296
C001814715	11.976	1.092	16.337	1	8	0	0.37	152	20.69	248.22	0.354
C002004010	14.630	1.219	56.953	1	7	0	0.61	178	20.69	248.22	0.449
C009123545	9.805	1.956	15.981	1	5	0	-0.01	165	20.69	248.22	0.488
C007004115	17.882	1.241	39.775	1	6	0	0.74	152	20.69	248.22	0.465
C007203805	8.839	1.784	8.222	1	5	0	0.15	152	20.69	248.22	0.448
C001900815	15.240	1.575	38.726	1	6	0	0.18	152	20.69	248.22	0.413
C005606105	10.331	1.692	27.549	1	6	0	0.22	178	20.69	248.22	0.448
C005901517	8.839	1.676	21.700	1	6	0	0.08	178	20.69	248.22	0.439
C001105220	15.062	1.695	26.289	0	6	0	0.03	152	20.69	248.22	0.438
C005904610	9.296	1.016	7.527	1	8	0	0.03	152	20.69	248.22	0.347
C002003505	16.154	1.219	75.747	1	7	0	0.61	178	20.69	248.22	0.438
C007100625	14.840	1.775	58.437	1	6	0	0.25	203	24.13	344.75	0.453
C005913030	10.363	1.676	26.430	1	6	0	0.08	178	20.69	248.22	0.446

C008902125	12.192	1.753	36.118	1	6	15	-0.11	165	27.58	248.22	0.446
C007112340	10.668	1.781	43.257	1	6	30	0.20	203	20.69	248.22	0.409
C002902505	18.288	1.496	59.278	1	5	30	0.13	152	20.69	248.22	0.418
C000800705	9.246	1.570	21.556	1	6	0	0.23	178	27.58	344.75	0.411
C006514240	8.807	1.583	11.939	1	6	0	0.00	178	27.58	344.75	0.399
C004804115	18.593	1.765	58.865	0	5	0	0.13	152	20.69	248.22	0.499
C003314210	18.593	1.753	84.536	1	5	0	0.46	165	20.69	248.22	0.416

11.3.2 Shear ANN Training and Testing Data

The manila-colored cells designate bridges that were used in the design set. The green-colored cells designate bridges that were used in the design-set size for some ANNs and additional testing bridges in reduced size ANNs. The aqua-colored cells designate bridges that were used in the independent testing set.

Bridges	L (m)	s (m)	Kg (Gmm^4)	CF (1 or 0)	#girders	Skew (deg.)	de (m)	Deck ts(mm)	fc' (MPa)	fy (MPa)	Shear $GDF_{maximum}$
C002001220	8.687	1.219	20.175	0	7	40	0.61	178	20.69	248.22	0.663
C006607105P	21.031	2.350	103.109	1	4	0	0.79	178	20.69	248.22	0.782
C006710205	24.384	2.057	135.193	1	4	0	0.60	178	20.69	248.22	0.679
C007025010	24.866	1.905	140.400	1	5	0	0.15	152	20.69	248.22	0.644
C001403305P	24.079	1.702	89.674	1	5	0	-0.09	127	20.69	248.22	0.596
C004702203	6.909	1.791	5.314	0	5	0	0.07	127	20.69	248.22	0.585
C001903310	11.887	0.864	10.805	1	10	0	0.00	152	20.69	248.22	0.348
C007103415	8.807	0.864	8.264	1	11	0	0.25	203	27.58	248.22	0.339
C005463410	7.283	0.813	8.579	1	10	0	-0.02	178	20.69	248.22	0.363
C006313310P	7.010	1.438	4.954	1	6	15	0.06	152	20.69	248.22	0.397
C002014017	6.096	1.219	16.448	1	7	0	0.61	178	20.69	248.22	0.520
C008101013P	6.096	1.295	23.279	1	6	0	0.42	152	20.69	248.22	0.435
C007932415	14.630	1.372	32.621	1	5	35	0.61	203	20.69	227.54	0.417
C004802905	8.534	2.057	31.555	1	5	45	0.05	178	20.69	248.22	0.480
C007443235	9.347	1.778	17.229	1	5	30	0.10	152	20.69	248.22	0.433
C002702510	14.732	1.727	40.802	1	5	25	0.20	152	20.69	248.22	0.429
C000602505	9.144	1.118	15.005	1	5	15	0.77	152	17.24	206.85	0.576
C007010905	11.278	0.975	19.264	1	7	0	0.73	133	17.24	206.85	0.573
C000103420	15.215	0.972	17.697	1	9	0	0.05	165	20.69	248.22	0.538

C009133625	14.935	0.861	23.405	1	7	0	0.48	159	20.69	248.22	0.444
C006305115	8.230	1.194	8.161	1	7	20	0.06	152	20.69	248.22	0.396
C001424750	15.697	2.216	144.110	0	5	0	0.14	178	20.69	248.22	0.774
C006300825P	8.839	1.029	6.933	1	8	0	0.00	140	20.69	248.22	0.387
C005913903	11.735	1.118	10.396	1	8	0	0.28	152	20.69	248.22	0.400
C001210930	14.935	1.753	122.459	1	6	0	-0.11	178	20.69	248.22	0.604
C006311110	17.907	1.537	84.547	0	6	0	0.13	165	20.69	248.22	0.531
C003303710	18.288	1.219	41.497	1	8	0	0.30	152	20.69	248.22	0.417
C001201210	7.620	1.794	7.188	1	6	0	0.05	152	20.69	248.22	0.603
C009123545	9.805	1.956	15.981	1	5	0	-0.01	165	20.69	248.22	0.624
C004803915	8.763	0.838	16.033	0	8	0	0.11	140	17.24	206.85	0.372
C006341615	17.983	0.978	24.279	1	7	0	0.05	152	20.69	248.22	0.371
C002902505	18.288	1.496	59.278	1	5	30	0.13	152	20.69	248.22	0.434
C002602910	17.983	1.188	53.629	1	8	0	0.18	178	20.69	248.22	0.435
C005903110	11.582	0.965	11.722	1	9	0	-0.05	152	20.69	248.22	0.367
C008002310	12.268	1.981	42.313	1	5	0	0.38	178	20.69	248.22	0.654
C001111430	10.973	1.981	31.674	1	4	0	0.69	191	20.69	248.22	0.642
C009111705	9.626	1.600	19.540	1	5	0	0.77	200	20.69	248.22	0.622
C007802440	18.440	2.184	60.850	1	4	0	0.41	178	20.69	248.22	0.717
C002701945	14.707	1.778	26.389	1	5	0	0.71	178	20.69	248.22	0.644
C001401710	13.503	2.105	69.179	1	5	0	0.04	203	20.69	248.22	0.710
C009002115	18.288	0.864	32.374	0	8	0	0.03	140	17.24	206.85	0.364
C007824260	18.136	1.905	73.369	1	5	0	0.61	178	20.69	248.22	0.672
C007911205	14.808	2.057	120.415	1	5	20	0.38	203	24.13	248.22	0.630
C001103815	23.311	1.676	103.774	1	6	0	0.38	165	20.69	248.22	0.552
C005913505	18.288	1.422	20.935	1	6	0	0.03	152	20.69	248.22	0.531
C003413410	21.056	1.969	92.415	1	4	0	0.78	203	17.24	206.85	0.742
C001401535	10.668	2.121	27.515	1	5	30	0.03	178	27.58	248.22	0.558

C000604715	18.034	1.543	93.067	1	6	0	0.49	203	20.69	248.22	0.534
C007815273	12.497	1.918	67.504	1	4	32	0.70	178	20.69	248.22	0.506
C006924230	6.248	1.524	5.333	1	6	0	0.46	178	20.69	248.22	0.501
C004720810	7.468	1.448	5.617	0	5	0	0.15	152	20.69	248.22	0.496
C005904610	9.296	1.016	7.527	1	8	0	0.03	152	20.69	248.22	0.423
C005901825	8.839	1.956	25.751	0	5	45	0.05	152	20.69	248.22	0.609
C007112340	10.668	1.781	43.257	1	6	30	0.20	203	20.69	248.22	0.603
C008803505	8.814	1.295	6.782	1	5	0	0.46	127	20.69	227.54	0.476
C001201410	8.839	1.753	18.992	1	6	30	-0.11	178	20.69	248.22	0.607
C002001215	8.687	1.219	16.602	0	7	35	0.61	152	20.69	248.22	0.570
C001224325	17.983	1.753	90.872	1	6	0	-0.11	178	17.24	248.22	0.593
C008722020	11.887	1.753	40.644	1	6	15	-0.11	178	27.58	248.22	0.552
C005901805	18.161	1.397	51.664	1	7	0	-0.08	152	20.69	248.22	0.471
C000102908	23.063	2.032	113.440	1	5	0	0.26	152	20.69	248.22	0.656
C007603710	11.887	1.829	28.183	1	4	0	0.43	152	20.69	248.22	0.591
C007904705	7.141	2.057	27.549	1	5	23	0.00	178	24.13	248.22	0.609
C007203715	9.144	1.473	7.518	1	5	0	0.09	152	20.69	248.22	0.535
C002001505	8.534	1.295	20.192	0	7	0	0.62	178	20.69	248.22	0.633
C001205010	14.630	1.346	61.658	0	6	15	0.61	152	20.69	248.22	0.583
C003406020	12.573	1.524	20.712	1	5	0	0.61	178	20.69	248.22	0.599
C009114505	8.306	1.302	9.989	1	6	0	0.02	140	17.24	206.85	0.434
C001705805	7.798	1.219	8.479	1	7	0	0.58	152	20.69	248.22	0.604
C001902340	8.738	1.321	9.940	1	7	0	0.02	152	20.69	248.22	0.443
C009202210	12.192	1.219	15.479	1	6	0	0.25	152	20.69	248.22	0.413
C001823610	11.976	1.092	14.176	1	8	0	0.38	127	20.69	248.22	0.426
C003403910	15.240	1.981	55.171	1	4	0	0.69	165	20.69	248.22	0.657
C001301620	13.716	1.905	45.147	1	4	15	0.50	165	17.24	227.54	0.606

C003704805P	15.278	2.057	58.662	1	5	0	0.15	152	20.69	248.22	0.677
C000226205	12.192	1.905	35.412	1	5	0	0.15	191	24.13	248.22	0.620
C009102805	17.856	1.930	64.849	1	5	0	0.10	178	27.58	344.75	0.630
C008902125	12.192	1.753	36.118	1	6	15	-0.11	165	27.58	248.22	0.582
C008404020	9.550	1.829	25.698	0	5	0	0.00	152	17.24	227.54	0.621
C005900525	11.735	0.991	8.455	1	7	0	0.00	140	20.69	227.54	0.382
C005121315P	9.144	1.822	22.898	1	5	0	0.01	152	20.69	248.22	0.629
C007202710	11.887	1.581	23.774	1	6	0	0.01	152	20.69	248.22	0.507
C006301204P	17.983	0.984	25.870	1	7	0	0.02	152	17.24	206.85	0.380
C001900130	9.144	1.791	22.898	1	6	0	0.09	152	20.69	248.22	0.609
C001716105	14.675	1.775	56.245	1	6	45	0.27	178	24.13	344.75	0.549
C005900505	11.811	1.753	45.724	0	5	0	0.08	178	20.69	248.22	0.592
C005913020	11.836	1.168	18.100	1	7	0	0.08	152	20.69	248.22	0.403
C007910405	8.534	1.794	21.569	1	6	0	0.16	178	20.69	248.22	0.612
C005922330	11.735	1.168	9.940	1	6	0	0.08	152	20.69	248.22	0.402
C002004725	11.582	1.219	26.896	1	7	0	0.61	178	20.69	248.22	0.537
C001712925	11.855	1.808	36.552	1	6	0	0.20	178	24.13	344.75	0.609
C008402410	11.963	1.473	23.128	1	5	0	0.03	152	20.69	248.22	0.558
C004507603	8.153	1.194	17.564	0	7	0	0.06	152	20.69	248.22	0.440
C002012040	8.534	1.219	26.669	0	7	0	0.61	178	20.69	248.22	0.538
C007602705	14.935	1.829	45.661	0	4	0	0.46	152	20.69	227.54	0.549
C004800415	18.745	1.829	88.995	1	5	0	0.53	165	20.69	248.22	0.592
C007102605	15.240	1.499	36.481	1	7	0	0.08	203	27.58	344.75	0.494
C005914820	11.836	1.524	37.880	1	6	20	0.15	178	20.69	248.22	0.529
C000805510P	7.315	1.191	11.320	1	7	0	0.16	178	20.69	248.22	0.415
C004903005	11.252	1.200	16.496	1	6	0	0.05	152	20.69	248.22	0.419
C006313105	11.887	0.991	12.518	1	7	0	0.00	152	17.24	206.85	0.373

C007203805	8.839	1.784	8.222	1	5	0	0.15	152	20.69	248.22	0.565
C007302705P	17.805	1.718	43.257	1	6	30	0.13	203	20.69	344.75	0.499
C001105220	15.062	1.695	26.289	0	6	0	0.03	152	20.69	248.22	0.578
C005902215	17.831	1.168	34.034	1	7	0	0.08	152	20.69	248.22	0.407
C009143435	15.570	1.286	23.607	1	5	0	0.40	165	20.69	248.22	0.480
C000102115	14.561	1.413	32.764	1	7	20	0.03	203	27.58	344.75	0.449
C000602310	11.278	1.168	21.091	0	6	0	0.05	165	17.24	227.54	0.419
C005901517	8.839	1.676	21.700	1	6	0	0.08	178	20.69	248.22	0.570
C002000707P	8.534	1.219	17.487	0	7	0	0.61	178	20.69	248.22	0.532
C006500230	9.093	0.854	10.914	1	11	0	0.00	178	27.58	344.75	0.351
C001400730	19.507	1.676	72.955	1	6	0	0.06	178	20.69	344.75	0.559
C005901830	14.935	1.676	38.359	1	6	0	0.08	203	20.69	248.22	0.540
C002003505	16.154	1.219	75.747	1	7	0	0.61	178	20.69	248.22	0.551
C006514240	8.807	1.583	11.939	1	6	0	0.00	178	27.58	344.75	0.524
C002704210P	15.240	1.524	34.988	1	5	20	0.61	178	20.69	248.22	0.523
C005900730	11.786	1.219	15.614	1	7	0	-0.03	152	20.69	248.22	0.415
C009314130	11.855	1.686	43.257	1	6	0	0.00	203	20.69	248.22	0.570
C002004010	14.630	1.219	56.953	1	7	0	0.61	178	20.69	248.22	0.551
C003314210	18.593	1.753	84.536	1	5	0	0.46	165	20.69	248.22	0.565
C001526720	8.785	1.822	30.955	1	5	20	0.01	178	20.69	248.22	0.572
C002012435	17.678	1.245	38.011	1	7	0	0.50	127	20.69	248.22	0.523
C005901410	17.882	1.397	35.029	1	7	0	0.03	152	20.69	248.22	0.506
C001814715	11.976	1.092	16.337	1	8	0	0.37	152	20.69	248.22	0.424
C001234905	17.983	1.829	48.628	1	4	33	0.33	165	20.69	248.22	0.491
C006602010	21.336	2.057	97.171	1	4	0	0.57	203	20.69	248.22	0.665
C008511515	7.925	1.321	25.798	0	7	0	0.30	203	20.69	248.22	0.458
C004712915	7.588	1.699	11.473	1	6	0	0.19	178	24.13	344.75	0.583
C007805310P	9.296	1.257	12.586	1	8	0	0.17	178	20.69	248.22	0.428

C000134022	8.839	1.702	24.582	1	6	0	0.01	152	20.69	248.22	0.589
C001900815	15.240	1.575	38.726	1	6	0	0.18	152	20.69	248.22	0.513
C002000823	7.010	1.219	14.137	0	7	0	0.61	178	20.69	248.22	0.512
C005900915	10.363	1.575	35.508	1	6	30	0.03	178	20.69	248.22	0.562
C002001627	6.401	1.219	18.400	0	7	0	0.61	178	20.69	248.22	0.524
C005901925	14.834	1.295	23.570	1	5	0	0.46	152	20.69	248.22	0.509
C005913030	10.363	1.676	26.430	1	6	0	0.08	178	20.69	248.22	0.570
C007000515	11.887	0.889	11.428	1	9	0	0.42	152	20.69	248.22	0.448
C001101705	14.935	1.753	39.173	1	5	0	0.15	165	20.69	248.22	0.569
C005606105	10.331	1.692	27.549	1	6	0	0.22	178	20.69	248.22	0.573
C003416235	10.541	1.295	20.054	1	7	0	-0.01	178	20.69	248.22	0.446
C000800705	9.246	1.570	21.556	1	6	0	0.23	178	27.58	344.75	0.529
C001202005	11.918	1.314	38.333	0	6	0	0.69	152	20.69	248.22	0.591
C007101130	14.780	1.770	75.551	1	6	30	0.27	203	20.69	344.75	0.549
C008602105P	17.888	1.791	96.927	1	5	0	0.00	178	27.58	248.22	0.600
C004529620	9.601	1.181	19.195	0	7	0	0.05	152	20.69	248.22	0.419
C002003405	8.534	1.219	18.908	0	7	0	0.61	178	20.69	248.22	0.540
C007602610	11.735	1.524	44.889	0	6	20	0.08	152	17.24	206.85	0.563
C004804115	18.593	1.765	58.865	0	5	0	0.13	152	20.69	248.22	0.589
C007001220	17.983	1.346	51.539	1	6	0	0.61	165	20.69	206.85	0.558
C001800605	11.989	1.092	16.517	1	8	0	0.41	165	20.69	248.22	0.439
C007004115	17.882	1.241	39.775	1	6	0	0.74	152	20.69	248.22	0.605
C002004730	8.712	1.219	20.175	0	7	0	0.60	178	20.69	248.22	0.531
C007213110	11.887	1.773	28.497	1	5	0	0.11	152	20.69	227.54	0.569
C004513915	13.884	1.321	35.222	1	7	0	0.00	178	20.69	248.22	0.456
C001411615P	16.764	1.670	60.705	1	6	20	0.09	178	27.58	248.22	0.504
C003302510	13.716	1.765	38.757	1	5	0	0.13	152	20.69	248.22	0.596
C002004730	8.534	1.219	20.044	0	7	0	0.69	178	20.69	248.22	0.564

C007012235	11.887	1.339	29.265	1	6	0	0.63	165	17.24	206.85	0.552
C007100625	14.840	1.775	58.437	1	6	0	0.25	203	24.13	344.75	0.601
C002705115	8.809	1.499	12.300	1	6	0	0.55	152	20.69	248.22	0.533
C002013720	7.087	1.219	15.218	0	7	0	0.61	178	20.69	248.22	0.530

11.3.3 Moment ANN Optimization Data

FE-based GDF	130 bridges	Training Algorithm: 'trainbr'					
ANN Architecture	10-(2-To-10)-1						
	Mean Error (%)				Max. Error (%)		
m	Design set	Indp. Test.	Addtl. Test.	CombinedTest.	Design set	Indp. Test.	Addtl. Test.
2	4.04	4.55			16.29	24.43	
3	4.00	3.76			15.45	20.46	
4	3.28	3.84			15.83	20.13	
5	3.05	3.96			16.03	23.28	
6	3.17	4.20			16.32	23.77	
7	3.21	3.79			14.66	19.68	
8	3.26	3.87			15.44	21.30	
9	3.03	3.89			15.18	22.17	
10	2.63	3.89			16.34	23.54	

FE-based GDF	130 bridges	Training Algorithm: 'trainbr'					
ANN Architecture	10-(2-To-10)-(2-To-10)-1						
	Mean Error (%)				Max. Error (%)		
m	Design set	Indp. Test.	Addtl. Test.	CombinedTest.	Design set	Indp. Test.	Addtl. Test.
2	3.69	4.68			15.71	22.65	
3	3.22	4.14			16.53	21.72	
4	3.08	4.10			17.22	22.19	
5	2.76	3.65			15.44	18.86	
6	17.31	8.84			69.22	48.00	
7	17.34	8.84			69.93	48.62	
8	17.37	8.83			70.60	49.20	
9	17.36	8.83			70.41	49.04	
10	1.79	6.72			17.46	25.08	

FE-based GDF	130 bridges	Training Algorithm: 'trainlm'					
ANN Architecture	10-(2-To-10)-1						
	Mean Error (%)				Max. Error (%)		
m	Design set	Indp. Test.	Addtl. Test.	CombinedTest.	Design set	Indp. Test.	Addtl. Test.
2	3.38	4.76			15.11	22.15	
3	3.21	4.37			14.56	21.05	
4	2.22	4.36			11.36	23.33	
5	2.05	4.27			13.59	17.29	
6	1.64	4.40			11.71	14.09	
7	1.46	4.99			13.07	19.76	
8	1.35	6.10			22.45	27.73	
9	1.21	7.89			22.89	26.63	
10	0.60	7.96			11.94	29.63	

FE-based GDF	130 bridges	Training Algorithm: 'trainlm'					
ANN Architecture	10-(2-To-10)-(2-To-10)-1						
	Mean Error (%)				Max. Error (%)		
m	Design set	Indp. Test.	Addtl. Test.	CombinedTest.	Design set	Indp. Test.	Addtl. Test.
2	3.31	4.03			13.90	22.78	
3	2.75	4.79			14.87	16.31	
4	1.95	5.79			17.97	19.06	
5	1.58	6.22			20.12	16.34	
6	0.97	7.48			17.20	17.91	
7	1.47	7.39			49.10	21.80	
8	1.46	7.15			31.95	23.50	
9	1.52	7.72			30.90	23.83	
10	1.29	6.73			24.44	24.82	

FE-based GDF	120 bridges	Training Algorithm: 'trainbr'					
ANN Architecture	10-(2-To-10)-1						
	Mean Error (%)				Max. Error (%)		
m	Design set	Indp. Test.	Addtl. Test.	CombinedTest.	Design set	Indp. Test.	Addtl. Test.
2	3.98	4.69	4.48	4.64	17.31	25.44	11.90
3	3.23	3.84	4.59	4.01	14.28	21.63	9.65
4	3.13	4.223	4.44	4.27	15.19	21.99	9.49
5	3.15	4.183	4.88	4.35	14.28	20.43	11.77
6	2.91	3.98	4.28	4.05	16.23	22.67	10.99
7	2.89	4.00	4.36	4.09	17.90	22.88	11.97
8	3.39	4.24	4.39	4.28	16.74	21.97	10.37
9	3.22	4.09	4.36	4.15	15.55	22.33	9.99
10	3.29	4.31	4.49	4.35	14.64	22.33	10.04

FE-based GDF	120 bridges	Training Algorithm: 'trainbr'					
ANN Architecture	10-(2-To-10)-(2-To-10)-1						
	Mean Error (%)				Max. Error (%)		
m	Design set	Indp. Test.	Addtl. Test.	CombinedTest.	Design set	Indp. Test.	Addtl. Test.
2	3.60	4.81	4.55	4.75	16.25	23.99	10.96
3	3.29	4.16	4.17	4.16	16.00	22.21	9.72
4	3.03	4.27	5.44	4.55	14.10	22.45	13.38
5	3.14	3.82	4.23	3.92	15.19	21.76	10.47
6	17.60	8.85	13.76	9.99	69.06	47.86	29.86
7	17.61	8.84	13.75	9.98	69.27	48.04	30.02
8	17.65	8.83	13.72	9.97	70.16	48.82	30.70
9	17.65	8.83	13.72	9.97	70.18	48.84	30.72
10	17.71	8.83	13.68	9.96	71.19	49.72	31.49

FE-based GDF	120 bridges	Training Algorithm: 'trainlm'					
ANN Architecture	10-(2-To-10)-1						
	Mean Error (%)				Max. Error (%)		
m	Design set	Indp. Test.	Addtl. Test.	CombinedTest.	Design set	Indp. Test.	Addtl. Test.
2	3.71	4.39	3.64	4.21	20.43	24.62	9.17
3	3.23	4.20	5.39	4.48	15.27	17.10	21.33
4	2.43	3.382	4.83	3.72	23.25	17.98	12.80
5	1.91	5.419	2.61	4.77	10.99	27.27	4.67
6	1.94	5.47	5.95	5.58	14.72	22.33	12.02
7	1.21	6.58	5.41	6.31	16.68	24.58	16.13
8	1.02	8.02	5.63	7.47	21.12	31.13	14.71
9	1.25	9.63	11.16	9.99	21.28	32.50	21.04
10	1.30	7.33	5.44	6.89	35.06	35.29	13.61

FE-based GDF	120 bridges	Training Algorithm: 'trainlm'					
ANN Architecture	10-(2-To-10)-(2-To-10)-1						
	Mean Error (%)				Max. Error (%)		
m	Design set	Indp. Test.	Addtl. Test.	CombinedTest.	Design set	Indp. Test.	Addtl. Test.
2	3.73	4.43	4.73	4.50	16.74	25.41	15.25
3	2.89	4.62	4.22	4.52	13.38	21.75	9.15
4	1.62	5.72	7.40	6.11	18.03	23.69	33.10
5	1.12	6.32	9.83	7.14	15.02	20.54	27.91
6	1.27	7.79	8.13	7.87	25.42	24.62	28.00
7	1.34	8.06	6.18	7.62	43.77	31.68	21.66
8	1.23	5.69	5.08	5.54	33.80	16.68	18.61
9	0.90	5.06	5.13	5.08	25.70	18.35	14.22
10	0.97	6.83	6.63	6.79	24.38	25.42	13.47

FE-based GDF	110 bridges	Training Algorithm: 'trainbr'						FE-based GDF	110 bridges	Training Algorithm: 'trainbr'					
ANN Architecture	10-(2-To-10)-1							ANN Architecture	10-(2-To-10)-(2-To-10)-1						
	Mean Error (%)				Max. Error (%)				Mean Error (%)				Max. Error (%)		
m	Design set	Indp. Test.	Addtl. Test.	CombinedTest.	Design set	Indp. Test.	Addtl. Test.	m	Design set	Indp. Test.	Addtl. Test.	CombinedTest.	Design set	Indp. Test.	Addtl. Test.
2	3.92	4.56	4.65	4.59	15.28	23.43	17.50	2	3.58	4.75	4.63	4.71	15.56	23.29	16.23
3	3.31	4.28	4.36	4.31	15.19	20.07	17.19	3	3.09	4.36	4.16	4.28	16.09	20.87	17.46
4	3.00	3.75	4.04	3.86	17.42	21.89	18.60	4	2.89	4.36	4.59	4.45	15.12	22.37	16.99
5	3.09	4.24	4.24	4.24	15.18	22.46	16.40	5	2.46	4.00	4.72	4.27	15.54	20.41	17.14
6	2.59	4.04	4.55	4.23	16.60	22.93	18.17	6	18.06	8.88	13.03	10.44	68.31	47.20	29.66
7	2.34	3.85	4.82	4.21	14.55	22.45	17.98	7	1.81	4.59	5.57	4.96	7.69	19.26	19.23
8	2.27	3.74	4.86	4.16	13.12	21.96	18.46	8	18.08	8.86	12.96	10.41	68.74	47.58	29.99
9	1.95	4.02	4.38	4.16	9.14	19.47	20.55	9	18.20	8.83	12.70	10.29	70.37	49.01	31.25
10	2.03	3.80	4.51	4.07	12.10	20.83	19.68	10	18.12	8.84	12.87	10.36	69.27	48.04	30.39

FE-based GDF	110 bridges	Training Algorithm: 'trainlm'						FE-based GDF	110 bridges	Training Algorithm: 'trainlm'					
ANN Architecture	10-(2-To-10)-1							ANN Architecture	10-(2-To-10)-(2-To-10)-1						
	Mean Error (%)				Max. Error (%)				Mean Error (%)				Max. Error (%)		
m	Design set	Indp. Test.	Addtl. Test.	CombinedTest.	Design set	Indp. Test.	Addtl. Test.	m	Design set	Indp. Test.	Addtl. Test.	CombinedTest.	Design set	Indp. Test.	Addtl. Test.
2	3.46	4.01	5.24	4.47	13.47	20.76	21.35	2	3.21	4.53	4.99	4.70	15.22	16.09	20.05
3	2.72	4.11	5.01	4.45	14.58	25.43	21.03	3	2.28	4.93	4.36	4.71	13.05	17.82	18.90
4	2.07	4.09	4.83	4.37	13.73	19.38	14.96	4	1.81	4.78	5.07	4.89	28.87	16.33	17.43
5	2.40	5.27	7.13	5.97	13.57	16.18	18.69	5	1.48	7.19	7.29	7.23	23.96	21.04	21.10
6	1.38	4.75	6.56	5.44	28.97	23.97	23.44	6	1.00	7.51	8.29	7.81	21.45	28.54	23.64
7	1.35	7.26	10.76	8.58	18.56	24.38	27.31	7	1.16	6.32	6.79	6.50	28.24	23.87	23.38
8	1.07	6.76	8.36	7.37	19.05	23.76	34.61	8	0.69	7.36	7.66	7.47	10.77	22.83	17.68
9	1.36	6.23	10.25	7.75	36.61	24.37	26.17	9	0.61	6.95	6.44	6.76	11.93	25.61	19.57
10	0.85	8.90	7.01	8.19	18.35	29.89	24.02	10	1.02	6.14	5.82	6.02	18.18	26.28	21.02

FE-based GDF	100 bridges	Training Algorithm: 'trainbr'					
ANN Architecture	10-(2-To-10)-1						
	Mean Error (%)				Max. Error (%)		
m	Design set	Indp. Test.	Addtl. Test.	CombinedTest.	Design set	Indp. Test.	Addtl. Test.
2	3.81	4.73	4.36	4.56	17.99	24.17	19.06
3	3.63	4.87	4.48	4.68	15.79	22.99	17.13
4	2.95	4.09	4.01	4.05	16.82	22.23	18.20
5	3.05	4.159	3.96	4.07	15.82	21.39	17.89
6	2.76	4.31	4.41	4.36	17.71	23.47	18.64
7	3.03	4.15	3.98	4.07	15.95	20.99	17.47
8	3.27	4.37	3.94	4.17	16.43	22.19	16.69
9	3.29	4.38	3.92	4.16	16.77	21.27	17.33
10	3.30	4.16	3.77	3.98	15.44	20.82	16.92

FE-based GDF	100 bridges	Training Algorithm: 'trainbr'					
ANN Architecture	10-(2-To-10)-(2-To-10)-1						
	Mean Error (%)				Max. Error (%)		
m	Design set	Indp. Test.	Addtl. Test.	CombinedTest.	Design set	Indp. Test.	Addtl. Test.
2	3.86	4.80	4.58	4.70	16.30	24.07	18.39
3	3.25	4.51	3.65	4.10	15.62	22.73	16.31
4	2.81	4.74	4.80	4.77	16.20	24.71	20.23
5	18.67	8.83	12.94	10.79	70.21	48.86	31.12
6	18.68	8.83	12.93	10.79	70.32	48.96	31.20
7	18.64	8.84	12.96	10.80	69.66	48.38	30.69
8	18.64	8.84	12.96	10.80	69.70	48.42	30.73
9	18.71	8.83	12.93	10.79	70.87	49.44	31.63
10	18.67	8.83	12.94	10.79	70.13	48.79	31.06

FE-based GDF	100 bridges	Training Algorithm: 'trainlm'					
ANN Architecture	10-(2-To-10)-1						
	Mean Error (%)				Max. Error (%)		
m	Design set	Indp. Test.	Addtl. Test.	CombinedTest.	Design set	Indp. Test.	Addtl. Test.
2	3.73	4.27	9.92	6.96	16.83	24.73	103.06
3	2.78	4.76	4.06	4.43	15.78	22.56	16.84
4	2.19	4.20	4.62	4.40	15.09	22.61	22.70
5	2.08	5.060	6.04	5.53	14.36	16.90	17.47
6	1.47	4.98	7.77	6.31	31.73	17.21	24.79
7	1.01	6.47	8.46	7.42	13.78	20.07	22.67
8	1.20	5.55	8.39	6.90	18.47	16.19	21.87
9	1.56	6.50	8.07	7.25	34.24	25.67	21.33
10	1.20	6.50	6.75	6.62	16.95	20.76	29.06

FE-based GDF	100 bridges	Training Algorithm: 'trainlm'					
ANN Architecture	10-(2-To-10)-(2-To-10)-1						
	Mean Error (%)				Max. Error (%)		
m	Design set	Indp. Test.	Addtl. Test.	CombinedTest.	Design set	Indp. Test.	Addtl. Test.
2	3.33	4.62	4.25	4.45	14.35	24.71	18.94
3	2.55	4.65	7.72	6.11	12.44	20.97	90.49
4	1.52	4.81	5.84	5.30	16.57	26.90	25.30
5	1.32	6.60	5.74	6.19	18.64	19.57	21.54
6	0.76	5.90	5.69	5.80	21.68	20.63	19.03
7	0.83	5.69	8.50	7.03	11.87	16.54	27.19
8	0.85	5.91	7.59	6.71	13.82	19.76	31.11
9	1.00	6.07	8.19	7.08	17.33	15.98	57.56
10	0.75	4.41	7.51	5.88	13.97	19.29	44.79

FE-based GDF	90 bridges	Training Algorithm: 'trainbr'						FE-based GDF	90 bridges	Training Algorithm: 'trainbr'					
ANN Architecture		10-(2-To-10)-1						ANN Architecture		10-(2-To-10)-(2-To-10)-1					
	Mean Error (%)				Max. Error (%)				Mean Error (%)				Max. Error (%)		
m	Design set	Indp. Test.	Addtl. Test.	CombinedTest.	Design set	Indp. Test.	Addtl. Test.	m	Design set	Indp. Test.	Addtl. Test.	CombinedTest.	Design set	Indp. Test.	Addtl. Test.
2	4.01	4.76	3.84	4.26	16.45	24.23	18.66	2	3.89	4.25	4.50	4.39	17.72	23.02	21.13
3	3.72	4.18	3.52	3.82	17.13	22.23	16.51	3	3.34	4.70	4.86	4.79	17.59	22.32	20.04
4	3.35	4.47	4.40	4.43	18.07	25.23	20.90	4	3.32	4.46	4.32	4.39	18.48	25.95	20.48
5	3.19	4.14	3.34	3.70	15.92	20.87	18.72	5	19.78	8.83	12.03	10.59	71.16	49.69	31.85
6	2.84	4.60	4.20	4.38	16.61	23.54	19.00	6	19.64	8.84	12.09	10.62	69.45	48.19	30.53
7	2.39	4.42	5.02	4.75	13.99	22.57	18.54	7	19.75	8.83	12.04	10.59	70.81	49.39	31.58
8	2.71	4.52	4.17	4.33	17.47	23.73	19.44	8	19.61	8.85	12.11	10.64	69.00	47.81	30.19
9	3.60	4.61	3.56	4.04	15.38	21.43	16.66	9	19.67	8.84	12.07	10.61	69.78	48.49	30.79
10	2.91	4.45	4.04	4.23	18.10	24.27	19.00	10	19.81	8.83	12.03	10.58	71.50	50.00	32.12

FE-based GDF	90 bridges	Training Algorithm: 'trainlm'						FE-based GDF	90 bridges	Training Algorithm: 'trainlm'					
ANN Architecture		10-(2-To-10)-1						ANN Architecture		10-(2-To-10)-(2-To-10)-1					
	Mean Error (%)				Max. Error (%)				Mean Error (%)				Max. Error (%)		
m	Design set	Indp. Test.	Addtl. Test.	CombinedTest.	Design set	Indp. Test.	Addtl. Test.	m	Design set	Indp. Test.	Addtl. Test.	CombinedTest.	Design set	Indp. Test.	Addtl. Test.
2	3.47	4.01	4.76	4.42	17.07	20.51	22.67	2	3.33	4.43	4.14	4.27	15.78	20.03	21.63
3	2.93	4.80	3.59	4.14	15.58	22.59	17.29	3	2.61	5.46	7.14	6.38	14.77	20.05	22.88
4	1.92	4.38	4.39	4.38	11.73	28.28	21.63	4	1.44	7.02	6.57	6.77	18.07	22.94	29.19
5	1.74	5.35	7.84	6.72	14.60	23.10	24.72	5	0.83	7.18	5.14	6.06	12.43	21.02	22.94
6	1.58	6.26	7.13	6.73	23.04	23.26	26.45	6	1.15	6.55	7.92	7.30	21.86	22.77	41.15
7	1.43	8.12	7.86	7.98	20.23	26.35	29.55	7	1.03	6.13	6.29	6.22	16.22	19.85	19.35
8	1.23	6.05	8.00	7.12	24.73	21.30	23.45	8	1.00	6.63	7.15	6.92	18.40	20.94	22.02
9	1.32	5.51	6.59	6.11	23.48	22.41	15.14	9	0.86	5.38	7.72	6.66	13.83	18.36	25.39
10	1.02	6.28	6.34	6.31	19.79	28.84	26.31	10	0.87	5.58	8.91	7.40	10.29	24.43	74.78

FE-based GDF	80 bridges	Training Algorithm: 'trainbr'					
ANN Architecture	10-(2-To-10)-1						
	Mean Error (%)				Max. Error (%)		
m	Design set	Indp. Test.	Addtl. Test.	CombinedTest.	Design set	Indp. Test.	Addtl. Test.
2	3.92	4.84	4.20	4.45	17.41	24.81	18.29
3	3.32	4.75	4.03	4.32	13.25	20.11	18.78
4	3.24	4.540	4.00	4.21	14.82	19.42	19.04
5	2.79	4.474	4.35	4.40	14.11	21.75	17.99
6	2.81	4.69	4.35	4.49	15.56	22.79	17.94
7	2.92	4.50	4.25	4.35	15.99	23.09	18.07
8	3.17	4.77	3.91	4.25	17.03	22.27	16.96
9	2.88	4.48	4.16	4.29	15.60	22.40	17.02
10	2.82	4.55	4.26	4.38	16.18	22.71	17.49

FE-based GDF	80 bridges	Training Algorithm: 'trainbr'					
ANN Architecture	10-(2-To-10)-(2-To-10)-1						
	Mean Error (%)				Max. Error (%)		
m	Design set	Indp. Test.	Addtl. Test.	CombinedTest.	Design set	Indp. Test.	Addtl. Test.
2	3.79	4.97	4.50	4.69	16.73	25.35	20.42
3	3.18	4.71	4.29	4.46	16.40	22.66	17.93
4	20.54	8.83	12.38	10.97	71.24	49.77	31.92
5	20.48	8.83	12.40	10.98	70.79	49.37	31.57
6	20.30	8.85	12.51	11.05	69.01	47.82	30.20
7	20.65	8.85	12.34	10.95	72.10	50.52	32.58
8	20.40	8.84	12.44	11.01	70.00	48.68	30.96
9	20.43	8.83	12.42	11.00	70.31	48.95	31.20
10	20.34	8.84	12.48	11.03	69.37	48.13	30.47

FE-based GDF	80 bridges	Training Algorithm: 'trainlm'					
ANN Architecture	10-(2-To-10)-1						
	Mean Error (%)				Max. Error (%)		
m	Design set	Indp. Test.	Addtl. Test.	CombinedTest.	Design set	Indp. Test.	Addtl. Test.
2	3.69	4.41	4.59	4.52	16.69	22.06	18.08
3	2.32	4.46	5.06	4.82	18.54	23.96	18.94
4	2.58	4.874	4.81	4.83	26.19	16.63	16.35
5	1.74	5.934	6.45	6.24	24.59	22.46	23.54
6	1.29	6.26	6.66	6.50	25.07	23.59	24.34
7	1.30	5.80	6.10	5.98	23.01	20.27	23.29
8	1.13	6.22	9.09	7.95	25.98	16.01	29.95
9	1.25	6.70	8.81	7.97	24.03	23.80	58.06
10	0.95	5.04	6.79	6.09	15.99	25.15	27.36

FE-based GDF	80 bridges	Training Algorithm: 'trainlm'					
ANN Architecture	10-(2-To-10)-(2-To-10)-1						
	Mean Error (%)				Max. Error (%)		
m	Design set	Indp. Test.	Addtl. Test.	CombinedTest.	Design set	Indp. Test.	Addtl. Test.
2	2.81	5.55	5.70	5.64	9.63	18.95	22.13
3	2.34	6.06	6.15	6.11	11.98	23.39	19.32
4	1.34	8.09	9.64	9.02	15.41	40.57	46.92
5	1.25	6.34	6.07	6.18	28.55	25.93	30.42
6	1.19	5.12	6.03	5.67	16.32	23.29	23.38
7	0.86	6.02	6.40	6.25	17.69	21.10	28.52
8	1.24	5.52	5.92	5.76	18.89	19.22	20.85
9	1.01	5.73	4.54	5.01	28.79	23.27	22.80
10	1.26	4.64	5.84	5.36	19.84	18.89	23.32

FE-based GDF	70 bridges	Training Algorithm: 'trainbr'					
ANN Architecture	10-(2-To-10)-1						
	Mean Error (%)				Max. Error (%)		
m	Design set	Indp. Test.	Addtl. Test.	CombinedTest.	Design set	Indp. Test.	Addtl. Test.
2	3.86	4.63	4.18	4.34	16.67	24.53	19.92
3	2.92	4.29	4.42	4.37	14.67	20.54	17.94
4	2.79	4.96	4.77	4.84	16.57	22.46	19.38
5	2.79	4.88	4.77	4.81	15.84	20.79	19.26
6	2.59	4.53	4.37	4.42	15.17	20.73	19.03
7	2.79	5.02	4.68	4.80	16.63	20.94	20.48
8	2.76	4.82	4.78	4.79	16.37	21.80	18.73
9	2.84	4.80	4.43	4.56	16.23	21.32	19.32
10	2.66	4.70	4.97	4.87	14.80	19.39	20.92

FE-based GDF	70 bridges	Training Algorithm: 'trainbr'					
ANN Architecture	10-(2-To-10)-(2-To-10)-1						
	Mean Error (%)				Max. Error (%)		
m	Design set	Indp. Test.	Addtl. Test.	CombinedTest.	Design set	Indp. Test.	Addtl. Test.
2	3.90	4.71	4.59	4.63	16.98	24.72	22.18
3	3.10	4.81	4.30	4.48	13.92	18.11	21.58
4	21.99	8.85	11.84	10.78	69.04	47.84	30.22
5	21.89	8.88	11.92	10.84	68.37	47.26	29.70
6	22.01	8.84	11.83	10.77	69.22	47.99	30.36
7	22.00	8.85	11.84	10.78	69.13	47.92	30.29
8	21.90	8.87	11.91	10.83	68.44	47.31	29.75
9	21.68	8.97	12.11	11.00	66.69	45.78	28.41
10	21.93	8.86	11.88	10.81	68.68	47.53	29.94

FE-based GDF	70 bridges	Training Algorithm: 'trainlm'					
ANN Architecture	10-(2-To-10)-1						
	Mean Error (%)				Max. Error (%)		
m	Design set	Indp. Test.	Addtl. Test.	CombinedTest.	Design set	Indp. Test.	Addtl. Test.
2	3.25	4.94	5.77	5.47	10.71	24.30	24.57
3	2.34	5.11	6.08	5.74	13.70	16.79	25.33
4	1.80	6.24	5.69	5.89	17.83	17.54	25.30
5	1.05	6.07	6.88	6.59	19.58	21.93	27.23
6	1.01	5.28	6.56	6.11	14.84	23.78	21.63
7	1.25	6.06	7.02	6.68	19.20	24.53	42.01
8	1.27	6.64	8.34	7.73	22.91	27.34	33.30
9	1.46	5.47	6.27	5.99	24.08	26.79	28.84
10	1.06	6.47	7.14	6.90	13.74	22.16	32.03

FE-based GDF	70 bridges	Training Algorithm: 'trainlm'					
ANN Architecture	10-(2-To-10)-(2-To-10)-1						
	Mean Error (%)				Max. Error (%)		
m	Design set	Indp. Test.	Addtl. Test.	CombinedTest.	Design set	Indp. Test.	Addtl. Test.
2	2.86	4.51	5.70	5.28	16.49	23.86	27.96
3	1.90	6.74	7.37	7.14	11.44	20.61	26.52
4	0.76	7.31	6.67	6.89	18.66	19.68	22.73
5	1.43	6.57	5.87	6.12	23.16	22.88	19.55
6	1.27	5.88	5.87	5.87	20.29	15.27	25.32
7	0.98	5.77	6.00	5.92	20.81	23.21	27.99
8	1.15	5.81	6.75	6.42	19.27	21.43	33.56
9	0.94	4.93	5.31	5.18	22.01	19.11	20.29
10	0.68	5.18	6.75	6.19	18.18	18.15	24.19

FE-based GDF	60 bridges	Training Algorithm: 'trainbr'					
ANN Architecture	10-(2-To-10)-1						
	Mean Error (%)				Max. Error (%)		
m	Design set	Indp. Test.	Addtl. Test.	CombinedTest.	Design set	Indp. Test.	Addtl. Test.
2	2.21	4.75	4.75	4.75	9.45	16.83	20.62
3	2.43	4.75	4.99	4.91	10.58	16.07	20.68
4	2.15	4.23	4.61	4.49	11.91	18.52	20.46
5	1.98	4.45	5.11	4.90	7.16	17.83	21.03
6	2.27	4.04	4.62	4.44	10.27	20.29	19.85
7	1.85	4.35	4.59	4.52	8.09	20.40	20.73
8	1.91	4.26	4.77	4.61	7.32	20.18	20.24
9	2.39	4.71	4.44	4.52	9.00	18.62	21.15
10	2.30	4.53	4.50	4.51	8.65	19.43	19.99

FE-based GDF	60 bridges	Training Algorithm: 'trainbr'					
ANN Architecture	10-(2-To-10)-(2-To-10)-1						
	Mean Error (%)				Max. Error (%)		
m	Design set	Indp. Test.	Addtl. Test.	CombinedTest.	Design set	Indp. Test.	Addtl. Test.
2	2.76	4.91	5.67	5.42	13.46	16.95	22.86
3	2.55	4.85	5.00	4.95	10.80	17.05	20.62
4	22.54	8.94	12.75	11.53	67.16	46.19	47.16
5	22.92	8.84	12.54	11.35	69.76	48.47	49.46
6	22.92	8.84	12.54	11.35	69.79	48.50	49.48
7	22.78	8.86	12.61	11.40	68.92	47.73	48.71
8	22.77	8.86	12.61	11.41	68.86	47.69	48.67
9	23.08	8.83	12.48	11.31	70.70	49.29	50.28
10	22.89	8.84	12.55	11.36	69.61	43.34	49.33

FE-based GDF	60 bridges	Training Algorithm: 'trainlm'					
ANN Architecture	10-(2-To-10)-1						
	Mean Error (%)				Max. Error (%)		
m	Design set	Indp. Test.	Addtl. Test.	CombinedTest.	Design set	Indp. Test.	Addtl. Test.
2	2.80	4.67	5.61	5.31	12.30	17.79	20.89
3	2.18	4.78	4.59	4.65	12.43	19.45	21.11
4	0.76	6.161	7.08	6.78	9.61	19.52	60.71
5	0.86	6.116	6.19	6.17	15.55	20.81	21.96
6	0.84	6.14	8.47	7.72	13.02	21.83	55.51
7	1.36	5.14	9.10	7.83	16.65	15.40	52.75
8	1.29	5.13	8.13	7.17	18.75	22.08	58.53
9	0.69	5.43	7.25	6.67	12.01	22.06	30.77
10	0.87	5.45	5.67	5.60	15.60	26.31	22.01

FE-based GDF	60 bridges	Training Algorithm: 'trainlm'					
ANN Architecture	10-(2-To-10)-(2-To-10)-1						
	Mean Error (%)				Max. Error (%)		
m	Design set	Indp. Test.	Addtl. Test.	CombinedTest.	Design set	Indp. Test.	Addtl. Test.
2	2.69	4.69	4.73	4.72	12.40	16.94	21.83
3	1.90	6.29	7.01	6.78	19.93	28.14	38.46
4	0.68	6.16	6.82	6.61	9.63	21.60	25.50
5	0.50	6.90	9.15	8.43	7.26	23.84	62.65
6	0.87	5.20	6.35	5.98	12.02	21.61	26.62
7	0.62	5.92	7.57	7.04	11.32	17.63	30.97
8	0.84	4.87	6.90	6.25	12.11	17.81	24.82
9	0.92	4.94	6.78	6.19	14.27	18.13	21.55
10	0.73	5.03	7.67	6.82	12.65	19.07	42.57

FE-based GDF	50 bridges	Training Algorithm: 'trainbr'					
ANN Architecture	10-(2-To-10)-1						
	Mean Error (%)				Max. Error (%)		
m	Design set	Indp. Test.	Addtl. Test.	CombinedTest.	Design set	Indp. Test.	Addtl. Test.
2	2.63	4.48	5.63	5.30	12.05	17.08	23.15
3	2.39	4.42	4.62	4.56	14.25	17.22	22.25
4	2.33	4.539	5.27	5.06	16.00	21.58	5.27
5	2.15	5.176	5.03	5.07	8.85	17.78	21.87
6	1.88	5.16	5.37	5.31	7.61	17.13	22.44
7	1.48	4.69	4.96	4.88	12.70	17.27	22.92
8	1.85	4.37	4.88	4.73	12.56	17.57	21.73
9	2.13	4.41	5.14	4.93	8.08	16.98	22.56
10	2.08	4.71	5.19	5.05	6.35	15.41	22.83

FE-based GDF	50 bridges	Training Algorithm: 'trainbr'					
ANN Architecture	10-(2-To-10)-(2-To-10)-1						
	Mean Error (%)				Max. Error (%)		
m	Design set	Indp. Test.	Addtl. Test.	CombinedTest.	Design set	Indp. Test.	Addtl. Test.
2	2.47	4.82	5.70	5.44	7.26	17.97	21.93
3	23.95	8.84	13.39	12.06	72.03	50.46	51.46
4	23.74	8.83	13.35	12.03	70.25	48.90	49.89
5	23.75	8.83	13.35	12.03	70.32	48.96	49.95
6	23.84	8.83	13.36	12.04	71.08	49.63	50.62
7	24.01	8.88	13.41	12.08	72.53	50.90	51.90
8	23.82	8.83	13.36	12.04	70.89	49.46	50.45
9	23.84	8.83	13.36	12.04	71.09	49.63	50.62
10	24.02	8.88	13.41	12.09	72.63	50.98	51.98

FE-based GDF	50 bridges	Training Algorithm: 'trainlm'					
ANN Architecture	10-(2-To-10)-1						
	Mean Error (%)				Max. Error (%)		
m	Design set	Indp. Test.	Addtl. Test.	CombinedTest.	Design set	Indp. Test.	Addtl. Test.
2	2.48	4.85	5.79	5.52	11.28	19.94	26.48
3	1.76	4.52	5.09	4.92	22.48	18.21	21.36
4	0.84	6.226	8.13	7.57	12.28	22.68	33.02
5	1.24	4.186	5.57	5.17	29.73	18.78	20.26
6	0.80	5.60	5.77	5.72	11.98	19.74	26.18
7	1.00	5.63	6.78	6.44	12.13	16.87	28.47
8	0.75	5.31	6.33	6.03	9.45	21.09	32.19
9	0.88	5.58	6.68	6.36	16.82	16.74	27.55
10	1.11	4.83	5.48	5.29	18.02	20.58	24.38

FE-based GDF	50 bridges	Training Algorithm: 'trainlm'					
ANN Architecture	10-(2-To-10)-(2-To-10)-1						
	Mean Error (%)				Max. Error (%)		
m	Design set	Indp. Test.	Addtl. Test.	CombinedTest.	Design set	Indp. Test.	Addtl. Test.
2	1.76	5.07	5.64	5.47	9.60	16.63	23.27
3	0.65	5.87	5.58	5.67	9.37	19.91	22.47
4	1.22	5.20	6.39	6.04	15.59	16.21	51.48
5	0.96	5.02	7.78	6.98	13.48	16.82	39.00
6	0.99	5.65	7.58	7.02	11.88	20.66	55.19
7	0.73	5.20	5.75	5.59	7.67	21.46	22.26
8	0.73	5.83	7.37	6.92	8.61	14.56	58.03
9	1.08	5.54	7.55	6.96	18.49	20.40	54.73
10	0.63	5.88	7.81	7.25	10.16	18.51	49.26

FE-based GDF	40 bridges	Training Algorithm: 'trainbr'					
ANN Architecture	10-(2-To-10)-1						
	Mean Error (%)				Max. Error (%)		
m	Design set	Indp. Test.	Addtl. Test.	CombinedTest.	Design set	Indp. Test.	Addtl. Test.
2	3.52	4.80	4.55	4.62	13.64	27.90	20.49
3	25.47	8.89	13.95	12.59	72.68	51.03	66.41
4	2.68	5.282	6.04	5.84	19.12	25.14	23.63
5	1.89	4.437	5.68	5.35	5.94	17.61	25.66
6	1.61	4.67	5.38	5.19	6.74	17.37	23.79
7	1.51	4.55	5.88	5.53	10.40	17.23	23.89
8	1.38	4.80	6.34	5.93	10.22	17.82	25.07
9	1.76	4.51	5.22	5.03	7.22	20.08	21.10
10	1.89	4.16	5.00	4.78	8.54	19.64	20.81

FE-based GDF	40 bridges	Training Algorithm: 'trainbr'					
ANN Architecture	10-(2-To-10)-(2-To-10)-1						
	Mean Error (%)				Max. Error (%)		
m	Design set	Indp. Test.	Addtl. Test.	CombinedTest.	Design set	Indp. Test.	Addtl. Test.
2	1.87	5.17	6.08	5.83	6.10	17.11	25.59
3	25.52	8.92	13.97	12.61	73.12	51.41	66.83
4	25.29	8.83	13.89	12.53	71.17	49.70	64.94
5	25.33	8.83	13.90	12.54	71.55	50.04	65.32
6	25.16	8.84	13.87	12.52	70.07	48.74	63.89
7	25.36	8.83	13.91	12.55	71.75	50.21	65.50
8	25.26	8.83	13.88	12.53	70.93	49.49	64.72
9	25.53	8.93	13.97	12.62	73.23	51.51	66.93
10	25.37	8.84	13.91	12.55	71.82	50.27	65.57

FE-based GDF	40 bridges	Training Algorithm: 'trainlm'					
ANN Architecture	10-(2-To-10)-1						
	Mean Error (%)				Max. Error (%)		
m	Design set	Indp. Test.	Addtl. Test.	CombinedTest.	Design set	Indp. Test.	Addtl. Test.
2	3.24	4.44	5.16	4.97	19.33	27.24	24.80
3	0.82	6.20	6.22	6.22	11.91	26.22	30.95
4	0.65	6.177	7.83	7.39	8.48	17.92	31.62
5	1.00	5.731	7.43	6.97	14.02	23.69	21.39
6	1.24	5.23	5.28	5.27	17.48	20.99	22.62
7	0.95	4.69	6.16	5.77	24.10	16.29	20.01
8	0.88	4.82	6.62	6.14	10.68	17.29	20.47
9	0.59	5.56	6.98	6.59	8.45	19.80	32.72
10	0.99	5.22	5.43	5.37	10.26	19.28	21.72

FE-based GDF	40 bridges	Training Algorithm: 'trainlm'					
ANN Architecture	10-(2-To-10)-(2-To-10)-1						
	Mean Error (%)				Max. Error (%)		
m	Design set	Indp. Test.	Addtl. Test.	CombinedTest.	Design set	Indp. Test.	Addtl. Test.
2	1.64	6.12	7.43	7.08	11.19	18.48	24.80
3	1.56	5.83	7.89	7.33	18.25	24.10	24.16
4	0.46	6.57	8.59	8.05	5.84	21.10	39.97
5	0.88	4.20	6.65	5.99	16.42	15.78	27.05
6	1.17	4.91	7.44	6.76	14.73	21.18	38.28
7	0.80	5.33	8.43	7.60	11.23	25.57	46.07
8	0.88	6.55	8.26	7.80	11.65	23.25	22.66
9	0.85	5.63	7.59	7.07	13.35	22.62	24.97
10	0.38	6.30	7.91	7.48	7.21	15.83	32.61

FE-based GDF	30 bridges	Training Algorithm: 'trainbr'					
ANN Architecture	10-(2-To-10)-1						
	Mean Error (%)				Max. Error (%)		
m	Design set	Indp. Test.	Addtl. Test.	CombinedTest.	Design set	Indp. Test.	Addtl. Test.
2	21.64	8.83	14.30	12.95	67.20	45.77	65.28
3	2.42	5.41	6.59	6.30	15.20	25.14	23.17
4	2.53	5.722	6.51	6.32	15.34	26.35	24.06
5	24.75	10.153	16.24	14.73	79.24	56.76	72.72
6	0.66	5.72	6.07	5.98	9.50	21.44	22.21
7	1.34	4.78	5.47	5.30	19.68	20.72	21.24
8	1.41	5.36	5.57	5.52	5.89	25.49	20.68
9	2.49	5.18	6.28	6.01	14.98	25.84	25.85
10	0.77	4.43	5.81	5.47	8.50	21.56	41.00

FE-based GDF	30 bridges	Training Algorithm: 'trainbr'					
ANN Architecture	10-(2-To-10)-(2-To-10)-1						
	Mean Error (%)				Max. Error (%)		
m	Design set	Indp. Test.	Addtl. Test.	CombinedTest.	Design set	Indp. Test.	Addtl. Test.
2	23.21	9.23	14.79	13.41	71.41	48.76	63.93
3	24.83	10.47	16.51	15.01	80.54	57.90	73.98
4	14.33	8.42	10.20	9.76	43.86	39.34	49.25
5	24.74	10.11	16.20	14.69	79.07	56.61	72.56
6	24.75	10.15	16.24	14.73	79.22	56.74	72.97
7	24.72	10.03	16.13	14.62	78.73	56.31	72.23
8	24.80	10.34	16.40	14.89	80.03	57.45	73.48
9	24.67	9.86	16.01	14.48	78.04	55.71	71.56
10	24.70	9.56	16.08	14.46	78.43	56.05	71.94

FE-based GDF	30 bridges	Training Algorithm: 'trainlm'					
ANN Architecture	10-(2-To-10)-1						
	Mean Error (%)				Max. Error (%)		
m	Design set	Indp. Test.	Addtl. Test.	CombinedTest.	Design set	Indp. Test.	Addtl. Test.
2	1.75	5.90	7.94	7.44	15.69	19.37	49.67
3	1.38	5.49	6.31	6.11	12.11	26.33	36.24
4	0.42	6.119	8.54	7.94	5.57	30.69	75.64
5	0.20	5.260	6.51	6.20	3.57	17.70	32.36
6	0.50	5.12	6.40	6.08	7.10	20.33	26.20
7	0.90	5.40	7.12	6.69	9.87	20.71	23.30
8	0.66	5.17	7.25	6.73	6.34	19.30	67.13
9	0.74	5.42	6.53	6.25	9.19	16.43	28.91
10	1.92	5.01	7.69	7.02	23.64	18.02	26.62

FE-based GDF	30 bridges	Training Algorithm: 'trainlm'					
ANN Architecture	10-(2-To-10)-(2-To-10)-1						
	Mean Error (%)				Max. Error (%)		
m	Design set	Indp. Test.	Addtl. Test.	CombinedTest.	Design set	Indp. Test.	Addtl. Test.
2	0.21	7.24	7.78	7.65	1.94	26.27	31.41
3	1.19	5.56	6.17	6.02	13.12	18.36	35.39
4	0.81	5.83	8.82	8.08	9.00	21.34	44.91
5	0.87	5.89	7.12	6.82	11.49	22.38	30.13
6	0.69	5.85	8.94	8.17	11.52	18.65	40.73
7	0.71	6.29	7.19	6.97	6.05	23.53	39.63
8	1.50	5.76	8.21	7.60	25.59	19.12	30.44
9	1.30	6.95	8.96	8.46	18.65	25.85	41.64
10	0.95	6.03	8.30	7.74	12.96	15.22	28.50

FE-based GDF	20 bridges	Training Algorithm: 'trainbr'					
ANN Architecture	10-(2-To-10)-1						
	Mean Error (%)				Max. Error (%)		
m	Design set	Indp. Test.	Addtl. Test.	CombinedTest.	Design set	Indp. Test.	Addtl. Test.
2	2.07	6.52	8.37	7.94	10.47	27.01	39.45
3	2.11	6.47	7.66	7.39	5.45	26.93	32.89
4	24.05	9.850	16.90	15.27	77.99	55.67	74.05
5	2.14	6.174	7.61	7.28	9.17	26.47	31.07
6	2.38	6.32	7.54	7.26	9.76	27.57	28.52
7	2.26	6.28	7.54	7.25	7.57	27.52	28.71
8	1.86	5.55	7.17	6.79	8.97	27.94	27.29
9	1.75	5.61	7.05	6.72	8.15	27.23	26.27
10	2.34	5.72	6.96	6.67	11.25	24.54	27.42

FE-based GDF	20 bridges	Training Algorithm: 'trainbr'					
ANN Architecture	10-(2-To-10)-(2-To-10)-1						
	Mean Error (%)				Max. Error (%)		
m	Design set	Indp. Test.	Addtl. Test.	CombinedTest.	Design set	Indp. Test.	Addtl. Test.
2	23.63	8.72	16.57	14.76	74.65	52.49	70.39
3	22.05	9.31	15.98	14.44	73.07	50.56	69.01
4	19.08	9.57	13.83	12.85	52.06	36.41	49.19
5	24.06	10.03	17.04	15.42	78.75	56.34	74.80
6	24.07	10.04	17.04	15.42	78.76	56.35	74.81
7	21.20	8.16	15.81	14.04	54.69	38.13	59.58
8	15.83	7.53	13.28	11.95	38.58	21.30	54.24
9	24.08	10.21	17.18	15.57	79.47	56.96	75.50
10	24.10	10.38	17.32	15.72	80.19	57.59	76.20

FE-based GDF	20 bridges	Training Algorithm: 'trainlm'					
ANN Architecture	10-(2-To-10)-1						
	Mean Error (%)				Max. Error (%)		
m	Design set	Indp. Test.	Addtl. Test.	CombinedTest.	Design set	Indp. Test.	Addtl. Test.
2	0.54	6.22	6.07	6.11	5.88	20.82	25.05
3	0.96	5.82	10.02	9.05	13.37	20.06	45.05
4	0.65	5.677	8.28	7.68	9.10	21.84	57.88
5	1.24	6.804	10.61	9.73	14.47	18.59	52.71
6	1.09	5.19	8.29	7.57	9.87	21.05	48.43
7	0.86	4.84	7.73	7.07	9.81	21.66	29.24
8	0.88	6.18	9.11	8.44	6.83	24.99	41.85
9	1.21	5.92	7.65	7.25	10.50	22.96	54.54
10	0.67	5.29	8.50	7.76	10.87	21.98	45.57

FE-based GDF	20 bridges	Training Algorithm: 'trainlm'					
ANN Architecture	10-(2-To-10)-(2-To-10)-1						
	Mean Error (%)				Max. Error (%)		
m	Design set	Indp. Test.	Addtl. Test.	CombinedTest.	Design set	Indp. Test.	Addtl. Test.
2	0.94	6.40	8.60	8.09	9.57	31.52	52.27
3	0.40	6.75	7.01	6.95	5.49	21.28	34.68
4	0.99	6.14	8.35	7.84	13.29	25.97	53.20
5	1.17	6.01	10.55	9.51	16.29	28.38	71.25
6	1.14	5.32	7.51	7.01	16.01	24.32	46.08
7	1.26	6.16	8.70	8.11	12.15	19.70	42.32
8	0.76	6.62	7.96	7.65	7.29	23.13	28.78
9	2.63	5.88	11.61	10.28	34.31	22.20	76.23
10	0.49	7.49	9.65	9.15	6.45	25.04	68.30

11.3.4 Shear ANN Optimzation Data

FE-based GDF	130 bridges	Training Algorithm: 'trainbr'					
ANN Architecture	10-(2-To-10)-1						
	Mean Error (%)				Max. Error (%)		
m	Design set	Indp. Test.	Addtl. Test.	CombinedTest.	Design set	Indp. Test.	Addtl. Test.
2	4.86	4.81			27.26	17.01	
3	4.12	3.94			27.83	13.63	
4	3.69	4.07			27.64	11.38	
5	3.70	4.11			21.27	10.97	
6	3.25	3.75			21.98	9.99	
7	3.42	3.76			22.35	11.79	
8	3.59	4.17			22.54	11.01	
9	3.63	4.02			22.62	11.58	
10	3.46	3.22			22.42	10.43	

FE-based GDF	130 bridges	Training Algorithm: 'trainbr'					
ANN Architecture	10-(2-To-10)-(2-To-10)-1						
	Mean Error (%)				Max. Error (%)		
m	Design set	Indp. Test.	Addtl. Test.	CombinedTest.	Design set	Indp. Test.	Addtl. Test.
2	5.71	4.66			26.61	13.47	
3	4.23	2.88			26.65	15.55	
4	3.78	4.15			23.19	11.33	
5	3.52	3.86			24.06	12.08	
6	16.86	7.92			56.63	26.72	
7	16.84	7.98			56.04	26.25	
8	16.87	7.90			56.90	26.94	
9	16.84	7.96			56.18	26.36	
10	3.59	5.58			51.28	18.61	

FE-based GDF	130 bridges	Training Algorithm: 'trainlm'					
ANN Architecture	10-(2-To-10)-1						
	Mean Error (%)				Max. Error (%)		
m	Design set	Indp. Test.	Addtl. Test.	CombinedTest.	Design set	Indp. Test.	Addtl. Test.
2	6.25	4.15			24.69	15.88	
3	4.07	4.70			28.33	11.52	
4	2.97	4.43			24.28	17.47	
5	2.75	5.21			31.01	12.34	
6	1.95	6.74			14.13	22.57	
7	1.90	7.02			36.53	32.03	
8	2.46	7.22			33.83	43.77	
9	1.67	7.66			39.89	30.96	
10	1.61	6.38			28.85	21.33	

FE-based GDF	130 bridges	Training Algorithm: 'trainlm'					
ANN Architecture	10-(2-To-10)-(2-To-10)-1						
	Mean Error (%)				Max. Error (%)		
m	Design set	Indp. Test.	Addtl. Test.	CombinedTest.	Design set	Indp. Test.	Addtl. Test.
2	5.39	3.67			27.99	11.50	
3	3.35	4.27			29.21	13.74	
4	2.51	6.43			24.61	24.86	
5	1.91	6.02			37.72	19.39	
6	1.79	9.74			32.02	27.18	
7	1.56	5.68			31.27	16.45	
8	1.21	6.96			31.92	19.70	
9	1.41	6.75			39.95	30.40	
10	1.24	6.55			23.76	18.62	

FE-based GDF	120 bridges	Training Algorithm: 'trainbr'					
ANN Architecture	10-(2-To-10)-1						
	Mean Error (%)				Max. Error (%)		
m	Design set	Indp. Test.	Addtl. Test.	CombinedTest.	Design set	Indp. Test.	Addtl. Test.
2	5.02	5.11	5.06	5.10	27.45	17.41	12.45
3	4.68	4.10	4.87	4.29	27.60	13.41	12.62
4	4.26	3.971	4.31	4.05	25.12	11.83	10.10
5	3.82	3.849	4.50	4.01	24.52	11.56	8.65
6	3.68	3.87	6.16	4.42	23.35	10.86	14.35
7	3.53	4.03	5.65	4.42	19.85	10.65	15.23
8	3.62	3.34	5.02	3.75	23.40	10.72	12.79
9	3.28	4.00	5.67	4.40	21.28	11.00	14.63
10	3.09	3.45	4.23	3.64	19.79	9.56	15.04

FE-based GDF	120 bridges	Training Algorithm: 'trainbr'					
ANN Architecture	10-(2-To-10)-(2-To-10)-1						
	Mean Error (%)				Max. Error (%)		
m	Design set	Indp. Test.	Addtl. Test.	CombinedTest.	Design set	Indp. Test.	Addtl. Test.
2	6.02	4.14	6.48	4.71	28.67	14.76	16.21
3	4.55	3.54	4.65	3.81	28.05	15.67	7.39
4	3.83	4.29	4.62	4.37	21.58	12.89	9.02
5	3.75	4.35	4.18	4.30	24.06	12.57	8.87
6	17.21	7.95	12.51	9.07	56.25	26.42	24.93
7	17.26	7.88	12.83	9.08	57.76	27.64	26.13
8	3.63	4.73	5.24	4.86	27.06	13.20	15.09
9	3.63	4.73	5.24	4.86	27.06	13.20	15.09
10	17.24	7.88	12.74	9.07	57.34	27.30	25.80

FE-based GDF	120 bridges	Training Algorithm: 'trainlm'					
ANN Architecture	10-(2-To-10)-1						
	Mean Error (%)				Max. Error (%)		
m	Design set	Indp. Test.	Addtl. Test.	CombinedTest.	Design set	Indp. Test.	Addtl. Test.
2	5.44	3.91	6.69	4.59	28.55	12.69	15.29
3	4.13	4.93	3.44	4.57	28.80	12.73	6.75
4	3.77	3.760	5.90	4.28	21.21	15.11	13.36
5	3.33	5.281	7.20	5.75	32.38	13.46	22.85
6	1.82	5.41	8.05	6.05	27.15	15.09	22.54
7	2.18	5.88	11.07	7.15	40.63	16.02	34.78
8	1.99	7.42	16.59	9.65	33.26	29.25	54.96
9	1.87	6.71	8.38	7.11	38.88	35.63	20.55
10	1.85	6.43	9.76	7.24	51.19	27.75	29.52

FE-based GDF	120 bridges	Training Algorithm: 'trainlm'					
ANN Architecture	10-(2-To-10)-(2-To-10)-1						
	Mean Error (%)				Max. Error (%)		
m	Design set	Indp. Test.	Addtl. Test.	CombinedTest.	Design set	Indp. Test.	Addtl. Test.
2	5.45	4.38	7.52	5.14	27.78	12.98	23.83
3	2.98	5.10	4.77	5.02	27.26	24.20	11.06
4	2.82	7.11	11.61	8.21	25.55	18.95	40.37
5	1.68	7.97	18.71	10.59	22.06	26.19	66.50
6	1.02	8.98	11.71	9.65	24.16	33.55	58.39
7	1.18	9.06	8.74	8.98	24.95	24.70	25.32
8	1.43	6.01	7.88	6.46	23.01	24.41	22.49
9	0.83	7.55	9.55	8.04	14.95	28.13	19.37
10	1.26	6.94	12.58	8.32	18.09	22.75	30.03

FE-based GDF	110 bridges	Training Algorithm: 'trainbr'					
ANN Architecture	10-(2-To-10)-1						
	Mean Error (%)				Max. Error (%)		
m	Design set	Indp. Test.	Addtl. Test.	CombinedTest.	Design set	Indp. Test.	Addtl. Test.
2	5.27	5.85	5.37	5.66	26.32	16.37	14.56
3	4.79	4.69	6.06	5.22	25.64	13.31	13.90
4	3.89	3.96	5.34	4.50	21.48	12.22	34.38
5	3.85	4.40	5.72	4.92	23.77	13.98	10.96
6	3.45	4.13	6.12	4.91	21.35	13.13	15.86
7	3.40	3.46	5.38	4.22	22.28	11.74	10.27
8	3.58	3.68	5.54	4.41	22.45	11.72	11.37
9	3.98	4.47	5.45	4.86	20.74	10.10	19.40
10	2.99	3.40	6.55	4.63	19.04	8.99	27.17

FE-based GDF	110 bridges	Training Algorithm: 'trainbr'					
ANN Architecture	10-(2-To-10)-(2-To-10)-1						
	Mean Error (%)				Max. Error (%)		
m	Design set	Indp. Test.	Addtl. Test.	CombinedTest.	Design set	Indp. Test.	Addtl. Test.
2	5.05	5.47	5.33	5.41	26.92	16.69	12.96
3	4.45	4.56	4.53	4.55	25.95	12.25	17.31
4	3.99	4.21	5.29	4.63	24.31	11.41	14.71
5	3.31	5.44	6.14	5.71	20.16	12.81	25.92
6	3.20	5.92	6.71	6.23	21.27	19.02	15.95
7	3.16	6.71	7.06	6.85	26.61	27.62	21.89
8	17.84	7.88	11.82	9.42	57.62	27.53	52.23
9	17.78	7.97	11.70	9.43	56.14	26.33	50.81
10	17.78	7.92	11.74	9.42	56.60	26.70	51.24

FE-based GDF	110 bridges	Training Algorithm: 'trainlm'					
ANN Architecture	10-(2-To-10)-1						
	Mean Error (%)				Max. Error (%)		
m	Design set	Indp. Test.	Addtl. Test.	CombinedTest.	Design set	Indp. Test.	Addtl. Test.
2	5.81	4.71	5.46	5.00	29.50	16.65	12.84
3	3.66	3.74	69.39	29.49	27.08	13.58	1305.61
4	3.39	4.61	8.60	6.17	17.46	15.07	44.97
5	3.09	7.00	7.20	7.08	18.81	21.06	38.36
6	2.39	7.02	15.42	10.31	34.32	20.20	73.45
7	1.87	8.36	10.43	9.17	19.10	49.74	28.11
8	1.58	8.66	12.41	10.13	27.69	40.98	34.86
9	1.55	10.95	15.53	12.74	21.08	39.55	41.47
10	1.78	8.17	19.04	12.43	31.47	23.38	86.53

FE-based GDF	110 bridges	Training Algorithm: 'trainlm'					
ANN Architecture	10-(2-To-10)-(2-To-10)-1						
	Mean Error (%)				Max. Error (%)		
m	Design set	Indp. Test.	Addtl. Test.	CombinedTest.	Design set	Indp. Test.	Addtl. Test.
2	5.12	4.07	5.31	4.56	27.47	13.82	16.13
3	2.97	4.50	7.01	5.49	24.16	13.58	23.21
4	2.58	6.29	12.70	8.80	40.91	26.79	86.86
5	1.51	7.84	7.82	7.83	29.72	34.82	29.18
6	1.20	6.36	7.07	6.64	32.07	17.98	22.01
7	1.51	7.14	16.26	10.72	28.02	29.17	69.71
8	1.33	6.97	9.76	8.06	33.22	23.06	24.44
9	1.18	6.89	12.87	9.23	20.68	30.61	34.08
10	1.56	6.04	10.75	7.89	24.65	21.43	31.95

FE-based GDF	100 bridges	Training Algorithm: 'trainbr'					
ANN Architecture	10-(2-To-10)-1						
	Mean Error (%)				Max. Error (%)		
m	Design set	Indp. Test.	Addtl. Test.	CombinedTest.	Design set	Indp. Test.	Addtl. Test.
2	5.34	5.81	5.80	5.81	25.92	16.07	16.18
3	4.58	4.07	4.52	4.29	27.05	13.00	14.72
4	4.02	4.78	5.82	5.29	21.97	21.02	41.03
5	3.42	4.421	7.80	6.08	18.94	11.99	34.56
6	3.65	4.05	5.55	4.79	20.68	15.69	35.40
7	3.40	4.16	6.53	5.33	18.35	14.55	30.77
8	3.34	4.71	7.12	5.90	19.72	23.65	41.52
9	3.17	4.77	8.68	6.69	18.35	15.54	32.61
10	8.10	4.45	5.82	5.13	25.37	15.17	19.35

FE-based GDF	100 bridges	Training Algorithm: 'trainbr'					
ANN Architecture	10-(2-To-10)-(2-To-10)-1						
	Mean Error (%)				Max. Error (%)		
m	Design set	Indp. Test.	Addtl. Test.	CombinedTest.	Design set	Indp. Test.	Addtl. Test.
2	6.40	4.42	5.02	4.72	26.72	14.52	11.97
3	4.48	5.12	6.69	5.89	25.88	21.15	35.07
4	3.73	4.48	7.14	5.79	21.17	11.68	27.12
5	18.09	7.87	13.37	10.57	58.72	28.42	53.30
6	18.06	7.87	13.30	10.54	58.33	28.10	52.91
7	18.02	7.88	13.13	10.47	57.34	27.30	51.96
8	18.02	7.88	13.11	10.46	57.20	27.19	51.83
9	18.06	7.87	13.28	10.53	58.20	27.99	52.79
10	18.02	7.88	13.15	10.47	57.45	27.39	52.07

FE-based GDF	100 bridges	Training Algorithm: 'trainlm'					
ANN Architecture	10-(2-To-10)-1						
	Mean Error (%)				Max. Error (%)		
m	Design set	Indp. Test.	Addtl. Test.	CombinedTest.	Design set	Indp. Test.	Addtl. Test.
2	6.07	3.97	5.68	4.81	29.04	11.98	15.32
3	4.31	6.22	8.29	7.24	24.60	22.22	38.87
4	2.79	5.37	5.43	5.40	32.15	15.99	47.97
5	3.14	7.347	9.06	8.19	29.86	24.28	33.63
6	2.20	9.26	11.57	10.39	25.35	21.31	38.32
7	2.21	9.91	9.38	9.65	30.66	35.78	38.51
8	1.64	10.08	16.71	13.34	35.12	31.12	70.72
9	0.73	9.80	14.33	12.02	17.68	44.12	65.73
10	1.43	9.90	14.07	11.95	29.75	23.44	75.28

FE-based GDF	100 bridges	Training Algorithm: 'trainlm'					
ANN Architecture	10-(2-To-10)-(2-To-10)-1						
	Mean Error (%)				Max. Error (%)		
m	Design set	Indp. Test.	Addtl. Test.	CombinedTest.	Design set	Indp. Test.	Addtl. Test.
2	5.12	3.88	9.92	6.85	27.31	12.98	125.83
3	3.62	6.18	19.50	12.73	25.44	19.70	343.63
4	2.18	5.53	10.17	7.81	30.86	18.57	35.13
5	1.71	10.35	17.80	14.02	24.03	34.33	56.84
6	1.71	7.16	8.78	7.96	33.41	21.67	28.39
7	1.45	7.53	9.40	8.45	38.33	21.39	51.15
8	1.32	9.21	10.24	9.72	18.86	24.13	32.35
9	0.86	7.82	10.23	9.00	23.77	43.59	28.72
10	1.03	7.96	11.08	9.49	22.19	25.67	55.01

FE-based GDF	90 bridges	Training Algorithm: 'trainbr'					
ANN Architecture	10-(2-To-10)-1						
	Mean Error (%)				Max. Error (%)		
m	Design set	Indp. Test.	Addtl. Test.	CombinedTest.	Design set	Indp. Test.	Addtl. Test.
2	5.13	7.65	7.27	7.43	24.64	20.83	19.60
3	4.46	4.98	7.53	6.41	25.17	14.07	28.78
4	3.87	5.22	6.07	5.70	23.49	18.48	29.97
5	4.15	4.24	5.24	4.81	23.81	22.10	31.72
6	3.49	5.82	7.90	6.99	18.30	14.00	31.48
7	3.76	4.51	5.92	5.31	18.84	13.52	20.26
8	4.12	5.70	7.18	6.54	25.57	17.73	25.90
9	4.14	4.44	6.79	5.77	25.03	10.20	22.16
10	4.22	4.82	7.30	6.22	23.85	14.16	31.21

FE-based GDF	90 bridges	Training Algorithm: 'trainbr'					
ANN Architecture	10-(2-To-10)-(2-To-10)-1						
	Mean Error (%)				Max. Error (%)		
m	Design set	Indp. Test.	Addtl. Test.	CombinedTest.	Design set	Indp. Test.	Addtl. Test.
2	6.65	4.35	5.29	4.88	26.92	10.87	22.11
3	4.48	6.29	7.35	6.89	25.35	16.10	23.48
4	4.14	5.81	7.30	6.65	23.21	20.70	37.68
5	18.80	7.87	12.96	10.74	58.74	28.43	53.31
6	18.91	7.89	13.25	10.91	60.19	29.61	54.72
7	4.04	7.57	9.19	8.48	23.59	19.86	34.86
8	18.78	7.87	12.94	10.72	58.57	28.29	53.15
9	18.77	7.87	12.89	10.70	58.24	28.02	52.83
10	18.82	7.86	13.02	10.77	59.05	28.68	53.61

FE-based GDF	90 bridges	Training Algorithm: 'trainlm'					
ANN Architecture	10-(2-To-10)-1						
	Mean Error (%)				Max. Error (%)		
m	Design set	Indp. Test.	Addtl. Test.	CombinedTest.	Design set	Indp. Test.	Addtl. Test.
2	5.98	5.12	7.46	6.44	28.02	19.75	24.80
3	3.04	6.59	9.46	8.20	15.94	24.38	54.46
4	2.90	7.80	9.57	8.79	23.40	19.61	58.63
5	2.02	8.80	12.27	10.75	17.92	28.28	40.00
6	2.60	11.54	10.77	11.11	23.99	24.99	35.55
7	1.43	12.28	14.72	13.65	18.47	37.13	58.38
8	1.21	7.79	13.28	10.88	17.35	30.19	72.34
9	1.85	11.20	16.50	14.19	28.81	30.65	72.25
10	0.96	9.09	13.82	11.76	13.77	36.40	67.43

FE-based GDF	90 bridges	Training Algorithm: 'trainlm'					
ANN Architecture	10-(2-To-10)-(2-To-10)-1						
	Mean Error (%)				Max. Error (%)		
m	Design set	Indp. Test.	Addtl. Test.	CombinedTest.	Design set	Indp. Test.	Addtl. Test.
2	5.94	4.58	29.78	18.78	27.99	19.28	946.46
3	3.72	7.62	7.99	7.82	29.80	19.62	22.03
4	2.05	7.50	12.66	10.40	75.29	23.96	72.42
5	1.98	7.58	12.80	10.52	45.14	26.31	47.36
6	1.32	10.26	15.74	13.35	18.52	45.61	51.38
7	1.88	8.91	14.59	12.11	22.66	25.86	90.94
8	1.66	7.17	8.78	8.08	24.40	17.36	28.32
9	1.37	9.09	9.53	9.34	28.01	23.77	30.76
10	1.49	8.13	10.10	9.24	25.28	20.47	39.44

FE-based GDF	80 bridges	Training Algorithm: 'trainbr'						FE-based GDF	80 bridges	Training Algorithm: 'trainbr'					
ANN Architecture	10-(2-To-10)-1							ANN Architecture	10-(2-To-10)-(2-To-10)-1						
	Mean Error (%)				Max. Error (%)				Mean Error (%)				Max. Error (%)		
m	Design set	Indp. Test.	Addtl. Test.	CombinedTest.	Design set	Indp. Test.	Addtl. Test.	m	Design set	Indp. Test.	Addtl. Test.	CombinedTest.	Design set	Indp. Test.	Addtl. Test.
2	5.50	7.23	7.33	7.29	22.92	19.36	22.73	2	6.84	5.17	6.57	6.03	24.64	13.28	25.58
3	4.97	5.23	7.64	6.72	22.54	15.81	26.08	3	4.51	6.16	7.31	6.87	24.38	14.72	26.60
4	4.00	4.473	7.14	6.12	22.73	11.58	26.07	4	19.03	7.88	13.53	11.37	57.68	27.57	52.29
5	4.38	4.946	6.77	6.07	24.23	12.51	24.00	5	19.19	7.88	13.91	11.60	60.13	29.56	54.65
6	4.07	4.87	6.99	6.18	23.53	11.43	27.34	6	19.07	7.87	13.61	11.41	58.38	28.14	52.96
7	4.19	4.54	6.26	5.60	25.34	13.55	23.06	7	19.12	7.86	13.73	11.48	59.14	28.76	53.70
8	8.40	5.10	7.13	6.35	24.93	18.46	24.66	8	19.07	7.87	13.63	11.42	58.48	28.22	53.06
9	4.27	5.48	7.15	6.51	23.49	12.53	26.73	9	19.08	7.87	13.63	11.43	58.54	28.27	53.12
10	3.96	5.31	7.25	6.51	23.01	11.65	29.70	10	19.23	7.90	14.01	11.67	60.68	30.00	55.19

FE-based GDF	80 bridges	Training Algorithm: 'trainlm'						FE-based GDF	80 bridges	Training Algorithm: 'trainlm'					
ANN Architecture	10-(2-To-10)-1							ANN Architecture	10-(2-To-10)-(2-To-10)-1						
	Mean Error (%)				Max. Error (%)				Mean Error (%)				Max. Error (%)		
m	Design set	Indp. Test.	Addtl. Test.	CombinedTest.	Design set	Indp. Test.	Addtl. Test.	m	Design set	Indp. Test.	Addtl. Test.	CombinedTest.	Design set	Indp. Test.	Addtl. Test.
2	5.91	4.57	6.34	5.66	27.28	18.07	21.90	2	5.94	4.40	7.98	6.61	25.82	17.06	49.79
3	3.58	7.52	7.67	7.61	23.19	19.51	21.56	3	3.08	8.59	10.41	9.72	23.10	25.36	69.68
4	3.39	7.268	10.63	9.34	30.71	18.36	57.58	4	1.41	10.57	14.96	13.28	24.94	27.37	67.16
5	2.53	10.143	10.90	10.61	27.70	24.55	41.44	5	1.47	10.49	13.27	12.21	20.91	25.62	50.67
6	2.71	9.67	11.19	10.61	69.91	27.89	38.89	6	1.78	10.61	9.77	10.09	34.59	25.06	49.03
7	2.00	8.74	11.65	10.54	28.67	23.48	97.87	7	1.62	8.04	10.16	9.35	40.01	24.90	89.61
8	2.38	8.97	10.77	10.08	34.95	25.84	29.09	8	1.20	7.97	11.49	10.14	21.06	20.94	60.48
9	1.60	9.64	10.06	9.90	27.98	42.49	51.34	9	1.62	8.64	11.40	10.35	29.81	18.69	67.11
10	1.98	9.35	14.42	12.48	44.07	23.38	64.13	10	1.33	7.53	15.78	12.62	19.37	24.30	90.50

FE-based GDF	70 bridges	Training Algorithm: 'trainbr'						FE-based GDF	70 bridges	Training Algorithm: 'trainbr'					
ANN Architecture	10-(2-To-10)-1							ANN Architecture	10-(2-To-10)-(2-To-10)-1						
	Mean Error (%)				Max. Error (%)				Mean Error (%)				Max. Error (%)		
m	Design set	Indp. Test.	Addtl. Test.	CombinedTest.	Design set	Indp. Test.	Addtl. Test.	m	Design set	Indp. Test.	Addtl. Test.	CombinedTest.	Design set	Indp. Test.	Addtl. Test.
2	7.46	6.60	10.18	8.96	23.73	25.01	59.58	2	5.74	5.56	5.98	5.83	25.25	11.88	20.93
3	5.18	5.34	6.78	6.29	22.46	15.63	23.56	3	5.44	5.73	7.07	6.61	23.53	15.92	31.06
4	4.24	4.97	6.24	5.81	23.61	12.09	33.64	4	19.00	7.87	14.63	12.33	58.53	28.26	53.11
5	9.13	5.30	7.70	6.88	28.93	18.50	26.88	5	18.99	7.87	14.63	12.32	58.47	28.22	53.05
6	8.89	4.85	6.73	6.09	25.47	15.88	23.09	6	19.02	7.87	14.66	12.35	58.83	28.50	53.40
7	8.80	5.88	7.31	6.82	24.73	19.71	27.64	7	18.98	7.87	14.62	12.32	58.38	28.14	52.96
8	4.34	4.14	6.72	5.84	24.51	10.55	27.43	8	18.94	7.88	14.58	12.30	57.83	27.70	52.44
9	8.83	4.87	6.87	6.19	24.94	16.88	22.61	9	19.02	7.87	14.66	12.35	58.83	28.51	53.40
10	8.74	5.36	6.71	6.25	25.56	18.22	25.85	10	19.02	7.87	14.66	12.34	58.81	28.49	53.38

FE-based GDF	70 bridges	Training Algorithm: 'trainlm'						FE-based GDF	70 bridges	Training Algorithm: 'trainlm'					
ANN Architecture	10-(2-To-10)-1							ANN Architecture	10-(2-To-10)-(2-To-10)-1						
	Mean Error (%)				Max. Error (%)				Mean Error (%)				Max. Error (%)		
m	Design set	Indp. Test.	Addtl. Test.	CombinedTest.	Design set	Indp. Test.	Addtl. Test.	m	Design set	Indp. Test.	Addtl. Test.	CombinedTest.	Design set	Indp. Test.	Addtl. Test.
2	6.54	5.77	7.75	7.07	27.90	24.20	28.81	2	6.24	6.37	8.21	7.59	26.15	16.38	31.46
3	4.44	8.30	8.30	8.30	22.29	22.75	76.03	3	3.21	9.38	12.75	11.60	22.30	21.45	74.18
4	3.17	9.47	8.41	8.77	32.05	25.10	30.58	4	2.04	13.90	15.29	14.82	36.82	47.33	69.97
5	2.55	12.11	19.75	17.15	47.05	31.82	293.07	5	1.62	11.36	11.77	11.63	32.79	38.29	73.50
6	1.62	11.59	15.17	13.95	25.70	38.47	72.88	6	1.80	10.73	14.51	13.22	42.58	36.30	68.63
7	2.00	10.57	13.73	12.65	36.97	35.77	86.14	7	2.39	8.69	13.58	11.92	41.97	30.26	53.89
8	1.91	9.23	10.91	10.34	32.43	18.14	58.51	8	1.73	10.09	12.54	11.71	23.90	22.01	71.36
9	1.89	12.22	13.09	12.79	27.59	26.05	69.16	9	1.59	9.56	10.07	9.89	22.90	35.83	38.06
10	1.64	11.56	12.71	12.32	37.74	32.76	49.47	10	2.31	8.93	9.26	9.15	37.29	21.77	55.94

FE-based GDF	60 bridges	Training Algorithm: 'trainbr'					
ANN Architecture	10-(2-To-10)-1						
	Mean Error (%)				Max. Error (%)		
m	Design set	Indp. Test.	Addtl. Test.	CombinedTest.	Design set	Indp. Test.	Addtl. Test.
2	6.09	5.39	6.11	5.89	23.59	13.42	19.74
3	4.82	5.37	7.20	6.64	22.10	16.52	27.55
4	9.45	5.07	7.28	6.60	24.54	17.09	23.94
5	9.56	4.80	6.99	6.32	23.72	16.64	22.05
6	9.35	5.16	7.17	6.55	24.41	16.78	25.51
7	8.99	5.06	7.14	6.50	26.14	16.01	24.15
8	9.23	4.69	7.06	6.33	24.77	15.39	22.24
9	9.38	5.05	6.86	6.30	25.39	17.89	23.84
10	9.23	4.96	7.26	6.55	25.05	18.03	24.86

FE-based GDF	60 bridges	Training Algorithm: 'trainbr'					
ANN Architecture	10-(2-To-10)-(2-To-10)-1						
	Mean Error (%)				Max. Error (%)		
m	Design set	Indp. Test.	Addtl. Test.	CombinedTest.	Design set	Indp. Test.	Addtl. Test.
2	6.10	7.81	6.77	7.09	22.87	18.93	24.43
3	4.76	5.15	7.97	7.11	23.81	15.09	36.48
4	19.95	7.87	14.36	12.37	57.98	27.81	52.58
5	19.85	7.89	14.34	12.36	57.15	27.15	51.78
6	19.84	7.89	14.34	12.36	57.05	27.06	51.68
7	19.83	7.90	14.34	12.36	56.98	27.01	51.61
8	19.84	7.89	14.34	12.36	57.06	27.08	51.69
9	19.76	7.99	14.33	12.39	56.01	26.22	50.67
10	19.89	7.88	14.35	12.36	57.55	27.47	52.16

FE-based GDF	60 bridges	Training Algorithm: 'trainlm'					
ANN Architecture	10-(2-To-10)-1						
	Mean Error (%)				Max. Error (%)		
m	Design set	Indp. Test.	Addtl. Test.	CombinedTest.	Design set	Indp. Test.	Addtl. Test.
2	6.46	5.65	7.75	7.10	27.62	24.91	33.22
3	3.86	7.35	14.16	12.07	27.85	21.33	74.09
4	2.25	9.198	10.77	10.29	28.00	39.97	49.21
5	2.48	8.467	12.97	11.59	40.28	33.72	52.17
6	1.81	9.70	10.75	10.43	25.54	30.58	39.32
7	1.11	11.83	15.76	14.55	14.67	36.96	87.65
8	2.05	11.14	11.16	11.16	31.40	29.67	46.15
9	1.17	8.22	15.53	13.29	24.17	30.53	141.17
10	1.39	8.37	12.64	11.33	25.03	53.49	100.19

FE-based GDF	60 bridges	Training Algorithm: 'trainlm'					
ANN Architecture	10-(2-To-10)-(2-To-10)-1						
	Mean Error (%)				Max. Error (%)		
m	Design set	Indp. Test.	Addtl. Test.	CombinedTest.	Design set	Indp. Test.	Addtl. Test.
2	6.04	7.16	8.37	8.00	43.96	25.07	38.99
3	1.67	10.49	16.43	14.61	27.37	61.73	226.36
4	2.22	10.35	14.81	13.44	54.62	39.89	58.54
5	2.57	7.62	10.42	9.56	48.51	32.71	50.14
6	1.72	9.63	10.57	10.29	27.50	23.20	45.43
7	2.09	10.06	13.54	12.47	21.86	27.37	67.88
8	1.93	7.78	11.27	10.20	20.58	19.25	98.83
9	1.30	9.14	11.00	10.43	34.74	23.48	36.49
10	1.46	9.86	10.29	10.15	25.68	25.62	39.90

FE-based GDF	50 bridges	Training Algorithm: 'trainbr'						FE-based GDF	50 bridges	Training Algorithm: 'trainbr'					
ANN Architecture	10-(2-To-10)-1							ANN Architecture	10-(2-To-10)-(2-To-10)-1						
	Mean Error (%)				Max. Error (%)				Mean Error (%)				Max. Error (%)		
m	Design set	Indp. Test.	Addtl. Test.	CombinedTest.	Design set	Indp. Test.	Addtl. Test.	m	Design set	Indp. Test.	Addtl. Test.	CombinedTest.	Design set	Indp. Test.	Addtl. Test.
2	5.51	6.87	10.21	9.28	25.61	26.46	51.78	2	5.26	7.56	10.79	9.89	22.84	26.94	60.34
3	4.96	5.69	7.77	7.19	22.69	25.94	29.42	3	21.40	7.99	13.99	12.31	56.01	26.22	50.68
4	8.69	5.159	7.56	6.89	27.67	18.40	23.80	4	21.58	7.88	13.99	12.28	57.57	27.49	52.19
5	8.78	5.150	7.71	6.99	26.96	18.59	23.22	5	21.49	7.90	13.98	12.28	56.89	26.93	51.53
6	8.94	4.97	7.51	6.80	27.83	18.64	23.58	6	21.66	7.87	14.00	12.29	58.06	27.88	52.66
7	8.69	4.87	7.71	6.92	28.98	18.48	22.82	7	21.50	7.90	13.98	12.28	56.96	26.99	51.59
8	8.60	5.30	7.71	7.04	27.72	19.14	23.44	8	21.74	7.87	14.01	12.29	58.53	28.26	53.11
9	9.16	4.82	7.66	6.87	28.71	18.76	23.67	9	21.70	7.87	14.00	12.29	58.33	28.10	52.92
10	8.79	5.03	7.99	7.16	28.91	18.75	23.05	10	21.44	7.92	13.98	12.29	56.53	26.64	51.18

FE-based GDF	50 bridges	Training Algorithm: 'trainlm'						FE-based GDF	50 bridges	Training Algorithm: 'trainlm'					
ANN Architecture	10-(2-To-10)-1							ANN Architecture	10-(2-To-10)-(2-To-10)-1						
	Mean Error (%)				Max. Error (%)				Mean Error (%)				Max. Error (%)		
m	Design set	Indp. Test.	Addtl. Test.	CombinedTest.	Design set	Indp. Test.	Addtl. Test.	m	Design set	Indp. Test.	Addtl. Test.	CombinedTest.	Design set	Indp. Test.	Addtl. Test.
2	4.91	9.62	19.75	16.92	23.05	33.20	456.72	2	4.72	9.09	10.86	10.36	41.24	25.70	40.39
3	2.61	8.29	10.45	9.84	25.14	23.59	47.28	3	3.16	10.66	12.58	12.05	48.56	27.45	37.51
4	2.15	12.139	13.26	12.95	30.99	34.45	55.38	4	1.75	9.08	12.10	11.26	27.45	30.08	64.24
5	1.47	7.521	12.94	11.42	30.85	25.18	84.48	5	2.21	7.89	8.13	8.06	33.77	26.01	30.03
6	1.77	9.70	13.73	12.60	25.66	26.51	143.27	6	2.42	7.90	9.46	9.02	39.47	22.36	32.37
7	1.99	8.41	11.32	10.51	28.82	28.29	38.77	7	1.27	8.27	10.05	9.56	32.90	20.38	65.60
8	1.66	8.40	11.21	10.43	31.26	39.32	71.05	8	1.53	8.87	11.73	10.93	28.17	33.14	43.53
9	1.89	6.73	11.38	10.08	33.33	24.12	83.45	9	0.90	9.17	10.03	9.79	13.10	26.42	50.36
10	1.57	8.40	11.41	10.57	35.48	25.06	57.37	10	1.64	7.05	9.79	9.02	32.78	19.01	51.26

FE-based GDF	40 bridges	Training Algorithm: 'trainbr'					
ANN Architecture	10-(2-To-10)-1						
	Mean Error (%)				Max. Error (%)		
m	Design set	Indp. Test.	Addtl. Test.	CombinedTest.	Design set	Indp. Test.	Addtl. Test.
2	8.54	7.24	8.67	8.30	26.00	19.15	28.88
3	8.84	6.43	8.53	7.99	25.69	18.19	26.79
4	8.61	6.825	8.84	8.32	25.17	18.99	28.04
5	8.97	6.512	8.75	8.18	25.59	19.61	28.95
6	8.79	6.41	8.63	8.06	25.41	18.68	26.83
7	8.48	6.26	8.59	8.00	26.03	16.96	26.15
8	8.76	6.28	8.70	8.08	24.82	17.88	27.51
9	8.30	6.57	8.84	8.26	25.82	18.98	27.25
10	8.79	6.12	8.54	7.92	25.79	17.45	26.59

FE-based GDF	40 bridges	Training Algorithm: 'trainbr'					
ANN Architecture	10-(2-To-10)-(2-To-10)-1						
	Mean Error (%)				Max. Error (%)		
m	Design set	Indp. Test.	Addtl. Test.	CombinedTest.	Design set	Indp. Test.	Addtl. Test.
2	23.72	7.88	13.89	12.35	57.64	27.54	52.25
3	23.47	7.96	13.90	12.38	56.18	26.36	50.84
4	23.55	7.91	13.89	12.35	56.73	26.81	51.38
5	23.50	7.94	13.89	12.37	56.38	26.52	51.03
6	23.64	7.89	13.88	12.35	57.19	27.18	51.81
7	23.60	7.90	13.88	12.35	57.00	27.02	51.63
8	23.31	8.14	13.94	12.45	55.14	25.52	49.83
9	23.22	8.25	13.96	12.50	54.56	25.05	49.27
10	23.30	8.16	13.94	12.46	55.05	25.45	49.75

FE-based GDF	40 bridges	Training Algorithm: 'trainlm'					
ANN Architecture	10-(2-To-10)-1						
	Mean Error (%)				Max. Error (%)		
m	Design set	Indp. Test.	Addtl. Test.	CombinedTest.	Design set	Indp. Test.	Addtl. Test.
2	23.30	8.16	13.94	12.46	55.05	25.45	49.75
3	2.47	11.24	17.27	15.73	43.82	51.31	87.01
4	1.50	10.267	13.28	12.51	40.92	30.33	78.71
5	1.69	9.351	14.67	13.31	22.56	28.01	69.27
6	1.33	8.69	9.74	9.47	26.58	27.54	50.54
7	2.28	8.73	11.12	10.51	37.61	26.36	74.76
8	1.74	7.52	10.81	9.96	33.77	25.04	59.39
9	1.67	7.04	10.16	9.36	32.02	28.65	54.43
10	1.44	8.68	10.92	10.35	30.67	29.82	37.70

FE-based GDF	40 bridges	Training Algorithm: 'trainlm'					
ANN Architecture	10-(2-To-10)-(2-To-10)-1						
	Mean Error (%)				Max. Error (%)		
m	Design set	Indp. Test.	Addtl. Test.	CombinedTest.	Design set	Indp. Test.	Addtl. Test.
2	1.46	11.97	15.55	14.63	13.57	34.92	68.47
3	2.09	12.47	17.76	16.40	27.25	39.65	112.72
4	1.32	10.74	13.03	12.44	27.48	26.58	90.17
5	1.72	9.45	11.11	10.68	33.83	30.04	56.94
6	2.24	8.92	12.95	11.92	28.23	43.68	71.22
7	1.27	7.71	10.03	9.44	33.58	22.27	64.90
8	0.75	10.69	14.64	13.63	12.67	22.98	117.02
9	1.74	7.38	11.30	10.29	29.51	22.58	85.38
10	2.04	5.40	8.78	7.92	32.72	17.99	57.50

FE-based GDF	30 bridges	Training Algorithm: 'trainbr'						FE-based GDF	30 bridges	Training Algorithm: 'trainbr'					
ANN Architecture	10-(2-To-10)-1							ANN Architecture	10-(2-To-10)-(2-To-10)-1						
	Mean Error (%)				Max. Error (%)				Mean Error (%)				Max. Error (%)		
m	Design set	Indp. Test.	Addtl. Test.	CombinedTest.	Design set	Indp. Test.	Addtl. Test.	m	Design set	Indp. Test.	Addtl. Test.	CombinedTest.	Design set	Indp. Test.	Addtl. Test.
2	11.48	5.94	8.88	8.18	26.55	20.42	30.17	2	22.86	8.00	15.03	13.37	55.95	26.18	50.62
3	11.66	5.85	8.95	8.21	27.99	21.24	31.52	3	22.90	7.97	15.02	13.35	56.14	26.33	50.80
4	10.82	5.839	8.91	8.18	23.38	18.65	28.38	4	22.63	8.22	15.07	13.45	54.71	25.17	49.42
5	11.55	5.076	8.59	7.76	24.55	17.46	28.59	5	22.47	8.40	15.12	13.53	53.86	24.48	48.60
6	10.92	6.01	8.41	7.84	24.51	19.83	28.40	6	22.60	8.24	15.07	13.46	54.56	25.05	49.28
7	11.46	5.73	9.27	8.43	23.62	18.11	30.55	7	22.51	8.35	15.10	13.50	54.06	24.65	48.79
8	11.54	5.44	8.64	7.88	24.14	18.71	29.05	8	22.65	8.20	15.06	13.44	54.83	25.27	49.54
9	10.96	5.59	8.35	7.69	24.44	18.96	28.59	9	22.37	8.52	15.16	13.58	53.30	24.03	48.06
10	10.31	6.27	8.71	8.13	25.01	19.30	29.99	10	22.12	8.88	15.27	13.76	51.65	22.70	46.47

FE-based GDF	30 bridges	Training Algorithm: 'trainlm'						FE-based GDF	30 bridges	Training Algorithm: 'trainlm'					
ANN Architecture	10-(2-To-10)-1							ANN Architecture	10-(2-To-10)-(2-To-10)-1						
	Mean Error (%)				Max. Error (%)				Mean Error (%)				Max. Error (%)		
m	Design set	Indp. Test.	Addtl. Test.	CombinedTest.	Design set	Indp. Test.	Addtl. Test.	m	Design set	Indp. Test.	Addtl. Test.	CombinedTest.	Design set	Indp. Test.	Addtl. Test.
2	3.98	12.05	20.02	18.13	40.55	41.78	76.49	2	22.18	8.79	15.24	13.72	52.04	23.01	46.84
3	1.74	10.77	13.14	12.58	30.57	28.67	83.69	3	1.63	10.33	14.84	13.77	28.93	48.43	49.73
4	2.08	9.412	9.85	9.75	25.71	34.66	31.52	4	1.72	10.63	15.63	14.45	23.39	32.45	52.02
5	2.77	8.649	10.98	10.43	32.95	29.53	45.09	5	0.58	12.01	14.44	13.86	7.70	37.43	47.34
6	3.23	7.36	9.57	9.05	35.84	31.88	30.40	6	2.18	12.12	12.84	12.67	18.40	32.06	48.18
7	2.79	10.60	10.18	10.28	41.60	35.84	53.99	7	1.78	7.92	13.92	12.50	17.46	28.39	81.36
8	2.60	8.24	12.46	11.46	34.88	23.51	72.40	8	2.22	7.30	12.46	11.24	34.34	25.61	72.82
9	1.42	10.30	14.33	13.38	13.73	27.26	68.10	9	0.77	12.44	16.10	15.24	7.16	36.71	102.03
10	2.06	10.32	8.53	8.95	32.33	23.56	45.34	10	2.30	8.42	12.01	11.16	32.83	28.10	55.59

FE-based GDF	20 bridges	Training Algorithm: 'trainbr'					
ANN Architecture	10-(2-To-10)-1						
	Mean Error (%)				Max. Error (%)		
m	Design set	Indp. Test.	Addtl. Test.	CombinedTest.	Design set	Indp. Test.	Addtl. Test.
2	22.17	7.97	15.87	14.14	56.15	26.33	50.81
3	22.43	7.88	15.89	14.13	57.41	27.35	52.03
4	22.43	7.881	15.89	14.13	57.41	27.35	52.03
5	22.06	8.053	15.88	14.16	55.63	25.92	50.31
6	22.33	7.90	15.88	14.12	56.95	26.99	51.57
7	22.21	7.94	15.87	14.13	56.38	26.52	51.03
8	22.14	7.98	15.87	14.13	56.05	26.27	50.70
9	22.22	7.93	15.87	14.12	56.44	26.59	51.08
10	22.23	7.93	15.87	14.13	56.48	26.60	51.12

FE-based GDF	20 bridges	Training Algorithm: 'trainbr'					
ANN Architecture	10-(2-To-10)-(2-To-10)-1						
	Mean Error (%)				Max. Error (%)		
m	Design set	Indp. Test.	Addtl. Test.	CombinedTest.	Design set	Indp. Test.	Addtl. Test.
2	22.17	7.97	15.87	14.14	56.15	26.33	50.81
3	22.09	8.03	15.88	14.15	55.78	26.04	50.46
4	22.19	7.95	15.87	14.13	56.26	26.43	50.92
5	22.12	8.00	15.88	14.14	55.94	26.17	50.61
6	21.89	8.20	15.89	14.20	54.80	25.25	49.51
7	21.91	8.18	15.89	14.20	54.91	25.34	49.62
8	22.03	8.08	15.88	14.17	55.49	25.80	50.17
9	21.95	8.15	15.89	14.19	55.10	25.49	49.80
10	21.75	8.34	15.91	14.25	54.12	24.69	48.85

FE-based GDF	20 bridges	Training Algorithm: 'trainlm'					
ANN Architecture	10-(2-To-10)-1						
	Mean Error (%)				Max. Error (%)		
m	Design set	Indp. Test.	Addtl. Test.	CombinedTest.	Design set	Indp. Test.	Addtl. Test.
2	2.16	9.65	15.52	14.23	27.94	36.77	65.21
3	2.91	9.27	16.36	14.80	37.48	33.15	82.85
4	3.42	9.932	12.75	12.13	34.45	35.85	46.85
5	4.01	9.285	16.47	14.89	45.91	37.53	85.50
6	1.06	12.13	16.84	15.80	9.71	41.51	72.12
7	2.23	8.68	15.41	13.93	41.68	31.65	67.15
8	3.97	9.62	17.12	15.47	29.43	29.48	62.70
9	1.99	10.01	15.30	14.14	21.73	36.40	74.56
10	4.07	9.73	15.05	13.88	56.09	30.28	66.58

FE-based GDF	20 bridges	Training Algorithm: 'trainlm'					
ANN Architecture	10-(2-To-10)-(2-To-10)-1						
	Mean Error (%)				Max. Error (%)		
m	Design set	Indp. Test.	Addtl. Test.	CombinedTest.	Design set	Indp. Test.	Addtl. Test.
2	4.07	9.73	15.05	13.88	56.09	30.28	66.58
3	1.53	9.28	14.82	13.60	13.25	30.87	66.51
4	0.43	10.88	16.76	15.47	7.52	29.32	75.85
5	2.27	10.34	15.83	14.62	28.29	34.56	81.47
6	2.29	9.54	14.57	13.46	26.66	48.83	68.45
7	5.24	10.20	14.56	13.60	45.04	32.89	51.68
8	0.56	12.38	13.68	13.40	7.37	36.09	61.72
9	3.18	9.12	12.22	11.54	26.33	29.64	53.23
10	0.45	11.42	14.73	14.00	3.69	41.88	68.54

11.4 Rating Factors

Note that ANN rating factors are not shown for bridges that were identified as outliers. Bridges 1-100 are bridges that were gathered for this current study. Bridges 101-174 were made available by Sofi's pilot study (2017).

Table 51. Operating Rating Factors for Bridges in this Study

		Moment LRFR Operating RF			Shear LRFR Operating RF			ANN Benefit	
Bridge #	Bridge ID	AASHTO	FEM	ANN	AASHTO	FEM	ANN	Moment ANN Benefit	Shear ANN Benefit
1	C006313310P	1.48	1.81	1.60	1.27	1.99	1.72	1.08	1.36
2	C006305115	1.78	2.11	2.10	1.85	2.67	2.78	1.18	1.50
3	C001705805	1.61	2.16	2.02	1.89	1.84	1.99	1.25	1.05
4	C001902340	1.82	2.11	1.93	2.22	2.74	2.53	1.06	1.14
5	C005922330	0.92	1.09	1.02	2.03	2.59	2.39	1.12	1.18
6	C001903310	0.74	1.58	#N/A	1.72	2.96	2.65	#N/A	1.54
7	C001823610	1.11	1.41	1.38	2.54	3.00	2.76	1.24	1.09
8	C007443235	1.89	2.24	2.01	2.02	3.50	3.36	1.07	1.66
9	C009133625	0.82	1.40	1.31	2.46	3.32	3.27	1.61	1.33
10	C001111430	1.92	2.20	2.16	2.62	2.88	2.69	1.13	1.03
11	C008402410	1.48	1.59	1.56	2.75	2.88	2.99	1.05	1.08
12	C005901410	1.08	1.24	1.14	3.03	3.38	3.34	1.06	1.10
13	C003403910	1.43	1.63	1.62	3.37	3.63	3.45	1.13	1.02
14	C002902505	1.36	1.61	1.51	3.56	5.41	5.30	1.11	1.49
15	C001403305P	0.99	1.12	0.97	4.27	4.58	4.47	0.98	1.05
16	C007424540	1.18	1.40	1.34	4.25	5.85	#N/A	1.14	#N/A

17	C006710205	1.22	1.45	1.37	4.41	4.71	4.60	1.13	1.04
18	C007025010	1.33	1.55	1.41	4.96	5.31	5.30	1.06	1.07
19	C000102908	1.35	1.59	1.46	5.08	5.58	5.38	1.09	1.06
20	C000134022	2.92	3.18	3.01	3.78	4.11	4.05	1.03	1.07
21	C000602505	1.21	1.65	1.55	1.90	2.30	2.26	1.28	1.19
22	C001101705	1.35	1.60	1.45	2.94	3.37	3.10	1.07	1.05
23	C001800605	1.24	1.65	1.62	2.64	3.03	2.81	1.30	1.07
24	C001814715	1.26	1.62	1.59	2.82	3.35	3.11	1.27	1.10
25	C002000707P	2.37	3.07	2.85	2.98	3.36	3.24	1.20	1.09
26	C002000823	2.59	3.37	3.05	2.60	3.05	2.81	1.18	1.08
27	C002001505	2.58	2.97	3.04	2.85	2.73	3.03	1.17	1.06
28	C002004725	1.60	2.16	2.11	2.89	3.23	3.12	1.32	1.08
29	C002004730	2.44	3.23	2.95	2.69	3.04	2.94	1.21	1.09
30	C002701945	0.94	1.14	1.08	3.08	3.15	2.96	1.15	0.96
31	C002702510	1.48	1.78	1.62	2.80	4.63	4.05	1.10	1.45
32	C002704210P	1.17	1.43	1.37	2.64	3.30	3.19	1.17	1.21
33	C003303710	1.18	1.51	1.35	4.62	5.75	5.09	1.15	1.10
34	C003314210	1.65	2.31	1.82	6.33	7.31	6.80	1.11	1.07
35	C003406020	1.16	1.51	1.38	2.25	2.25	2.27	1.19	1.01
36	C003413410	0.74	1.00	0.94	2.40	2.41	2.36	1.28	0.98
37	C003704805P	1.65	1.81	1.74	3.22	3.45	3.36	1.05	1.05
38	C004800415	1.61	1.79	1.73	4.12	4.67	4.32	1.08	1.05
39	C004802905	3.80	4.72	4.02	2.40	4.44	4.14	1.06	1.73
40	C004803915	1.42	2.72	2.54	2.39	3.84	3.77	1.79	1.58
41	C004804115	1.32	1.38	1.23	2.14	2.38	2.27	0.93	1.06
42	C004813220	1.72	2.19	#N/A	9.01	10.46	#N/A	#N/A	#N/A

43	C005137305	1.83	2.16	#N/A	5.95	6.24	#N/A	#N/A	#N/A
44	C005900525	0.61	0.98	0.92	1.40	2.20	2.24	1.52	1.60
45	C005900730	1.34	1.66	1.46	2.89	3.62	3.30	1.09	1.14
46	C005901502	2.02	2.31	1.99	1.39	5.30	#N/A	0.99	#N/A
47	C005901805	1.30	1.50	1.36	4.68	5.61	5.05	1.05	1.08
48	C005901830	1.41	1.63	1.51	3.08	3.62	3.27	1.07	1.06
49	C005901925	1.00	1.20	1.18	2.89	3.06	3.09	1.18	1.07
50	C005902215	1.12	1.41	1.22	3.20	4.04	3.75	1.09	1.17
51	C005903110	0.87	1.59	1.49	2.52	4.12	3.83	1.71	1.52
52	C005913020	1.56	1.95	1.75	3.36	4.29	4.01	1.13	1.19
53	C005913903	0.99	1.20	1.19	1.47	1.86	1.69	1.20	1.15
54	C005940620	1.11	2.10	#N/A	9.98	16.58	#N/A	#N/A	#N/A
55	C006300507	0.83	1.35	#N/A	0.92	1.50	#N/A	#N/A	#N/A
56	C006300825P	1.10	1.82	1.71	1.90	2.95	2.96	1.56	1.56
57	C006301204P	0.48	0.79	0.71	2.32	3.66	3.41	1.50	1.47
58	C006313105	0.65	1.04	0.99	1.89	3.04	2.95	1.51	1.56
59	C006341615	0.61	1.08	0.95	2.31	3.73	3.50	1.56	1.52
60	C006602010	1.18	1.41	1.40	2.91	3.18	3.04	1.19	1.04
61	C006607105P	1.04	1.30	1.27	2.70	2.86	2.77	1.22	1.02
62	C007001220	0.96	1.23	1.14	3.19	3.43	3.47	1.19	1.09
63	C007004115	0.85	1.20	1.03	2.97	3.25	3.27	1.22	1.10
64	C007010905	0.87	1.26	1.18	1.71	2.01	1.90	1.35	1.11
65	C007012235	1.20	1.53	1.52	2.42	2.67	2.40	1.26	0.99
66	C007202710	1.64	1.90	1.71	2.87	3.45	3.05	1.04	1.07
67	C007203715	1.18	1.29	1.23	1.73	1.88	1.92	1.04	1.11
68	C007203805	1.36	1.61	1.38	1.73	2.02	1.91	1.01	1.11

69	C007213110	1.57	1.82	1.63	2.86	3.31	3.16	1.04	1.10
70	C007602705	1.44	1.48	1.35	2.87	3.50	3.32	0.93	1.16
71	C007603710	1.50	1.75	1.68	2.68	3.05	3.01	1.12	1.12
72	C007802440	1.10	1.29	1.24	2.80	2.95	2.90	1.12	1.04
73	C007805310P	2.00	2.38	2.21	2.45	3.03	2.83	1.11	1.16
74	C007815273	2.54	2.93	2.80	4.59	7.07	6.86	1.10	1.49
75	C007932415	1.12	1.59	1.45	2.53	4.10	3.69	1.29	1.46
76	C008002310	1.99	2.32	2.17	3.04	3.28	3.24	1.09	1.07
77	C008101013P	4.75	5.60	5.28	4.82	5.98	5.22	1.11	1.08
78	C008803505	1.12	1.33	1.27	2.02	2.29	2.19	1.14	1.08
79	C009002115	0.56	0.94	#N/A	2.45	4.04	3.93	#N/A	1.60
80	C009111705	1.88	2.28	2.16	2.55	2.72	2.59	1.15	1.01
81	C009114505	1.47	1.70	1.60	1.92	2.40	2.24	1.09	1.16
82	C009143435	0.87	1.07	1.05	1.93	2.16	2.13	1.20	1.11
83	C009202210	1.24	1.48	1.43	3.34	4.21	3.84	1.15	1.15
84	C000103420	0.68	1.05	1.14	2.62	2.92	3.63	1.69	1.39
85	C001132713	0.93	1.83	#N/A	0.99	1.93	#N/A	#N/A	#N/A
86	C001234905	1.04	1.22	1.16	2.69	4.23	4.18	1.11	1.55
87	C002012435	1.00	1.10	1.14	3.48	3.63	3.68	1.14	1.06
88	C002602910	1.59	1.70	1.75	5.04	5.97	5.39	1.09	1.07
89	C002713535	0.93	2.52	#N/A	0.88	1.92	#N/A	#N/A	#N/A
90	C005904610	0.99	1.33	1.55	1.34	1.91	2.08	1.56	1.55
91	C005913505	0.59	0.55	0.61	2.15	2.31	2.34	1.03	1.09
92	C007000515	0.77	1.46	1.30	1.94	2.60	2.52	1.70	1.30
93	C007824260	1.48	1.84	1.64	4.78	4.91	4.86	1.11	1.02
94	C009123545	1.71	1.90	1.61	2.58	2.89	2.62	0.94	1.02

95	C002705115	1.82	2.18	2.07	2.84	3.15	2.86	1.14	1.01
96	C003302510	1.57	1.81	1.66	3.05	3.35	3.25	1.06	1.07
97	C005121315P	2.45	2.68	2.36	2.99	3.18	3.19	0.97	1.07
98	C001103815	1.30	1.41	1.40	4.51	5.18	4.97	1.08	1.10
99	C001900130	2.41	2.71	2.55	3.03	3.28	3.26	1.06	1.08
100	C001900815	1.41	1.63	1.54	3.14	3.73	3.46	1.09	1.10
101	C000621615	3.89	4.53	4.38	4.74	4.68	#N/A	1.13	#N/A
102	C000800705	3.82	4.39	4.12	4.20	4.83	5.01	1.08	1.19
103	C000805510P	2.69	3.14	2.83	2.69	3.35	3.26	1.05	1.21
104	C001201410	2.61	3.97	2.76	2.35	2.91	2.95	1.06	1.26
105	C001210930	3.39	4.44	3.77	6.25	6.75	6.43	1.11	1.03
106	C001224325	1.79	2.27	2.02	4.08	4.49	3.97	1.13	0.97
107	C000226205	2.13	2.72	2.18	2.62	2.92	2.85	1.02	1.09
108	C001401535	2.39	3.59	2.43	2.23	3.39	3.28	1.02	1.47
109	C001401710	2.43	2.93	2.44	3.65	3.79	3.66	1.00	1.00
110	C001411615P	2.03	2.70	2.12	3.36	4.56	4.36	1.04	1.30
111	C001526720	3.50	4.76	3.48	2.92	3.70	3.47	0.99	1.19
112	C002001220	2.49	3.76	3.56	2.49	2.38	2.42	1.43	0.97
113	C001716105	2.55	3.95	3.55	4.27	6.26	6.16	1.39	1.44
114	C002001627	3.52	4.35	4.06	3.19	3.65	3.43	1.15	1.08
115	C002003405	2.50	3.12	3.00	3.03	3.37	3.29	1.20	1.09
116	C002003505	1.90	2.57	2.46	4.23	4.61	4.56	1.30	1.08
117	C002004010	1.81	2.39	2.36	4.36	4.74	4.70	1.30	1.08
118	C002012040	3.14	3.89	3.71	3.55	3.95	3.83	1.18	1.08
119	C002013720	2.72	3.40	3.19	2.89	3.27	3.12	1.17	1.08
120	C002014017	3.56	4.42	4.27	2.88	3.32	3.16	1.20	1.10

121	C002313205	3.02	3.45	#N/A	6.51	7.53	#N/A	#N/A	#N/A
122	C000604715	1.88	2.25	2.25	4.62	5.19	4.93	1.20	1.07
123	C003416235	2.08	2.45	2.17	2.77	3.35	3.11	1.04	1.12
124	C004507603	3.11	3.97	3.38	3.39	3.97	3.93	1.09	1.16
125	C004513915	1.87	2.24	2.01	3.43	4.11	3.77	1.07	1.10
126	C004712915	3.03	3.49	3.12	2.78	3.05	2.98	1.03	1.07
127	C000201005	3.30	3.69	#N/A	2.10	2.12	#N/A	#N/A	#N/A
128	C005463410	1.67	3.64	2.88	2.24	3.71	3.49	1.73	1.55
129	C005606105	2.22	2.57	2.41	2.84	3.16	3.11	1.08	1.09
130	C005900505	2.62	2.95	2.40	3.47	3.82	3.64	0.91	1.05
131	C005900915	2.91	4.22	3.26	2.97	3.65	3.93	1.12	1.32
132	C005901517	2.81	3.31	2.82	2.68	2.98	2.88	1.00	1.08
133	C005913030	2.24	2.61	2.30	2.42	2.69	2.59	1.03	1.07
134	C005914820	2.29	2.93	2.59	2.97	3.64	3.72	1.13	1.25
135	C007904705	4.01	6.88	4.49	2.70	3.52	3.53	1.12	1.31
136	C006514240	3.06	3.81	3.15	3.14	3.66	3.44	1.03	1.09
137	C007100625	2.55	3.05	2.99	5.18	5.66	5.75	1.17	1.11
138	C007101130	3.02	4.09	3.89	5.16	7.00	6.58	1.29	1.28
139	C007103415	1.54	2.95	2.84	1.70	3.00	2.88	1.84	1.70
140	C001712925	2.69	3.21	3.04	4.25	4.64	4.58	1.13	1.08
141	C007112340	2.78	3.99	3.32	2.97	3.72	3.72	1.19	1.25
142	C007910405	2.78	3.32	2.94	2.97	3.21	3.20	1.06	1.08
143	C007911205	3.10	3.71	3.51	4.47	5.52	5.47	1.13	1.22
144	C008001215	1.83	2.54	#N/A	2.05	2.08	#N/A	#N/A	#N/A
145	C008602105P	2.40	2.84	2.35	4.75	5.24	5.26	0.98	1.11
146	C008722020	2.82	3.74	2.84	3.26	4.09	3.75	1.01	1.15

147	C008902125	2.44	3.21	2.44	3.07	3.65	3.64	1.00	1.19
148	C001201210	1.65	2.02	1.69	1.43	1.57	1.54	1.03	1.08
149	C009102805	2.29	2.71	2.48	5.14	5.67	5.64	1.08	1.10
150	C009314130	2.52	2.99	2.52	3.35	3.74	3.56	1.00	1.06
151	C004702203	1.44	1.79	1.38	1.43	1.62	1.63	0.96	1.14
152	C006924230	1.83	2.08	1.96	1.34	1.60	1.46	1.07	1.09
153	C004720810	1.67	1.77	1.46	1.60	1.86	1.79	0.87	1.12
154	C002004730	2.48	3.15	2.99	2.65	2.97	2.88	1.20	1.08
155	C005901825	3.10	4.74	2.93	2.44	3.41	3.34	0.94	1.37
156	C002001215	2.11	3.07	2.87	2.61	2.79	2.53	1.36	0.97
157	C008511515	4.17	4.63	4.30	3.82	4.56	4.30	1.03	1.13
158	C004529620	2.49	2.95	2.71	2.93	3.60	3.42	1.09	1.17
159	C008404020	2.03	2.49	1.95	2.43	2.62	2.53	0.96	1.04
160	C004903005	1.51	1.84	1.65	2.69	3.32	3.13	1.10	1.16
161	C000602310	1.71	1.84	1.63	3.33	4.08	3.88	0.95	1.17
162	C007602610	1.97	2.70	2.26	3.18	3.62	3.33	1.15	1.05
163	C001202005	1.82	2.22	2.08	3.21	3.46	3.32	1.14	1.03
164	C001301620	1.30	1.56	1.48	2.49	3.00	2.98	1.14	1.20
165	C001105220	1.18	1.26	1.08	2.39	2.64	2.53	0.91	1.06
166	C001205010	1.91	2.35	2.26	4.51	4.65	4.46	1.19	0.99
167	C001424750	3.01	3.66	3.15	5.04	4.97	4.85	1.05	0.96
168	C006311110	2.09	2.35	2.19	5.12	5.79	5.45	1.05	1.06
169	C001400730	2.01	2.43	2.26	5.47	6.20	5.91	1.12	1.08
170	C009103005	1.42	1.74	1.45	3.89	3.80	#N/A	1.02	#N/A
171	C007102605	2.32	2.95	2.76	4.14	4.95	4.75	1.19	1.15
172	C000102115	2.45	3.36	3.04	4.09	5.74	5.47	1.24	1.34

173	C007302705P	1.47	2.08	1.91	3.37	5.07	4.72	1.30	1.40
174	C006500230	2.03	4.35	3.81	3.21	5.48	5.07	1.87	1.58

11.5 Load Test Documentation

Table 52. Strain Gauge ID and Locations for Yutan Load Test 1

Sensor ID	Girder # (1-8)	Cross Section Location (South Abut., Midspan, North Abut.)	Sensor Location (West or East Bottom Flange, Top of Web)	BDI Sensor ID
1	1	South Abutment	Top of Web	5404
2	1	South Abutment	West Bottom Flange	4526
3	1	South Abutment	East Bottom Flange	4523
4	2	South Abutment	Top of Web	4546
5	2	South Abutment	West Bottom Flange	5397
6	2	South Abutment	East Bottom Flange	5328
7	3	South Abutment	Top of Web	5381
8	3	South Abutment	West Bottom Flange	5401
9	3	South Abutment	East Bottom Flange	6182
10	4	South Abutment	Top of Web	5395
11	4	South Abutment	West Bottom Flange	6326
12	4	South Abutment	East Bottom Flange	5410
13	5	South Abutment	Top of Web	7039
14	5	South Abutment	West Bottom Flange	5412
15	5	South Abutment	East Bottom Flange	4520
16	8	South Abutment	Top of Web	6190
17	8	South Abutment	West Bottom Flange	6181
18	8	South Abutment	East Bottom Flange	5406
19	1	Midspan	Top of Web	4535
20	1	Midspan	West Bottom Flange	6876
21	1	Midspan	East Bottom Flange	6192
22	2	Midspan	Top of Web	7033
23	2	Midspan	West Bottom Flange	7030
24	2	Midspan	East Bottom Flange	7032
25	3	Midspan	Top of Web	7051
26	3	Midspan	West Bottom Flange	7041
27	3	Midspan	East Bottom Flange	7040
28	4	Midspan	Top of Web	7035
29	4	Midspan	West Bottom Flange	7052
30	4	Midspan	East Bottom Flange	7054
31	5	Midspan	Top of Web	5408

32	5	Midspan	West Bottom Flange	6178
33	5	Midspan	East Bottom Flange	4524
34	8	Midspan	Top of Web	7031
35	8	Midspan	West Bottom Flange	7044
36	8	Midspan	East Bottom Flange	7042
37	1	North Abutment	Top of Web	7053
38	1	North Abutment	West Bottom Flange	7048
39	1	North Abutment	East Bottom Flange	7050
40	2	North Abutment	Top of Web	7038
41	2	North Abutment	West Bottom Flange	6191
42	2	North Abutment	East Bottom Flange	4531
43	3	North Abutment	Top of Web	7058
44	3	North Abutment	West Bottom Flange	7037
45	3	North Abutment	East Bottom Flange	7060
46	4	North Abutment	Top of Web	5398
47	4	North Abutment	West Bottom Flange	4541
48	4	North Abutment	East Bottom Flange	5411
49	5	North Abutment	Top of Web	7029
50	5	North Abutment	West Bottom Flange	5384
51	5	North Abutment	East Bottom Flange	7055

Table 53. Strain Gauge ID and Locations for Yutan Load Test 2

Sensor ID	**Girder # (1-8)**	**Cross Section Location (South Abut., Midspan, North Abut.)**	**Sensor Location (Bottom Flange, Top of Web)**	**BDI Sensor ID**
1	1	South Abutment	Top of Web	7060
2	1	South Abutment	Bottom Flange	7031
3	2	South Abutment	Top of Web	7057
4	2	South Abutment	Bottom Flange	5395
5	3	South Abutment	Top of Web	7032
6	3	South Abutment	Bottom Flange	7051
7	4	South Abutment	Top of Web	5398
8	4	South Abutment	Bottom Flange	4524
9	5	South Abutment	Top of Web	7029

10	5	South Abutment	Bottom Flange	7045
11	6	South Abutment	Top of Web	6178
12	6	South Abutment	Bottom Flange	7030
13	7	South Abutment	Top of Web	7043
14	7	South Abutment	Bottom Flange	6192
15	8	South Abutment	Top of Web	7040
16	8	South Abutment	Bottom Flange	7047
17	1	Midspan	Top of Web	7049
18	1	Midspan	Bottom Flange	5401
19	2	Midspan	Top of Web	5412
20	2	Midspan	Bottom Flange	4523
21	3	Midspan	Top of Web	7035
22	3	Midspan	Bottom Flange	5384
23	4	Midspan	Top of Web	7053
24	4	Midspan	Bottom Flange	7037
25	5	Midspan	Top of Web	7052
26	5	Midspan	Bottom Flange	6876
27	6	Midspan	Top of Web	7046
28	6	Midspan	Bottom Flange	6181
29	7	Midspan	Top of Web	7042
30	7	Midspan	Bottom Flange	5397
31	8	Midspan	Top of Web	7036
32	8	Midspan	Bottom Flange	5410
33	1	North Abutment	Top of Web	4520
34	1	North Abutment	Bottom Flange	6191
35	2	North Abutment	Top of Web	7041
36	2	North Abutment	Bottom Flange	7056
37	3	North Abutment	Top of Web	7061
38	3	North Abutment	Bottom Flange	4541
39	4	North Abutment	Top of Web	6182
40	4	North Abutment	Bottom Flange	5411
41	5	North Abutment	Top of Web	7055
42	5	North Abutment	Bottom Flange	7054
43	6	North Abutment	Top of Web	4546
44	6	North Abutment	Bottom Flange	4526

12 References

Adeli, H. (2001). Neural Networks in Civil Engineering: 1989-2000. *Computer-Aided Civil and Infrastructure Engineering*, 16(2), pp.126-142.

American Institute of Steel Construction (2017). *Design Guide 21: Welded Connections--A Primer for Engineers*.

Alipour, M., Harris, D., Barnes, L., Ozbulut, O. and Carroll, J. (2017). Load-Capacity Rating of Bridge Populations through Machine Learning: Application of Decision Trees and Random Forests. *Journal of Bridge Engineering*.

American Association of State Highway and Transportation Officials (AASHTO). (2019).*The Manual for Bridge Evaluation*, 3rd Ed., 2019 Interim Revisions,Washington, DC.

American Association of State Highway and Transportation Officials (AASHTO). (2013).*The Manual for Bridge Evaluation*, 2nd Ed., 2011 and 2013 Interim Revisions,Washington, DC.

American Association of State Highway and Transportation Officials (AASHTO). (2015).*AASHTO LRFD Bridge Design Specifications*, 7th Ed., 2015 Interim Revisions,Washington, DC.

Anderson, D., Hines, E., Arthur, S. and Eiap, E. (1997). Application of Artificial Neural Networks to the Prediction of Minor Axis Steel Connections. *Computers & Structures*, 63(4), pp.685-692.

Armendariz, R. and Bowman, M. (2018). Bridge Load Rating. *Joint Transportation Research Program*, (FHWA/IN/JTRP-2018/07).

Bae, H. and Oliva, M. (2012). Moment and Shear Load Distribution Factors for Multigirder Bridges Subjected to Overloads. *Journal of Bridge Engineering*, 17(3), pp.519-527.

Bakht, B. and Jaeger, L. (1990). Bridge Testing—A Surprise Every Time. *Journal of Structural Engineering*, 116(5), pp.1370-1383.

Bakht, B. and Jaeger, L. (1988). Bearing Restraint in Slab-on-Girder Bridges. *Journal of Structural Engineering*, 114(12), pp.2724-2740.

Bandara, R., Chan, T. and Thambiratnam, D. (2014). Frequency Response Function Based damage Identification Using Principal Component Analysis and Pattern Recognition Technique. *Engineering Structures*, 66, pp.116-128.

Barker, M. (2001). Quantifying Field-Test Behavior for Rating Steel Girder Bridges. *Journal of Bridge Engineering*, 6(4), pp.254-261.

Barth, K. and Wu, H. (2006). Efficient Nonlinear Finite Element Modeling of Slab on Steel Stringer Bridges. *Finite Elements in Analysis and Design*, 42(14-15), pp.1304-1313.

Bechtel, A., McConnell, J. and Chajes, M. (2009). Destructive Testing and Finite Element Analysis to Determine Ultimate Capacity of Skewed Steel I-Girder Bridges. *Transportation Research Record: Journal of the Transportation Research Board*, 2131(1), pp.49-56.

Bechtel, A., McConnell, J. and Chajes, M. (2011). Ultimate Capacity Destructive Testing and Finite-Element Analysis of Steel I-Girder Bridges. *Journal of Bridge Engineering*, 16(2), pp.197-206.

Bell, E., Lefebvre, P., Sanayei, M., Brenner, B., Sipple, J. and Peddle, J. (2013). Objective Load Rating of a Steel-Girder Bridge Using Structural Modeling and Health Monitoring. *Journal of Structural Engineering*, 139(10), pp.1771-1779.

Bishara, A., Liu, M. and El-Ali, N. (1993). Wheel Load Distribution on Simply Supported Skew I-Beam Composite Bridges. *Journal of Structural Engineering*, 119(2), pp.399-419.

Bowman, M. D. and Chou, R. (2014). Review of Load Rating and Posting Procedures and Requirements. *Indiana Department of Transportation*.

Burdette, E. and Goodpasture, D. (1971). Full-Scale Bridge Testing: An Evaluation of Bridge Design Criteria.

Cai, C. and Shahawy, M. (2003). Understanding Capacity Rating of Bridges from Load Tests. *Practice Periodical on Structural Design and Construction*, 8(4), pp.209-216.

Cattan, J. and Mohammadi, J. (1997). Analysis of Bridge Condition Rating Data Using Neural Networks. *Computer-Aided Civil and Infrastructure Engineering*, 12(6), pp.419-429.

Chajes, M., Mertz, D. and Commander, B. (1997). Experimental Load Rating of a Posted Bridge. *Journal of Bridge Engineering*, 2(1), pp.1-10.

Chen, H., Tsai, K., Qi, G., Yang, J. and Amini, F. (1995). Neural Network for Structure Control. *Journal of Computing in Civil Engineering*, 9(2), pp.168-176.

Chen, Y. (1995). Prediction of Lateral Distribution of Vehicular Live Loads on Bridges with Unequally Spaced Girders. *Computers & Structures*, 54(4), pp.609-620.

Cheung, M., Gardner, N. and Ng, S. (1987). Load Distribution Characteristics of Slab-on-Girder Bridges at Ultimate. *Canadian Journal of Civil Engineering*, 14(6), pp.739-752.

Chuang, P., Goh, A. and Wu, X. (1998). Modeling the Capacity of Pin-Ended Slender Reinforced Concrete Columns Using Neural Networks. *Journal of Structural Engineering*, 124(7), pp.830-838.

Chung, W. and Sotelino, E. (2006). Three-dimensional Finite Element Modeling of Composite Girder Bridges. *Engineering Structures*, 28(1), pp.63-71.

Chung, W., Liu, J. and Sotelino, E. (2006). Influence of Secondary Elements and Deck Cracking on the Lateral Load Distribution of Steel Girder Bridges. *Journal of Bridge Engineering*, 11(2), pp.178-187.

Conner, S. and Huo, X. (2006). Influence of Parapets and Aspect Ratio on Live-Load Distribution. *Journal of Bridge Engineering*, 11(2), pp.188-196.

Desayi, P. and Krishnan, S. (1964). Equation for the Stress-Strain Curve of Concrete. *ACI Journal Proceedings*, 61(3).

Eamon, C. and Nowak, A. (2002). Effects of Edge-Stiffening Elements and Diaphragms on Bridge Resistance and Load Distribution. *Journal of Bridge Engineering*, 7(5), pp.258-266.

Ebeido, T. and Kennedy, J. (1996). Girder Moments in Continuous Skew Composite Bridges. *Journal of Bridge Engineering*, 1(1), pp.37-45.

Ebeido, T. and Kennedy, J. (1996). Shear and Reaction Distributions in Continuous Skew Composite Bridges. *Journal of Bridge Engineering*, 1(4), pp.155-165.

Eom, J. and Nowak, A. (2001). Live Load Distribution for Steel Girder Bridges. *Journal of Bridge Engineering*, 6(6), pp.489-497.

Fu, K. and Lu, F. (2003). Nonlinear Finite-Element Analysis for Highway Bridge Superstructures. *Journal of Bridge Engineering*, 8(3), pp.173-179.

Galambos, T., Leon, R., French, C., Barker, M. and Dishongh, B. (1992). Inelastic Rating Procedures for Steel Beam and Girder Bridges. *NCHRP*, Report 352.

Gheitasi, A. and Harris, D. (2015). Failure Characteristics and Ultimate Load-Carrying Capacity of Redundant Composite Steel Girder Bridges: Case Study. *Journal of Bridge Engineering*, 20(3), p.05014012.

Gheitasi, A. and Harris, D. (2015). Overload Flexural Distribution Behavior of Composite Steel Girder Bridges. *Journal of Bridge Engineering*, 20(5).

Ghosn, M. and Moses, F. (1998). Redundancy in Highway Bridge Superstructures. *NCHRP*, Report 406.

Ghosn, M., Moses, F. and Gobieski, J. (1986). Evaluation of Steel Bridges Using In-Service Testing. *Transportation Research Record*.

Guzelbey, I., Cevik, A. and Gögüş, M. (2006). Prediction of Rotation Capacity of Wide Flange Beams Using Neural Networks. *Journal of Constructional Steel Research*, 62(10), pp.950-961.

Hadi, M. (2003). Neural Networks Applications in concrete Structures. *Computers & Structures*, 81(6), pp.373-381.

Hall, J. and Kostem, C. (1981). *Inelastic Overload Analysis of Continuous Steel Multi-Girder Highway Bridges by the Finite Element Method*. Ph.D. Lehigh University.

Harris, D., Civitillo, J. and Gheitasi, A. (2016). Performance and Behavior of Hybrid Composite Beam Bridge in Virginia: Live Load Testing. *Journal of Bridge Engineering*, 21(6), p.04016022.

Harris, D. (2010). Assessment of Flexural Lateral Load Distribution Methodologies for Stringer Bridges. *Engineering Structures*, 32(11), pp.3443-3451.

Harris, D., Cousins, T., Murray, T. and Sotelino, E. (2008). Field Investigation of a Sandwich Plate System Bridge Deck. *Journal of Performance of Constructed Facilities*, 22(5), pp.305-315.

Harris, D. and Gheitasi, A. (2013). Implementation of an Energy-Based Stiffened Plate formulation for Lateral Load Distribution characteristics of Girder-Type Bridges. *Engineering Structures*, 54, pp.168-179.

Hasançebi, O. and Dumlupınar, T. (2013). Detailed Load Rating Analyses of Bridge Populations Using Nonlinear Finite Element Models and Artificial Neural Networks. *Computers & Structures*, 128, pp.48-63.

Hasançebi, O. and Dumlupınar, T. (2011). A Neural Network Approach for Approximate Force Response Analyses of a Bridge Population. *Neural Computing and Applications*, 22(3-4), pp.755-769.

Hearn, G. (2014). *NCHRP Synthesis 453: State Bridge Load Posting Processes and Practices*.

Hegazy, T., Tully, S. and Marzouk, H. (1998). A Neural Network Approach for Predicting the Structural Behavior of Concrete Slabs. *Canadian Journal of Civil Engineering*, 25(4), pp.668-677.

Helba, A. and Kennedy, J. (1994). Parametric Study on Collapse Loads of Skew Composite Bridges. *Journal of Structural Engineering*, 120(5), pp.1415-1433.

Hosteng, T., and Phares, B., (2013) Demonstration of Load Rating Capabilities Through Physical Load Testing: Ida County Bridge Case Study," Iowa. Dept. of Transportation.

Hosteng, T., and Phares, B., (2013) Demonstration of Load Rating Capabilities Through Physical Load Testing: Sioux County Bridge Case Study," Iowa. Dept. of Transportation.

Huang, C. and Loh, C. (2001). Nonlinear Identification of Dynamic Systems Using Neural Networks. *Computer-Aided Civil and Infrastructure Engineering*, 16(1), pp.28-41.

Huang, H., Shenton, H. and Chajes, M. (2004). Load Distribution for a Highly Skewed Bridge: Testing and Analysis. *Journal of Bridge Engineering*, 9(6), pp.558-562.

Jaramilla, B. and Huo, S. (2005). FHWA-HRT-05-006: Looking to Load and Resistance Factor Rating. *Federal Highway Administration*, 69(1).

Jeffrey, A., Breña, S. and Civjan, S. (2009). Evaluation of Bridge Performance and Rating through Non-destructive Load Testing.

Kathol, S., Azizinamini, A. and Luedke, J. (1995). *Strength Capacity of Steel Girder Bridges: Final Report*. Nebraska Department of Roads.

Khaleel, M. and Itani, R. (1990). Live-Load Moments for Continuous Skew Bridges. *Journal of Structural Engineering*, 116(9), pp.2361-2373.

Khaloo, A. and Mirzabozorg, H. (2003). Load Distribution Factors in Simply Supported Skew Bridges. *Journal of Bridge Engineering*, 8(4), pp.241-244.

Kim, S. and Nowak, A. (1997). Load Distribution and Impact Factors for I-Girder Bridges. *Journal of Bridge Engineering*, 2(3), pp.97-104.

Kim, Y., Tanovic, R. and Wight, R. (2013). A Parametric Study and Rating of Steel I-Girder Bridges Subjected to Military Load Classification Trucks. *Engineering Structures*, 56, pp.709-720.

Kulicki, J., Prucz, Z., Clancy, C., Mertz, D. and Nowak, A., 2007. Updating the Calibration Report for AASHTO LRFD Code. *NCHRP*, Project 20-07 Task 186.

Kushida, M., Miyamoto, A. and Kinoshita, K. (1997). Development of Concrete Bridge Rating Prototype Expert System with Machine Learning. *Journal of Computing in Civil Engineering*, 11(4), pp.238-247.

Lichtenstein, A., Moses, F. and Bakht, B. (1998). *Manual for Bridge Rating Through Load Testing*. Research Results Digest Number 234.

Mabsout, M., Tarhini, K., Frederick, G. and Kesserwan, A. (1998). Effect of Continuity on Wheel Load Distribution in Steel Girder Bridges. *Journal of Bridge Engineering*, 3(3), pp.103-110.

Mabsout, M., Tarhini, K., Frederick, G. and Kobrosly, M. (1997). Influence of Sidewalks and Railings on Wheel Load Distribution in Steel Girder Bridges. *Journal of Bridge Engineering*, 2(3), pp.88-96.

MacKay, D.J.C. (1992) "Bayesian Interpolation," *Neural Comput.*, 4(3), 415-447

Marquardt, D. (1963). An Algorithm for Least-Squares Estimation of Nonlinear Parameters. *Journal of the Society for Industrial and Applied Mathematics*, 11(2), pp.431-441.

Marx, H., Khachaturian, N. and Gamble, W. (1986). *Report FHWA/IL/UI-210: Development of Design Criteria for Simply Supported Skew Slab-And-Girder Bridges*. Illinois Department of Transportation.

Masri, S., Chassiakos, A. and Caughey, T. (1993). Identification of Nonlinear Dynamic Systems Using Neural Networks. *Journal of Applied Mechanics*, 60(1), p.123.

Masri, S., Smyth, A., Chassiakos, A., Caughey, T. and Hunter, N. (2000). Application of Neural Networks for Detection of Changes in Nonlinear Systems. *Journal of Engineering Mechanics*, 126(7), pp.666-676.

McConnell, J., Chajes, M. and Michaud, K. (2015). Field Testing of a Decommissioned Skewed Steel I–Girder Bridge: Analysis of System Effects. *Journal of Structural Engineering*, 141(1), p.D4014010.

Mikami, I., Tanaka, S. and Hiwatashi, T. (1998). Neural Network System for Reasoning Residual Axial Forces of High-Strength Bolts in Steel Bridges. *Computer-Aided Civil and Infrastructure Engineering*, 13(4), pp.237-246.

Moses, F. (2001). NCHRP Report 454, Calibration of Load Factors for LRFR Bridge Evaluation.

Moses, J., Harries, K., Earls, C. and Yulismana, W. (2006). Evaluation of Effective Width and Distribution Factors for GFRP Bridge Decks Supported on Steel Girders. *Journal of Bridge Engineering*, 11(4), pp.401-409.

Mukherjee, A. and Deshpande, J. (1995). Modeling Initial Design Process using Artificial Neural Networks. *Journal of Computing in Civil Engineering*, 9(3), pp.194-200.

Mukherjee, A., Deshpande, J. and Anmala, J. (1996). Prediction of Buckling Load of Columns Using Artificial Neural Networks. *Journal of Structural Engineering*, 122(11), pp.1385-1387.

Murdock, M. (2009). *Comparative Load Rating Study Under LRFR and LFR Methodologies for Alabama Highway Bridges*. Ph.D. Auburn University.

National Cooperative Highway Research Program (1998). *NCHRP Report 406: Redundancy in Highway Bridge Superstructures*. Washington D.C.: National Academy Press.

National Cooperative Highway Research Program (1993). *NCHRP Report 352: Inelastic Rating Procedures for Steel Beam and Girder Bridges*. Washington D.C.: National Academy Press.

NBI (National Bridge Inventory). (2019).

Nowak, A., Kim, S. and Stankiewicz, P. (2000). Analysis and diagnostic testing of a bridge. *Computers & Structures*, 77(1), pp.91-100.

Nowak, A. (1999). NCHRP Report 368, Calibration of LRFD Bridge Design Code.

Pandey, P. and Barai, S. (1995). Multilayer Perceptron in Damage Detection of Bridge Structures. *Computers & Structures*, 54(4), pp.597-608.

Pendharkar, U., Chaudhary, S. and Nagpal, A. (2007). Neural Network for Bending Moment in Continuous Composite Beams Considering Cracking and Time Effects in Concrete. *Engineering Structures*, 29(9), pp.2069-2079.

Phares, B., Wipf, T., Klaiber, F. and Abu-Hawash, A. (2003). Bridge Load Rating Using Physical Testing.

Razaqpur, A.G. and Nofal, M. (1990). Analytical Modeling of Nonlinear Behavior of Composite Bridges. *Journal of Structural Engineering*, 116(6), pp.1715-1733.

Razaqpur, A.G., Shedid, M. and Nofal, M. (2012). Inelastic Load Distribution in Multi-Girder Composite Bridges. *Engineering Structures*, 44, pp.234-247.

Sakr, M. and Sakla, S. (2009). Long-term Deflection of Cracked Composite Beams with Nonlinear Partial Shear Interaction — A Study Using Neural Networks. *Engineering Structures*, 31(12), pp.2988-2997.

Sanayei, M., Phelps, J., Sipple, J., Bell, E. and Brenner, B. (2012). Instrumentation, Nondestructive Testing, and Finite-Element Model Updating for Bridge Evaluation Using Strain Measurements. *Journal of Bridge Engineering*, 17(1), pp.130-138.

Sebastian, W. and McConnel, R. (2000). Nonlinear FE Analysis of Steel-Concrete Composite Structures. *Journal of Structural Engineering*, 126(6), pp.662-674.

Sheikh-Ahmad, J., Twomey, J., Kalla, D. and Lodhia, P. (2007). Multiple Regression and Committee Neural Network Force Prediction Models in Milling FRP. *Machine Science and Technology*, 11(3), pp.391-412.

Shu, J., Zhang, Z., Gonzalez, I. and Karoumi, R. (2013). The Application of a Damage Detection Method using Artificial Neural Network and Train-Induced Vibrations on a Simplified Railway Bridge Model. *Engineering Structures*, 52, pp.408-421.

Sirca, G. and Adeli, H. (2004). Counterpropagation Neural Network Model for Steel Girder Bridge Structures. *Journal of Bridge Engineering*, 9(1), pp.55-65.

Sofi, F. and Steelman, J., (2019). Nonlinear Flexural Distribution Behavior and Ultimate System Capacity of Skewed Steel Girder Bridges. *Engineering Structures*, 197, p.109392.

Sofi, F. and Steelman, J., (2017). Parametric Influence of Bearing Restraint on Nonlinear Flexural Behavior and Ultimate Capacity of Steel Girder Bridges. *Journal of Bridge Engineering*, 22(7), p.04017033.

Sofi, F. (2017). Structural System-Based Evaluation of Steel Girder Highway Bridges and Artificial Neural Network (ANN) Implementation for Bridge Asset Management. Ph.D. University of Nebraska-Lincoln.

Sotelino, E., Liu, J., Chung, W. and Phuvoravan, K. (2004). *FHWA/IN/JTRP-2004/20: Simplified Load Distribution Factor for Use in LRFD Design*.

Stallings, J. and Yoo, C. (1993). Tests and Ratings of Short-Span Steel Bridges. *Journal of Structural Engineering*, 119(7), pp.2150-2168.

Szerszen, M., Linzell, D., Azam, S., Al-Hajami, A., Steelman, J. and Wood, R., (2019). *Protocol To Evaluate And Load Rate Existing Bridges Using Field Testing*.

Tabsh, S. and Tabatabai, M. (2001). Live Load Distribution in Girder Bridges Subject to Oversized Trucks. *Journal of Bridge Engineering*, 6(1), pp.9-16.

Tadesse, Z., Patel, K., Chaudhary, S. and Nagpal, A. (2012). Neural networks for prediction of deflection in composite bridges. *Journal of Constructional Steel Research*, 68(1), pp.138-149.

Tarhini, K. and Frederick, G. (1992). Wheel Load Distribution in I-Girder Highway Bridges. *Journal of Structural Engineering*, 118(5), pp.1285-1294.

Wipf, T. and Hosteng, T. (2010). *Diagnostic Load Testing May Reduce Embargoes*. Tech Transfer Summary.

Wipf, T., Phares, B., Wood, D., Mellingen, E. and Samuelson, A. (2003). *Iowa DOT Report TR-445: Development of Bridge Load Testing Process for Load Evaluation*. Center for Transportation Research and Education.

Yarnold, M., Golecki, T. and Weidner, J. (2018). Identification of Composite Action Through Truck Load Testing. *Frontiers in Built Environment*, 4.

Yousif, Z. and Hindi, R. (2007). AASHTO-LRFD Live Load Distribution for Beam-and-Slab Bridges: Limitations and Applicability. *Journal of Bridge Engineering*, 12(6), pp.765-773.

Zheng, L., Huo, X. and Hayworth, R. (2007). Comparison of Load Factor Rating (LFR) to Load and Resistance Factor Rating (LRFR) of Prestressed Concrete I-Beam Bridges. *American Society of Civil Engineers Structures Congress*.

Zokaie, T. (2000). AASHTO-LRFD Live Load Distribution Specifications. *Journal of Bridge Engineering*, 5(2), pp.131-138.

END OF DOCUMENT